Numerical methods for nondestructive identification of defects
Doctoral thesis

Guillermo Rus Carlborg
Department of Structural Mechanics, University of Granada, Spain.
grus@ugr.es tlf: +34958249431 fax: +34958249959

Advisor: Prof. Rafael Gallego Sevilla

June 2001

Author: Guillermo Rus Carlborg

Advisor: Rafael Gallego Sevilla

ISBN: 84-699-6762-2
Depósito legal: GR 1866/01

Contents

Acknowledgements:

The present thesis would only have been possible with the help of some people I gratefully wish to mention and give my thanks to.

- *Prof. Rafael Gallego Sevilla has wisely and providently directed the whole track, patiently aiding me whenever I asked.*
- *Prof. Javier Suárez Medina cleared the way of this subject and efficiently encouraged me straight on.*
- *Prof. Juan José Granados Romera got me out of the jam more than once.*
- *The whole Department, with no exception has daily supported me and created an optimistic atmosphere.*
- *Outside this Institute, Prof. Francisco Chirino Godoy generously provided us with useful source code.*
- *And at last, I am especially grateful to Prof. Marc Bonnet for the direct contribution to a chapter of this thesis and the paternity of its ground ideas, besides for his guidance in the scientific world.*

*T*o my parents.

Part I

Preliminaries

Chapter 1

Objectives

The purpose of this work is to study a class of inverse problems arising in mechanics with emphasis on the Boundary Element Method (BEM). An Identification Inverse Problem (IIP) means that the unknown is a hidden part of the geometry (internal cavities, inclusions, etc.) instead of the displacements or stresses. The search is performed with the help of additional data in form of measurements of the mechanical response (nondestructive testing). The Boundary Element Method is especially well suited because of a lower need of computational effort and a better adaptivity to varying geometry.

The central point is a sensitivity integral equation with respect to the geometry, which provides an useful gradient for minimization algorithms of cost functions.

The main objectives are summarized in the following points,

- Survey on IP strategies, clarifying the main benefits, drawbacks and areas of applications of each one (see chapter 4).

- Direct derivation of sensitivity to geometry. This is the point in which most effort has been invested. The derivation is done in an analytic and completely generic way, before any definition of parametrization or discretization (chapter 5).

- Sensitivity by the adjoint variable method. This method extended to the derivation of the sensitivity to a crack geometry in bidimensional elastodynamics by means of a boundary only equation (chapter 6).

- Topological derivative. A method based on the linearized estimation of the presence of a circular cavity or straight crack is presented. It appears to be extremely fast in comparison with the solution of a whole direct problem and still give more than enough precision for initialization or even detection purposes (see chapter 10).

- Comparison of the most interesting minimization methods in a systematic way in order to reveal the scope of each one in a practical framework, within the limits of the impossibility to demonstrate mathematically any property in this direction.

- All the developed methods are thoroughly tested numerically, including simulated errors, control of distance from the exact solutions, and means to attain better convergence, in order to provide ready-for-use techniques. Several parametrizations are suggested and tested (see chapter 8; part III contains an abstract of the most revealing results).

- A very simple regularization formula for hypersingular integrals that does not require the calculation of any derivative and only requires to program one loop. This is developed together with a review in appendix B.

- A programmable algebra for tensorial expressions with a high number of indices is developed. The advantages are facility for the programming and lower likelihood of bugs and errors (see appendix C).
- A generalized formula for the quarter point element is made to allow higher order elements to represent accurately the $\sqrt{r}$ behaviour of crack tips, in chapter 7.
- A close relationship between the optimization methods and the observation equation approach was found in the form of an equivalence of both methods. This link will be widened and may make it possible to interchange adjoint tools between each other. This is explained in chapter 11.3.

Chapter 2

Introduction

2.1 The problem

The necessity for nondestructive detection appears in many fields of engineering and other applied sciences:

- The great number of structures in civil engineering, architecture, and aeronautical engineering during the economical growth of the last half century has left to our generation the need for the *sustainable maintenance*, control and conservation of these complex elements during their active life and to raise their longevity. This requires accurate and cheap massive techniques to detect the appearance of defects during service loads. A critical example would be the accurate detection of fatigue cracks in an aeroplane wing beam, lengthening its profitable life and guaranteeing its safety.

- Industrial production and civil engineering structures take immediate advantage of nondestructive methods in the stage of *quality* control, in the search of defects in materials and structures (subsurface flaws, inclusions or cracks). This earns special relevance for high performance advanced materials.

- There is an emerging field in *biomechanics*, where these techniques are needed for tomography, identification and even diagnosis of physically conmensurable abnormal elements.

- The search of antipersonnel mines is also being developed by inverse problems in some Universities.

- One of the most traditional fields of nondestructive detection comes from *geotechnics* and geophysics, not due to the desire of leaving unaltered the structure but for the impossibility to accede deep and extensive areas.

  For instance, mineralogical prospection (detection of oil, water, configuration of layers, etc.), which is traditionally divided into strategic operations (several hundreds of square kilometers) and tactical operations (some dozens), is divided into three successive stages:

  - Study of the terrain, mainly consulting the geological and geographical information.
  - Search for source points by indirect methods, classified into teledetection, physical and chemical methods.
  - Control of source points, by cartography, physical and chemical prospection, and destructive drilling.

  The main techniques used here are:

  - Teledetection and aerial photography.

- Geophysics, from air or ground, divided into radioactivity, magnetism, resistivity, gravity, and structural discontinuities.
- Geochemistry.
- Drilling.
- Washing of alluvium.
- Other techniques based on geological knowledge.

The specific procedure of oil prospection is divided in two phases, one aimed at finding the oil fields:

- by stratigraphy, sedimentology, tectonics, etc.;
- by teledetection;
- by magnetometry;
- by gravimetry;
- seismic or deep echography;
- stratigraphical drilling, in special cases.

The second phase consists in finding out the size of the field in order to decide its practical exploitability and its profitability, besides finding a favourable drilling point.

At this point, there are two areas in which the procedure may be enhanced. The seismic echography carried out from the surface is usually insufficient in practice. The second point is that the determination of the size and shape of the field, at the very last stage, requires drillings, which, apart of being expensive, do not allow for much precision.

In daily practice, the methods used for these issues are quite empiric and rudimentary, requiring either approximations to get analytic solutions, or the interpretation of the measured data (ultrasonic or X-ray plots, or gravimetry or condictivity measurements) by an experienced person on observation, giving therefore poor quantitative data.

Some practical attempts to use sytematic identification algorithms have given promising results. But the identification is a good example of ill posed problems: neither the existence nor the unicity need to exist, and the result may be very sensitive to the measures. This makes it necessary to find robust methods.

Currently, the main problems, which define the direction of the present work, are:

- need for a fast and accurate computation of gradients with respect to the geometrical variation,
- small scope of convergence of the classical optimization algorithms, together with a
- lack of criteria for the choice of algorithms, and
- lack of criteria for the initialization of the algorithms,
- need of a technique for global search in an affordable computing time.

It is important to note an effect of the multidisciplinarity of the subject: many of the contributions of this work (the discussed techniques for the derivation of the gradient, the survey on soft computing, mathematical programming and some tests about them) as well as many of the tools used here are common to *structural optimization* and design.

2.2 What to measure

When seeking defects or flaws inside a body, any physical magnitude that propagates inside it and that manifests on an accessible part of it may be studied in principle in order to obtain information about what is happening inside. The identification can be based on *propagation* phenomena of elastic properties (such as elastic deformation, wave propagation, acoustics, etc.), governed by partial differential equations; electric, thermal or other flow measurements, described by similar *potential* equations; or based on *radiation* (X-rays, reconstruction by photography, etc.). The latter is actually a particular case of the first problem in large scales from the point of view of the frequency (see [36]). The problems tackled here belong to the first type.

On the other hand another classification can be made distinguishing *acoustic emission* (where the "sound" generated by the crack growth is monitored) from *acoustic response* (where the waveform transferred after a dynamic excitation is analyzed).

The present work concerns the study of the response of propagated elastic waves.

2.3 Concept of Inverse Problem

Due to its mathematical properties and conditioning this problem is classified inside the discipline of so called inverse problems.

A direct problem can be stated as the calculation of the response (certain displacements u and stress vectors q) in a specific body defined by its geometry Ω, mechanical properties (k), behavior model (operator L) and boundary conditions (some known values of u and q). As a counterpart of this, an inverse problem is one in which we do not know part of the information above, for example a part of the geometry, or its mechanical properties.

If a generic direct problem (not necessarily elastic) is defined as:

$$L(k)u = q \qquad on \quad \Omega$$

the nature of the unknown yields the following classification of inverse problems by Kubo [74]:

- Identification: a part of the geometry (Ω). This is the problem we are dealing with here.
- Modelization: the mathematical equations that govern the behavior (L).
- Reconstruction: the boundary or initial conditions.
- External actions: q.
- Material properties: some parameters characterizing the material (k).

In order to find this data, supplementary information has to be provided, in form of some extra measurements of u or q made on an accessible area of the specimen.

2.4 How to measure

Although the present work regards mainly steady state harmonic elastic waves (and also static response, as the simplified theoretical solution), there are other possibilites to study.

The use of *static displacement* or traction vector magnitudes is in general less useful than steady state harmonic magnitudes and phase data. The reason is the higher error that may be accumulated and, more important, the difficulty in the measurement, which would only be reliable with laser transducers.

The measurement of *steady state* time-periodic excitation is used here mainly because of a reduction in the amount of data involved, in comparison with the transient dynamic (pulse) testing, without loosing the advantages of having a dynamical signal. This data may be read and produced by means of usual piezoelectric transducers with an appropriate range of frequency response.

A third choice would be to use the *modal* data of the specimen. But eigenvalues and eigenvectors, as happens with static data, are not always significantly influenced by small changes of the geometrical and stiffness data of a structure, leading to problems of low accuracy of the data despite the high accuracy of the eigenfrequency measurement methods. Moreover, for large changes of the crack quantities, besides the appearance of new eigenfrequencies, a change in the order of the system's eigenmodal quantities may arise (i.e. the first mode may become the second for a certain change in the position of the crack). This would require an additional effort to trace these changes. Contrarywise, in the case of small-scale specimens, it is not always efficient to perform an accurate modal analysis test since the mass and stiffness of the required machinery are big enough to influence the measured quantities.

Transient dynamics response (echo) to an impact-type dynamic loading (e.g. a hammer) is based on the waveform matching techniques. The simple variant is based on using only the resonance peaks and delay instead of a complete FFT (frequency-domain) or time-domain data. This ultrasonic backscattering has been studied in the simplified way by Wooh [132] and Nakahata [90] for experimental setups, and using the complete wave data by Stavroulakis [110], and earlier in a partial manner by Takadoya [116] among others.

The steady-state analysis can be enhanced by the analysis of the *harmonic waveform*. If a non-sinusoidal wave is applied at the excitation, i.e. containing several harmonics corresponding to the same base frequency, the resulting steady state waveform will be able to be split into the same harmonics, modified in amplitude and phase. This makes it possible to obtain very rich information using one actuator and only one transducer for the measurement (at only one point, if desired). This possibility is qualitatively tested at the end of the numerical tests. This has an equivalence with the technique of measuring several load cases in the case of static or harmonic detection.

An important limitation of the use of steady-state dynamic data for crack detection should be pointed out here. In this work, *no unilateral effects* or contact phenomena are considered in the crack for the following reasons:

- The frequency domain based postprocessing is usually not applicable anymore.
- The nonlinearities that appear on the model convert the optimization functions into non-differentiable ones, making the choice of optimization algorithm very different from the ones used for cavity and inclusion identification. The differentiation of the boundary integral equation becomes a nontrivial task.
- The solution of the nonlinear problem as well as the optimization algorithm, which would require bilevel techniques (a lower iteration level for the nonlinear system solution and an upper one for the optimization), are dramatically more expensive computationally. This moves the balance towards non-contact testing.

The absence of contact has its field of applicability when the crack is initially open and kept so during the excitation. This happens as long as the small harmonic excitation load is applied on a preloaded structure where the crack is already open, which will be the usual case, when the load motivates the creation of the crack. This way, the specimen can be studied in service or working conditions, and the small harmonic load will not alter the null contact conditions of the crack.

The case of crack identification with unilateral contact is thoroughly studied for the first time by Stavroulakis (2000) [110].

At this point one may distinguish two ways of tackling the problem of identification: one studying the exact problem solving direct ones in an iterative way (our case), and the deduction of a simplified relationship between the excitation and the response (transition function) which substitutes the solution of a direct problem (see Wooh et al. [132] or Bostrom et al. [21] [20]).

Chapter 3

Preliminary concepts

3.1 Boundary Element Method

In some class of Inverse Problems, the use of the Boundary Element Method (BEM) provides clear advantages in comparison with the finite element method and others:

- It does not require a remesh of the domain of the body at each iteration. This reduces both the computational effort and eliminates small but important perturbations due to the changes of the mesh.
- The application of these methods to real problems may require many iterations, as well as big precision in the intermediate solutions, so the use of finite elements would be very expensive.
- In the case of ultrasonic detection, the need to model small waves augments very much the required number of degrees of freedom, which would increase with one more dimension in the case of domain versus boundary discretization.

A conceptual approach to the BEM could be the following. The method is divided in two steps:

1. First of all we build an integral equation. It has to include the constitutive and continuity equations and relate the unknowns. Integral equations are internal products with a kernel evaluated at a pole. When solved numerically, they should be of the Fredholm second type[1], to avoid ill-conditioning. The advantage of the method comes when the integrals are evaluated only on the boundary. The ones used for the elasticity BEM come from the reciprocity theorem of Betti, and include in the kernels Green functions.
2. Secondly, we need to discretize the equation to be able to solve it numerically. Among the methods available (collocation, BEM[2], Nyström[3] or Galerkin[4]), we are going to use the BEM. This is done in two stages:
   - We divide the boundary in elements and assimilate the geometry and the unknown variables on each element by the product of base functions multiplied by discrete nodal values ($\mathbf{x} = \sum \phi_i \mathbf{x}_i$, $\mathbf{u} = \sum \phi_i \mathbf{u}_i$, $\mathbf{q} = \sum \phi_i \mathbf{q}_i$). This is called discretization.
   - In order to get the necessary number of equations we evaluate the integral equation at as many poles or collocation points as unknowns.

A description of the Boundary Element Method for static elasticity follows.

[1] Integral equation of Fredholm's second type: $f(\boldsymbol{\xi}) = \int a(\mathbf{x}, \boldsymbol{\xi}) f(\mathbf{x}) dx$, where a is the kernel.

[2] BEM: the collocation points lie on the boundary.

[3] Nyström method: the collocation points, unknowns and integration points are identical. This method is useful for high kernel evaluation / equation system solving time ratio.

[4] Galerkin approach: involves a further modification of the integral equation. This method is not considered here (see [15]).

3.1.1 Governing equations for elasticity

In our problems, the basic magnitudes and equations in elastostatics at any point of a domain Ω enclosed by a boundary Γ, are the following (basic references on Timoshenko [102], Doblaré [35] or Paris [94]):

σ_{ij} Stress tensor

ϵ_{ij} Strain tensor

u_i Displacements

b_i Body forces

q_i Stress vector at a normal n_j ($q_i = \sigma_{ij} n_j$)

Equilibrium equations:

$$\sigma_{ij,j} + b_i = 0 \qquad in \quad \Omega \tag{3.1}$$

Compatibility equations:

$$\epsilon_{ij} = \frac{1}{2}(u_{i,j} + u_{j,i}) \tag{3.2}$$

Constitutive equations:

$$\sigma_{ij} = \lambda \delta_{ij} \epsilon_{kk} + 2\mu \epsilon_{ij} \tag{3.3}$$

δ_{ij} Kroenecker delta

λ, μ Lamé constants, that can be expressed in terms of:

E, ν Shear modulus, Elasticity modulus and Poisson ratio

$$\mu = \frac{E}{2(1+\nu)} \qquad \lambda = \frac{\nu E}{(1+\nu)(1-2\nu)}$$

An elasticity problem consists of finding a solution of the equations above in a domain Ω bounded by Γ, with some boundary conditions on two non-overlapping partitions of $\Gamma_1 + \Gamma 2 = \Gamma$,

$$\begin{cases} u_k(\mathbf{x}) = \overline{u}_k(\mathbf{x}) & \mathbf{x} \in \Gamma_1 \\ q_k(\mathbf{x}) = n_j(\mathbf{x})\sigma_{jk}(\mathbf{x}) = \overline{q}_k(\mathbf{x}) & \mathbf{x} \in \Gamma_2 \end{cases}$$

3.1.2 Fundamental solution

We are going to restrict ourselves to plane strain ($\epsilon_{33} = 0$) for 2D elasticity. In order to solve a plane stress problem, we just have to substitute the elastic constants by:

$$\nu' = \frac{\nu}{1+\nu} \qquad E' = E(1 - \nu'^2)$$

In order to fulfill the constitutive and compatibility conditions in the adjoint solution used in the reciprocity theorem, we use as kernel functions the fundamental or Kelvin solutions.

Combining the three basic equations (3.1, 3.2 and 3.3) we get the Navier equation:

$$\left(\frac{1}{1-2\nu}\right) u_{j,ji} + u_{i,jj} + \frac{1}{\mu} b_i = 0$$

The Kelvin solutions are the displacement and the stress observed at $\mathbf{x}$, due to a concentrated load (δ of Dirac) applied at the pole $\boldsymbol{\xi}$ towards the direction of the canonical vector e_k,

$$b_i = \delta(\mathbf{x} - \boldsymbol{\xi}) e_i$$

The solution of this problem in 2D elastostatics is (see Domínguez [36], Brebbia [22] and Alarcón [4], [99]):

$$u_k^i = \frac{1}{8\pi\mu(1-\nu)}\left[(3-4\nu)\log\frac{1}{r}\delta_{ik} + r_{,i}r_{,k}\right]$$

$$\sigma_{jk}^i = \frac{-1}{4\pi(1-\nu)r}\left[(1-2\nu)\left\{\delta_{ik}r_{,j} + \delta_{jk}r_{,i} - \delta_{ij}r_{,k}\right\} + 2r_{,i}r_{,j}r_{,k}\right]$$

$$q_k^i = \sigma_{jk}^i n_j = \frac{-1}{4\pi(1-\nu)r}\left[(1-2\nu)\left\{\delta_{ik}r_{,n} + n_k r_{,i} - n_i r_{,k}\right\} + 2r_{,i}r_{,k}r_{,j}n_j\right]$$

where $r_k = x_k - \xi_k$, $r = \sqrt{r_1^2 + r_2^2}$.

3.1.3 Integral equation

The integral equation we use for the BEM is one that directly relates u_i and p_i. If we begin from the equilibrium equation (3.1), we use the principle of the inner product or weak formulation, defining a weight function w_i (this principle is the origin of many numerical methods):

$$\int_\Omega (\sigma_{ij,j} + b_i) w_i d\Omega = 0$$

If we choose the Kelvin solution u_k^i as the kernel function, and integrate it by parts twice the first component, we obtain Betti's reciprocity theorem:

$$\int_\Omega \sigma_{jk,j}^i u_k d\Omega + \int_\Omega b_i u_k^i d\Omega = -\int_\Gamma \sigma_{jk} n_j u_k^i d\Gamma + \int_\Gamma \sigma_{jk}^i n_j u_k d\Gamma \tag{3.4}$$

The process followed so far is analogous to the proof of the Green theorem between two fields u_k and u_k^*, taking into account that $\sigma_{jk,j} + b_k = 0$.

The advantage of our chosen fundamental solution is that the identity $\sigma_{jk,j}^i + \delta(\mathbf{x} - \boldsymbol{\xi})e_i = 0$ converts the first domain integral into a puntual value, giving:

$$-u_i(\boldsymbol{\xi}) + \int_\Omega b_k u_k^i d\Omega = -\int_\Gamma \sigma_{jk} n_j u_k^i d\Gamma + \int_\Gamma \sigma_{jk}^i n_j u_k d\Gamma$$

Reorganizing the terms, and in the case in which we can neglect body forces, we get an integral equation that we only need to evaluate at the boundary:

$$u_i(\boldsymbol{\xi}) = \int_\Gamma (q_k u_k^i - q_k^i u_k) d\Gamma \tag{3.5}$$

3.1.4 Limit to the boundary

The former equation can be turned into a boundary integral equation if we take the pole to the boundary. In this case the integrals can turn singular. To analyze it, we evaluate them with the pole inside the domain, modified by a hemispherical protuberance of radius $\epsilon \to 0$ (figure 3.1). We decompose the integral into the sum of a Cauchy Principal Value (avoiding the hemisphere) and a analytic term (over the hemisphere):

$$\int_\Gamma f d\Gamma = \lim_{\epsilon\to 0}\left(\int_{\Gamma-\Gamma_\epsilon} f d\Gamma\right) + \lim_{\epsilon\to 0}\left(\int_{\Gamma_\epsilon} f d\Gamma\right) \tag{3.6}$$

1. First integral ($\int_\Gamma (q_k u_k^i) d\Gamma$) The first component (on $\Gamma - \Gamma_\varepsilon$) is singular of order $log\left(\frac{1}{r}\right)$, so it should be numerically handled with care. The second component (on Γ_ε) tends to 0.

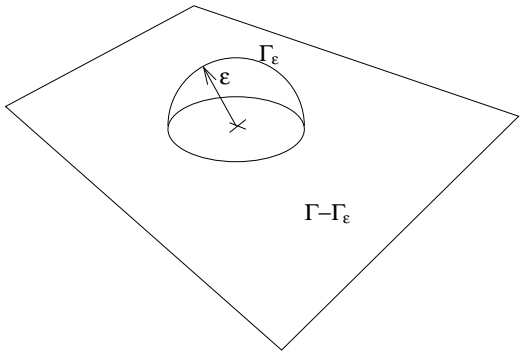

Figure 3.1: Artifice to make the limit to the boundary.

2. Second integral ($\int_\Gamma(-q_k^i u_k)d\Gamma$) The first component (on $\Gamma-\Gamma_\varepsilon$) is also singular of order $\frac{1}{r}$. The second one (on Γ_ε) has the following limit:

$$\lim_{\epsilon\to 0}\left(\int_{\Gamma_\epsilon} q_k^i d\Gamma\right) = c_k^i - \delta_k^i$$

where $c_k^i(\mathbf{x})$ gives the free term, which depends on the position of the collocation point $\boldsymbol{\xi}$ ($c_k^i = 0$ if $\boldsymbol{\xi} \notin \Omega\bigcup\Gamma$; $c_k^i = 1$ if $\boldsymbol{\xi} \in \Omega$ and its value depends on the local geometry of the boundary if $\boldsymbol{\xi} \in \Gamma$). If the boundary is smooth at the pole, $c_k^i = \frac{1}{2}\delta_{ik}$).

Hence, the integral equation 3.5 turns into:

$$c_k^i(\boldsymbol{\xi})u_k(\boldsymbol{\xi}) + \int\!\!\!\!\!\!-_\Gamma \left[q_k^i(\mathbf{x};\boldsymbol{\xi})u_k(\mathbf{x}) - u_k^i(\mathbf{x};\boldsymbol{\xi})q_k(\mathbf{x})\right] d\Gamma(\mathbf{x}) = 0 \tag{3.7}$$

where the integrals have the sense of Cauchy Principal Value. $\mathbf{x}$ is the integration or observation point whereas $\boldsymbol{\xi}$ is the pole or collocation point.

3.1.5 Steady state dynamics

The formulation above can be easily extended to the frequency domain dynamics with the aid of a complex variable $\overline{u}_k$ or $\overline{q}_k$ (being $i = \sqrt{-1}$ the imaginary unit). If the excitation has a frequency ω, every magnitude (u_k or q_k) will accomplish,

$$u_k(t) = u_k^0 \sin(\omega t + \psi) = A_k \sin\omega t - B_k \cos\omega t = \mathrm{RE}((A_k + B_k i)e^{i\omega t}) = \mathrm{RE}(\overline{u}_k e^{i\omega t})$$

The only differences are that the equilibrium equation reads $\sigma_{ij,j} + b_i = \rho\ddot{u}_i$, whereas the reciprocity theorem is identical, as long as the phases coincide. The fundamental solution is now sought to a point load that varies sinusoidally with frequency ω yielding,

$$u_k^i = \frac{1}{2\pi\mu}\left[\psi\delta_{ik} - \chi r_{,i} r_{,k}\right] \tag{3.8}$$

Functions ψ and χ take the value:

$$\begin{aligned}
\psi &= K_0(z_s) + \frac{1}{z_s}[K_1(z_s) - \frac{c_s}{c_p}K_1(z_p)] \\
\chi &= [K_0(z_s) + \frac{2}{z_s}K_1(z_s))] - \frac{c_s^2}{c_p^2}[K_0(z_p) + \frac{2}{z_p}K_1(z_p)] \\
& z_s = \frac{i\omega r}{c_s}; z_s = \frac{i\omega r}{c_s}
\end{aligned}$$

where $K_\alpha(z)$ are the modified Bessel functions of order α, c_s and c_p are the S (shear or irrotational) and P (dilatational or isovolumic) wave velocities, which depend on the Lamé constants λ, μ and on the density ρ.

$$c_s^2 = \frac{\lambda + 2\mu}{\rho} \qquad c_p^2 = \frac{\mu}{\rho}$$

3.1.6 Hypersingular BEM

Another boundary integral equation can be obtained by applying Hooke's law to the former one. It is often used for crack modelization because of the problems that singular BIE give since necessary terms vanish due to the coincidence of the geometry of both crack lips. Other authors also use it on regular boundaries with Neumann conditions.

The following points and hypothesis have to be reviewed from the definition and treatment of the BIE in the BEM in order to derive the sensitivity equations rigurously.

The displacement integral equation for an internal point is:

$$\delta_k^i u_k(\boldsymbol{\xi}) + \int_\Gamma \left[q_k^i(\mathbf{x};\boldsymbol{\xi}) u_k(\mathbf{x}) - u_k^i(\mathbf{x};\boldsymbol{\xi}) q_k(\mathbf{x}) \right] d\Gamma(\mathbf{x}) = 0 \qquad \text{for } \boldsymbol{\xi} \text{ interior.} \tag{3.9}$$

It is interesting to note that q_k^i can be written as:

$$q_k^i(\mathbf{x},\boldsymbol{\xi}) = \sigma_{jk}^i(\mathbf{x},\boldsymbol{\xi}) n_j(\mathbf{x}) = (\lambda \delta_{jk} u_{m,m}^i(\mathbf{x},\boldsymbol{\xi}) + \mu(u_{k,j}^i(\mathbf{x},\boldsymbol{\xi}) + u_{j,k}^i(\mathbf{x},\boldsymbol{\xi})))n_j(\mathbf{x})$$

Since the fundamental solutions are C^∞ we can apply the operator

$$\left(\lambda \delta_{ij} \frac{\partial \{eq\}^m}{\partial \xi_m}(\mathbf{x},\boldsymbol{\xi}) + \mu \left(\frac{\partial \{eq\}^i}{\partial \xi_j}(\mathbf{x},\boldsymbol{\xi}) + \frac{\partial \{eq\}^j}{\partial \xi_i}(\mathbf{x},\boldsymbol{\xi}) \right) \right) n_j(\boldsymbol{\xi})$$

to the component i (referred to the collocation point $\boldsymbol{\xi}$) of equation 3.9 ($\{eq\}^i$), we obtain:

$$\delta_k^i q_k(\boldsymbol{\xi}) + \int_\Gamma \left[d_{jk}^i(\mathbf{x};\boldsymbol{\xi}) n_j(\boldsymbol{\xi}) q_k(\mathbf{x}) - s_{jkl}^i(\mathbf{x};\boldsymbol{\xi}) n_j(\boldsymbol{\xi}) n_l(\mathbf{x}) u_k(\mathbf{x}) \right] d\Gamma(\mathbf{x}) = 0 \qquad \text{for } \boldsymbol{\xi} \text{ interior} \tag{3.10}$$

which can be written written as:

$$c_k^i(\boldsymbol{\xi}) q_k(\boldsymbol{\xi}) + \int_\Gamma \left[d_k^i(\mathbf{x};\boldsymbol{\xi}) q_k(\mathbf{x}) - s_k^i(\mathbf{x};\boldsymbol{\xi}) u_k(\mathbf{x}) \right] d\Gamma(\mathbf{x}) = 0 \qquad \text{for } \boldsymbol{\xi} \text{ interior}$$

The kernels in this integral equation (stress BIE or *qbie* for short) are obtained from the ones in 3.7 (referred to as *ubie* in the sequel) using Hooke's law,

$$\begin{aligned}
d_k^i(\mathbf{x},\boldsymbol{\xi}) &= d_{jk}^i(\mathbf{x},\boldsymbol{\xi}) n_j(\boldsymbol{\xi}) \\
s_k^i(\mathbf{x},\boldsymbol{\xi}) &= s_{jk}^i(\mathbf{x},\boldsymbol{\xi}) n_j(\boldsymbol{\xi}) = s_{jkl}^i(\mathbf{x},\boldsymbol{\xi}) n_j(\boldsymbol{\xi}) n_l(\mathbf{x}) \\
d_{jk}^i(\mathbf{x},\boldsymbol{\xi}) &= \lambda \delta_{ij} u_{k,m}^m(\mathbf{x},\boldsymbol{\xi}) + \mu(u_{k,j}^i(\mathbf{x},\boldsymbol{\xi}) + u_{k,i}^j(\mathbf{x},\boldsymbol{\xi})) \\
s_{jkl}^i(\mathbf{x},\boldsymbol{\xi}) &= \lambda \delta_{ij} \sigma_{kl,m}^m(\mathbf{x},\boldsymbol{\xi}) + \mu(\sigma_{kl,j}^i(\mathbf{x},\boldsymbol{\xi}) + \sigma_{kl,i}^j(\mathbf{x},\boldsymbol{\xi}))
\end{aligned}$$

where the derivatives are performed with respect to the coordinates of $\mathbf{x}$, and the fact that $\partial/\partial x_m = -\partial/\partial \xi_m$ for the kernels has been taken into account since they are functions of the distance r.

If we apply this equation on a cracked body defined by the boundaries $\Gamma = \Gamma_e + \Gamma_+ + \Gamma_-$ (see figure 3.2) we can make the following observations:

$$\begin{aligned}
d_{jk}^i(\mathbf{x}^+,\boldsymbol{\xi}) = d_{jk}^i(\mathbf{x}^-,\boldsymbol{\xi}) \quad &\text{since} \quad u_{k,j}^i(\mathbf{x}^+,\boldsymbol{\xi}) = u_{k,j}^i(\mathbf{x}^-,\boldsymbol{\xi}) \\
s_{jk}^i(\mathbf{x}^+,\boldsymbol{\xi}) = -s_{jk}^i(\mathbf{x}^-,\boldsymbol{\xi}) \quad &\text{since} \quad \sigma_{kl}^i(\mathbf{x}^+,\boldsymbol{\xi}) = \sigma_{kl}^i(\mathbf{x}^+,\boldsymbol{\xi}) \text{ and } n_l^+ = -n_l^- \\
\Delta u_k(\mathbf{x}^+) \quad &= \quad u_k(\mathbf{x}^+) - u_k(\mathbf{x}^-)
\end{aligned}$$

If we assume stress free or induced stress in cracks, which is the usual case,

$$\Delta q_k(\mathbf{x}^+) = 0 = q_k(\mathbf{x}^+) + q_k(\mathbf{x}^-) \quad \Leftrightarrow \quad q_k(\mathbf{x}^+) = -q_k(\mathbf{x}^-)$$

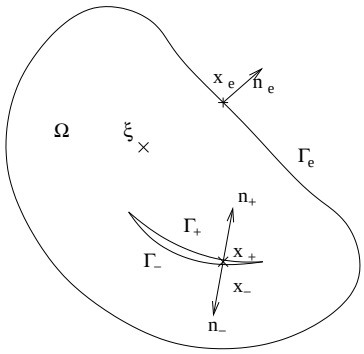

Figure 3.2: Definitions in a cracked body.

Expanding the integral extension into the former sum of boundaries, some terms happen to vanish, and the unknowns can be grouped into the $\Delta u_k(\mathbf{x}^+)$ only (crack opening displacement):

$$\delta^i_k q_k(\boldsymbol{\xi}) + \int_{\Gamma_e} \left[d^i_{jk}(\mathbf{x};\boldsymbol{\xi}) n_j(\boldsymbol{\xi}) q_k(\mathbf{x}) - s^i_{jkl}(\mathbf{x};\boldsymbol{\xi}) n_j(\boldsymbol{\xi}) n_l(\mathbf{x}) u_k(\mathbf{x}) \right] d\Gamma(\mathbf{x}) + \int_{\Gamma_+} \left[-s^i_{jkl}(\mathbf{x};\boldsymbol{\xi}) n_j(\boldsymbol{\xi}) n_l(\mathbf{x}) u_k(\mathbf{x}) \right] d\Gamma(\mathbf{x}) = 0 \qquad \text{for } \boldsymbol{\xi} \text{ interior.}$$

The reason why the q_k terms vanish and not the u_k terms is that there is an intervention of a normal vector $n_j(\boldsymbol{\xi})$ evaluated at the collocation point which keeps it from changing the sign across the two crack lips.

If one defines an unique set of variables along all the boundaries as,

$$\begin{cases} \Gamma = \Gamma_e \Rightarrow & \begin{cases} \mathbf{u} \leftarrow \mathbf{u} \\ \mathbf{q} \leftarrow \mathbf{q} \end{cases} \\ \Gamma = \Gamma_+ \Rightarrow & \begin{cases} \mathbf{u} \leftarrow \Delta\mathbf{u} \\ \mathbf{q} \leftarrow 0 \end{cases} \end{cases}$$

equation 3.10 is recovered

$$\delta^i_k q_k(\boldsymbol{\xi}) + \int_{\Gamma} \left[d^i_{jk}(\mathbf{x};\boldsymbol{\xi}) n_j(\boldsymbol{\xi}) q_k(\mathbf{x}) - s^i_{jkl}(\mathbf{x};\boldsymbol{\xi}) n_j(\boldsymbol{\xi}) n_l(\mathbf{x}) u_k(\mathbf{x}) \right] d\Gamma(\mathbf{x}) = 0 \qquad \text{for } \boldsymbol{\xi} \text{ interior.} \tag{3.11}$$

but now $\Gamma = \Gamma_e + \Gamma_+$.

The complex limiting process has to be done carefully to demonstrate the existence of this integral equation at the limit to the boundary. In fact the equation in this form is only valid at interior points or smooth boundary points where, again, $c^i_k = 1/2\delta^i_k$. In this last case the integral is understood in the sense of the Hadamard Finite Part:

$$c^i_k(\boldsymbol{\xi}) q_k(\boldsymbol{\xi}) + \oint_{\Gamma} \left[d^i_k(\mathbf{x};\boldsymbol{\xi}) q_k(\mathbf{x}) - s^i_k(\mathbf{x};\boldsymbol{\xi}) u_k(\mathbf{x}) \right] d\Gamma(\mathbf{x}) = 0 \tag{3.12}$$

Important literature on the original development of these formulas and necessary considerations about fracture mechanics are found in Blandford [10], Dominguez [80], Ewalds [42], Popelar [67], Gallego [45], [46], Saez [103], Bonnet [17], Sensale [107], Cruse [32], Chirino [30], Elices [38], Broek [23], Polch [95] and Young [134].

3.1.7 Discretization

Any of the equations above are valid for a continuum problem. As mentioned above we express the continuum in terms of discrete values by

$$x_k = \sum \phi_{kj} x_j \qquad u_k = \sum \phi_{kj} u_j \qquad q_k = \sum \phi_{kj} q_j$$

(or

$$x_k = \sum \phi_j x_k^j \qquad u_k = \sum \phi_j u_k^j \qquad q_k = \sum \phi_j q_k^j$$

depending on the structure of the data), which transforms any equation into algebraic one (see figure 3.3). On the other hand, writing it for as many collocation points and directions as unknowns

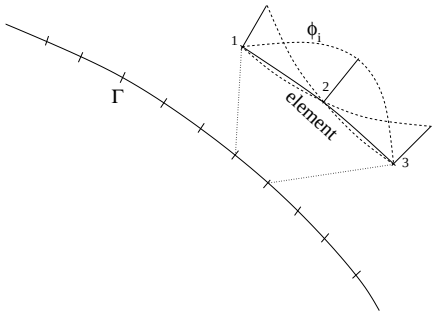

Figure 3.3: Element discretization

allows to construct a defined system of equations.

$$\mathbf{Hu} = \mathbf{Gq} \tag{3.13}$$

where the coefficient matrices $\mathbf{H}$ and $\mathbf{G}$ are mounted adding

$$\mathbf{H} = \{h_{ij}\} = \begin{cases} c_k^i(\boldsymbol{\xi})\phi_{kj}(\boldsymbol{\xi}) + \int_\Gamma q_k^i(\mathbf{x};\boldsymbol{\xi})\phi_{kj}(\mathbf{x})d\Gamma(\mathbf{x}) & \text{for the } ubie \\ \int_\Gamma s_k^i(\mathbf{x};\boldsymbol{\xi})\phi_{kj}(\mathbf{x})d\Gamma(\mathbf{x}) & \text{for the } qbie \end{cases} \tag{3.14}$$

$$\mathbf{G} = \{g_{ij}\} = \begin{cases} \int_\Gamma u_k^i(\mathbf{x};\boldsymbol{\xi})\phi_{kj}(\mathbf{x})d\Gamma(\mathbf{x}) & \text{for the } ubie \\ c_k^i(\boldsymbol{\xi})\phi_{kj}(\boldsymbol{\xi}) + \int_\Gamma d_k^i(\mathbf{x};\boldsymbol{\xi})\phi_{kj}(\mathbf{x})d\Gamma(\mathbf{x}) & \text{for the } qbie \end{cases} \tag{3.15}$$

and the vectors $\mathbf{u}$ and $\mathbf{q}$ collect the displacements and tractions.

The boundary conditions basically imply that at each point either $\mathbf{u}$ or $\mathbf{q}$ is known. This permits to multyply by its coefficients then known terms and perform the column addition yielding a system vector $\mathbf{b}$, whereas the other half of the unknown $\mathbf{u}$ and $\mathbf{q}$ are grouped with its coefficients giving the system matrix $\mathbf{A}$ and unknowns vector $\mathbf{v}$.

$$\mathbf{Av} = \mathbf{b} \tag{3.16}$$

3.1.8 Regularization of the integrals

As it usually happens with integral equation methods, the integrals have singularities of different orders. After the limiting process the integrals are defined outside the "artificial ball" around the pole, and divided into a first one that may have a singularity, and turns to be a Cauchy Principal Value (CPV: $⨍_a^b = \lim_{\epsilon\to 0}\left(\int_a^{-\epsilon} + \int_\epsilon^b\right)$) or Hadamard Finite Part (HFP: $⨍\!\!\!\!-_a^b = \lim_{\epsilon\to 0}\left(\int_a^{-\epsilon} + \int_\epsilon^b - C\frac{1}{\epsilon}\right)$), and a second integral that tends to a so called free term, calculated in the appendix:

$$\int_\Gamma f d\Gamma = \lim_{\epsilon\to 0}\left(\int_{\Gamma-\Gamma_\epsilon} f d\Gamma\right) + \lim_{\epsilon\to 0}\left(\int_{\Gamma_\epsilon} f d\Gamma\right)$$

When some values at this point tend to infinite, the first term has singularities: $\log\frac{1}{r}$, $\frac{1}{r}$, $\frac{1}{r^2}$. In order to be able to compute them numerically in an efficient way, we need to use a combination of some techniques:

- Decomposing the kernel in a sum of a regular part (continuous and differentiable, and not tending to infinite), which will be integrated numerically, and a simpler singular part, to be integrated analytically ($\int = \int_{regular} + \int_{analytic}$).

- Placing the collocation points a bit separated from the ends of the elements when necessary.
- Integrating by special gauss quadratures, as in the case of logaritmic kernels.

Chapter 4

State of the art

In this chapter, am ordered sample of strategies to tackle inverse problems is presented. In the second part, a more extensive survey of authors is made focusing on the critical point of the method for gradient obtention.

In the specific field of identification inverse problems by boundary integral equations, a brief survey of the work done so far, to our knowledge, is presented.

The study of inverse problems in engineering has become an active area of research in the last two decades (see Tanaka and Dulikravich [120]; Delaunay and Jarny [33]; Zabaras, Woodbury and Raynaud [136], other authors: [40], [26], [106], [7], and edited proceedings and journals: [117], [118], [120], [121], [119]). Recent and good surveys and works were written by Bui [25] and Stavroulakis [110]. General surveys can be found by Kubo [74] or Nishimura and Kobayashi [93].

4.1 Strategies for solving Inverse Problems

There are several methods that can be used to solve IP. An approximate classification of them depending on the scope of the convergence is shown in figure 4.1.

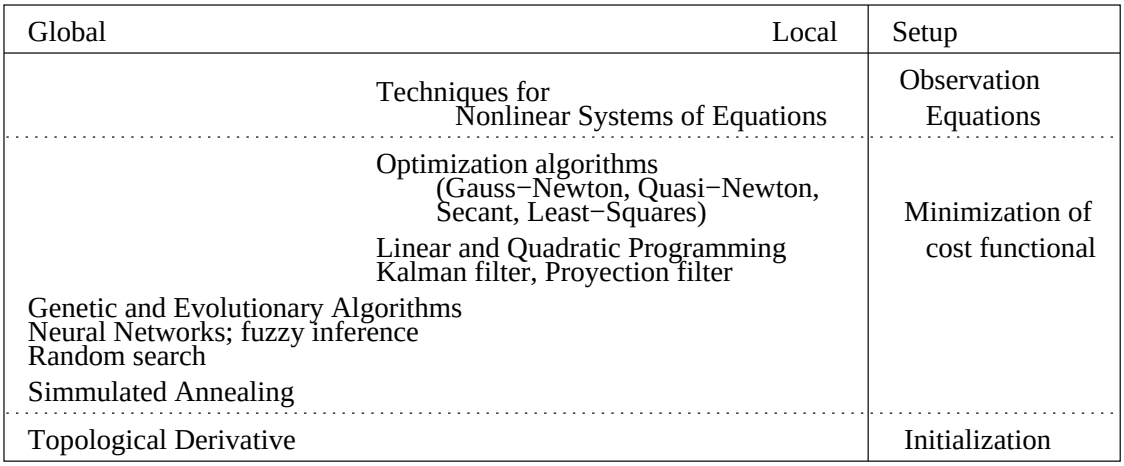

Figure 4.1: A classification of IP strategies.

The ideal algorithm should cover the whole scope, in order to start from a completely unknown configuration and end up with any required approximation (1: accuracy). The way to achieve this at an affordable computational cost (2: effectivity) and a good likelihood for a successfull solution (3: convergence), is throughout several stages ranging global to local methods successively.

The methods treated here are the optimization algorithms, and in particular the Secant and Least squares (local scope) for being the most suitable a priori.

1. **Observation equation methods**

   They are based on establishing a direct correspondence between computed and experimental values,

   $$F(x) = u^{exp}$$

   x is the parameter set (note that for simplicity reasons and congruence with usual literature, the parameter set called P in the rest of the thesis is here denoted by x).

   u is the data to compare (measurements, grouping displacements and stress vectors).

   $()^{exp}$ refers to experimental data.

   F is the operator that maps (implicitly) the parameters to the computed displacements / stress vectors (direct problem).

   The outline of this problem is tackled through a linearization of the relationship by the following decomposition:

   $$F(u_0) + \left.\frac{dF(u)}{dx}\right|_{x_0} \delta x \approx u^{exp} \tag{4.1}$$

   where δx is extracted for the update of x and the obtention of a hopefully better approximation.

   The observation equations have been solved numerically in the following ways,

   - Finite differentiation. If we denote $Ax = b$ the discretized system of equations for the behaviour of the supposed model, $\tilde{A}\tilde{x} = \tilde{b}$ the modified one, and $\delta x = \tilde{x} - x$ the sensitivity, we just have to solve both problems and substract the solution vectors.
   - Analytical differentiation. This is the fastest and most ellaborated method. If we write the modified model equations as a series expansion centered at the assumed one, substract them and elliminate higher order terms, we obtain directly the variation vector. This is the method treated most deeply in this work.
   - It is possible to calculate this vector by finite differenciation as follows, which may enlighten the meaning of the analytical method: $\tilde{A}\tilde{x} - \tilde{b} = (A + \delta A)(x + \delta x) - (b + \delta b) = Ax - b + \delta Ax + A\delta x + \delta A\delta x - \delta b$. Substracting the equations of the modified and assumed model, and neglecting second order terms, we get $A\delta x = -\delta Ax + \delta b$. The right term does not need the solution of any system of equations, and the matrix A of the left term is already factorized after calculating x.
   - An easier numerical method, as it does not require the calculation of the variation of δA, comes from the more straightforward expression $A\delta x = \tilde{A}x - \tilde{b}$.

2. **Optimization theory**

   To tackle this problem with the optimization theory, we have to start with an initial guess of the geometry x, and define a cost functional to miminize $f = \frac{1}{2}R^T R$ where $R = F(x) - u^m$ is the residual. This definition can be altered adding some term $A(x)$, which would lead to a regularization technique due to Tikhonov. The optimization problem is therefore defined as,

   $$\min_x f : \Re^n \to \Re$$

   The definition adopted for the cost functional as a least squares sum has a probabilistic justification since it basically implies that the deviation from the exact solution will be minimal. It can also be seen as the substitution of the vector R with a L^2 norm, which in turn can be interpreted as the solution at the least distance from the exact one. Some gaussian probabilistic interpretations of this definition were developed by Abdallah [1], Suzuki [115] from a bayesian point of view and [86] for a general overview.

The techniques for the minimization of the cost functional are very varied. In an attempt to clarify a classification of them, from the surveys made on the subject and using as a basis the incomplete set of methods that has been tested for identification inverse problems together with the BEM, the following overview is made. A brief description is organized in the following two big groups: soft computing and the classical mathematical programming, and outlined on figure 11.1.

Special emphasis is made on some mathematical programming methods. The observation equation methods are here shown to be closely related to the Gauss-Newton method in 11.3.

General surveys about optimization techniques applied to inverse problems are found on Menke [86], Dennis [64] [34] and Hansen [60].

4.2 Derivation of the gradient

Many methods for IP require the gradient of the cost functional ∇f or the matrix of derivatives $A = \frac{-\delta F(x)}{\delta x}$. Such minimization can be performed by different techniques, but any efficient algorithm would need an analytical computation of the gradient of the cost functional, when available. A classification of them with respect to the computational cost may be the following,

Higher cost		Lower cost
Finite differences (FD)	Adjoint variable (AVM)	Direct derivation (DD)

- *Finite differences* imply solving an additional direct problem at a finite distance from the original one (unless the use of central differences) for each term or vector of the matrix. The drawbacks of this technique are the limited precision of the values and the high computational cost since at least a new direct problem has to be solved for each parameter, at every iteration.

  This approach has been extensively used as well, to regular, strongly, and even hypersingular BIE (Mellings and Aliabadi [84], Bonnet [13]; Matsumoto et al. [83]; Nishimura and Kobayashi [92]; Kirsch [69]). Bonnet [13] demonstrated that the differentiation formulas used for regular integrals can be applied to strongly singular or hypersingular integration as well, providing a firmer mathematical basis to the earlier works.

  Mitra and Das [88] use minimization algorithms for a cost functional, where the gradient is obtained by finite differences, and still require measurements on all the boundary. Mellings and Aliabadi [84] and [85] apply a similar technique.

  Nishimura and Kobayashi [92], [93] use a similar approach for the identification of cracks, starting from the gradient of the *ubie*, which is solved by a Galerkin method. Very good convergence was attained, although they needed measurements along the whole boundary and the use of Tikhonov regularization. Nishimura [91] developed extensions to threedimensional and curved cracks in transient elastodynamics. The gradient is obtained directly from the discretized equations, which is only possible explicitly for constant boundary elements. Neither special elements are used to capture $\sqrt{r}$ crack tip behaviour.

  The direct use of optimization algorithms with finite difference gradient obtention is the most extended: Bezerra and Saigal [9] for elastostatics, Zabaras et al. [105] for material properties, Mura et al. [89] identify cavities, Kagawe [66] uses acoustics whereas Yao [133] uses elasticity, Kassab et al. [68] perform experimental applications with laser speckel photography and static elasticity for cavity detection. Bryan et al. [24] show experimental results on crack reconstruction by impedance tomography.

- The advantage of the *Adjoint variable method* is that one only needs to compute the original and the adjoint direct problems whatever the number of variables, and then making some faster calculations to obtain each derivative. The problem of this method may be the complexity of the formulation.

This method has been employed by several authors in different applications, for example Aithal and Saigal [3], Bonnet [11] for two-dimensional thermal problems; Bonnet [14] for 3D inverse scattering problems by hard and penetrable obstacles; Meric [87] for shape optimization in potential fields; Burczyński [27] applied to stochastic shape sensitivity analysis; Lewis [76] studied some numerical aspects of the approach to general problems. Bui [6] studied the evaluation of the plane containing a three dimensional crack. Calvo [28] developed adjoint problems for optimization of several different functionals.

Bonnet [11], [12], [13], [14], [17] has contributed giving many theoretical formulations and useful ideas to understand the procedure, even for threedimensional acoustic scattering. His later work relies on the obtention of the derivative of a complete cost function by the adjoint variable method, first for closed boundaries and later for cracks [16], [19], [18].

- The basis for the *direct derivative* came from the finite variations formulation used directly for IP.

  Zeng and Saigal [137] developed a formulation for potential fields based on variations, but lack numerical treatment and implementation. Tanaka and Masuda [122], Tanaka and Yamagiwa [127] and Matsumoto and Tanaka [82] developed a similar approach years earlier using Taylor expansions of the kernels and weights in the BIE, leading to a sensitivity equation to the geometry variation. The proposed method requires the solution of three systems: the direct problem, the sensitivity equations and an overdefined system for the parameters. An important drawback is that internal stressed are required as measurements, for which the derivated equation is the more complicated *qbie*. In these papers, the authors propose a different approach from the minimization of a cost functional: the observation equations, but failed to proof its reliability, due to mathematical inconsistences (Tanaka et al.[122]) or simply because no numerical application is carried out (Zeng and Saigal, [137]). Similar partial solutions were provided later by Burczynski et al. [27].

  Gallego and Suarez [114] developed the variation Boundary Integral Equation (δBIE) for the two-dimensional potential problem in a rigorous way, through a series expansion of the kernels and weights of the integral equation, followed by a rigurous limit to the boundary before discretization, considering lacking terms in [137] and [122], and therefore achieving better numerical results. Being the first attempt in this direction it still lacks some basis regarding material derivative and optimization techniques. They presented some numerical results using the observation equation approach in [49], [50], [48], [51], as well as Rus and Gallego [100].

- *Automatic differenciation* is performed automatically by recently developed software that treats directly FORTRAN and C++ source code (see [39], [43]). Like explicit derivation after discretization [84], both methods show inconsistencies while handling singular and hypersingular integration, besides not taking into account the appearance of free terms. An additional problem of AD is the number of limitations imposed on the source code.

Part II

Contributions

Chapter 5

Direct Derivation of geometrical sensitivity

The goal is to calculate the derivative of the displacements or stress vectors (grouped in $\mathbf{v}$) with respect to the geometrical change of the geometry ($\frac{d\mathbf{v}}{d\delta\mathbf{x}}$). This variation will in principle be described as a variation field $\delta\mathbf{x}$ in the sense that any point will move $\tilde{x}_i = x_i + \delta x_i(\mathbf{x})$. This field will later be described in terms of a finite set of parameters $\mathbf{P}$ by a procedure called parametrization.

The definition of this derivative in a generic way, before parametrization, follows the steps:

1. The starting point will be the integral equations used for the regular boundary element method (*ubie* and *qbie*).
2. The procedure starts defining the sensitivity of the whole equation to a generic variation of the geometry.
3. As in the usual boundary element method, the resulting integral equation has to be taken to the boundary (the variation equations *δubie* and *δqbie*). This step together with the discretization needs some care due to the appearance of singular integrals.
4. Finally, this sensitivity equation is discretized by the usual BEM techniques, and the necessary reorganization of the equations is carried out to extract the desired $\frac{dv_i}{dP_g}$.

The second point is the most complicated and its obtention, as shown in figure 5.1, is synthesized in the following steps:

- Layout of problems to compare. We present two problems, one known (at a certain iteration), and one perturbed, a part of whose geometry is altered by a differential deformation field $\delta\mathbf{x}$. The information of the former will be considered known since the direct problem is solved, but not the perturbed one.
- Linear approximation of unknown terms by series decomposition. The perturbed geometry involves terms which we do not know, and we will approximate them by known terms by means of a series decomposition "centered" at the analogous known term, and decomposed with respect to the geometry variation.
- Variation integral equation. After substracting both equations and truncating the terms of variation of the geometry variation to the first order (linearization), we obtain a variation integral equation.

If the oject to minimize were a generic cost or objective functional J defined as,

$$J(\Gamma_c) = \int_{\Gamma_q} \varphi_u(\mathbf{u})d\Gamma + \int_{\Gamma_u} \varphi_q(\mathbf{q})d\Gamma + \int_{\Gamma} \psi(\mathbf{x})d\Gamma$$

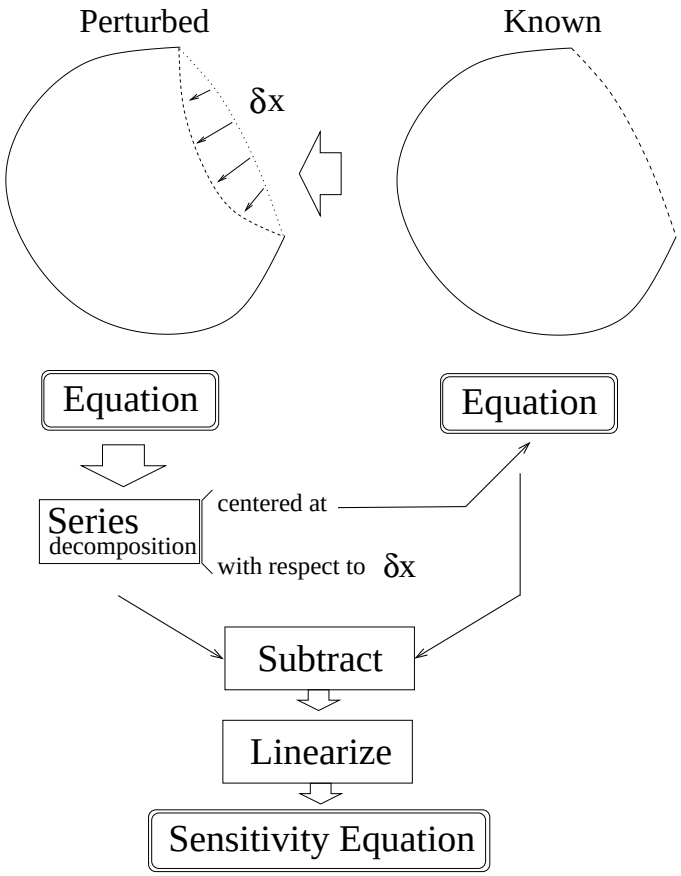

Figure 5.1: Procedure for the variation integral equation

its gradient could be obtained based on the sensitivity ($\frac{d\mathbf{v}}{d\delta\mathbf{x}}$ so that $\delta\mathbf{v} = \frac{d\mathbf{v}}{d\delta\mathbf{x}}\delta\mathbf{x}$) simply applying the chain rule:

$$\delta J(\Gamma_c) = \int_{\Gamma_q} \frac{\partial \varphi_u}{\partial \mathbf{u}} \delta\mathbf{u} d\Gamma + \int_{\Gamma_u} \frac{\partial \varphi_q}{\partial \mathbf{q}} \delta\mathbf{q} d\Gamma + \int_{\Gamma} \frac{\partial \psi}{\partial \mathbf{x}} \delta\mathbf{x} d\Gamma$$

5.1 Preliminary concepts

5.1.1 Representation of some useful geometrical variation terms

Starting from a generic variation field $\delta\mathbf{x}(\mathbf{x})$, that converts an assumed geomety domain, boundary and points $(\Omega, \Gamma, \mathbf{x})$ into a varied one $(\tilde{\Omega}, \tilde{\Gamma}, \tilde{\mathbf{x}})$, and with the aid of series expansion, one may represent explicitly all the needed geometrical variation terms that appear in the sensitivity equation (see figure 5.2 for a simplified idea).

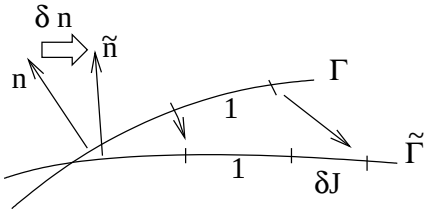

Figure 5.2: Sense of some geometrical definitions: $\tilde{\mathbf{n}} = \mathbf{n} + \delta\mathbf{n}$ and $d\tilde{\Gamma} = (1 + \delta J)d\Gamma$

The variations of some geometrical quantities needed later can be expressed in terms of the

normal $\mathbf{n}$ and tangent $\mathbf{t}$ and some derivatives of the variation field with the help of a series expansion and the following differential geometrical interpretations. Figure 5.3 shows the necessary definitions: a point $\mathbf{x}$ and its surroundings (a differential $\delta\mathbf{x} \times \delta\mathbf{y}$) on the boundary Γ is deformed by $\delta\mathbf{x}$ as a displacement (discontinuous line) and a distortion (dotted line).

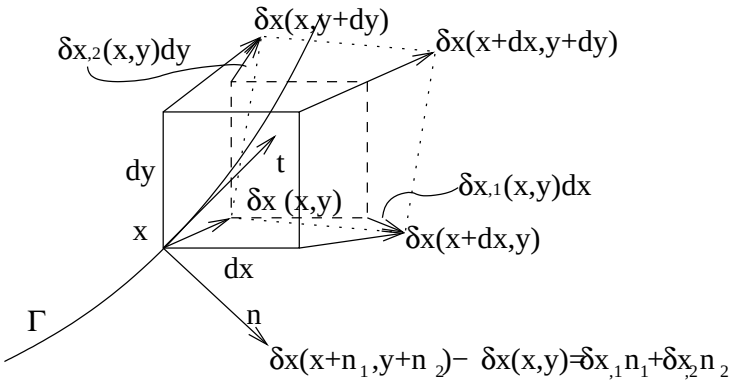

Figure 5.3: Differential geometrical interpretations in the vicinity of ξ.

If δn_j is the variation in the normal to a boundary subject to $\delta\mathbf{x}$, δJ is the unitary variation in the length of that boundary, then

$$\begin{aligned}
\delta r_l &= \delta x_l - \delta \xi_l \\
\delta n_j &= t_j t_l \epsilon_{lp} \lim_{\varepsilon \to 0^+} \left(\frac{1}{\varepsilon} (\delta x_p(\boldsymbol{\xi} + \mathbf{t}\varepsilon) - \delta x_l(\boldsymbol{\xi})) \right) = t_j t_l \epsilon_{lp} \delta x_{p,m} t_m \\
\delta J &= t_l \lim_{\varepsilon \to 0^+} \left(\frac{1}{\varepsilon} (\delta x_l(\boldsymbol{\xi} + \mathbf{t}\varepsilon) - \delta x_l(\boldsymbol{\xi})) \right) = t_l \delta x_{l,m} t_m \\
\epsilon_{ij} &= \begin{pmatrix} 0 & 1 \\ -1 & 0 \end{pmatrix} \text{ (permutation tensor)}
\end{aligned}$$

5.1.2 Starting equations

The starting equations at an internal point and the names and indexes to be used in the sequel are:

$u_k(\mathbf{x})$ Displacement vector in the real state (value at point $\mathbf{x}$, component k).

$q_k(\mathbf{x})$ Stress vector in the real state (value at point $\mathbf{x}$, component k).

$u_k^i(\mathbf{x}, \boldsymbol{\xi})$ Displacement vector of the Kelvin solution (value at point $\mathbf{x}$, component k of displacement when the fundamental load is applied at direction i, point $\boldsymbol{\xi}$).

$q_k^i(\mathbf{x}, \boldsymbol{\xi}) = \sigma_{jk}^i(\mathbf{x}, \boldsymbol{\xi}) n_j(\mathbf{x})$ (Stress vector of the Kelvin solution (value at point x, component k of stress when the fundamental load is applied at direction i, point $\boldsymbol{\xi}$).

$\sigma_{jk}^i(\mathbf{x}, \boldsymbol{\xi})$ (Stress tensor of the fundamental solution (value at point $\mathbf{x}$, components jk (symmetric) of stress when the fundamental load is applied at direction i, point $\boldsymbol{\xi}$).

δ_k^i Kroenecker delta.

$\mathbf{x}$ Integration point.

$\boldsymbol{\xi}$ Collocation point of fundamental load.

i Index for fundamental load direction.

k Index for component of any field.

The displacement integral equation is (*ubie*):

$$\delta_k^i u_k(\boldsymbol{\xi}) + \int_\Gamma q_k^i(\mathbf{x},\boldsymbol{\xi}) u_k(\mathbf{x}) d\Gamma(\mathbf{x}) = \int_\Gamma u_k^i(\mathbf{x},\boldsymbol{\xi}) q_k(\mathbf{x}) d\Gamma(\mathbf{x}) \qquad \text{for } \xi \text{ interior.} \tag{5.1}$$

and the stress integral equation is (*qbie*):

$$\delta_k^i q_k(\boldsymbol{\xi}) + \int_\Gamma s_{jkl}^i(\mathbf{x},\boldsymbol{\xi}) n_j(\boldsymbol{\xi}) n_l(\mathbf{x}) u_k(\mathbf{x}) d\Gamma(\mathbf{x}) = \int_\Gamma d_{jk}^i(\mathbf{x},\boldsymbol{\xi}) n_j(\boldsymbol{\xi}) q_k(\mathbf{x}) d\Gamma(\mathbf{x}) \qquad \text{for } \xi \text{ interior.} \tag{5.2}$$

5.2 Derivation of the equation

5.2.1 How to obtain the gradient of a boundary integral equation

The derivation of the equation is made by the limiting definition of the derivative, $\delta\{eq\} = \lim_{\delta\mathbf{x}\to 0}\left(\{\tilde{eq}\} - \{eq\}\right)$. The term $\{\tilde{eq}\}$ represents the original integral equation $\{eq\}$ altered by an infinitesimal geometrical deformation field $\delta\mathbf{x}$ (see as an example figure 5.4), that only affects the desired part of the geometry (the unknown flaw or the zone to be optimized). This altered state need not be defined yet, giving more generality to the results. The alteration will be defined later by means of a parametrization of the geometry.

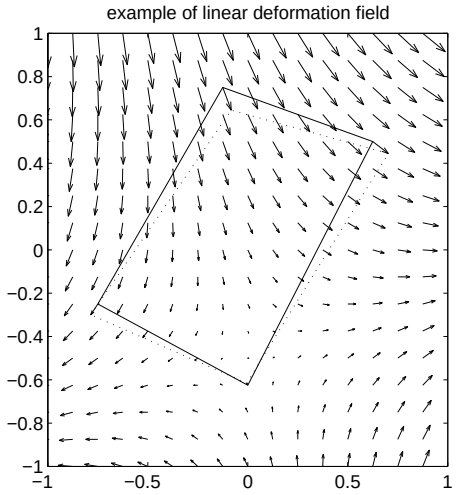

Figure 5.4: Example of $\delta\mathbf{x}(\mathbf{x})$ field.

In order to be able to subtract the two equations in the limit, we have to express them in common terms. This is done by doing a series expansion of the altered one with respect to $\delta\mathbf{x}$ and centered at the original equation. This expansion has to be done by first expanding each of the terms and then substituting them in the integral equation.

The other needed step consists of performing the limit to the boundary of the integral equations. In practice, this implies studying the order of variation of each crossed terms (products of each of the terms of the expansion) after the subtraction. This will lead to keeping all the first order terms and eliminating the rest for the following reasons: (1) the order-zero terms will vanish identically during the subtraction since they will be identical but of inverse sign, and (2) the second and higher order terms will vanish since they will be very small in comparison with first order terms when $\delta\mathbf{x} \to 0^+$. The order in which these limits are carried out may be inverted (see [13]). A safe strategy would be to do the limit to the boundary after the limit to the derivative. This way, the derivative is made of an internal equation with no singularities, but complicated free terms

appear during the limit to the boundary. The opposite order may be applied when the collocation point (pole of the integral equation) is placed at a smooth point. In chapter 5.3, both methods are compared, yielding the same results at smooth collocation points.

A similar procedure, but taking into account terms of one higher term, can in principle be carried out for the computation of the hessian instead of the gradient. This is not as interesting as the gradient since the most powerful optimization algorithms for the identification problem only work with gradients. The hessian or double derived equation would require all the kernels and weights to fulfill one higher order of derivability.

The procedure for the obtention of the derivative is carried out as follows, for each of the internal point equations.

5.2.2 Derivative of the *ubie*

The original and the altered integral equations ($\{\tilde{eq}\}$ and $\{eq\}$) are:

$$\{\tilde{eq}\}: \qquad \tilde{u}_i(\boldsymbol{\xi}) + \int_{\tilde{\Gamma}} \left[\tilde{u}_k \tilde{q}^i_k - \tilde{u}^i_k \tilde{q}_k\right] d\tilde{\Gamma} = 0$$

$$\{eq\}: \qquad u_i(\boldsymbol{\xi}) + \int_{\Gamma} \left[u_k q^i_k - u^i_k q_k\right] d\Gamma = 0$$

The displacements and tractions of the altered configurations are directly expressed in terms of the original one, defining their difference as δu_k and δq_k (where the symbol δ refers in general to a difference in the magnitude between the two mentioned configurations):

$$\begin{aligned} \tilde{u}_k &= u_k + \delta u_k \\ \tilde{q}_k &= q_k + \delta q_k \end{aligned}$$

whereas the kernels have to be expanded in a series in which only the first terms are important for a differential perturbation. The series expansion is carried out differentiating with respect to $\mathbf{x}$ ($f_{i,j} = \frac{df_i}{dx_j}$). When doing the material derivative of $u^i_k(\mathbf{x}, \boldsymbol{\xi})$, both $\mathbf{x}$ and $\boldsymbol{\xi}$ are displaced. Only the first term will be kept, denoting the rest as *hot.* (higher order terms).

$$\tilde{u}^i_k \simeq u^i_k + \frac{du^i_k}{dx_m}\delta x_m + \frac{du^i_k}{d\xi_m}\delta\xi_m + hot. = u^i_k + \frac{du^i_k}{dx_m}\delta x_m - \frac{du^i_k}{dx_m}\delta\xi_m + hot. = u^i_k + u^i_{k,m}\delta r_m + hot.$$

since $r_k = x_k - \xi_k$ and because of the radial nature of u^i_k. In general,

$$\begin{aligned} \tilde{u}^i_k &\simeq u^i_k + u^i_{k,m}\delta r_m + hot. \\ \tilde{q}^i_k &= \tilde{\sigma}^i_{jk}\tilde{n}_j(\mathbf{x}) \simeq q^i_k + \sigma^i_{jk}\delta n_j(\mathbf{x}) + \sigma^i_{jk,m}\delta r_m n_j(\mathbf{x}) + hot. \end{aligned}$$

and finally, the variation of the normal $n_j(\mathbf{x})$ and the integral domain can be expressed by means of the previously defined $\delta n_j(\mathbf{x})$ and δJ, as shown in figure 5.2:

$$\begin{aligned} \tilde{n}_j(\mathbf{x}) &= n_j(\mathbf{x}) + \delta n_j(\mathbf{x}) \\ d\tilde{\Gamma} &= [1 + \delta J] d\Gamma \end{aligned}$$

The resulting *δubie* after the substitution of the expansions above in $\{\tilde{eq}\}$ and the subtraction to $\{eq\}$ is:

$$\begin{aligned} \delta^i_k \delta u_k(\boldsymbol{\xi}) + \int_\Gamma &\left[\sigma^i_{jk}(\mathbf{x},\boldsymbol{\xi}) n_j(\mathbf{x}) \delta u_k(\mathbf{x}) - u^i_k(\mathbf{x},\boldsymbol{\xi})\delta q_k(\mathbf{x})\right] d\Gamma(\mathbf{x}) \\ + \int_\Gamma &\left[(\sigma^i_{jk,m}(\mathbf{x},\boldsymbol{\xi}) n_j(\mathbf{x}) u_k(\mathbf{x}) - u^i_{k,m}(\mathbf{x},\boldsymbol{\xi}) q_k)\delta r_m(\mathbf{x},\boldsymbol{\xi})\right. \\ &+(\sigma^i_{jk}(\mathbf{x},\boldsymbol{\xi}) n_j(\mathbf{x}) u_k(\mathbf{x}) - u^i_k(\mathbf{x},\boldsymbol{\xi}) q_k)\delta J(\mathbf{x}) \\ &\left.+\sigma^i_{jk}(\mathbf{x},\boldsymbol{\xi}) u_k(\mathbf{x}) \delta n_j(\mathbf{x})\right] d\Gamma(\mathbf{x}) = 0 \qquad (5.3) \\ &\text{for } \boldsymbol{\xi} \text{ interior} \end{aligned}$$

5.2.3 Derivative of the *qbie*

The original and the altered integral equations ($\{\tilde{eq}\}$ and $\{eq\}$) are:

$$\{\tilde{eq}\}: \qquad \tilde{q}_i(\boldsymbol{\xi}) + \int_{\tilde{\Gamma}} \left[\tilde{q}_k \tilde{d}^i_k - \tilde{s}^i_k \tilde{u}_k\right] d\tilde{\Gamma} = 0$$

$$\{eq\}: \qquad q_i(\boldsymbol{\xi}) + \int_{\Gamma} \left[q_k d^i_k - s^i_k u_k\right] d\Gamma = 0$$

The additional series expansions of the individual terms are:

$$\begin{aligned}
\tilde{n}_j(\boldsymbol{\xi}) &= n_j(\boldsymbol{\xi}) + \delta n_j(\boldsymbol{\xi}) \\
\tilde{d}^i_{jk} &= d^i_{jk} + d^i_{jk,m}\delta r_m + hot. \\
\tilde{s}^i_{jk} &= \tilde{s}^i_{jkl}\tilde{n}_l(\mathbf{x}) \simeq s^i_{jk} + s^i_{jkl}\delta n_l(\mathbf{x}) + s^i_{jkl,m}\delta r_m n_l(\mathbf{x}) + hot.
\end{aligned}$$

The resulting *δqbie* after the substitution and subtraction is:

$$\begin{aligned}
\delta^i_k \delta q_k(\boldsymbol{\xi}) + \int_{\Gamma} &\left[d^i_{jk}(\mathbf{x},\boldsymbol{\xi}) n_j(\boldsymbol{\xi}) \delta q_k(\mathbf{x}) - s^i_{jkl}(\mathbf{x},\boldsymbol{\xi}) n_j(\boldsymbol{\xi}) n_l(\mathbf{x}) \delta u_k(\mathbf{x})\right] d\Gamma(\mathbf{x}) \\
&+ \int_{\Gamma} \left[(d^i_{jk}(\mathbf{x},\boldsymbol{\xi}) n_j(\boldsymbol{\xi}) q_k(\mathbf{x}) - s^i_{jkl}(\mathbf{x},\boldsymbol{\xi}) n_j(\boldsymbol{\xi}) n_l(\mathbf{x}) u_k)\delta J(\mathbf{x}) \right. \\
&\quad + (d^i_{jk}(\mathbf{x},\boldsymbol{\xi}) q_k - s^i_{jkl}(\mathbf{x},\boldsymbol{\xi}) n_l(\mathbf{x}) u_k(\mathbf{x}))\delta n_j(\boldsymbol{\xi}) \\
&\quad + (d^i_{jk,m}(\mathbf{x},\boldsymbol{\xi}) n_j(\boldsymbol{\xi}) q_k(\mathbf{x}) - s^i_{jkl,m}(\mathbf{x},\boldsymbol{\xi}) n_l(\mathbf{x}) n_j(\boldsymbol{\xi}) u_k)\delta r_m(\mathbf{x},\boldsymbol{\xi}) \\
&\quad \left. - s^i_{jkl}(\mathbf{x},\boldsymbol{\xi}) n_j(\boldsymbol{\xi}) u_k \delta n_l(\mathbf{x})\right] d\Gamma(\mathbf{x}) = 0 \qquad (5.4) \\
&\qquad \text{for } \boldsymbol{\xi} \text{ interior}
\end{aligned}$$

5.2.4 Derivation of kernels

The succesive terms of the series expansion yield some derivated terms in addition to the original ones. The definition in terms of the fundamental functions of all the kernels involved in both variation equations are:

$$d^i_{jk}(\mathbf{x},\boldsymbol{\xi}) = \lambda\delta_{ij}u^n_{k,n}(\mathbf{x},\boldsymbol{\xi}) + \mu(u^i_{k,j}(\mathbf{x},\boldsymbol{\xi}) + u^j_{k,i}(\mathbf{x},\boldsymbol{\xi})) \qquad (5.5)$$

$$s^i_{jkl}(\mathbf{x},\boldsymbol{\xi}) = \lambda\delta_{ij}\sigma^n_{kl,n}(\mathbf{x},\boldsymbol{\xi}) + \mu(\sigma^i_{kl,j}(\mathbf{x},\boldsymbol{\xi}) + \sigma^j_{kl,i}(\mathbf{x},\boldsymbol{\xi})) \qquad (5.6)$$

$$d^i_{jk,m}(\mathbf{x},\boldsymbol{\xi}) = \lambda\delta_{ij}u^n_{k,nm}(\mathbf{x},\boldsymbol{\xi}) + \mu(u^i_{k,jm}(\mathbf{x},\boldsymbol{\xi}) + u^j_{k,im}(\mathbf{x},\boldsymbol{\xi})) \qquad (5.7)$$

$$s^i_{jkl,m}(\mathbf{x},\boldsymbol{\xi}) = \lambda\delta_{ij}\sigma^n_{kl,nm}(\mathbf{x},\boldsymbol{\xi}) + \mu(\sigma^i_{kl,jm}(\mathbf{x},\boldsymbol{\xi}) + \sigma^j_{kl,im}(\mathbf{x},\boldsymbol{\xi})) \qquad (5.8)$$

where

$$\begin{aligned}
\sigma^i_{jk}(\mathbf{x},\boldsymbol{\xi}) &= \lambda\delta_{jk}u^i_{n,n}(\mathbf{x},\boldsymbol{\xi}) + \mu(u^i_{j,k}(\mathbf{x},\boldsymbol{\xi}) + u^i_{k,j}(\mathbf{x},\boldsymbol{\xi})) \\
\sigma^i_{jk,l}(\mathbf{x},\boldsymbol{\xi}) &= \lambda\delta_{jk}u^i_{n,nl}(\mathbf{x},\boldsymbol{\xi}) + \mu(u^i_{j,kl}(\mathbf{x},\boldsymbol{\xi}) + u^i_{k,jl}(\mathbf{x},\boldsymbol{\xi})) \\
\sigma^i_{jk,lm}(\mathbf{x},\boldsymbol{\xi}) &= \lambda\delta_{jk}u^i_{n,nlm}(\mathbf{x},\boldsymbol{\xi}) + \mu(u^i_{j,klm}(\mathbf{x},\boldsymbol{\xi}) + u^i_{k,jlm}(\mathbf{x},\boldsymbol{\xi}))
\end{aligned}$$

The only needed term is the fundamental solution given earlier and its derivatives. In the two-dimensional generic case of an harmonically dynamic load (which gives the static solution as the limit to null frequency) the displacement field was given by (see equation 3.8 and following):

$$u^i_k = \frac{1}{2\pi\mu}\left[\psi\delta_{ik} - \chi r_{,i} r_{,k}\right]$$

For more compact expressions we can define the tensors:

$$\begin{aligned}
e_{abij} &= \delta_{ai}\delta_{bj} + \delta_{aj}\delta_{bi} \\
e_{abcijk} &= \delta_{ai}\delta_{bj}\delta_{ck} + \delta_{aj}\delta_{bk}\delta_{ci} + \delta_{ak}\delta_{bi}\delta_{cj}
\end{aligned}$$

Thus, the successive derivatives of the fundamental solution are:

$$\begin{aligned}
u^a_b &= \tfrac{1}{2\pi\mu} \quad [\psi\delta_{ab} - \chi r_{,a}r_{,b}] \\
u^a_{b,c} &= \tfrac{1}{2\pi\mu} \quad [\psi'\delta_{ab}r_{,c} - \chi' r_{,a}r_{,b}r_{,c} - \chi e_{abij}r_{,i}r_{,jc}] \\
u^a_{b,cd} &= \tfrac{1}{2\pi\mu} \quad [\psi''\delta_{ab}r_{,c}r_{,d} + \psi'\delta_{ab}r_{,cd} - \chi'' r_{,a}r_{,b}r_{,c}r_{,d} - \chi' r_{,a}r_{,b}r_{,cd} \\
&\quad -e_{abij}(\chi' e_{cdkl}r_{,i}r_{,k}r_{,jl} + \chi r_{,icd}r_{,j} + \chi r_{,ic}r_{,jd})] \\
u^a_{b,cde} &= \tfrac{1}{2\pi\mu} \quad [\psi'''\delta_{ab}r_{,c}r_{,d}r_{,e} + (-r\psi'' + \psi')\delta_{ab}r_{,cde} - \chi''' r_{,a}r_{,b}r_{,c}r_{,d}r_{,e} \\
&\quad -\chi''[e_{abcijk}e_{delm}r_{,i}r_{,j}r_{,kl}r_{,m} + e_{abeijm}r_{,ic}r_{,j}r_{,d}r_{,m}] \\
&\quad -\chi'[e_{abcijk}(r_{,ie}r_{,b}r_{,kd} + r_{,i}r_{,je}r_{,kd} + r_{,i}r_{,j}r_{,kde}) \\
&\quad +e_{abij}(r_{,i}r_{,jc}r_{,de} + e_{delm}(r_{,im}r_{,jc}r_{,l}))] \\
&\quad -\chi e_{abij}[r_{,ide}r_{,jc} + r_{,id}r_{,jce} + r_{,ie}r_{,jcd} + r_{,jcde}r_{,i}]]
\end{aligned}$$

where $r_a = x_a - \xi_a$, $r = \sqrt{r_1^2 + r_2^2}$, and $r_{,a} = \frac{\partial r}{\partial x_a}$. Therefore,

$$\begin{aligned}
r_{,a} &= \frac{r_a}{r} \\
r_{,ab} &= \frac{1}{r}(\delta_{ab} - r_{,a}r_{,b}) \\
r_{,abc} &= \frac{-1}{r}e_{abcijk}r_{,ij}r_{,k} \\
r_{,abcd} &= \frac{-1}{r}(r_{,abc}r_{,d} + e_{abcijk}(r_{,ijd}r_{,k} + r_{,ij}r_{,kd}))
\end{aligned}$$

It is interesting to see the order of singularity of each term with respect to r, by a Taylor expansion to the first order:

$$\begin{aligned}
r &= r^1 \\
r_{,a} &= A + O(r^1) \\
r_{,ab} &= B\frac{1}{r} + O(r^0) \\
r_{,abc} &= C\frac{1}{r^2} + O(r^{-1}) \\
r_{,abcd} &= D\frac{1}{r^3} + O(r^{-2})
\end{aligned}$$

$$\begin{aligned}
\psi &= \frac{-1}{2}\left[\left[\frac{1}{2} + \gamma + \ln\left(\frac{i\omega r}{2c_s}\right)\right] + \left[\frac{-1}{2} + \gamma + \ln\left(\frac{i\omega r}{2c_p}\right)\right]\frac{c_s^2}{c_p^2}\right] + O(r^2) \\
\psi' = \frac{\partial\psi}{\partial r} &= \frac{-1}{2}\left[1 + \frac{c_s^2}{c_p^2}\right]\frac{1}{r} + O(r^1) \\
\psi'' = \frac{\partial^2\psi}{\partial r^2} &= \frac{1}{2}\left[1 + \frac{c_s^2}{c_p^2}\right]\frac{1}{r^2} + O(r^0) \\
\psi''' = \frac{\partial^3\psi}{\partial r^3} &= -\left[1 + \frac{c_s^2}{c_p^2}\right]\frac{1}{r^3} + O(r^{-1})
\end{aligned}$$

$$\begin{aligned}
\chi &= \frac{-1}{2}\left[1 - \frac{c_s^2}{c_p^2}\right] + O(r^2) \\
\chi' = \frac{\partial\chi}{\partial r} &= \frac{\omega^2}{4c_p^4c_s^2}\left[\left[\frac{-1}{4} + \gamma + \ln\left(\frac{i\omega r}{2c_s}\right)\right]c_p^4 - \left[\frac{-1}{4} + \gamma + \ln\left(\frac{i\omega r}{2c_p}\right)\right]c_s^4\right]r + O(r^3) \\
\chi'' = \frac{\partial^2\chi}{\partial r^2} &= \frac{\omega^2}{4c_p^4c_s^2}\left[\left[\frac{3}{4} + \gamma + \ln\left(\frac{i\omega r}{2c_s}\right)\right]c_p^4 - \left[\frac{3}{4} + \gamma + \ln\left(\frac{i\omega r}{2c_p}\right)\right]c_s^4\right] + O(r^2) \\
\chi''' = \frac{\partial^3\chi}{\partial r^3} &= \frac{\omega^2(c_p^4 - c_s^4)}{4c_p^4c_s^2}\frac{1}{r} + O(r^1)
\end{aligned}$$

where $\gamma \simeq 0.5772157...$ is the Euler gamma. Therefore,

$$\begin{aligned}
u^a_b &= (A + B\ln(r)) + O(r^2) \\
u^a_{b,c} &= (A + B\ln(r))\frac{1}{r} + O(r^1) \\
u^a_{b,cd} &= (A + B\ln(r))\frac{1}{r^2} + O(r^0) \\
u^a_{b,cde} &= (A + B\ln(r))\frac{1}{r^3} + O(r^{-1}) \\
\sigma^a_{bc} &= (A + B\ln(r))\frac{1}{r} + O(r^1) \\
\sigma^a_{bc,d} &= (A + B\ln(r))\frac{1}{r^2} + O(r^0) \\
\sigma^a_{bc,de} &= (A + B\ln(r))\frac{1}{r^3} + O(r^{-1}) \\
d^a_{bc} &= (A + B\ln(r))\frac{1}{r} + O(r^1) \\
d^a_{bc,d} &= (A + B\ln(r))\frac{1}{r^2} + O(r^0) \\
s^a_{bcd} &= (A + B\ln(r))\frac{1}{r^2} + O(r^0) \\
s^a_{bcd,e} &= (A + B\ln(r))\frac{1}{r^3} + O(r^{-1})
\end{aligned}$$

where the constants (A, B) are obviously not common.

One should notice that the next term in all the expansions is always two orders higher than the first one. This property will be very important in the sequel, since in the hypersingular sensitivity equation, two orders of the expansion are used: one that gives an infinity term and a second that gives a free term. The mentioned fact allows to take into consideration only one term in the expansion.

All the indices regarding directions of derivation can always be interchanged without any change of value. For instance,

$$u^a_{b,cde} = u^a_{b,dce} = u^a_{b,dec} = ...\text{(all 6 permutations)}$$

5.3 Limit to the boundary

5.3.1 Boundary versus internal integral

There are two possibilities when deriving the boundary integral equation.

1. One may obtain the integral equation for an internal point, proceeding as explained with the derivation, and later take the derived equation valid for an internal point to the boundary limit. This choice is safer because it does not require to be careful with what happens with every term at the boundary. Taking the equation to the limit is a dull process that will be carried out in the rest of the chapter.

2. The other possibility is to derive directly the boundary integral equation, ie., after taking the original one to the boundary limit. In the end it is shown that both techniques yield the same results as long as the collocation point lays on a smooth boudnary (C^∞).

   In the smooth case, the kernels have an univocally defined value around the collocation point, and so are the geometrical values δn_i, δJ, δr_i. Hence the substitution of the expanded terms in the boundary integral equations, and their subtraction yield:

ubie:

$$\frac{1}{2}\delta_k^i u_k(\boldsymbol{\xi}) + \int_\Gamma \left[q_k^i u_k(\mathbf{x}) - u_k^i q_k(\mathbf{x})\right] d\Gamma(\mathbf{x}) = 0$$

δubie:

$$\begin{aligned}\frac{1}{2}\delta_k^i \delta u_k + \int_\Gamma \big[\sigma_{jk}^i n_j(\mathbf{x})\delta u_k - u_k^i \delta q_k \\ +\sigma_{jk,m}^i n_j(\mathbf{x}) u_k \delta r_m - u_{k,m}^i q_k \delta r_m + \sigma_{jk}^i n_j(\mathbf{x}) u_k \delta J - u_k^i q_k \delta J + \sigma_{jk}^i u_k \delta n_j(\mathbf{x})\big]\, d\Gamma &= 0\end{aligned}$$

qbie:

$$\frac{1}{2}\delta_k^i q_k(\boldsymbol{\xi}) + \int_\Gamma \left[s_{jkl}^i n_j(\boldsymbol{\xi}) n_l(\mathbf{x}) u_k(\mathbf{x}) - d_{jk}^i n_j(\boldsymbol{\xi}) q_k(\mathbf{x})\right] d\Gamma(\mathbf{x}) = 0$$

δqbie:

$$\begin{aligned}\frac{1}{2}\delta_k^i \delta q_k + \int_\Gamma \big[d_{jk}^i n_j(\boldsymbol{\xi})\delta q_k - s_{jkl}^i n_j(\boldsymbol{\xi}) n_l(\mathbf{x})\delta u_k \\ +d_{jk}^i n_j(\boldsymbol{\xi}) q_k \delta J - s_{jkl}^i n_j(\boldsymbol{\xi}) n_l(\mathbf{x}) u_k \delta J + d_{jk}^i q_k \delta n_j(\boldsymbol{\xi}) - s_{jkl}^i n_l(\mathbf{x}) u_k \delta n_j(\boldsymbol{\xi}) \\ +d_{jk,m}^i n_j(\boldsymbol{\xi}) q_k \delta r_m - s_{jkl,m}^i n_l(\mathbf{x}) n_j(\boldsymbol{\xi}) u_k \delta r_m - s_{jkl}^i n_j(\boldsymbol{\xi}) u_k \delta n_l(\mathbf{x})\big]\, d\Gamma &= 0\end{aligned}$$

which are identical to the ones obtained by the limiting process after the derivation of the internal equations in the case of a smooth collocation point.

5.3.2 Limit to the boundary of the internal equations

The equations in 5.2 are written assuming that the collocation point $\boldsymbol{\xi}$ is placed at an interior point in the domain Ω bounded by Γ. In the usual BEM the equations are applied with $\boldsymbol{\xi}$ on the boundary Γ. Hence we have to approach the point to the boundary through a limiting process. The consequence of the limit is that the integrals are split into a Cauchy Principal Value or Hadamard Finite Part, and some free terms.

The limit is usually done by modifying the boundary locally so that it never touches the collocation point, but yields a definition capable to be taken to the limit. Some exhaustive works on the artifices for the limit to the boundary can be found in [79], [55], [56] and [72]. Here we decompose the boundary into a sector of a ball S_ε around $\boldsymbol{\xi}$, that will yield the free terms, and the rest of the boundary save for the ball $\Gamma - \Gamma_\varepsilon$, which is by definition a Cauchy Principal Value if the integrand is of the order $\frac{1}{r}$ or a Hadamard Finite Part for $\frac{1}{r^2}$.

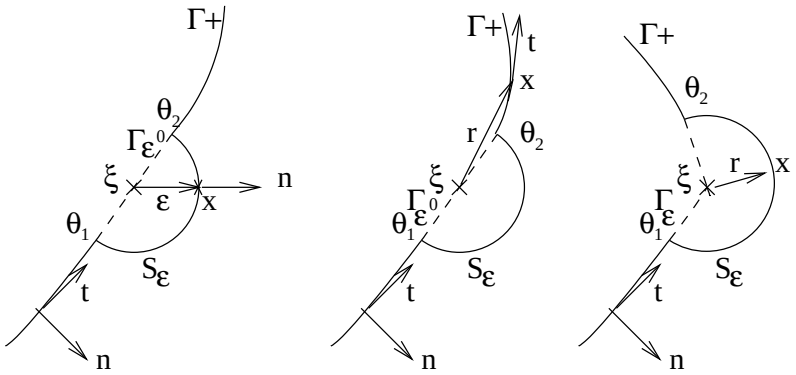

Figure 5.5: Artifice for limiting process. Left: $\mathbf{x} \in \Gamma_\varepsilon$. Middle: $\mathbf{x} \in \Gamma_+$ after Γ_ε. Right: case of a non-smooth boundary.

5.3.3 Order of singularity

The basic integral equations before the limit to the boundary (for $\boldsymbol{\xi}$ interior) are the following, and the order of each integrand when $\boldsymbol{\xi}$ approaches $\mathbf{x}$ are studied for a correct treatment of the integrals.

ubie:

$$\delta_k^i u_k(\boldsymbol{\xi}) + \int_\Gamma \left[\sigma_{jk}^i(\mathbf{x},\boldsymbol{\xi}) n_j(\mathbf{x}) u_k(\mathbf{x}) - u_k^i(\mathbf{x},\boldsymbol{\xi}) q_k(\mathbf{x})\right] d\Gamma(\mathbf{x}) = 0 \quad (\boldsymbol{\xi} \text{ interior})$$

Integrand	Order
$q_k^i(\mathbf{x},\boldsymbol{\xi}) u_k(\mathbf{x})$	r^{-1}
$u_k^i(\mathbf{x},\boldsymbol{\xi}) q_k(\mathbf{x})$	$\ln(r)$

δubie:

$$\begin{aligned}\delta_k^i \delta u_k(\boldsymbol{\xi}) + \int_\Gamma &\left[\sigma_{jk}^i(\mathbf{x},\boldsymbol{\xi}) n_j(\mathbf{x}) \delta u_k(\mathbf{x}) - u_k^i(\mathbf{x},\boldsymbol{\xi}) \delta q_k(\mathbf{x})\right] d\Gamma(\mathbf{x}) \\ + \int_\Gamma &\left[(\sigma_{jk,m}^i(\mathbf{x},\boldsymbol{\xi}) n_j(\mathbf{x}) u_k(\mathbf{x}) - u_{k,m}^i(\mathbf{x},\boldsymbol{\xi}) q_k) \delta r_m(\mathbf{x},\boldsymbol{\xi})\right. \\ &+(\sigma_{jk}^i(\mathbf{x},\boldsymbol{\xi}) n_j(\mathbf{x}) u_k(\mathbf{x}) - u_k^i(\mathbf{x},\boldsymbol{\xi}) q_k) \delta J(\mathbf{x}) \\ &\left.+\sigma_{jk}^i(\mathbf{x},\boldsymbol{\xi}) u_k(\mathbf{x}) \delta n_j(\mathbf{x})\right] d\Gamma(\mathbf{x}) = 0 \\ &(\boldsymbol{\xi} \text{ interior})\end{aligned}$$

Integrand	Order
$\sigma_{jk}^i u_k \delta n_j(\mathbf{x})$	r^{-1}
$\sigma_{jk,m}^i n_j(\mathbf{x}) u_k \delta r_m$	r^{-1}
$\sigma_{jk}^i n_j(\mathbf{x}) \delta u_k$	r^{-1}
$-u_{k,m}^i q_k \delta r_m$	r^0
$-u_k^i \delta q_k$	$\ln(r)$
$\sigma_{jk}^i n_j(\mathbf{x}) u_k \delta J$	r^{-1}
$-u_k^i q_k \delta J$	$\ln(r)$

qbie:

$$\delta_k^i q_k(\boldsymbol{\xi}) + \int_\Gamma \left[d_{jk}^i(\mathbf{x},\boldsymbol{\xi}) n_j(\boldsymbol{\xi}) q_k(\mathbf{x}) - s_{jkl}^i(\mathbf{x},\boldsymbol{\xi}) n_j(\boldsymbol{\xi}) n_l(\mathbf{x}) u_k(\mathbf{x})\right] d\Gamma(\mathbf{x}) = 0 \quad (\boldsymbol{\xi} \text{ interior})$$

Integrand	Order
$s_{jkl}^i(\mathbf{x},\boldsymbol{\xi}) n_j(\boldsymbol{\xi}) n_l(\mathbf{x}) u_k(\mathbf{x})$	r^{-2}
$d_{jk}^i(\mathbf{x},\boldsymbol{\xi}) n_j(\boldsymbol{\xi}) q_k(\mathbf{x})$	r^{-1}

δqbie:

$$\begin{aligned}\delta_k^i \delta q_k(\boldsymbol{\xi}) + \int_\Gamma &\left[d_{jk}^i(\mathbf{x},\boldsymbol{\xi}) n_j(\boldsymbol{\xi}) \delta q_k(\mathbf{x}) - s_{jkl}^i(\mathbf{x},\boldsymbol{\xi}) n_j(\boldsymbol{\xi}) n_l(\mathbf{x}) \delta u_k(\mathbf{x})\right] d\Gamma(\mathbf{x}) \\ + \int_\Gamma &\left[(d_{jk}^i(\mathbf{x},\boldsymbol{\xi}) n_j(\boldsymbol{\xi}) q_k(\mathbf{x}) - s_{jkl}^i(\mathbf{x},\boldsymbol{\xi}) n_j(\boldsymbol{\xi}) n_l(\mathbf{x}) u_k) \delta J(\mathbf{x})\right. \\ &+(d_{jk}^i(\mathbf{x},\boldsymbol{\xi}) q_k - s_{jkl}^i(\mathbf{x},\boldsymbol{\xi}) n_l(\mathbf{x}) u_k(\mathbf{x})) \delta n_j(\boldsymbol{\xi}) \\ &+(d_{jk,m}^i(\mathbf{x},\boldsymbol{\xi}) n_j(\boldsymbol{\xi}) q_k(\mathbf{x}) - s_{jkl,m}^i(\mathbf{x},\boldsymbol{\xi}) n_l(\mathbf{x}) n_j(\boldsymbol{\xi}) u_k) \delta r_m(\mathbf{x},\boldsymbol{\xi}) \\ &\left.-s_{jkl}^i(\mathbf{x},\boldsymbol{\xi}) n_j(\boldsymbol{\xi}) u_k \delta n_l(\mathbf{x})\right] d\Gamma(\mathbf{x}) = 0 \\ &(\boldsymbol{\xi} \text{ interior})\end{aligned}$$

Integrand	Order
$s^i_{jkl} n_j(\boldsymbol{\xi}) u_k \delta n_l(\mathbf{x})$	r^{-2}
$t^i_{jkl,m} n_l(\mathbf{x}) n_j(\boldsymbol{\xi}) u_k \delta r_m$	r^{-2}
$s^i_{jkl} n_j(\boldsymbol{\xi}) n_l(\mathbf{x}) \delta u_k$	r^{-2}
$-d^i_{jk,m} n_j(\boldsymbol{\xi}) q_k \delta r_m$	r^{-1}
$-d^i_{jk} n_j(\boldsymbol{\xi}) \delta q_k$	r^{-1}
$s^i_{jkl} n_j(\boldsymbol{\xi}) n_l(\mathbf{x}) u_k \delta J$	r^{-2}
$-d^i_{jk} n_j(\boldsymbol{\xi}) q_k \delta J$	r^{-1}
$s^i_{jkl} n_l(\mathbf{x}) u_k \delta n_j(\boldsymbol{\xi})$	r^{-2}
$-d^i_{jk} q_k \delta n_j(\boldsymbol{\xi})$	r^{-1}

5.3.4 Free terms

The free terms are the analytically calculable integrals along S_ε that appear in the decomposition of the boundary at the limit to the boundary. If the integral is made at a smooth point the integration can be done without loss of generality between $\delta x_1 = 0$ and $\delta x_2 = \pi$.

On the boundary S_ε, the radius r and its derivatives become exactly (see figure 5.5):

$$\begin{aligned}
r_i &= r n_i \\
r_{,a} &= \frac{r_a}{r} = \delta_{a\alpha} n_\alpha \\
r_{,ab} &= \frac{1}{r}(\delta_{ab} - r_{,a} r_{,b}) = \frac{1}{r} \epsilon_{a\alpha} \epsilon_{b\beta} n_\alpha n_\beta \\
r_{,abc} &= \frac{-1}{r} e_{abca'b'c'} r_{,a'b'} r_{,c'} = \frac{-1}{r^2} e_{abca'b'c'} \epsilon_{a'\alpha} \epsilon_{b'\beta} \delta_{c\gamma} n_\alpha n_\beta n_\gamma \\
r_{,abcd} &= \frac{-1}{r}(r_{,abc} r_{,d} + e_{abca'b'c'}(r_{,a'b'c'} r_{,d} + r_{,a'b'} r_{,c'd}))
\end{aligned}$$

where, $n_i = (\cos\theta, \sin\theta)^T$ and $\delta_{a\alpha}$ is the Kroenecker delta whereas $\epsilon_{a\alpha}$ is the permutation tensor.

The variations of the geometrical values can be expressed, in terms of the normal and the tangent and some derivatives of the variation field, with the help of a series expansion and the differential geometrical interpretations recalled from figure 5.6, where a point $\mathbf{x}$ on a boundary Γ has normal $\mathbf{n}$ and tangent $\mathbf{t}$, the zone is distorted by a variation field $\delta\mathbf{x}$, which is studied at a differential area $dx \times dy$.

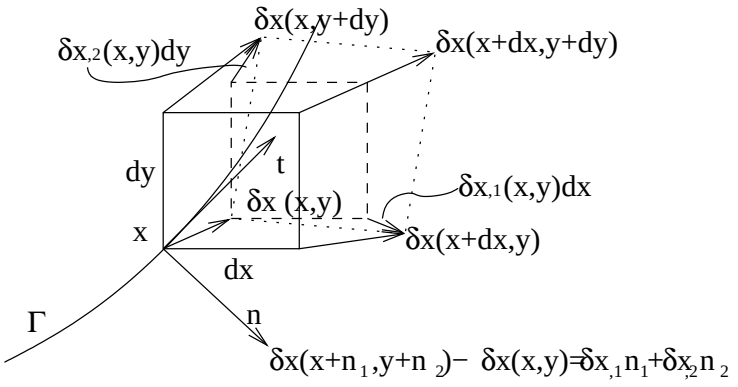

Figure 5.6: Differential geometrical interpretations in the vicinity of ξ.

In S_ε, the necessary considerations in terms of definitions and expansions of the terms in the

integrals are the following. The range of the integral and its differential are,

$$\begin{aligned} d\Gamma &= r d\theta \qquad \text{(the differential of line is converted into a differential of angle along the ball)} \\ \Gamma_\epsilon &\equiv \theta_1 \to \theta_2 \qquad \text{(limits of differentiation)} \\ r &= \varepsilon \end{aligned}$$

The value of the displacements and tractions in $\mathbf{x}$ can be expressed in terms of those in $\boldsymbol{\xi}$, as well as their variations,

$$\begin{aligned} u_i(\mathbf{x}) &= u_i(\boldsymbol{\xi}) + u_{i,j}(\boldsymbol{\xi}) r n_j(\mathbf{x}) + hot. \\ q_i(\mathbf{x}) &= \sigma_{ij}(\mathbf{x}) n_j(\mathbf{x}) \\ \sigma_{ij}(\mathbf{x}) &= \sigma_{ij}(\boldsymbol{\xi}) + \sigma_{ij,l}(\boldsymbol{\xi}) r n_l(\mathbf{x}) + hot. \\ \delta u_i(\mathbf{x}) &= \delta u_i(\boldsymbol{\xi}) + \delta u_{i,j}(\boldsymbol{\xi}) r n_j(\mathbf{x}) + hot. \\ \delta q_i(\mathbf{x}) &= \delta\sigma_{ij}(\mathbf{x}) n_j(\mathbf{x}) + \sigma_{ij}(\mathbf{x}) \delta n_j(\mathbf{x}) \\ \delta\sigma_{ij}(\mathbf{x}) &= \delta\sigma_{ij}(\boldsymbol{\xi}) + \delta\sigma_{ij,l}(\boldsymbol{\xi}) r n_l(\mathbf{x}) + hot. \end{aligned}$$

The value of the geometrical variations are also expressed as a series expansion in terms of their values at $\boldsymbol{\xi}$, and will therefore need more than one term in some cases:

$$\begin{aligned} \delta x_i(\mathbf{x}) &= \delta x_i(\boldsymbol{\xi}) + \delta x_{i,j}(\boldsymbol{\xi})(x_j - \xi_j) + hot. \quad \Rightarrow \\ \delta r_l &= \delta\xi_{l,m} r n_m + \delta x_{l,mn} r^2 n_m n_n + hot. \\ \delta x_{i,j}(\mathbf{x}) &= \delta x_{i,j}(\boldsymbol{\xi}) + \delta x_{i,jk} r n_k + hot. \quad \Rightarrow \\ \delta n_j(\mathbf{x}) &= t_j(\mathbf{x}) t_l(\mathbf{x}) \epsilon_{lk} \delta x_{k,m}(\boldsymbol{\xi}) t_m(\mathbf{x}) + r t_j(\mathbf{x}) t_l(\mathbf{x}) \epsilon_{lk} \delta x_{k,mn}(\boldsymbol{\xi}) t_m(\mathbf{x}) n_n(\mathbf{x}) + hot. \\ \delta J(\mathbf{x}) &= t_l(\mathbf{x}) t_m(\mathbf{x}) \delta x_{l,m}(\boldsymbol{\xi}) + r \delta x_{l,mn}(\boldsymbol{\xi}) t_l(\mathbf{x}) t_m(\mathbf{x}) n_n(\mathbf{x}) + hot. \\ \epsilon_{ij} &= \begin{pmatrix} 0 & 1 \\ -1 & 0 \end{pmatrix} \text{ (permutation tensor)} \end{aligned}$$

After a proper decomposition, the terms in $O(r^0)$ are regular integrals that can be evaluated numerically by a standard Gauss quadrature. The terms in $O(r^{-2})$ should vanish in order to have a computable expression. This only happens if $f(\mathbf{x})$ is continuous and derivable at 0, or $f(0) \in C^{1,\alpha}$. The terms in $O(r^{-1})$ may give a finite term in this case, called free term.

The free terms can also be calculated using the programmable transformation of the indicial algebra. For instance, one of the free terms in the hypersingular variation integrals would be computed as follows.

$$\lim_{\varepsilon \to 0^+} \int_{s_\varepsilon} s^i_{jkl} n_j(\boldsymbol{\xi}) u_k \delta n_l(\mathbf{x}) d\Gamma = \lim_{\varepsilon \to 0^+} \int_{s_\varepsilon} I d\theta$$

Substituting the expansions $u_k(\mathbf{x}) = u_k(\boldsymbol{\xi}) + u_{k,n}(\boldsymbol{\xi}) r n_n(\mathbf{x})$ and $\delta n_l = t_l t_m \epsilon_{mp} \delta x_{p,o} t_o + t_l t_m \epsilon_{mp} \delta x_{p,oq} t_o n_q$ we get four terms in I. The term of order ε^1 vanishes in the limit. The term of order ε^{-1} yields a number that tends to infinity. The integral of one of the two terms of order ε^0 is

$$I = s^i_{jkl} n_j(\boldsymbol{\xi}) u_{k,n} n_n t_l t_m \epsilon_{mp} \delta x_{p,o} t_o$$

Taking into account that all the terms are evaluated at the integration point $\mathbf{x}$ excepting $n_j(\boldsymbol{\xi})$, one may define the free term DQ^i_{jklmn} following figure 5.7. DQ is named after the initials of $\delta qbie$. We start from right to left we have eight indices (i, j, k, l, m, n, o, p) corresponding to s^i_{jkl} the four first (which is decomposed into matrix tt multiplied by $u^{*''}$, as can be deduced from the Hooke laws in equation 5.8 and following) and to n_p, n_n, t_o, t_l the rest. Internally, the indices are treated as numbers, since they are redefined several times, and follow the lines in the flow chart. δ_{48} is the

Kroenecker delta between the fourth and eigth index, condensing them. We have therefore defined the free term coefficient tensor in a matricial way as $DQ^i_{jklmn} = \delta_{48} \times tt \times u^{*''} \times n_p n_n t_o t_{l'}$, and the new indices correspond to the terms on the left $(direction, \mathbf{n}, \mathbf{u}', \delta\mathbf{x})$. This finally leads to the term,

$$DQ^i_{jklmn} n_j(\boldsymbol{\xi}) u_{k,m} \delta x_{l,n}$$

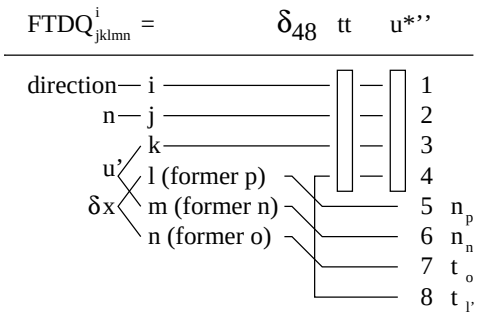

Figure 5.7: Flow chart of the indicial algebraic transformation.

The resulting free terms are the following, in the case of a smooth boundary at the collocation point.

Free terms for the *ubie***:**

1.

$$\lim_{\varepsilon \to 0^+} \int_{s_\varepsilon} q^i_k(\mathbf{x}, \boldsymbol{\xi}) u_k(\mathbf{x}) d\Gamma \quad = \quad \frac{1}{2}\delta^i_k u_k(\boldsymbol{\xi}) = u_k(\boldsymbol{\xi}) U1^i_k \qquad U1^i_k = \frac{1}{2}\delta_{ik}$$

2.

$$\lim_{\varepsilon \to 0^+} \int_{s_\varepsilon} u^i_k(\mathbf{x}, \boldsymbol{\xi}) q_k(\mathbf{x}) d\Gamma \quad = \quad 0$$

Therefore, as expected,

$$\frac{1}{2}\delta^i_k u_k(\boldsymbol{\xi}) + \oint_\Gamma \left[q^i_k u_k(\mathbf{x}) - u^i_k q_k(\mathbf{x}) \right] d\Gamma(\mathbf{x}) = 0 \qquad \text{for } \xi \in \Gamma \tag{5.9}$$

Free terms for the *δubie***:**

1.

$$\lim_{\varepsilon \to 0^+} \int_{s_\varepsilon} \sigma^i_{jk} u_k \delta n_j(\mathbf{x}) d\Gamma \quad = \quad u_k(\boldsymbol{\xi}) \delta x_{l,m}(\boldsymbol{\xi}) DU1^i_{kml}$$

2.

$$\lim_{\varepsilon \to 0^+} \int_{s_\varepsilon} \sigma^i_{jk,m} n_j(\mathbf{x}) u_k \delta r_m d\Gamma \quad = \quad u_k(\boldsymbol{\xi}) \delta x_{l,m}(\boldsymbol{\xi}) DU2^i_{kml}$$

3.

$$\lim_{\varepsilon \to 0^+} \int_{s_\varepsilon} \sigma^i_{jk} n_j(\mathbf{x}) \delta u_k d\Gamma \quad = \quad \delta u_k(\boldsymbol{\xi}) DU3^i_k \qquad DU3^i_k = \frac{1}{2}\delta_{ik}$$

4.

$$\lim_{\varepsilon\to 0^+}\int_{s_\varepsilon} -u^i_{k,m}q_k\delta r_m d\Gamma \quad = \quad 0$$

5.

$$\lim_{\varepsilon\to 0^+}\int_{s_\varepsilon} -u^i_{k}\delta q_k d\Gamma \quad = \quad 0$$

6.

$$\lim_{\varepsilon\to 0^+}\int_{s_\varepsilon} \sigma^i_{jk}n_j(\mathbf{x})u_k\delta J d\Gamma \quad = \quad u_k(\boldsymbol{\xi})\delta x_{l,m}(\boldsymbol{\xi})DU6^i_{kml}$$

7.

$$\lim_{\varepsilon\to 0^+}\int_{s_\varepsilon} -u^i_{k}q_k\delta J d\Gamma \quad = \quad 0$$

It happens that $DU1^i_{kml} + DU2^i_{kml} + DU6^i_{kml} = 0$.
The resulting boundary integral equations for smooth boundaries is simplified as follows,

$$\begin{aligned}\frac{1}{2}\delta^i_k\delta u_k(\boldsymbol{\xi}) + \oint_\Gamma \left[\sigma^i_{jk}(\mathbf{x},\boldsymbol{\xi})n_j(\mathbf{x})\delta u_k(\mathbf{x}) - u^i_k(\mathbf{x},\boldsymbol{\xi})\delta q_k(\mathbf{x})\right] d\Gamma(\mathbf{x}) \\ + \oint_\Gamma \left[(\sigma^i_{jk,m}(\mathbf{x},\boldsymbol{\xi})n_j(\mathbf{x})u_k(\mathbf{x}) - u^i_{k,m}(\mathbf{x},\boldsymbol{\xi})q_k)\delta r_m(\mathbf{x},\boldsymbol{\xi})\right. \\ +(\sigma^i_{jk}(\mathbf{x},\boldsymbol{\xi})n_j(\mathbf{x})u_k(\mathbf{x}) - u^i_k(\mathbf{x},\boldsymbol{\xi})q_k)\delta J(\mathbf{x}) \\ \left.+\sigma^i_{jk}(\mathbf{x},\boldsymbol{\xi})u_k(\mathbf{x})\delta n_j(\mathbf{x})\right] d\Gamma(\mathbf{x}) \quad = \quad 0 \qquad (5.10)\\ \text{for } \boldsymbol{\xi}\in\Gamma\end{aligned}$$

Free terms for the *qbie*:

1.

$$\lim_{\varepsilon\to 0^+}\int_{s_\varepsilon} s^i_{jkl}(\mathbf{x},\boldsymbol{\xi})n_j(\boldsymbol{\xi})n_l(\mathbf{x})u_k(\mathbf{x})d\Gamma \quad = \quad n_l u_j IQ1^i_{jl}\lim_{\varepsilon\to 0^+}\frac{1}{\varepsilon} + n_l u_{j,k}Q1^i_{jkl}$$

2.

$$\lim_{\varepsilon\to 0^+}\int_{s_\varepsilon} d^i_{jk}(\mathbf{x},\boldsymbol{\xi})n_j(\boldsymbol{\xi})q_k(\mathbf{x})d\Gamma \quad = \quad n_l\sigma_{jk}Q2^i_{jkl}$$

The terms $n_l u_{j,k}Q1^i_{jkl} + n_l\sigma_{jk}Q2^i_{jkl}$ group into $-\frac{1}{2}\delta^i_k q_k(\boldsymbol{\xi})$ taking into account that $q_k = \sigma_{jk}n_j(\mathbf{x}) = (\lambda\delta_{jk}u_{m,m} + \mu(u_{k,j} + u_{j,k}))n_j(\mathbf{x})$.

In the *qbie* and *δqbie* there are some terms that tend to infinite when the radius ε disappears (terms in $\lim_{\varepsilon\to 0^+}\frac{1}{\varepsilon}$). Since all equations should take finite values in order to have a physical sense, the sum of all those terms cancel out with similar divergent terms in the integral along $\Gamma - \Gamma_\varepsilon$. The infinite terms are named with a starting initial I (e.g. $IQ1$ is the Infinite free term of the *qbie* number 1).

$$\frac{1}{2}\delta^i_k q_k(\boldsymbol{\xi}) + \oint_\Gamma \left[s^i_{jkl}n_j(\boldsymbol{\xi})n_l(\mathbf{x})u_k(\mathbf{x}) - d^i_{jk}n_j(\boldsymbol{\xi})q_k(\mathbf{x})\right] d\Gamma(\mathbf{x}) = 0 \qquad \text{for } \xi\in\Gamma_e$$

Free terms for the $\delta qbie$:

1.
$$\begin{aligned}\lim_{\varepsilon\to 0^+}\int_{s_\varepsilon} s^i_{jkl}n_j(\boldsymbol{\xi})u_k\delta n_l(\mathbf{x})d\Gamma &= n_j u_k\delta x_{l,m}IDQ1^i_{jklm}\lim_{\varepsilon\to 0^+}\frac{1}{\varepsilon}\\ &\quad +n_j u_{k,m}\delta x_{l,n}DQ1^i_{jklmn}\\ &\quad +n_j u_k\delta x_{l,mn}DQ5^i_{jklmn}\end{aligned}$$

2.
$$\begin{aligned}\lim_{\varepsilon\to 0^+}\int_{s_\varepsilon} s^i_{jkl,m}n_l(\mathbf{x})n_j(\boldsymbol{\xi})u_k\delta r_m d\Gamma &= n_j u_k\delta x_{l,m}IDQ2^i_{jklm}\lim_{\varepsilon\to 0^+}\frac{1}{\varepsilon}\\ &\quad +n_j u_{k,m}\delta x_{l,n}DQ2^i_{jklmn}\\ &\quad +n_j u_k\delta x_{l,mn}DQ6^i_{jklmn}\end{aligned}$$

3.
$$\lim_{\varepsilon\to 0^+}\int_{s_\varepsilon} s^i_{jkl}n_j(\boldsymbol{\xi})n_l(\mathbf{x})\delta u_k d\Gamma = n_l u_j IQ1^i_{jl}\lim_{\varepsilon\to 0^+}\frac{1}{\varepsilon} + n_l\delta u_{j,k}DQ11^i_{jkl}$$

4.
$$\lim_{\varepsilon\to 0^+}\int_{s_\varepsilon} -d^i_{jk,m}n_j(\boldsymbol{\xi})q_k\delta r_m d\Gamma = n_j\sigma_{km}\delta x_{l,n}DQ8^i_{jklmn}$$

5.
$$\begin{aligned}\lim_{\varepsilon\to 0^+}\int_{s_\varepsilon} -d^i_{jk}n_j(\boldsymbol{\xi})\delta q_k d\Gamma &= n_l\delta\sigma_{jk}DQ12^i_{jkl}\\ &\quad +\delta n_l\sigma_{jk}DQ13^i_{jkl}\end{aligned}$$

6.
$$\begin{aligned}\lim_{\varepsilon\to 0^+}\int_{s_\varepsilon} s^i_{jkl}n_j(\boldsymbol{\xi})n_l(\mathbf{x})u_k\delta J d\Gamma &= n_j u_k\delta x_{l,m}IDQ3^i_{jklm}\lim_{\varepsilon\to 0^+}\frac{1}{\varepsilon}\\ &\quad +n_j u_{k,m}\delta x_{l,n}DQ3^i_{jklmn}\\ &\quad +n_j u_k\delta x_{l,n}DQ7^i_{jklmn}\end{aligned}$$

7.
$$\lim_{\varepsilon\to 0^+}\int_{s_\varepsilon} -d^i_{jk}n_j(\boldsymbol{\xi})q_k\delta J d\Gamma = n_j\sigma_{km}\delta x_{l,n}DQ9^i_{jklmn}$$

8.
$$\lim_{\varepsilon\to 0^+}\int_{s_\varepsilon} s^i_{jkl}n_l(\mathbf{x})u_k\delta n_j(\boldsymbol{\xi})d\Gamma = \delta n_l u_j IDQ4^i_{jl}\lim_{\varepsilon\to 0^+}\frac{1}{\varepsilon} + \delta n_l u_{j,k}DQ4^i_{jkl}$$

9.
$$\lim_{\varepsilon\to 0^+}\int_{s_\varepsilon} -d^i_{jk}q_k\delta n_j(\boldsymbol{\xi})d\Gamma = \delta n_l\sigma_{jk}DQ10^i_{jkl}$$

The terms $\delta n_l u_{j,k}DQ4^i_{jkl} + \delta n_l\sigma_{jk}DQ10^i_{jkl}$ group into $-\frac{1}{2}\delta^i_k\sigma_{kl}(\boldsymbol{\xi})\delta n_l(\boldsymbol{\xi})$ taking into account that $q_k = \sigma_{jk}n_j(\mathbf{x}) = (\lambda\delta_{jk}u_{m,m} + \mu(u_{k,j} + u_{j,k}))n_j(\mathbf{x})$.

Terms $n_l \delta u_{j,k} DQ11^i_{jkl} + n_l \delta \sigma_{jk} DQ12^i_{jkl}$ also group into $-\frac{1}{2}\delta^i_k \delta\sigma_{kl}(\boldsymbol{\xi}) n_l(\boldsymbol{\xi})$ for the same reason. These last two grouped terms reduce further to $-\frac{1}{2}\delta^i_k \delta q_k$.

The sum of terms in $DQ8^i_{jklmn}, DQ9^i_{jklmn}, DQ13^i_{jkl}$ should be equal to zero, although this has still not been confirmed analytically.

If the equation were to be used at a regular boundary, we will see that the equation would turn into,

$$\begin{aligned}
\frac{1}{2}\delta^i_k \delta q_k(\boldsymbol{\xi}) + \oint\!\!\!\!\!\!-_\Gamma \left[d^i_{jk}(\mathbf{x},\boldsymbol{\xi}) n_j(\boldsymbol{\xi}) \delta q_k(\mathbf{x}) - s^i_{jkl}(\mathbf{x},\boldsymbol{\xi}) n_j(\boldsymbol{\xi}) n_l(\mathbf{x}) \delta u_k(\mathbf{x}) \right] d\Gamma(\mathbf{x}) \\
+ \oint\!\!\!\!\!\!-_\Gamma \left[(d^i_{jk}(\mathbf{x},\boldsymbol{\xi}) n_j(\boldsymbol{\xi}) q_k(\mathbf{x}) - s^i_{jkl}(\mathbf{x},\boldsymbol{\xi}) n_j(\boldsymbol{\xi}) n_l(\mathbf{x}) u_k) \delta J(\mathbf{x}) \right. \\
+ (d^i_{jk}(\mathbf{x},\boldsymbol{\xi}) q_k - s^i_{jkl}(\mathbf{x},\boldsymbol{\xi}) n_l(\mathbf{x}) u_k(\mathbf{x})) \delta n_j(\boldsymbol{\xi}) \\
+ (d^i_{jk,m}(\mathbf{x},\boldsymbol{\xi}) n_j(\boldsymbol{\xi}) q_k(\mathbf{x}) - s^i_{jkl,m}(\mathbf{x},\boldsymbol{\xi}) n_l(\mathbf{x}) n_j(\boldsymbol{\xi}) u_k) \delta r_m(\mathbf{x},\boldsymbol{\xi}) \\
\left. - s^i_{jkl}(\mathbf{x},\boldsymbol{\xi}) n_j(\boldsymbol{\xi}) u_k \delta n_l(\mathbf{x}) \right] d\Gamma(\mathbf{x}) \quad = \quad 0 \\
\text{for } \xi \in \Gamma_e
\end{aligned}$$

The so called hypersingular integral equation or stress integral equation 3.12 is transformed into itself during the limiting process to a collocation point on the crack (as long as $\Delta q = 0$, since $q(x^+) = q(x^-)$), since the domain exists on both sides of the crack boundaries, as if it were an interior point. The free terms carried out above for a regular boundary do not count,

qbie:

$$\delta^i_k q_k(\boldsymbol{\xi}) + \oint\!\!\!\!\!\!-_\Gamma \left[s^i_{jkl} n_j(\boldsymbol{\xi}) n_l(\mathbf{x}) u_k(\mathbf{x}) - d^i_{jk} n_j(\boldsymbol{\xi}) q_k(\mathbf{x}) \right] d\Gamma(\mathbf{x}) = 0 \qquad \text{for } \xi \in \Gamma_+ \tag{5.11}$$

δqbie:

$$\begin{aligned}
\delta^i_k \delta q_k(\boldsymbol{\xi}) + \oint\!\!\!\!\!\!-_\Gamma \left[d^i_{jk}(\mathbf{x},\boldsymbol{\xi}) n_j(\boldsymbol{\xi}) \delta q_k(\mathbf{x}) - s^i_{jkl}(\mathbf{x},\boldsymbol{\xi}) n_j(\boldsymbol{\xi}) n_l(\mathbf{x}) \delta u_k(\mathbf{x}) \right] d\Gamma(\mathbf{x}) \\
+ \oint\!\!\!\!\!\!-_\Gamma \left[(d^i_{jk}(\mathbf{x},\boldsymbol{\xi}) n_j(\boldsymbol{\xi}) q_k(\mathbf{x}) - s^i_{jkl}(\mathbf{x},\boldsymbol{\xi}) n_j(\boldsymbol{\xi}) n_l(\mathbf{x}) u_k) \delta J(\mathbf{x}) \right. \\
+ (d^i_{jk}(\mathbf{x},\boldsymbol{\xi}) q_k - s^i_{jkl}(\mathbf{x},\boldsymbol{\xi}) n_l(\mathbf{x}) u_k(\mathbf{x})) \delta n_j(\boldsymbol{\xi}) \\
+ (d^i_{jk,m}(\mathbf{x},\boldsymbol{\xi}) n_j(\boldsymbol{\xi}) q_k(\mathbf{x}) - s^i_{jkl,m}(\mathbf{x},\boldsymbol{\xi}) n_l(\mathbf{x}) n_j(\boldsymbol{\xi}) u_k) \delta r_m(\mathbf{x},\boldsymbol{\xi}) \\
\left. - s^i_{jkl}(\mathbf{x},\boldsymbol{\xi}) n_j(\boldsymbol{\xi}) u_k \delta n_l(\mathbf{x}) \right] d\Gamma(\mathbf{x}) \quad = \quad 0 \\
\text{for } \xi \in \Gamma_+
\end{aligned} \tag{5.12}$$

with the following redefinitions,

$$\begin{cases} \Gamma = \Gamma_e \Rightarrow & \begin{cases} u \leftarrow u & \delta u \leftarrow \delta u \\ q \leftarrow q & \delta q \leftarrow \delta q \end{cases} \\ \Gamma = \Gamma_+ \Rightarrow & \begin{cases} u \leftarrow \Delta u & \delta u \leftarrow \delta \Delta u \\ q \leftarrow 0 & \delta q \leftarrow 0 \end{cases} \end{cases}$$

5.3.5 Non-smooth points

The first two equations can be written as follows, in the case of a cornered boundary. In this case, the *δubie* has two somewhat more complicated terms. It would make no sense to do this calculation for the stress boundary equations since they should be written for points within the elements, which will be smooth.

ubie:

$$u_k(\boldsymbol{\xi}) U1^i_k + \oint\!\!\!\!\!\!-_\Gamma \left[q^i_k u_k(\mathbf{x}) - u^i_k q_k(\mathbf{x}) \right] d\Gamma(\mathbf{x}) = 0 \tag{5.13}$$

Component	Should be (in *ubie*)	Should be (in *δubie*)	Should be (in *qbie*)	Should be (in *δqbie*)
u_k	$C^{0,\alpha}$	$C^{0,\alpha}$	$C^{1,\alpha}$	$C^{1,\alpha}$
q_k	bounded	bounded	$C^{0,\alpha}$	$C^{0,\alpha}$
σ_{kl}	–	$C^{0,\alpha}$	$C^{1,\alpha}$	$C^{1,\alpha}$
δx_l	–	$C^{1,\alpha}$	–	$C^{2,\alpha}$
δu_l	–	$C^{0,\alpha}$	–	$C^{1,\alpha}$
δq_l	–	$C^{0,\alpha}$	–	$C^{1,\alpha}$
$\delta\sigma_{kl}$	–	–	–	$C^{1,\alpha}$

Table 5.1: Conditions of derivability of each component

δubie:

$$\begin{aligned}
&\delta u_k(\boldsymbol{\xi})DU1^i_k + u_k(\boldsymbol{\xi})\delta x_{l,j}(\mathbf{x},\boldsymbol{\xi})DU2^i_{jkl} \\
&+ \int\!\!\!\!\!\!-_\Gamma \left[\sigma^i_{jk}(\mathbf{x},\boldsymbol{\xi})n_j(\mathbf{x})\delta u_k(\mathbf{x}) - u^i_k(\mathbf{x},\boldsymbol{\xi})\delta q_k(\mathbf{x})\right] d\Gamma(\mathbf{x}) \\
&+ \int\!\!\!\!\!\!-_\Gamma \left[(\sigma^i_{jk,m}(\mathbf{x},\boldsymbol{\xi})n_j(\mathbf{x})u_k(\mathbf{x}) - u^i_{k,m}(\mathbf{x},\boldsymbol{\xi})q_k)\delta r_m(\mathbf{x},\boldsymbol{\xi})\right. \\
&\quad +(\sigma^i_{jk}(\mathbf{x},\boldsymbol{\xi})n_j(\mathbf{x})u_k(\mathbf{x}) - u^i_k(\mathbf{x},\boldsymbol{\xi})q_k)\delta J(\mathbf{x}) \\
&\quad \left. +\sigma^i_{jk}(\mathbf{x},\boldsymbol{\xi})u_k(\mathbf{x})\delta n_j(\mathbf{x})\right] d\Gamma(\mathbf{x}) \quad = \quad 0
\end{aligned} \tag{5.14}$$

where the free term take some more complicated values, listed in the appendix.

5.3.6 Conditions of derivability

In the preceding integrals we have used a limited number of terms in the series expansions of every term in the kernels. These terms can only vanish if all the terms fulfill some conditions of derivability. From the conditions pointed out at each integral, one can list the conditions for every component to be accomplished around the collocation point as in table 5.1. – means no conditions to fulfill, $C^{1,\alpha}$ means the Hölder condition, with $0 \leq \alpha < 1$. This implies that if $u_j \in C^{1,\alpha}$, then $u_j(\mathbf{x}) = u_j(\boldsymbol{\xi}) + u_{j,h}(\boldsymbol{\xi})(x_h - \xi_h) + O(r^{1+\alpha})$.

These conditions have crucial importance in the discretization and collocation method used to solve numerically the equations. This is discussed in chapter 7.

5.3.7 Remark on the singularity of the variation equations

The reason that the order of the variation equation does not increase with respect to the direct equation is the following.

In the modified state we are changing both the position of the integration points at the same time as the collocation points (material derivative). When we take the terms that vary in the first order, there appear terms both in δx and in $\delta\xi$. Moreover, they appear with opposite signs because of the radial nature of the fundamental solution, giving the possibility of grouping both terms into δr. These new terms tends to zero as $O(r)$, reducing in 1 the order of the whole kernel. This compensates the increase in 1 order of the fundamental function.

The terms not depending on δx or $\delta\xi$ have a non-derived fundamental function, having therefore the same order as the origin.

Chapter 6

Adjoint Variable Method

The objective here is to find the gradient of a cost functional J used for e.g. geometry identification, with respect to the variation of the geometry by a set P of parameters ($\frac{dJ}{dP}$).

The main advantage of this method is that there is no need to calculate any gradient of $\mathbf{u}$ or $\mathbf{q}$. It is obtained by solving the direct problem, an adjoint problem defined in a specific way, and apply some simple formulas that yield the gradient of J.

6.1 Objective function

In an inverse problem like a crack detection, the goal is to find the optimum geometry in the sense that the behaviour of the supposed problem fits our measurements on the real specimen, i.e. some set of data (stress vectors and displacements q_i, u_i) equals the measured set (q_i^{exp}, u_i^{exp}). This can be done choosing an objective function,

$$J(\Gamma_c) = \int_0^T \int_{\Gamma_q} \varphi_u d\Gamma dt + \int_0^T \int_{\Gamma_u} \varphi_q d\Gamma dt + \int_\Gamma \psi d\Gamma \tag{6.1}$$

where,

$$\varphi_u = \varphi_u(u_i, \mathbf{x}, t) \qquad \varphi_q = \varphi_q(q_i, \mathbf{x}, t) \qquad \psi = \psi(\mathbf{x})$$

The generic formulation achieved here will eventually be tested using the functions,

$$\begin{aligned} \varphi_u &= \begin{cases} \frac{1}{2}(u_i^{exp} - u_i)^2 & \Gamma^{m_u} \\ 0 & \text{otherwise} \end{cases} \\ \varphi_q &= \begin{cases} \frac{1}{2}(q_i^{exp} - q_i)^2 & \Gamma^{m_q} \\ 0 & \text{otherwise} \end{cases} \\ \psi &= 0 \end{aligned} \tag{6.2}$$

A perturbation of the crack boundary Γ can be described by a transformation of the domain $\tilde{x}_i = x_i + \delta x_i(\mathbf{x})$, where P is a time-like parameter, and δx_i an instantaneous velocity vector, fulfilling that $\delta x_i = 0$ on Γ_e. This definition is equivalent to the former one, in which $\delta x_i = \Theta_{ig} P_g$, being δx_i the variation field and the time-like parameter is generalized to a vector P_g of g parameters.

We are going to use the material or Lagrangian derivatives of the fields with respect to the variable P, defined as $\delta f_i = \frac{\partial f_i}{\partial P_g}\delta P_g + \frac{\partial f_i}{\partial x_j}\delta x_j$.

6.2 Adjoint variable method

6.2.1 Basics

Our problem is to express the derivative of the derivative of a cost functional with respect to some geometrical parameters in an effective way. A detailed description of the full mathematical process for a continuous problem is given by M. Bonnet in [16]. Another good overview can be found in [28]. The basic ideas and process are the following, and can be presented from the reciprocity and from the lagrangian approaches.

For the sake of simplicity, the sequel is written for a discretized generic problem $A_{ij}(P)u_j = b_i$, instead of the continuous problem $(c_1^2 - c_2^2)u_{i,jj} + c_1^2 u_{j,ij} - \rho\ddot{u}_j = 0$.

Reciprocity approach

As stated above, we have a cost functional that depends directly on u and indirectly on some geometrical parameter(s) P,

$$J(P) = J(u(P), P)$$

We are searching its derivative with respect to P,

$$\delta J = J_{,u_i}\,\delta u_i + J_{,P}\,\delta P$$

Now, we can define a new problem with the same behaviour, which means the same system matrix in the discrete problem, or the same constitutive equilibrium and compatibility equations in the continuous problem, as $A_{ij}(P)u'_j = b'_i$. For the discrete problem we can do the following multiplications and subtraction, which are equivalent to the derivation of the Betti reciprocity theorem for the continuous one. If we differentiate the problem definition,

$$A_{ij}(P)u_j = b_i \qquad \Rightarrow \qquad A_{ij}\delta u_j + \delta A_{ij}u_j = 0$$

and multiply by an adjoint state and a derived state, with the goal of elliminating the explicit calculation of δu_i,

$$\left.\begin{array}{c} u'_i[A_{ij}\delta u_j + \delta A_{ij}u_j = 0] \\ \delta u_i[A_{ij}(P)u'_j = b'_i] \end{array}\right\} \qquad \Rightarrow \qquad u_i\delta A_{ij}u'_j = -b'_i\delta u_i$$

With the particular choice of $b'_i = -J_{,u_i}$, we can substitute this expression in the expression of $\frac{\partial J}{\partial P}$, giving

$$\delta J = u_i\delta A_{ij}u'_j + J_{,P}\,\delta P$$

Lagrangian approach

This is the most convenient approach for the continuous problem. If we add to the cost function a lagrangian term that vanishes as the direct problem is fulfilled, and derive it,

$$L = J + A = J + u'_i[A_{ij}u_j - b_i] \qquad \Rightarrow \qquad \delta L = J_{,P}\,\delta P + J_{,u_i}\,\delta u_i + u'_i[A_{ij}u'_j + \delta A_{ij}u_j = 0]$$

Again, if we choose $b'_i = -J_{,u_i}$ and substitute it, we have

$$\delta L = u_i\delta A_{ij}u'_j + J_{,P}\,\delta P$$

In this expression, neither u_i or u'_i depend on P, which is the reason why there is only need for calculating one adjoint problem. To complete the problem, the term $u_i\delta A_{ij}u'_j$ can be treated (apllying Gauss theorems and developing the crack tip terms, as shown in [16]), so as to have a boundary integral in δA_{ij}

6.2.2 Adjoint problem

Following M. Bonnet [16], we define the following Lagrangian, involving the test functions u'_i, p'_i which act as Lagrange multipliers.

$$L = J + A = J + \int_0^T \int_\Omega [\sigma_{ij} u'_{i,j} + \rho \ddot{u}_i u'_i] d\Omega dt$$
$$- \int_0^T \int_{\Gamma_u} (u_i - u_i^{exp}) q'_i d\Gamma dt - \int_0^T \int_{\Gamma_u} q_i u'_i d\Gamma dt - \int_0^T \int_{\Gamma_q} q_i^{exp} u'_i d\Gamma dt \tag{6.3}$$

The adjoint problem will be defined now by the same governing equations 6.4, below, and the boundary conditions, governed by the same field equations, elastic constants and angular frequency ω. It will be labeled using $(')$.

$$(c_1^2 - c_2^2) u'_{i,jj} + c_1^2 u'_{j,ij} - \rho \ddot{u}'_j = 0$$
$$q'_i = -\frac{\partial \varphi_u}{\partial u_i} (\text{ on } \Gamma_q) \qquad u'_i = \frac{\partial \varphi_q}{\partial q_i} (\text{ on } \Gamma_u) \qquad q'_i = 0 (\text{ on } \Gamma_c) \tag{6.4}$$

The total derivative of L with respect to a domain perturbation is deduced in [16],

$$\begin{aligned}
\delta L \;=\; & \int_{\Gamma_c^+} (\delta x_k n_k) \int_0^T [[\sigma_{ij} u'_{i,j} - \rho \dot{u}_i \dot{u'}_i]] dt d\Gamma \\
& - \frac{1}{\mu} \int_{\delta\Gamma_c} (\delta x_k \nu_k) \int_0^T \{(1-\nu)[K_I K'_I + K_{II} K'_{II}] + K_{III} K'_{III}\} dt d\Gamma \\
& - \frac{1-\nu}{\mu} \int_{\delta\Gamma_c} (\delta x_k n_k) \int_0^T [K_I K'_{II} + K_{II} K'_I] dt d\Gamma \\
& + \int_{\Gamma_c} [\psi_i \delta x_i + \psi (\delta x_{i,i} - n_i \delta x_{i,j} n_j)] d\Gamma_c
\end{aligned}$$

where $\delta\Gamma_c$ is the crack tip, $[[f]] = f(x^+) - f(x^-)$ (discontinuity of f across Γ), n_i is the normal on Γ and Σ_ε. After the limiting process, ν_i denotes the unit outward normal to $\delta\Gamma$ lying on the tangent plane to Γ_c, and N_i is the normal to Γ_c^+ (see figure 6.1).

6.2.3 Reduction to bidimensional cracks in frequency domain

The problem is going to be solved for an harmonic load at a single frequency ω. The static case is immediately deducted by obviating any complex components and the $\frac{\Pi}{\omega}$ factor at the beginning. The values of displacements, stress vectors and stress intensity factors will therefore be represented with complex numbers $f(x) = [a(x) \quad b(x)] = a(x) + b(x)\sqrt{-1}$ that fulfill $f(x,t) = Re\left[f(x)e^{i\omega t}\right]$.

Taking into account the definition of the adjoint problem, the test functions, and reducing the problem to a plane strain problem, we get the expression 6.5 for the gradient of the Lagrangian in a more explicit way. The definitions are clarified in figure 6.1.

If we take into consideration the following points,

- $\tilde{\omega} = \omega \qquad \tilde{c}_1 = c_1 \qquad \tilde{c}_2 = c_2 \qquad \tilde{\rho} = \rho$
- $u_i(y,t) = \text{Re}\left[u_i(x)e^{i\omega t}\right] \qquad q_i(y,t) = \text{Re}\left[q_i(x)e^{i\omega t}\right]$
- $K_n(y,t) = \text{Re}\left[K_n(x)e^{i\omega t}\right]$
- $\int_0^{T=\frac{2\pi}{\omega}} \cos^2 \omega t dt = \frac{\pi}{\omega} \qquad \int_0^T \sin^2 \omega t dt = \frac{\pi}{\omega} \qquad \int_0^T \cos \omega t \sin \omega t dt = 0$

Doing the following generic operation, we can transform the time integrals:

$$\begin{aligned}\int_0^T F_n(t)F'_n(t)dt &= \int_0^T (a_n\cos\omega t - b_n\sin\omega t)(a'_n\cos\omega t - b'_n\sin\omega t)dt \\ &= \left[a_n a'_n\int_0^T \cos^2\omega t dt + b_n b'_n\int_0^T \sin^2\omega t dt\right. \\ &\left. -a_n b'_n\int_0^T \sin\omega t\cos\omega t dt - b_n a'_n\int_0^T \sin\omega t\cos\omega t dt\right] \\ &= \frac{\pi}{\omega}\left[a_n a'_n + b_n b'_n\right] = \frac{\pi}{\omega}\mathrm{Re}\left[F_n\overline{F'}_n\right]\end{aligned}$$

$$\begin{aligned}\int_0^T c_{ijkl}u_{i,j}(\mathbf{x},t)u'_{k,l}(\mathbf{x},t)dt &= \frac{\pi}{\omega}\mathrm{Re}\left[c_{ijkl}u_{i,j}\overline{u'}_{k,l}\right] \\ \int_0^T \rho\dot{u}_i(\mathbf{x},t)\dot{u'}_i(\mathbf{x},t)dt &= \frac{\pi}{\omega}\mathrm{Re}\left[\rho\omega^2 u_i\overline{u'}_i\right] \\ \int_0^T K_n(t)K'_n(t)dt &= \frac{\pi}{\omega}\mathrm{Re}\left[K_n\overline{K'}_n\right]\end{aligned}$$

and we reach the expression,

$$\begin{aligned}\delta L = \frac{\pi}{\omega}\mathrm{Re}\Bigg[&\int_{\Gamma_c}(\delta x_k n_k)[[c_{ijkl}u_{i,j}\overline{u'}_{k,l} - \rho\omega^2 u_i\overline{u'}_i]]d\Gamma \\ &-\sum_{tips}\left\{\frac{1}{\mu}(\delta x_k\nu_k)\left\{(1-\nu)[K_I\overline{K'}_I + K_{II}\overline{K'}_{II}] + K_{III}\overline{K'}_{III}\right\}\right. \\ &\left.+\frac{1-\nu}{\mu}(\delta x_k N_k)[K_I\overline{K'}_{II} + K_{II}\overline{K'}_I]\right\}\Bigg]\end{aligned} \tag{6.5}$$

where $\overline{a}$ stands for the conjugate of the complex value a.

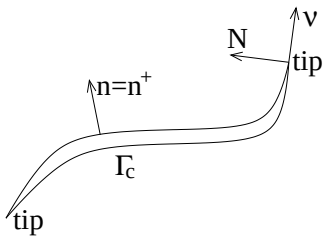

Figure 6.1: Some definitions of the geometry

The term involving the gradient of the displacements can be calculated in terms of boundary values only with the help of the expression 6.6, derived below. ∇_s means the surface gradient, which is the proyection of the gradient onto the surface. div_s is also the proyection of the divergence

on the surface.

$$\begin{aligned}
\sigma : \nabla\overline{u'} &= \mu\left\{\frac{2\nu}{1-\nu} div_s u div_s \overline{u'}\right. \\
&\left. +\frac{1}{2}(\nabla_S u + \nabla_S^T u) : (\nabla_S \overline{u'} + \nabla_S^T \overline{u'}) - (n\nabla_S u)(n\nabla_S \overline{u'})\right\} \\
\mathrm{div}_S u &= u_{t,t} \\
\nabla_S u &= \begin{bmatrix} 0 & 0 \\ u_{n,t} & u_{t,t} \end{bmatrix} \\
u_{t,t} &= u_{i,\xi} t_i \frac{1}{J} \\
\sigma_{ij}\overline{u'}_{i,j} &= \mu\left\{\frac{2\nu}{1-\nu} u_{t,t}\overline{u'}_{t,t} + \frac{1}{2}(2u_{n,t}\overline{u'}_{n,t} + 2u_{t,t}\overline{u'}_{t,t}) - u_{n,t}\overline{u'}_{n,t}\right\} \\
&= \frac{2\mu}{J^2(1-\nu)} u_{i,\xi} t_i \overline{u'}_{j,\xi} t_j
\end{aligned} \tag{6.6}$$

6.2.4 Summary

The adjoint problem to solve for this particular case is finally defined in 6.8, with identical constants and frequency to the direct one. The different parts of the boundary are shown in figure 6.2.

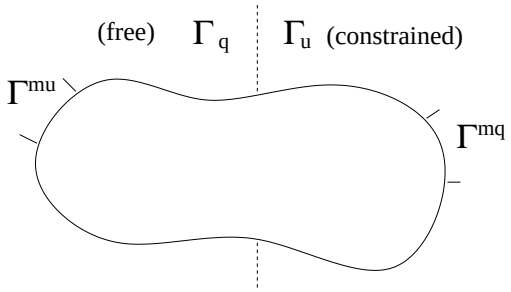

Figure 6.2: Generic definition of the boundary division

$$\begin{aligned}
(c_1^2 - c_2^2)u'_{i,jj} + c_1^2 u'_{j,ij} = \rho\ddot{u}'_i \qquad & \text{with,} \\
q'_i &= \begin{cases} (u_i^{exp} - u_i) & \Gamma^{m_u} \\ 0 & \Gamma_q/\Gamma^{m_u} \end{cases} \\
u'_i &= \begin{cases} (q_i - q_i^{exp}) & \Gamma^{m_q} \\ 0 & \Gamma_u/\Gamma^{m_q} \end{cases} \\
q'_i &= 0 \text{ on } \Gamma_c
\end{aligned} \tag{6.7}$$

Chapter 7

Numerical treatment

7.1 Discretization

The boundary is divided into a number of elements, and at each one, the following variables are defined as stated, in the known state and in the perturbed one (see figure 7.1):

$$\mathbf{x} = \sum_{n=1}^{N} \phi_n \mathbf{x}_n \qquad \mathbf{u} = \sum_{n=1}^{N} \phi_n \mathbf{u}_n \qquad \mathbf{q} = \sum_{n=1}^{N} \phi_n \mathbf{q}_n$$
$$\tilde{\mathbf{x}} = \sum_{n=1}^{N} \phi_n \tilde{\mathbf{x}}_n \qquad \tilde{\mathbf{u}} = \sum_{n=1}^{N} \phi_n \tilde{\mathbf{u}}_n \qquad \tilde{\mathbf{q}} = \sum_{n=1}^{N} \phi_n \tilde{\mathbf{q}}_n$$

ϕ_n Interpolation or base functions.

n Index for node at a certain element of order $N-1$ ($n = \{1, 2, 3\}$ for quadratic elements, $N = 2$).

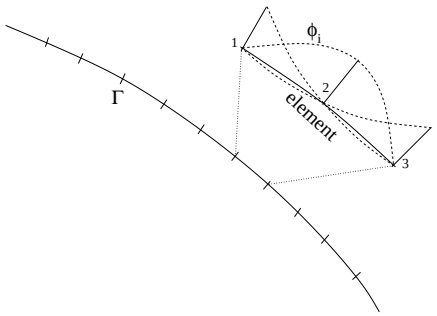

Figure 7.1: Element discretization

In fact, the perturbed geometry $\tilde{}$ is never discretized, but only the variation, which can be defined for $\mathbf{u}$ and $\mathbf{x}$ as,

$$\delta\mathbf{u} = \sum_{n=1}^{N} \phi_n \delta\mathbf{u}_n \qquad \delta\mathbf{q} = \sum_{n=1}^{N} \phi_n \delta\mathbf{q}_n$$

The variation of the geometry $\delta\mathbf{x}$ can be defined in two ways:

$$\delta\mathbf{x} = \sum_{n=1}^{N} \phi_n \delta\mathbf{x}_n \qquad \text{where} \qquad \delta\mathbf{x}_n = \Theta_{ig}(\mathbf{x}_n) P_g$$

or

$$\delta \mathbf{x} = \Theta_{ig}(\mathbf{x}) P_g \qquad \text{where} \qquad \mathbf{x} = \sum_{n=1}^{N} \phi_n \mathbf{x}_n$$

Both methods were tested, and the second was kept since it gave better results.

7.1.1 High order shape functions

A systematic procedure to obtain the shape functions and their derivatives of any order, easy to implement, using Lagrange polynomials, is the following:

$$\phi_i = \prod_{i \neq j} \frac{\xi - \xi_j}{\xi_i - \xi_j} \qquad \frac{d\phi_i}{d\xi} = \sum_{i \neq k} \prod_{i \neq k, i \neq j} \frac{\xi - \xi_j}{\xi_i - \xi_j} \frac{1}{\xi_i - \xi_k}$$

This has only been implemented for the direct derivation package.

7.1.2 Collocation

If a standard element method is used, the obtained conditions at different points of the boundary are,

Component	Between elements	Inside elements
u_k	(1)	C^∞
q_k	(1)	C^∞
σ_{kl}	(1)	C^∞
δx_l	(2)	(2)
δu_l	(1)	C^∞
δq_l	(1)	C^∞
$\delta \sigma_{kl}$	(1)	C^∞

(1) It is $C^{0,\alpha}$ if a standard discretization is taken. It is possible to choose some degree of coincidence of some derivatives (tangential elements, by means of Overhouser elements [131] or splines, etc.), giving $C^{1,\alpha}$ or higher.

(2) It is C^∞ if a continuous variation field is chosen, which is our case. This is an important limitation in the choice of parametrization. Other choices such as a parametrization based on a spline or dependent on the discretization should be studied for every particular case.

These results show that in neither the *qbie* nor *δqbie* the collocation points cannot be placed in between elements, but displaced some quantity towards the center. In the *δubie*, the collocation points can be on interelemental nodes as long as the normal and geometrical definition satisfy the continuity.

7.1.3 $\sqrt{r}$ crack tips for high order elements

When the boundary element of any order is placed on a crack tip, one may prove that a particular collocation of the nodes may be sufficient to express or model the $\sqrt{r}$ behaviour of the displacements and stresses. The only condition is that the element must be straight.

In a straight element, the displacements/stresses (tangential and normal, or equivalently horizontal and vertical) depend asymptotically on the distance from the tip, equivalent to the local x direction as $u = c\sqrt{x}$.

On the other hand, the discretization of the displacements/stresses is made by writing $u = \sum \phi_i(\xi) u_i$.

If we are capable of defining a local variable η that varies from $\eta = 0$ at the tip, and $\eta = 1$ at the end of the element such that $x = L\xi^2$, and we use any set of shape functions that is capable of modelling the identity, there will be some shape function or combination of them that will be linear:

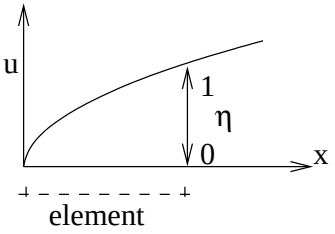

Figure 7.2: Definitions for the crack tip element.

$\phi = \eta$ (any of the spaces of linear or higher order mentioned above). Substituting everything, we obtain what we looked for,

$$u = c'\eta = c\sqrt{x}$$

The necessary relationship $x = L\eta^2$ is simply obtained by placing the nodes regularily spaced in terms of the variable η. Hence, in a three noded element the central element is placed at $\eta = 0.5$, or equivalently at $x = L0.5^2 = 0.25L$, which is the defintion of a quarter point element. In a higher order (n) element, the coordinates of the middle nodes are $\xi = [\frac{1}{n}, \frac{2}{n}, ...\frac{n-1}{n}]$ or $x = L[\frac{1}{n^2}, \frac{2^2}{n^2}, ...\frac{(n-1)^2}{n^2}]$.

The further components of the shape function space will yield the terms of the displacements/stresses:

$$u = \{1, \sqrt{x}, x, x^{\frac{3}{2}}, x^2, ...\}$$

which are coincident with the series expansion of the analytical solutions at crack tips.

The goodness of these elements has been tried giving excellent results.

7.2 Applying the parametrization

If we substitute the desired parametrization (see chapter 8),

$$\delta x_i \quad = \quad \Theta_{ig}\delta P_g$$

where Θ_{ig} is the parameterization matrix, and P_g the vector of discrete parameters, the following expressions are derived,

$$\delta r_i = (\Theta_{ig}(\xi) - \Theta_{ig}(x))\delta P_g; \quad \delta n_i = t_i t_m t_l \epsilon_{mk}\Theta_{kg,l}\delta P_g; \quad \delta J = t_k t_l \Theta_{lg,k}\delta P_g$$

Substituting 7.1 in 5.11 and 5.12, the systems of equations can be written as,

δubie:

$$c^i_k\delta u_k(\boldsymbol{\xi}) + \int_\Gamma \left[\sigma^i_{jk}(\mathbf{x},\boldsymbol{\xi})n_j(\mathbf{x})\delta u_k(\mathbf{x}) - u^i_k(\mathbf{x},\boldsymbol{\xi})\delta q_k(\mathbf{x})\right] d\Gamma(\mathbf{x}) = {}^gU^i_g(\xi)\delta P_g$$

$$\begin{aligned} {}^gU^i_g(\xi)\delta P_g = -\int_\Gamma \big[&(\sigma^i_{jk,m}(\mathbf{x},\boldsymbol{\xi})n_j(\mathbf{x})u_k(\mathbf{x}) - u^i_{k,m}(\mathbf{x},\boldsymbol{\xi})q_k)\delta r_m(\mathbf{x},\boldsymbol{\xi}) \\ &+(\sigma^i_{jk}(\mathbf{x},\boldsymbol{\xi})n_j(\mathbf{x})u_k(\mathbf{x}) - u^i_k(\mathbf{x},\boldsymbol{\xi})q_k)\delta J(\mathbf{x}) \\ &+\sigma^i_{jk}(\mathbf{x},\boldsymbol{\xi})u_k(\mathbf{x})\delta n_j(\mathbf{x})\big]\, d\Gamma(\mathbf{x}) \end{aligned} \tag{7.1}$$

δqbie:

$$c^i_k\delta q_k(\boldsymbol{\xi}) + \int_\Gamma \left[d^i_{jk}(\mathbf{x},\boldsymbol{\xi})n_j(\boldsymbol{\xi})\delta q_k(\mathbf{x}) - s^i_{jkl}(\mathbf{x},\boldsymbol{\xi})n_j(\boldsymbol{\xi})n_l(\mathbf{x})\delta u_k(\mathbf{x})\right] d\Gamma(\mathbf{x}) = {}^gQ^i_g(\xi)\delta P_g$$

$$\begin{aligned} {}^gQ^i_g(\xi)\delta P_g = -\int_\Gamma \big[&(d^i_{jk}(\mathbf{x},\boldsymbol{\xi})n_j(\boldsymbol{\xi})q_k(\mathbf{x}) - s^i_{jkl}(\mathbf{x},\boldsymbol{\xi})n_j(\boldsymbol{\xi})n_l(\mathbf{x})u_k)\delta J(\mathbf{x}) \\ &+(d^i_{jk}(\mathbf{x},\boldsymbol{\xi})q_k - s^i_{jkl}(\mathbf{x},\boldsymbol{\xi})n_l(\mathbf{x})u_k(\mathbf{x}))\delta n_j(\boldsymbol{\xi}) \\ &+(d^i_{jk,m}(\mathbf{x},\boldsymbol{\xi})n_j(\boldsymbol{\xi})q_k(\mathbf{x}) - s^i_{jkl,m}(\mathbf{x},\boldsymbol{\xi})n_l(\mathbf{x})n_j(\boldsymbol{\xi})u_k)\delta r_m(\mathbf{x},\boldsymbol{\xi}) \\ &-s^i_{jkl}(\mathbf{x},\boldsymbol{\xi})n_j(\boldsymbol{\xi})u_k\delta n_l(\mathbf{x})\big]\, d\Gamma(\mathbf{x}) \end{aligned} \tag{7.2}$$

7.3 Organizing the equations

The discretization of either the singular or hypersingular variation boundary integral equation, and the substitution of the variation of the geometry by the parametrization definition, yields the following expression in matricial form,

$$\mathbf{H}\delta\mathbf{u} - \mathbf{G}\delta\mathbf{q} = \Delta\delta\mathbf{P}$$

where $\mathbf{u}$ and $\mathbf{q}$ are the displacement and stress vectors and $\mathbf{P}$ is the parameter set. $\mathbf{H}$ and $\mathbf{G}$ are identical to the system matrices in the usual BEM. Δ is a matrix that groups the rest of the integrals, in which $\delta\mathbf{n}$, δJ and $\delta\mathbf{r}$ have to be substituted, and then $\delta\mathbf{P}$ becomes a common factor to be extracted.

$$\Delta = \begin{cases} {}^{g}U_g^i(\xi) & \text{for the } \delta qbie \\ {}^{g}Q_g^i(\xi) & \text{for the } \delta qbie \end{cases}$$

The application of the boundary conditions yield the same coefficients of the system matrix $\mathbf{A}$ as the usual BEM, since the prescribed values have zero variation. These variations are therefore not unknowns, as if they were prescribed:

$$\mathbf{A}\delta\mathbf{v} = \Delta\delta\mathbf{P}$$

where $\delta\mathbf{v}$ groups the non prescribed terms of $\delta\mathbf{u}$ and $\delta\mathbf{q}$ in the sequel, as done in the BEM. The solutions of the latter system for each column of Δ can be performed and grouped into $\mathbf{J}$, that will later be called jacobian, so that it accomplishes,

$$\delta\mathbf{v} = \mathbf{J}\delta\mathbf{P} \quad \Rightarrow \quad \mathbf{J} = \{j_{ig}\} = \frac{dv_i}{dP_g}$$

From a computational point of view, this procedure is very cheap since the system matrix $\mathbf{A}$ is already computed and factorized from the direct problem, so the remaining operations are the successive substitutions of the columns of Δ.

Chapter 8

Parametrization

8.1 Why and how to parametrize?

The variation of the geometry during a step in the iterative inverse solution is always represented by a so called parametrization, which means a representation of the geometrical definition by a finite set of values. A generic and exact representation would need an infinite number of parameters. When the problem is discretized for the sake of solving it numerically, the geometry is then defined by some nodal coordinates. Taking as parameters each of these nodal coordinates, would yield the complete parametrization of this geometry, involving a finite but big number of data.

In the approach to inverse and optimization problems there are two important points to be taken into account at this stage. Both are related to the used iterative numerical methods for highly nonlinear and ill-conditioned equations they deal with. The numerical optimization algorithms used in these problems are never guaranteed to converge, but the "probability" of convergence highly depend on the number of parameters to optimize.

This ill-conditioning is rooted in the physical meaning of the problem, so this difficulty cannot be avoided by purely mathematical manipulations. But there are some modifications in the global strategy that allow to partly overcome this problem. The two aspects one can manipulate are the regularization and the choice of parametrization. The regularization basically consists of adding some a priori information on the expected solution. The second aspect directly consists of reducing the number of parameters by expressing the geometry by a fewer number of data. Both can eventually be related in the sense that in the reduced parametrization we are introducing assumed information in the form of relationships in the values of the surplus nodal coordinates since they are all expressed in terms of a few parameters.

8.1.1 Choice of parametrizacion

There is a great freedom in the choice and invention of parametrizations. The most usual ones are based on a definition of the complete geometry by splines of all kinds and orders, (in aeronautical shape optimization, usually cubic B-splines, NURBS, described often in the literature [5], or Bezier-curves [130]). In identification problems, the geometry is usually defined by simple geometrical entities, in turn defined by a few parameters (like ellipses defined by the coordinates of the center, the axes length and an angle of orientation [9], [133] [85]).

Modification field

A more advanced concept put forward first by Gallego and Suárez [48] consists in defining directly the modification field instead of the geometry. This means applying a deformation field to some initial geometry (as complicated as you want), that is capable of moving it until any possible solution. Now, it is this field which is defined by a set of parameters (for example a linear deformation

field that in 2D is defined by 6 parameters, which has been used in [100], [114]). This field is only non-zero for the sought part of the geometry (the flaw or the zone to be optimized).

Mesh-dependent parametrization

Another more conceptual strategy consists of a mesh-dependent parametrization, that can basically be understood as grouping nodes or defining a superimposed mesh with a few nodes (= parameters), more or less directly related to the model mesh (see [19] and [18]). This parametrization is developed in detail in the next sections.

The choice of parametrization also has effects on the order of derivability or smoothness of the boundary of the geometry.

Since every parametrization has advantages and disadvantages, and since this is a key point, everyone should be beared in mind when approaching an identification or optimization problem, in order to choose a proper one, or set of ones, in an harmonic global strategy.

8.1.2 Field of variation

In any parametrization the variation of the geometry can be derived from to the variation of the value of each parameter.

In the case of the sensitivity equation the choice of a field of deformation is a good one. In this work, this will be our choice. One reason is the congruence of the sense of the derivative of the field, not only on the boundary but in its vicinity. Another reason is that a field can be applied to any geometry without a change of parametrization.

The field of deformation δx_i can be defined as a vectorial field, expressing the change of position of each material point:

$$\tilde{x}_i = x_i + \delta x_i$$

The main advantge is that the field can be manipulated before defining any parametrization. This allows to define and implement the main sensitivity calculation with complete generality with respect to the choice of parametrization. In particular, the variation equation will only depend explicitly on the terms,

$$\delta x_i \quad \text{and} \quad \frac{\partial \delta x_i}{\partial x_m}$$

where they will have to fulfill some conditions, as shown in chapter 5.3.6. The parametrization is defined as:

$$\delta x_i(\mathbf{x}) = \Theta_{ig} \delta P_g$$

where δx_i is a continuous and finite vectorial field definition that depends, in a multiplicative sense, on a parametrization matrix Θ_{ig} and on a vector P_g of g parameters.

Global strategy and parametrization: big parameters

At a certain step k in the iterative optimization procedure, one may have a modified state by a vector of parameters P_g^k yielding a deformation field $\delta \mathbf{x}^k$ and a geometry Γ^k.

There is an important consideration related to the way different optimization techniques perform the iterations. There are two ways to use the parametrization:

1.

$$\begin{aligned} x_i^k &= x_i^{k-1} + \delta x_i^k(\mathbf{x}^{k-1}) \\ \delta x_i^k &= \Theta_{ig}(\mathbf{x}^{k-1}) \delta P_g \end{aligned}$$

If one uses the observation equation approach, in which the only information used for a step k is the setup in step $k-1$, one may apply to the geometry $k-1$ a parameter set that will only last one iteration, and that will start and be applied to the geometry $k-1$. This may be called incremental parametrization.

2.

$$\begin{aligned} x_i^k &= x_i^0 + \Delta x_i^k(\mathbf{x}^0) \\ \Delta x_i^k &= \Theta_{ig}(\mathbf{x}^0) P_g \end{aligned}$$

If the iterative method is more complicated one may need more information than just the last step. Therefore one may not use a one step parameter as before, but some history. It is possible to store artificially the necessary information, but there is a conceptually clearer procedure, which is to use a parameter that evolves throughout the iterative method. This parameter will be calculated from the initial geometry 0. This allows the parameter to be treated independently, as a black box, by the optimization algorithm.

Both methods can coincide only in the case that, for any couple of iterations a and b, $\Theta(\mathbf{x}^a) = \Theta(\mathbf{x}^b)$, which happens when the parametrization is obtained after integrating each incremental one as a differential element. This can generally not be done because of a dependence of the path followed by each simultaneous parameter. On the other hand this integration is generally impracticable.

The global parametrization is more convenient for global optimization algorithms since they require information about previous steps (during updates or line searches, for instance), and in the case of a hessian update method, the latter is built in an additive sense from the initial one, based on information of all the history of the parameter vector.

The incremental parametrization gives much more flexibility and more clarity to its definition since it only regards the last step in order to construct a new field, besides breaking the limitations of the initial configuration.

This has an important consequence on the definition of the geometrical terms with respect to the parameter, as they take big values, referred to a geometry far from the current one, and in which the geometry 0 and $k-1$ are qualitatively different. A simple example to show this difference is depicted in 8.1. If we choose some initial geometry 0 that becomes $k-1$, and the parameter is for example the scaling magnitude, different values are needed to arrive at the same geometry k, depending on the method.

The implications of this on the definition of the geometrical values appear in terms of the choice of which terms of the expression relate to geometry 0 and which relate to geometry $k-1$. The geometrical considerations are explained in figure 8.2. If we have an initial state 0 and a final one f,

$$\begin{aligned} t_i &= \frac{dx_i}{|dx|} \\ \lim_{r\to 0} \delta r_l^f &= \frac{\delta x^0_{l,m}(\xi) dx^0_m}{|dx^f|} r + \frac{\delta x^0_{l,mn}(\xi) dx^0_m dx^0_n}{|dx^f||dx^0|} r^2 + hot. \qquad \text{(when integrating singularities)} \\ \delta J &= \frac{dx^f_l \delta x^0_{l,m} dx^0_m}{|dx^f||dx^f|} \\ \delta n_j &= \frac{dx^f_j dx^f_l \epsilon_{l,p} \delta x^0_{p,m} dx^0_m}{|dx^f||dx^f||dx^f|} \end{aligned}$$

The equivalent expressions for an incremental parametrization (when the difference in 0 and f

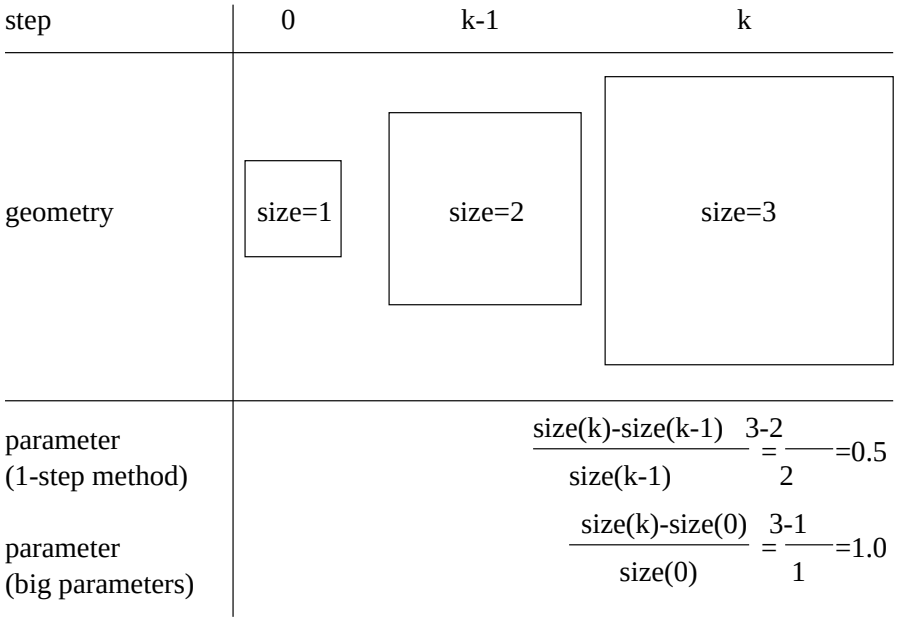

Figure 8.1: Comparison of parametrization types.

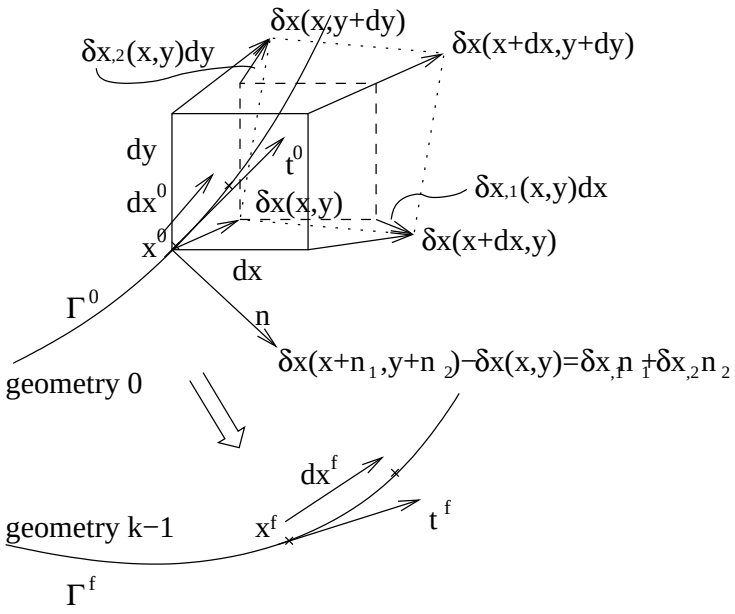

Figure 8.2: Geometrical definitions.

is negligible) were obtained in chapter 5.1.1:

$$\begin{aligned} \delta r_l &= \delta x_{l,m}(\xi) r_m + \delta x_{l,mn}(\xi) r_m r_n + hot. \\ \delta n_j &= t_j t_l \epsilon_{lp} \delta x_{p,m} t_m \\ \delta J &= t_l \delta x_{l,m} t_m \end{aligned}$$

The incremental parametrization has been used in this work with the direct derivation of the sensitivity, with global optimization algorithms, althought the global parameters have also been tested with the AVM gradient obtention. The reason for the eventual choice of incremental parametrization is that it gives some more freedom in the possible deformations, since it is not linked to the initial shape.

The procedure to the use of incremental parametrization follows, as well as some considerations. Two values of the parameters are used: an internal value P for the optimization algorithm, and an incremental one δP as external for the gradient calculation and geometry variation (only geometry $k-1$ is stored, and is updated with $\delta P^{k-1} = P^k - P^{k-1}$). At each iteration we update the geometry and reset the external parameter to zero. The variation of the geometry at the iteration is made using as external parameter only the increment of internal parameter at the current step.

The drawback of this procedure is that there is not an univocal relationship between internal parameter value and geometry, which may introduce some degree of unpredictability in the optimization algorithm. The univocal relationship does not exist since, in general, $\Theta(\mathbf{x}^k) \neq \Theta(\mathbf{x}^{k-1})$. One trick to overcome this, at least for the line searches, would be to recover the biyective relationshhip between internal parameter value and geometry by computing the geometry through a numerical integration of the increment.

Cautions

A nonlinear variation field may alter the ratio in the positions of the nodes making the resulting real shape functions become of a different order than the original. For example, a normal element could in an extreme case turn into something similar to a quarter point element.

Conversely, the order of a quarter point element at the end of a crack can be modified to a non $\sqrt{r}$ by an inconvenient relative displacement of the nodes. This can be overridden by identifying the element and imposing a linear modification at that zone.

8.1.3 Relationship with discretization

There are two main ways to use the parametrization inside the discretized sensitivity boundary integral equation:

- $\delta\mathbf{x} = \delta\mathbf{x}(\mathbf{x})$ This means that at an integration point x, the value of the matrix $\delta\mathbf{x}$ is computed once at $\mathbf{x}$ itself. This is the most close to the analytical definition.

- $\delta\mathbf{x} = \sum \delta\mathbf{x}^i \phi^i$ means that the value of the matrix $\delta\mathbf{x}$ evolves as the rest of the variables following the interpolation by the shape functions ϕ^i. Thus $\delta\mathbf{x}^i$ is only evaluated at the nodes i.

The first method has proved a better behaviour.

8.2 Tested parametrizations

The first five parametrizations are tested for the direct derivation sensitivity computation and for the solution of complete identification problems. The remaining parametrizations are tested together with the AVM, for both sensitivity and solution of inverse problems.

8.2.1 Basic linear deformation field

A linear perturbation field is described by a field of a constant deformation tensor plus a displacement of the field (6 parameters).

A definition of more physical meaning, in the sense that it comes from a deformation tensor, is the following:

$$\Theta^6_{ig} = \begin{bmatrix} 1 & 0 & x_2 & x_1 & x_1 & x_2 \\ 0 & 1 & -x_1 & x_2 & -x_2 & x_1 \end{bmatrix}$$

where $\mathbf{x} = \mathbf{x}^{real} - \mathbf{x}^{cg}$ (x with respect of the centroid of the flaw), i is the index for the direction and g is the index for the parameter vector P_g, which gives each parameter a clear sense:

$$P_g = \begin{bmatrix} \delta x_1^{cg} \\ \delta x_2^{cg} \\ \delta\omega \\ \delta\epsilon_m \\ \delta\epsilon' \\ \delta\epsilon_{12} \end{bmatrix} = \begin{bmatrix} \text{First coordinate of the centroid of the flaw} \\ \text{Second coordinate of the centroid of the flaw} \\ \text{Angle of rotation} \\ \text{Spheric strain} \\ \text{Horizontal elongation} \\ \text{Distortion} \end{bmatrix}$$

One may see that this parametrization is the complete linear deformation by decomposing it into a canonical set, in the sense that if we uncouple the directions i we can write the polynomial expansion of δx_i around the two dimensions x_1, x_2:

$$\delta x_1 = \begin{bmatrix} 1 & x_1 & x_2 & ... \end{bmatrix} \begin{bmatrix} \delta a_1^1 \\ \delta a_1^2 \\ \delta a_1^3 \\ ... \end{bmatrix} \qquad \delta x_2 = \begin{bmatrix} 1 & x_1 & x_2 & ... \end{bmatrix} \begin{bmatrix} \delta a_2^1 \\ \delta a_2^2 \\ \delta a_2^3 \\ ... \end{bmatrix}$$

$$\Theta_{ig}^6 = \begin{bmatrix} 1 & 0 & x_1 & 0 & x_2 & 0 \\ 0 & 1 & 0 & x_1 & 0 & x_2 \end{bmatrix}$$

and the corresponding parameters are,

$$P_g = \begin{bmatrix} \delta a_1^1 & \delta a_2^1 & \delta a_1^2 & \delta a_2^2 & \delta a_1^3 & \delta a_2^3 \end{bmatrix}^T$$

8.2.2 Fourier parametrization for cracks

Ideally, a crack should be able to be represented by a curved line with a higher order than just quadratic, in order to adopt for example the shape of an S.

Besides, a lower number of parameters should be used as only deformations in the sense of the normal should be needed, eliminating all the tangential components that would appear, in a field defined with more generality in the x and y direction.

A parametrization based on a Fourier series decomposition has the following advantages:

- The ends of the crack are straight in the limit (zero curvature), maintaining the $\sqrt{r}$ behaviour of the crack tips.
- A Fourier series is capable of representing any shape with a sufficient number of terms.
- It is very simple to add terms as the identification proceeds without need for redefining previous parameters, as would happen with Lagrange polynomials.
- Fourier series have good properties from the point of view of the regularization (see [96]).

The suggested parametrization is the following:

$$\Theta_{ig}^{crack} = \begin{bmatrix} 1-\xi & 0 & \xi & 0 & -\sin\alpha\sin 1\pi\xi & -\sin\alpha\sin 2\pi\xi & ... & -\sin\alpha\sin n\pi\xi \\ 0 & 1-\xi & 0 & \xi & \cos\alpha\sin 1\pi\xi & \cos\alpha\sin 2\pi\xi & ... & \cos\alpha\sin n\pi\xi \end{bmatrix}$$

where ξ is a normalized distance between the tips A and B, $\xi = \frac{(x_1-x_1^A)(x_1^B-x_1^A)+(x_2-x_2^A)(x_2^B-x_2^A)}{(x_1^B-x_1^A)^2+(x_2^B-x_2^A)^2}$ and $n = 1...\infty$. $-\sin\alpha$ and $\cos\alpha$ are the director cosines of the segment that joins the crack tips (see figure 8.3).

$$\Theta_{ig,k}^{crack} = \begin{bmatrix} -\frac{\partial\xi}{\partial x_k} & 0 & \frac{\partial\xi}{\partial x_k} & 0 & -\sin\alpha\cos n\pi\xi\frac{\partial\xi}{\partial x_k}... \\ 0 & -\frac{\partial\xi}{\partial x_k} & 0 & \frac{\partial\xi}{\partial x_k} & \cos\alpha\cos n\pi\xi\frac{\partial\xi}{\partial x_k}... \end{bmatrix}$$

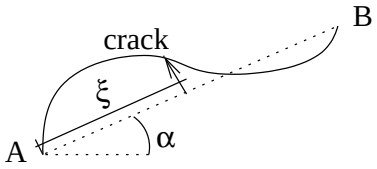

Figure 8.3: Definition of the crack parametrization.

8.2.3 2-point by 6 parametrization

This idea is based on a linear combination of two basic parametrizations of six variables each centered at two points. The linear combination is made proportional to the distance to each point.

$$\Theta_{ig}^{2point} = \Theta_{ig}^{6A}(1-\xi) + \Theta_{ig}^{6B}(\xi)$$

$$\Theta_{ig}^{2point} = \begin{bmatrix} 1-\xi & 0 & (x_2 - x_2^B)(1-\xi)... & \xi & 0 & (x_2 - x_2^B)(\xi)... \\ 0 & 1-\xi & -(x_1 - x_1^B)(1-\xi)... & 0 & \xi & -(x_1 - x_1^B)(\xi)... \end{bmatrix}$$

where the unitary distance $A-B$, $\xi = \frac{(x_1-x_1^A)(x_1^B-x_1^A)+(x_2-x_2^A)(x_2^B-x_2^A)}{(x_1^B-x_1^A)^2+(x_2^B-x_2^A)^2}$.

8.2.4 Polar Fourier parametrization

This idea comes from a generalization of a segment-wise polar parametrization used by other authors. This modification brings some advantages:

- It keeps continuity and infinite derivability at every formerly smooth point.
- A Fourier series capable of representing any shape with a sufficient number of terms.
- It is very simple to add terms as the identification proceeds without any need for redefining previous parameters, as would happen with Lagrange polynomials.

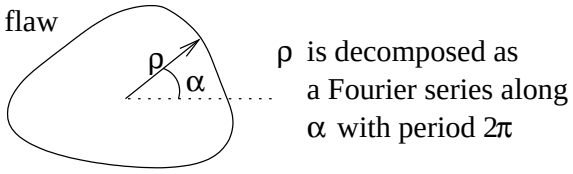

Figure 8.4: Definition of the Fourier polar parametrization.

The suggested parametrization is the following (see figure 8.4):

$$\Theta_{ig}^{crack} = \begin{bmatrix} 1 & 0 & \cos\alpha & \cos\alpha\sin 1\alpha & \cos\alpha\cos 1\alpha & \cos\alpha\sin 1\alpha & \cos\alpha\cos 1\alpha & ... & \cos\alpha\sin n\alpha & \cos\alpha\cos n\alpha \\ 0 & 1 & \sin\alpha & \sin\alpha\sin 1\alpha & \sin\alpha\cos 1\alpha & \sin\alpha\sin 1\alpha & \sin\alpha\cos 1\alpha & ... & \sin\alpha\sin n\alpha & \sin\alpha\cos n\alpha \end{bmatrix}$$

where $n = 1...\infty$.

8.2.5 Uncoupled quadratic field

By expanding the canonical set up to the second order, we obtain the following base with 12 parameters,

$$\Theta_{ig}^{12} = \begin{bmatrix} 1 & 0 & x_1 & 0 & x_2 & 0 & x_1x_2 & 0 & x_1^2 & 0 & x_2^2 & 0 \\ 0 & 1 & 0 & x_1 & 0 & x_2 & 0 & x_1x_2 & 0 & x_1^2 & 0 & x_2^2 \end{bmatrix}$$

8.2.6 Element-wise parametrization for cracks

This is based on the principle that the variation of the geometry of a crack is best defined in detail by $n_n + 2$ parameters, being n_n the number of nodes. The way they are chosen is shown in figure 8.5, aiming n parameters at the movement of the nodes perpendicularly to themselves, and 2 at the lengthening of the crack at each tip.

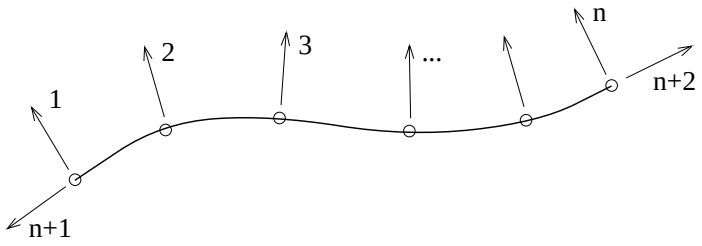

Figure 8.5: Elementary parametrization

The parameter matrix Θ_{ig} can be defined as,

$$\Theta_{ig} = \sum_g \phi_g n_i^+ \qquad 1 \leq g \leq n$$

$$\Theta_{i,n+1} = \phi^a \nu_i, \Theta_{i,n+2} = \phi^b \nu_i \qquad \text{for the tip growth parameters}$$

where n_i^+ and ν_i are the upper normal and tangent vectors (see 6.1). As shown in figure 8.6, ϕ_g is the set of quadratic shape functions of value 1 at node g and 0 elsewhere. ϕ^a and ϕ^b are linear shape functions that have value 1 at the corresponding node and decreases to zero at the opposite one. All these functions have null value outside the varying crack (i.e. at known boundaries and at further possible unknown cracks, which would be defined with another similar set of parameters).

We reduce the number of nodal parameters to one for every middle node, giving $n_e + 2$ parameters (n_e is the number of elements). Hence we avoid the possibility of curved crack end elements. The combination of shape functions eventually used to ensure C^1 variation and straight tip elements are displayed in figure 8.6.

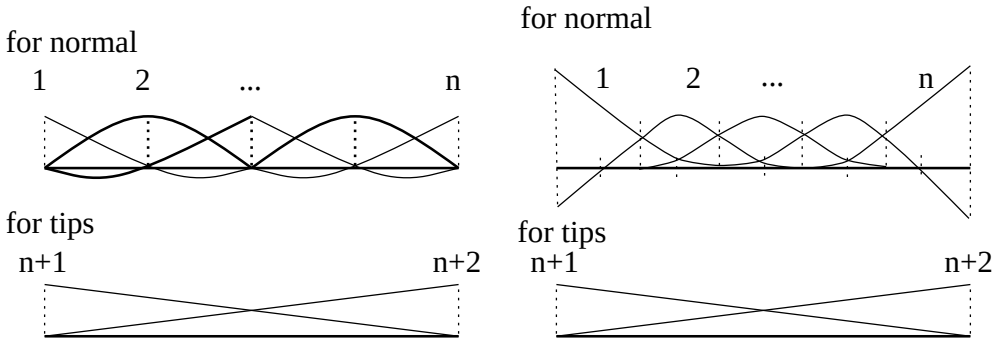

Figure 8.6: Shape functions for nodal parametrization (left) and elementary parametrization (right).

For the simplified case of a regular initial mesh (with a constant jacobian), the relationship between both sets of parameters is defined by the following $n_e + 2$ by $n_n + 2$ matrix. There are more complicated methods for general cases, as a modification of this one, the Overhouser elements, [131], or the use of different types of splines [77]. The two latter increase the order of interpolation

to cubic.

$$T = \frac{1}{8}\begin{pmatrix} 12 & 10 & 4 & 1 & 0 & 0 & 0 & 0 & \dots & 0 & 0 & 0 & 0 & 0 & 0 \\ -4 & -2 & 4 & 6 & 4 & 1 & 0 & 0 & \dots & 0 & 0 & 0 & 0 & 0 & 0 \\ 0 & 0 & 0 & 1 & 4 & 6 & 4 & 1 & \dots & 0 & 0 & 0 & 0 & 0 & 0 \\ 0 & 0 & 0 & 0 & 0 & 1 & 4 & 6 & \dots & 0 & 0 & 0 & 0 & 0 & 0 \\ \dots & \dots & \dots & \dots & \dots & \dots & \dots & \dots & \dots & \dots & \dots & \dots & \dots & \dots & \dots \\ 0 & 0 & 0 & 0 & 0 & 0 & 0 & 0 & \dots & 6 & 4 & -2 & -4 & 0 & 0 \\ 0 & 0 & 0 & 0 & 0 & 0 & 0 & 0 & \dots & 1 & 4 & 10 & 12 & 0 & 0 \\ 0 & 0 & 0 & 0 & 0 & 0 & 0 & 0 & \dots & 0 & 0 & 0 & 0 & 1 & 0 \\ 0 & 0 & 0 & 0 & 0 & 0 & 0 & 0 & \dots & 0 & 0 & 0 & 0 & 0 & 1 \end{pmatrix}$$

8.2.7 Extension to superimposed mesh

We suggest an intermediate and very general solution with the benefits of the increased number of parameters of the elementary parametrization and the convergence towards zero of the error with an enhacement of the discretization. This method consists basically in defining two superimposed but independent meshes for the parametrization and for the model, having the desired number of parameters $= n_e^{parametrization} + 2$ and a sufficient smooth mesh to ensure a good calculation (n_e^{model}).

We made a consideration to simplify greatly the implementation and ensuring a better behaviour, which consists of defining the superimposed mesh as a combination of the model mesh. Hence, this is defined on the basis of the elementary parametrization by defining new set of h parameters that depend on the g elementary parameters by,

$$\Theta_{ih}^{par} = \sum_j \phi_h^{par}(x_j)\Theta_{ij}^{model}(x_j)$$

$$\Theta_{i,tips}^{par} = \Theta_{i,tips}^{model} \qquad \text{for the tip growth parameters}$$

This means that there is a matrix S_{hj} that allow to $\delta x_{ih}^{par} = S_{hj}\Theta_{ij}^{model}$. Thus, in the AVM calculation, the nodal parameter vector is expressed in terms of the parameters of the superimposed mesh as $P_k^{nod} = S_{hj}T_{jk}P_h^{superimposed}$, and the gradient of this parametrization is expressed in terms of the nodal one as $L_k^{nod} = S_{hj}T_{jk}L_h^{superimposed}$.

It is possible to represent all of these parametrizations and many others in terms of the elementary parametrization, simplifying the programming tasks, and giving a sense of generality and modularity to the method.

Chapter 9

Sensitivity to material properties

Closely related to the IIP is the *material identification problem* (MIP) where the unknowns are the physical constants of the material (mechanical, electrical,... depending on the application) on the whole domain or a part of it (an inclusion for instance). Finite difference techniques have been successfully applied by e.g. Schnur et al. [105] and Yuan et al. [135], and the adjoint variable method by Constantinescu et al. [31].

The derivation and evaluation of the corresponding singular and hypersingular integral equations is much simpler for the case of the material properties. The structure of a the inverse problem is very similar as above, but using the value of the different material properties of each material used as a parameter. This vector of parameters can be appended to the vector of geometrical parameters. A global scaling of geometrical and mechanical values should prevent from any problems related to ill conditioning related to this coupling.

The derivatives of the BIEs are simply carried out directly under the integral symbol, since this and the derivative can be interchanged.

It should be noted that the following formulation has not been tested.

9.1 Derivative of integral equations

The two equations to derive are the singular and hypersingular ones, evaluated at smooth points:

ubie:

$$c_k^i u_k(\xi) + \int_\Gamma \left\{ q_k^i u_k(x) - u_k^i q_k(x) \right\} d\Gamma(x) = 0 \tag{9.1}$$

qbie:

$$c_k^i q_k(\xi) + \int_\Gamma \left\{ t_{jkl}^i n_j(\xi) n_l(x) u_k(x) - d_{jk}^i n_j(\xi) q_k(x) \right\} d\Gamma(x) = 0 \tag{9.2}$$

Taking into account how the only material dependent terms vary with respect to a material variable m:

$$\begin{aligned}
\tilde{u}_b^a &= u_b^a + \frac{du_b^a}{dm}\delta m + hot. \\
\tilde{u}_{b,c}^a &= u_{b,c}^a + \frac{du_{b,c}^a}{dm}\delta m + hot. \\
\tilde{u}_{b,cd}^a &= u_{b,cd}^a + \frac{du_{b,cd}^a}{dm}\delta m + hot. \\
\tilde{\sigma}_{bc}^a &= \sigma_{bc}^a + \frac{d\sigma_{bc}^a}{dm}\delta m + hot. \\
\tilde{\sigma}_{bc,d}^a &= \sigma_{bc,d}^a + \frac{d\sigma_{bc,d}^a}{dm}\delta m + hot.
\end{aligned}$$

One may get, substituting and subtracting the altered and original equations:
$\delta ubie_m$:

$$c_k^i \delta u_k + \int_\Gamma \{\sigma_{jk}^i n_j(x)\delta u_k - u_k^i \delta q_k + \frac{d\sigma_{jk}^i}{dm} n_j(x) u_k \delta m - \frac{du_k^i}{dm} q_k \delta m \Big\} d\Gamma = 0 \tag{9.3}$$

$\delta qbie_m$:

$$c_k^i \delta q_k + \int_\Gamma \{t_{jkl}^i n_j(\xi) n_l(x)\delta u_k - d_{jk}^i n_j(\xi)\delta q_k + \frac{t_{jkl}^i}{dm} n_l(x) n_j(\xi) u_k \delta m - \frac{d_{jk}^i}{dm} n_j(\xi) q_k \delta m \Big\} d\Gamma = 0 \tag{9.4}$$

9.2 Numerical treatment

The terms can be grouped after the discretization, the definition of the vector $m = \{m_m\}$ of m material parameters, and the formation of the system of equations as,
$\delta ubie_m$:

$$\begin{aligned} c_k^i \delta u_k + \int_\Gamma \{\sigma_{jk}^i n_j(x)\delta u_k - u_k^i \delta q_k\} d\Gamma &= {}^m U_m^i(\xi)\delta m_m \\ {}^m U_m^i(\xi) = -\frac{dc_k^i}{dm_m} u_k &+ \int_\Gamma \left\{ \frac{du_k^i}{dm_m} q_k - \frac{d\sigma_{jk}^i}{dm_m} n_j(x) u_k \right\} d\Gamma \end{aligned}$$

$\delta qbie_m$:

$$\begin{aligned} c_k^i \delta q_k + \int_\Gamma \{t_{jkl}^i n_j(\xi) n_l(x)\delta u_k - d_{jk}^i n_j(\xi)\delta q_k\} d\Gamma &= {}^m Q_m^i(\xi)\delta m_m \\ {}^m Q_m^i(\xi) = -\frac{dc_k^i}{dm_m} q_k &+ \int_\Gamma \left\{ \frac{d_{jk}^i}{dm} n_j(\xi) q_k - \frac{t_{jkl}^i}{dm} n_l(x) n_j(\xi) u_k \right\} \end{aligned}$$

In the case of a smooth collocation point, $\frac{dc_k^i}{dm_m}$ is null. The complete definitions of every weight and kernel can be found in the appendix.

The equations are again organized with the known data u_k and q_k, the measured data δu_k and δq_k to the right hand side coefficient matrix, and δm as a vector with all the material properties values at each material conforming the model.

$$A\delta u = {}^m\Delta \delta m$$

During an iteration, the system matrix A including the boundary conditions has already been computed and factorized for the direct problem. As in the case of identification IP, the solutions of the latter system for each column of ${}^m\Delta$ can be performed and grouped into ${}^m J$, so that it accomplishes,

$$\delta u = {}^m J \delta m \quad \Rightarrow \quad {}^m J = \frac{du}{dm}$$

The iterative process will imply the recalculation of the direct problem with the new material properties defined as $m^{k+1} = m^k + \delta m^k$ at iteration k.

Chapter 10

Topological derivative

The concept of topological derivative consists in the infinitesimal variation of the response when an infinitesimal flaw appears. This "derivative" can be seen as the first order term in the variation due to the sought flaw, and therefore a good approximation for small flaws in comparison to the specimen dimensions:

$$u(A_{flaw}) \quad = \quad u(0) + \frac{du(0)}{dA}\delta A + O(\delta A^2) \tag{10.1}$$

where $u(A)$ is the mechanical response when a flaw of volume A exists ($A = 0$ means no flaw, and therefore no discretization or modelization of it, and $A = A_{flaw}$ means the real flaw). The magnitude A is of the order r^n in $\Re^n$.

Very few works have been found in relationship with this idea. Theoretical work on elliptical equations and synthetic overviews appeared recently from Sokolowski [109], [108] (dealing with the topological derivative of energy in potential) and Masmoudi [81] (for the sensitivity to move an infinitesimal part of the domain at the boundary).

10.1 Boundary integral equation

The topological derivative is computed considering a modified state that contains an infinitesimal cavity. Since this cavity is small, the variables along its boundary can be computed by series approximations in terms of their values at the center of the cavity. A linearization and integration on the vanishing boundary of the ensuing expressions leads to the following definition.

In this chapter the expression of the topological derivative for a vanishing circular cavity and a crack is presented, but more general forms are dealt with elsewhere (see Gallego and Rus [47]).

In a homogeneous domain Ω whose exterior boundary is Γ_e, and subject to a static load, consider the appearance of a stress free circular cavity centered at point $\mathbf{z}$ and defined by its boundary Γ_z (see figure 10.1).

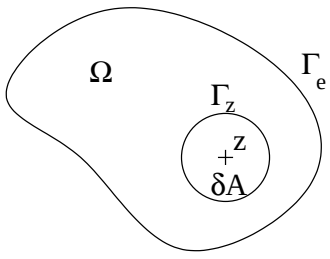

Figure 10.1: Boundaries for the topological derivative.

The standard boundary integral equation of the BEM can be split into the two boundaries Γ_e and Γ_z:

$$c_k^i(\boldsymbol{\xi})u_k(\boldsymbol{\xi}) + \int_{\Gamma_e} \left[q_k^i(\boldsymbol{\xi},\mathbf{x})u_k(\mathbf{x}) - u_k^i(\boldsymbol{\xi},\mathbf{x})q_k(\mathbf{x})\right] d\Gamma(\mathbf{x}) + \int_{\Gamma_z} \left[q_k^i(\boldsymbol{\xi},\mathbf{x})u_k(\mathbf{x}) - u_k^i(\boldsymbol{\xi},\mathbf{x})q_k(\mathbf{x})\right] d\Gamma(\mathbf{x}) = 0$$

On the second integral (inside the flaw) we assume that there is no stress ($q_k = 0$). We also study the value of $u_k(\mathbf{x})$: it can be split into the sum of a rigid solid motion (a single common displacement u_k^{solid}) plus a deformation along $\mathbf{x}$ with respect to the former displacement. For some choice of rigid solid motion, the latter component can further be assimilated to the deformation $u_k^{infinite}(\mathbf{x})$ of a flaw in an infinite medium subject to a constant stress state at the infinite σ_{ij} (see figure 10.2). This assumption is valid as long as the flaw is small enough, or conversely, far enough from any external boundary or variation of the stress field from σ_{ij}. Hence,

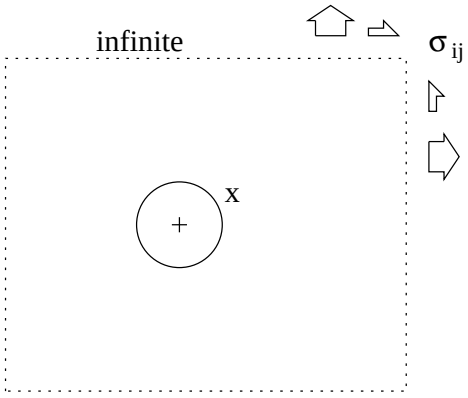

Figure 10.2: A small flaw in a big medium and constant stress field.

$$u_k(\mathbf{x}) = u_k^{solid} + u_k^{infinite}(\mathbf{x}) + hot.$$

Finally, $q_k^i(\boldsymbol{\xi},\mathbf{x}) = \sigma_{jk}^i(\boldsymbol{\xi},\mathbf{x})n_j(\mathbf{x})$, where $\sigma_{jk}^i(\boldsymbol{\xi},\mathbf{x}) = \sigma_{jk}^i(\boldsymbol{\xi},\mathbf{z}) + hot.$ The second integral turns therefore:

$$\begin{aligned}\int_{\Gamma_z} \left[q_k^i(\boldsymbol{\xi},\mathbf{x})u_k(\mathbf{x}) - u_k^i(\boldsymbol{\xi},\mathbf{x})q_k(\mathbf{x})\right] d\Gamma(\mathbf{x}) &= \int_{\Gamma_z} \left[\sigma_{jk}^i(\boldsymbol{\xi},\mathbf{x})n_j(\mathbf{x})u_k(\mathbf{x})\right] d\Gamma(\mathbf{x}) \\ &= \sigma_{jk}^i(\boldsymbol{\xi},\mathbf{z}) \int_{\Gamma_z} \left[n_j(\mathbf{x})(u_k^{solid} + u_k^{infinite}(\mathbf{x}) + hot.)\right] d\Gamma(\mathbf{x}) \\ = \sigma_{jk}^i(\boldsymbol{\xi},\mathbf{z})u_k^{solid} \int_{\Gamma_z} \left[n_j(\mathbf{x})\right] d\Gamma(\mathbf{x}) &+ \sigma_{jk}^i(\boldsymbol{\xi},\mathbf{z}) \int_{\Gamma_z} \left[n_j(\mathbf{x})u_k^{infinite}(\mathbf{x})\right] d\Gamma(\mathbf{x}) + hot.\end{aligned}$$

The first integral $\int_{\Gamma_z} [n_j(\mathbf{x})]\, d\Gamma(\mathbf{x})$ is exactly zero, meaning that the rigid solid motion of a flaw does not affect the integral. The second integral can be solved analytically substituting in $u_k^{infinite}(\mathbf{x})$ the analytical solution of the flaw in the infinite medium. This has been done of the case of a circle and a crack (see figure 10.3), yielding the tensor $-K_{jk}(z^z)$ defined later.

In conclusion, generalizing to several circular cavities centered at a set of points z^z,

$$c_k^i(\xi)\delta u_k(\xi) + \int_{\Gamma} \left[q_k^i(x,\xi)\delta u_k(x) - u_k^i(x,\xi)\delta q_k(x)\right] d\Gamma(x) = {}^tU_z^i(z^z;\xi)\delta A_z \tag{10.2}$$

where,

$${}^tU_z^i(z^z;\xi) = \sigma_{jk}^i(z^z;\xi)K_{jk}(z^z)$$

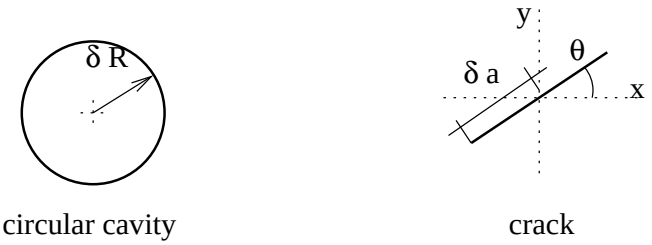

Figure 10.3: Description of cavity and ccrack.

The size parameter δA_z has the following definition for each case (see figure 10.3):

$$\delta A_z = \begin{cases} \pi \delta R^2 & \text{for a circular cavity} \\ \delta a^2 & \text{for a straight crack} \end{cases} \tag{10.3}$$

- In the case of a circular cavity, $K_{jk}(z^z)$ has the value,

$$\begin{pmatrix} K_{11} & K_{12} \\ K_{21} & K_{22} \end{pmatrix} = \frac{1}{E} \begin{pmatrix} 3\sigma_{11} - \sigma_{22} & 4\sigma_{12} \\ 4\sigma_{21} & 3\sigma_{22} - \sigma_{11} \end{pmatrix} \tag{10.4}$$

- In the case of a crack, $K_{jk}(z^z)$ is,

$$\begin{pmatrix} K_{11} & K_{12} \\ K_{21} & K_{22} \end{pmatrix} = \frac{2\pi(1-\nu^2)}{E} \begin{pmatrix} -\sigma_{12}^{'} \sin\theta\cos\theta + \sigma_{11}^{'} \sin\theta^2 & -\sigma_{11}^{'} \sin\theta\cos\theta - \sigma_{12}^{'} \sin\theta^2 \\ -\sigma_{11}^{'} \sin\theta\cos\theta + \sigma_{12}^{'} \cos\theta^2 & +\sigma_{12}^{'} \sin\theta\cos\theta - \sigma_{11}^{'} \cos\theta^2 \end{pmatrix} \tag{10.5}$$

where, in turn, $\sigma_{ij}^{'}$ is the local stress on the crack reference system:

$$\begin{aligned} \sigma_{11}^{'} &= \frac{\sigma_{11} + \sigma_{22}}{2} + \frac{\sigma_{22} - \sigma_{11}}{2} \cos 2\theta - \sigma_{12} \sin 2\theta \\ \sigma_{12}^{'} &= \frac{\sigma_{22} - \sigma_{11}}{2} \sin 2\theta + \sigma_{21} \sin 2\theta \end{aligned}$$

10.2 Numerical implementation

The discretization of the 10.2 leads to,

$$\mathbf{A}\delta\mathbf{v} = {}^t\Delta\delta A \tag{10.6}$$

where $\mathbf{A}$ is the same system matrix than for the direct problem and $\delta\mathbf{v}$ groups the variation values corresponding to the non prescribed displacement and stress vectors. ${}^t\Delta = {}^tU$ is the matrix $n \times m$ where n are the collocation points (number of equations in the direct problem) and m is the number of estimated flaws. $\delta\mathbf{A}$ is a vector with the volumes of these flaws. Solving $\mathbf{A}$ for each column of ${}^t\Delta$ we can define the derivative ${}^t\mathbf{J}$,

$$\mathbf{A}\,{}^t\mathbf{J} = {}^t\Delta \qquad \Rightarrow \qquad {}^tJ = \{{}^tj_{iz}\} = \frac{dv_i}{dA_z} \tag{10.7}$$

10.3 Procedure for the solution

The identification procedure can hence be structured as follows. The difference between the measured response $\mathbf{v}^{exp}$ and the computed one without flaw $\mathbf{v}^0$ is called $\delta\mathbf{v}$. The sought variables are stored in vector $\mathbf{x}$ (including all the centroids z^z and angles in the case of cracks). Any minimization algorithm can be used to search $\mathbf{x}$ that minimizes the cost function f defined as $f = \frac{1}{2}\mathbf{R}^T\mathbf{R}$ (giving

a the sense of the minimum distance of the residuals, or the highest similarity in the response), where the residual is,

$$\mathbf{R} = \mathbf{v}(\mathbf{A}) - \mathbf{v}^{exp} \approx v^0 + \frac{d\mathbf{v}(0)}{d\mathbf{A}}\delta\mathbf{A} - \mathbf{v}^{exp} = \delta\mathbf{v} + {}^t\mathbf{J}(\mathbf{x})\delta\mathbf{A}(\mathbf{x}) \tag{10.8}$$

At this point $\delta\mathbf{A}(x)$ can be optimized directly in order to minimize f for the given $\mathbf{x}$, by means of its linearity, through least squares:

$$\delta\mathbf{A}(x) = ({}^t\mathbf{J}(\mathbf{x})^T {}^t\mathbf{J}(\mathbf{x}))^{-1} {}^t\mathbf{J}(\mathbf{x})\delta\mathbf{v} \tag{10.9}$$

This method is very useful for the following reasons,

- The direct problem (computation of $\mathbf{v}$ and $\mathbf{A}$) is only done once for the whole search.
- Each iteration is extremely cheap in comparison with the solution of a direct problem, since:
  - $\mathbf{A}$ is already factorized and ready for substitution.
  - $K_{jk}(\mathbf{z}^z)$ basically needs to compute the value of the stress at points $\mathbf{z}^z$. This is the most time consuming step.
  - The evaluation of $\sigma^i_{jk}(\mathbf{z}^z;\xi)$ is immediate.
- The number of parameters to search is drastically reduced since $\delta\mathbf{A}$ is computed in the inner step, and only the centroid (and angle) of each flaw are allowed to vary.

The ability to easily search several simultaneous flaws gives the possibility of searching a undefined number of faults by allowing for a number of flaws in excess, and letting the non existing flaws vanish by themselves. This intuitive principle has earlier been suggested under the name of "bubble" technique, and was tested in [113] when comparing between the zero-one technique (absolute existence or nonexistence), in another context.

Chapter 11

The solution of the Inverse Problem

An overview of the most used methods in the literature for this task is presented in chapter 4. In this work the Levenberg-Marquardt method is mainly used to minimize the least squares sum of a residual vector with the gradient provided by Direct Differentiation, after having tested the Gauss-Newton and BFGS too. The minimization of the cost functional, derivated by the Adjoint Variable Method is minimized with the BFGS method.

An interesting unification of the strategies referenced in chapter 4, not seen by many authors, is explained at the end of this chapter.

11.1 Minimization algorithms

The approximate classification of the usual methods for IP solution depending on the scope of the convergence is recalled from chapter 4.2. 11.1.

Global	Local	Setup
	Techniques for Nonlinear Systems of Equations	Observation Equations
	Optimization algorithms (Gauss−Newton, Quasi−Newton, Secant, Least−Squares)	Minimization of cost functional
	Linear and Quadratic Programming Kalman filter, Proyection filter	
Genetic and Evolutionary Algorithms Neural Networks; fuzzy inference Random search Simmulated Annealing		
Topological Derivative		Initialization

Figure 11.1: A classification of IP strategies.

A description of the main unconstrained minimization methods follows, most of which have been used in the present work (see Rus and Gallego [101]).

11.1.1 Mathematical programming

The natural evolution of the currently available methods from the most simple to the most sophisticated ones is exposed here. A good survey on them was carried out by Dennis and Schnabel [64],

and others [97], [63].

The only methods tested for having chances to be best in our Identification IP were the BFGS, Gauss-Newton, damped Gauss-Newton and Levenberg-Marquardt methods.

Newton's method

By a multivariable Taylor series expansion until the second term, we can define an affine model of $f(x) : \Re^n \to \Re$ as,

$$m_c(x_c + p) = f(x_c) + \nabla f(x_c)^T p + \frac{1}{2} p^T \nabla^2 f(x_c) p + h^T h\epsilon(p)$$

where[1]

$\nabla_i f = \frac{\partial f}{\partial x_i}$ is the gradient.

$\nabla^2_{ij} f = \frac{\partial^2 f}{\partial x_i \partial x_j}$ is the Hessian, which will be symmetric if twice continuous differentiable.

The error will be bounded by,

$$\frac{1}{2} p^T (\nabla^2 f(z) - \nabla^2 f(x_c)) p \leq \frac{\gamma}{6} \parallel p \parallel^3$$

and γ is the Lipschitz constant.

If the gradient and the Hessian are not available, they are best calculated with the approximations,

$$\nabla f \simeq \frac{f(x+he_i) - f(x-he_i)}{2h} \qquad error \leq \frac{\gamma}{6} h^2 \tag{11.1}$$

$$\nabla^2 f \simeq \frac{f(x+he_i+he_j) - f(x-he_i) - f(x-he_j) + f(x))}{h^2} \qquad error \leq \frac{5\gamma h}{6} \tag{11.2}$$

For a good numerical computation, the perturbation should be chosen of the order $h_j \approx$ (machine epsilon)$^{\frac{1}{3}} max\{\mid x_j \mid, \text{typical } x_j\} sign(x_j)$.

The necessary conditions for the minimization are that $\nabla f = 0$ and $\nabla^2 f$ is positive semidefinite. The sufficient condition for x to be the minimum is that $\nabla^2 f$ is positive definite (which implies a convex geometry for the hypersurface f).

Newton's method consists in an iterative method in which from a starting guess x_k we repeat the following,

$$\nabla^2 f(x_k) s_k = -\nabla f(x_k) \tag{11.3}$$

$$x_{k+1} = x_k + s_k \tag{11.4}$$

The interesting property for us is that this method is locally q-quadratically convergent, i.e., $\mid x_{k+1} - x_k \mid \leq c_k \mid x_k - x_* \mid^2$.

Quasi-Newton method

This method comes after redefining the Hessian of the former method, and reads,

1. Compute $\nabla f(x_k)$
2. Compute $H_k = \nabla^2 f(x_k)$

[1] Note that other possible notation for the expansion is,

$$m_c(x_c + p) = f(x_c) + < \nabla f(x_c), p > + \frac{1}{2} < \nabla^2 f(x_c) p, p > + < p, p > \epsilon(h)$$

3. Factorize H_k and calculate the condition number. If it is ill-conditioned, perturb ($H_k = \nabla^2 f(x_k) + \mu_k I$, with $\mu_k <$ minimum eigenvalue).

4. $H_k s_k = -\nabla f(x_k)$

5. $x_{k+1} = x_k + s_k$ or choose x_{k+1} with a global strategy.

Line search is the most immediate of the so called global strategies (which here mean a somewhat larger scope, still far from the whole domain). The idea is that the step s_k given by any of the optimization algorithms may not lead to a better point (which often happens for big values of s_k), but it is possible to guarantee that, since the direction of s_k has a negative gradiend, a better solution can be found in the line defined by that direction. It is defined as $x_{k+1} = x_k + \lambda_k s_k$. It may be controlled by imposing two conditions that will define a permissible region (calling here $g(\lambda) = f(x + \lambda p)$):

$$g(\lambda) \leq g(0) + \alpha \lambda g'(0) \tag{11.5}$$

$$g'(\lambda) \geq \beta g'(0) \qquad \beta > \alpha \tag{11.6}$$

The exact value of λ is chosen in a backtracking algorithm, based on the information of the already evaluated points. Depending on the number of them and their relative relationships, there are dozens of different more or less heuristic algorithms, which use quadratic, cubic or mixed models of the line, when not bisection of any other technique. These are not described here (see [63]).

Model-trust region is the other big family of global strategies. They modify H_k instead of λ_k such that $s_k \leq \delta_c$, i.e. s_k is within the trust radius δ_c. Primarily, the step may be chosen by the "hook" step (by $(H_c + \mu I)s(\mu) = -\nabla f(x_c)$), or, as in our case, by the double dogleg step, which is the point located at a distance δ_c of the line joining the Newton solution ($-H^{-1}\nabla f$) with the Cauchy solution ($\frac{-\nabla f}{\|f\|}$). Secondly, the trust region can be reduced by yet another backtracking of $f(x_+) \leq f(x_c) + \alpha \nabla f(x_+ - x_c)$.

Secant methods

Broyden's method, or the secant update method for unconstrained minimization, is computed through the following steps,

1. $y_{k-1} = \nabla f(x_k) - \nabla f(x_{k-1})$

2. $H_k = H_{k-1} + \frac{(y_{k-1} - H_{k-1} s_{k-1}) s_{k-1}^T}{s_{k-1}^T s_{k-1}}$

3. $H_k s_k = -\nabla f(x_k)$

4. $x_{k+1} = x_k + s_k$

The main advantage of these methods is that they do not require a calculation of the Hessian. One theoretical explanation of the behavior of the method is that this update of the Hessian involves the minimum change in the Frobenius norm of the affine model. The practical interesting property of the method is that it converges q-superlinearly ($| x_{k+1} - x_k | \leq c_k | x_k - x_* |$).

For the initialization of the method, taking $H_0 = I$ uses to be a good choice. In this case, the first iteration will become equal to the steepest descent.

During the second step, which is the secant update, two numerical techniques can be used to perform this calculation, which can be interesting for bigger problems. The first one is a factorization, that makes the computation faster, and the second one consists of working with the inverse of the hessian directly, for the use with the third step.

There are other updates, such as the Powell-Symmetric-Broyden update, the Davidon-Fletcher-Powell update, and the Inverse-Positive-Definite-Secant update. But the practice has stated the

Broyden-Fletcher-Goldfarb-Shanno (BFGS) or Positive-Definite-Secant update as the best option. Then, the update is made using,

$$H_k = H_{k-1} + \frac{y_{k-1}y_{k-1}^T}{y_{k-1}^T s_{k-1}} + \frac{H_{k-1}s_{k-1}s_{k-1}^T H_{k-1}}{s_{k-1}^T H_{k-1} s_{k-1}}$$

Gauss-Newton method

This is not a further development of the former method, but another family that takes advantage of the structure of the nonlinear least squares. Since $f = \frac{1}{2}R^T R$, and calling $J = J_{ij} = \frac{\partial R_i}{\partial x_j}$, then $\nabla f = J^T R$; $\nabla^2 f = J^T J + \sum_i R_i \nabla^2 R_i$. If the residual tends to zero at the optimum ($R \to 0$) and R is not too nonlinear, we can neglect the second term of the hessian definition and write,

1. $J_k^T J_k s_k = -J_k^T R_k$
2. $x_{k+1} = x_k + s_k$

This algorithm converges quick q-linearly and even q-quadratically for a zero-residual problem. The disadvantage is that it is not necessarily globally convergent, and that it is not well defined if J does not have full column rank.

To overcome this there are two possible modifications:

Damped Gauss-Newton

1. $J_k^T J_k s_k = -J_k^T R_k$
2. $x_{k+1} = x_k + \lambda_k s_k$

where λ_k is calculated with a line search similar to the ones described above. This makes the method globally convergent.

Levenberg-Marquardt or Trust Region Approach

1. $(J_k^T J_k - \mu_k I)s_k = -J_k^T R_k$ subject to $\| x_{k+1} - x_k \|_2 \leq \delta_k$
2. $x_{k+1} = x_k + s_k$

This is performed as described above in the Model-Trust region. This improves the behaviour of the algorithm for J with not full column rank, and for big second terms $\sum_i r_i \nabla^2 r_i$. A line search can be added on this method, $x_{k+1} = x_k + \lambda_k s_k$.

There is yet another method in which the second term $\sum_i r_i \nabla^2 r_i$ is approximated by a secant approximation update (A) and included in the algorithm,

1. $A_k = A_{k-1} + \frac{(y_{k-1}^{II} - A_{k-1}s_{k-1})y_{k-1}^T + y_{k-1}(y_{k-1}^{II} - A_{k-1}s_{k-1})^T}{y_{k-1}^T s_{k-1}} -$
   $- \frac{<y_{k-1}^{II} - A_{k-1}s_{k-1}, s_{k-1}> y_{k-1}y_{k-1}^T}{(y_{k-1}^T s_{k-1})^2}$ where $y_{k-1}^{II} = A_k s_{k-1}$
2. $(J_k^T J_k + A_k)s_k = -J_k^T R_k$
3. $x_{k+1} = x_k + s_k$

Filtering

These methods, originally developed for linear inversion, are aimed at incorporate information about the noise in the measurements (basically shortening the step depending on that noise), and the error in the measurements (putting more weight on the safer data). Although not originally developed and grouped with the preceding algorithms, these methods are coincident with Gauss-Newton in the case of zero and identity covariance matrices Q and M respectively. These methods have not been implemented with explicitly known covariance data.

Some interesting applications of Kalman filter were done by Tanaka et al. [123], [124], Tosaka [129] or Suzuki et al. [115].

Extended Kalman filter. If a covariance matrix Q of the white measurement noise with zero mean is given, and the error covariance of the measurements is M, the algorithm reads:

1. $s_k = -[MJ_k^T(J_kMJ_k^T + Q)^{-1}]R_k$
2. $x_{k+1} = x_k + s_k$

The matrix $[MJ_k^T(J_kMJ_k^T + Q)^{-1}]$ is called filter gain.

Proyection filter

1. $s_k = -[(J_k^TQ^+J_k)^{-1}J_k^TQ^T]R_k$
2. $x_{k+1} = x_k + s_k$

where the superscript + denotes the Moore-Penrose generalized inverse of a matrix.

Among other tested techniques, simulated annealing is used to stabilize the convergence process ([75]), and linear and quadratic programming enclose efficient techniques for the addition of constraints to local optimization algorithms.

11.1.2 Soft computing

Random search

This lies in solving the direct problem a number of times, each one with a different supposed configuration chosen randomly.

Genetic and Evolutionary algorithms

One way to increase the efficiency of this and make it usable is through genetic algorithms (GA), or evolutionary algorithms (in the case of real coding instead of gray coding). The main advantages of this is the safety in the convergence, but the disadvantage is the enormous computing time required.

Many specialized references can be found (Goldberg [52]), and among the attempts to identify shapes with Boundary elements, one may cite [71], [41], [125], [113], [112] or [111].

Within the framework of genetic optimization, the set of parameters (x, "phenotype") is encoded as a chain of variables ("chromosomes"). Furthermore, due to the stochastic nature of this approach, a population of test flaws ("individuals") is assumed. For each set, the error function ($e(x) = -\log\sum(u^{computed} - u^{exp})^2$ has been implemented in our case) is calculated and transformed into a "fitness" to be maximized.

The problem is further inspired by Darwin's principle of survival through natural selection. In the "selection" step, individuals with better fitness values are given a higher probability to be mated and to inherit their characteristics to the next generation. A "crossover" operator permits parts of the encoding string of the parents to be exchanged within the reproduction step. Finally, arbitrary parts of the information are changed at random ("mutation") during the creation of the new generation. Sometimes very good individuals are allowed to pass through the whole procedure unchanged ("elitism"), i.e., they are copied as they are in the following generation.

Besides the facility to paralellize the computation, many other enhanced variants of the basic genetic algorithm described can be taken into account, such as dominance-diploidy-abeyance (number of chromosomes and the genotype to phenotype mapping), reordering (a mutation consisting in e.g. an inversion of alleles), segregation/translocation, duplication/deletion, sexual differenciation, speciation, multiobjective optimization (Pareto optimality: $(x < py) \Leftrightarrow (\forall i)(x_i \leq y_i)\&(\exists i)(x_i < y_i)$), knowledge-based techniques, hybtid schemes (involving a local search in the place of each function evaluation), or more sophisticated climbing algorithms, or struggling ones.

Neural networks

An artificial neural network is composed if a certain number of processing elements which are highly interconnected into a specified pattern and hierarchy. If to a given set of input data the corresponding wished output data are known, the whole set of input-output learning paradigms can be used to train the network (i.e. to adjust the variables which govern its behaviour) such as to be able to reconstruct the implicit highly nonlinear mapping between input and output variables.

Let us consider a simple processing element ("perceptron") where a given input vector x is transmitted to the processing unit j from a number of input nodes i through connection lines with synaptic weights w_{ij}. The signal received by the processing unit (node j) reads $r_j = \sum_i x_i w_{ij}$. The signal is processed in unit j through an activation function f_j to produce an output (response) $z_j = f_j(r_j)$.

Now, if a set of input-output paradigms $[x, y]$ is given, the weights w_{ij} can be adapted so that they represent the $[x, y]$ relation. A simple "Hebbian" error driven iterative learning technique reads $w_{ij}^{(k)} = w_{ij}^{(k-1)} + \eta_i (y - z^{(k)}(x)) x_i^{(k)}$, where η_i is the learning rate at iteration k. This simple "adaptive linear combiner" is enhanced by a multilayer connection in a hierarchical structure, making the resulting neural network capable of dealing with much more complicated objects.

The final goal is the determination of the values w_{ij} during the "back-propagation" (denoting a class of networks in opposition to "feed-forward" neural networks) of the errors $y - z^{(k)}(x)$ in the successive learning "epochs" (easily paralellized). Thus, when training is completed, the network responses with appropriate model-free estimates of the output values for each set of input variables.

Among other specialized references it is possible to cite [61] or [111], who imspired most of this description.

Fuzzy and neuro-fuzzy inference

Fuzzy inference methods are best suited for the processing of information where some existing experience is available in the form of rules, and is very interesting for the automatization of existing knowledge that cannot be integrated into a modelling environment but which is well documented and tested from human operators or external tests.

11.2 Implementation issues and control

11.2.1 Error

It is possible to have a guess of the likelihood of x being the optimum. The matrix J^{-1} itself gives directly the rate of deviation of the solution x for the variation of each data, since $J_{ij} = \frac{\partial R_i}{\partial x_j}$.

The variance-covariance matrix gives the variance/covariance of the answer x when the data has some uncertainty, and is defined as $\sigma^2 (J^T J)^{-1}$ (see Bates and Watts [8]) where σ is an appropriate statistical constant. When no more data is known, it can be taken as $\sigma = \frac{2f(x)}{m-n}$, being m and n the number of measured points and geometry parameters respectively.

11.2.2 Scaling

The scaling of the problem means that the units and magnitudes of the different parameters involved in the problem (for example the size of the hole with respect to the total size, or the mixture of displacement and stress measurements) may affect the solution.

Whereas Newton's and BFGS methods are unaffected by scaling, the steepest descent and therefore the trust region models are affected. Therefore, the values introduced in the algorithms should previously be modified by an scaling matrix D_x in the form, $\hat{x} = D_x x$.

There is a further effect that one should care. Too different magnitudes may also affect the conditioning of the matrices due to the computer precision, not only in the optimization algorithms, but also in the BEM calculations. The solution is similar as before.

The best way to do this may be in the stage of the preprocessing, which will stabilize the steps of communication between different modules besides lowering the risk of bugs in the codes due to their simplification.

11.2.3 Stopping

Another issue is the stopping of the iterative algorithm. The main methods in numerical optimization are,

- Gradient: $\| \nabla f \| \leq \varepsilon$. This can be improved so as it does not depend on the units, $max_i \mid \frac{\nabla f_i max\{|x_i|, typicalx_i\}}{max\{|f|, typicalf\}} \mid \leq tolerance$
- Step: $\frac{|x_k - x_{k-1}|}{max\{x_k, typicalx\}} \leq tolerance$. The drawback of this method is that it may be stuck in local minima (or flat regions).
- Residual: $f \leq tolerance$. The drawback of this method is that it requires the residual to become close to zero.

A good option is a combination of e.g. the last two methods.

11.2.4 Reduction of the step

One of the simplest regularization procedures, in the sense of making safer the convergence, is to affect the variation calculated at each step by a coefficient between 0 and 1: $x^{i+1} = x^i + \alpha \delta x^i$. The case of absence of regularization would be $\alpha = 1$. We have defined a value of α that evolves with the accuracy determined by the error ($f = \frac{1}{2} R^T R$), as $\alpha = \frac{1}{1+\beta f^2}$. If $\beta = 0$, this criterium is omitted, since $\alpha = 1$, whereas the bigger β is the slower but safer will the search proceed. This has only been implemented for the simple Gauss-Newton method in static cavity detection.

11.2.5 Banning impossible configurations

First of all, the easiest control is to ban every point of the flaws from crossing any boundary (this would avoid for instance that flaws jump out of the model, or that they overlap each other). This is done by checking that the segment defined by the variation vector of each point does not cross any segment joining two consecutive nodes. If id would do, then, the variation segment will be reduced until it does not cross. On the other hand, the variation parameters make all sense only if their values are within a certain interval. This interval can be shortened further in order to reduce the effect of the absence of second order effects. If the value of one iteration segment would surpass it, we just truncate it's value.

One procedure has been tested on all the examples for banning impossible configurations that occur when the sought flaw or crack exceeds the expected range of locations, such as the boundary or an area at a safe distance from it. It consists of a remapping of the parameter values which can be seen as a constraint of their values to some virtual box of allowed positions of the flaws. It is based on giving a legal value of each parameter regardless of the trial value of the optimization algorithm. An important point is to give it continuity and derivability so as to have a good conditioning and calculability of gradient and hessian. The suggested mappings of the value and gradient have the following form, being $x \in [-\infty, \infty]$ the trial parameter, $y \in [-r, r]$ the transformed parameter with physical meaning, $\frac{dy}{dp}$ and $\frac{dx}{dp}$ the gradients of y and x with respect to the parameter p, and r the limiting range,

$$y = arctan\left(\frac{\pi x}{2r}\right)\frac{2r}{\pi}$$

$$\frac{dy}{dp} = \frac{dx}{dp}\frac{dy}{dx} = \frac{dx}{dy}\left(1 + \left(\frac{\pi x}{2r}\right)^2\right)$$

11.3 Equivalence between Observation Equation and Gauss-Newton method

A so called sensitivity equation has previously been used directly for the solution of IP through the BEM by several authors ([122], [137], [114], [49], [50], [48], [51]). The method basically consisted in writing the integral equation and deriving it with respect to a generic geometry variation through a more or less complicated linearization and limiting process to the boundary. The resulting integral equations gave, after the discretization, the relationships between the variation of the measured displacements and the geometrical parameters (a system of equations called δBIE in the form $H(x)\delta u = \triangle(x)\delta x \Rightarrow A(x)\delta x = \delta u$). These data are easily related to the residual R and the geometrical description x respectively. The δBIE could be directly used in an iterative process starting from an initial guess of the geometry x_0,

1. Compute $A(x_k)$
2. Solve the non-square over-determined system of equations $A(x_k)\delta x_k = \delta u_k$ by least squares $(A_k^T A_k \delta x_k = A_k^T \delta u_k)$.
3. Update the geometry $x_{k+1} = x_k + \delta x_k$

Now, since $R = u - u^{exp} \Rightarrow \delta R = \delta u$ and calling $J = \frac{\partial R}{\partial x} = \frac{\partial u}{\partial x} = \frac{\delta u}{\delta x} = A$ for a sufficiently small iteration or within a linearized model, we can define a cost functional $f = \frac{1}{2}R^T R$. Gauss-Newton's method for this functional reads,

1. $J_k^T J_k s_k = -J_k^T R_k$
2. $x_{k+1} = x_k + s_k$

which is exactly the same as the process described above. This is yet another justification of the good behaviour of Gauss-Newton's method and unifies two methods formerly classified in different families.

This link between the two theories may allow the adaptation of techniques of each one into the other, opening a new area of research. Examples of possible study in this direction could be, to begin with:

- use the benefits of the singular value decomposition of linear observation equations onto minimization algorithms in order to damp higher singular values as a regularization technique (see [86], chapter 7, and [60], chapter 2),
- or application of theory of factor analysis (see [86], chapter 10), both after an adaptation to nonlinear theory.
- Application of truncated least squares techniques to the definition of the minimization functional (see [60], chapter 3).
- Application of error and probability theories to minimization theories, preconditioning, etc. (see [60]).

Part III

Numerical tests

Chapter 12

Sensitivity tests

12.1 Comparison with analytical solution. Direct derivation

12.1.1 Singular equation

In this point, we check the partial results corresponding to the sensitivity coefficients. A problem with a calculable analytical solution and sensitivity is the one consisting in a plate of infinite dimensions with a circular hole, and subjected to an uniform stress from the end as shown in figure 12.1.

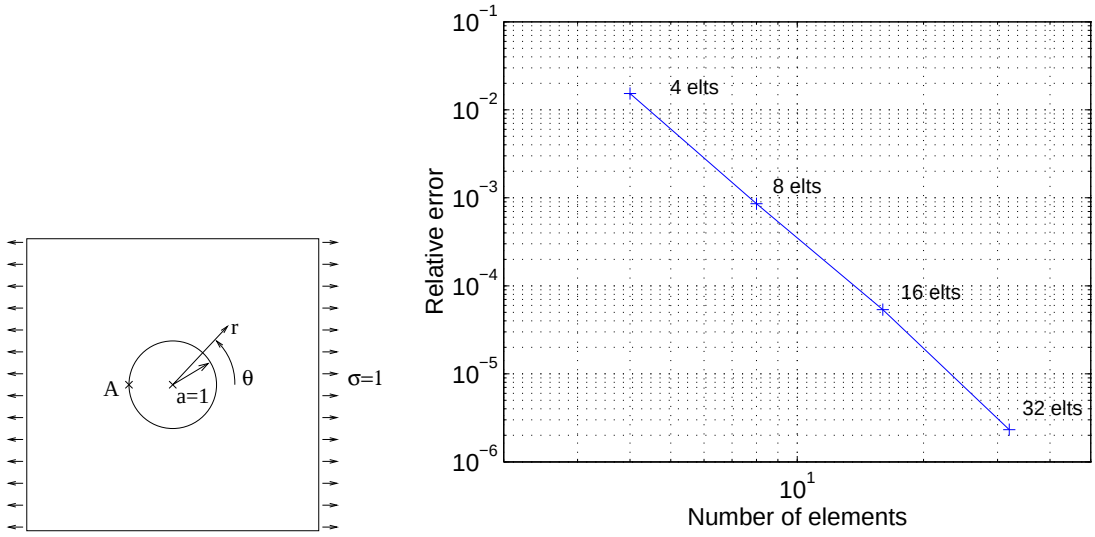

Figure 12.1: Infinite plate with hole. Model and numerical error.

The stress field was calculated by Kirsch [70] in 1898 and is confirmed by Timoschenko [102]. The exact solution of the displacements field can be derived, and yields:

$$
\begin{aligned}
u_x &= \frac{\sigma\cos\theta(a^4(1+\nu)-a^2(-3+\nu)r^2+2r^4-2a^2(1+\nu)(a^2-r^2)\cos 2\theta}{2Er^3} \\
u_y &= \frac{-\sigma(a^4(1+\nu)+a^2(1-3\nu)r^2+2\nu r^4+2a^2(1+\nu)(a^2-r^2)\cos 2\theta)\sin\theta}{2Er^3}
\end{aligned}
$$

The sensitivity to the radius of the hole in terms of the material derivative is, evaluated at the

boundary of the hole:

$$\begin{aligned} u_{x,a} &= \frac{3\sigma\cos\theta}{E} \\ u_{y,a} &= \frac{-\sigma\sin\theta}{E} \end{aligned}$$

In our process, we use this type of derivation, in comparison to the alternative used in previous jobs, that would give,

$$\begin{aligned} u_{x,a} &= \frac{-a\sigma\cos\theta(-2a^2(1+\nu)+(-3+\nu)r^2+2(1+\nu)(2a^2-r^2)\cos 2\theta}{Er^3} \\ u_{y,a} &= \frac{-a\sigma(2a^2(1+\nu)+(1-3\nu)r^2+2(1+\nu)(2a^2-r^2)\cos 2\theta)\sin\theta}{Er^3} \end{aligned}$$

The errors on the numerical calculations of these values at point A are shown in figure 12.1, for discretizations of the hole of 4, 8, 16 and 32 elements.

The following two graphics show the values of the two components of the variation vector for all the nodes versus the analytical solution in the case of 4 and 16 elements (figure 12.2).

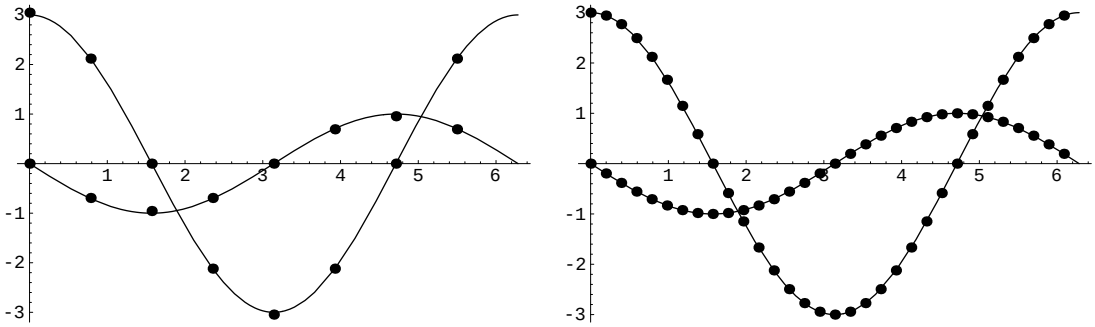

Figure 12.2: Variation along the boundary, 4 elements and 16 elements

12.1.2 Hypersingular equation

A similar example can be found for the case of the hypersingular equation applied to cracks. The exact solution of a straight crack in an infinite medium subjected to an uniform stress from the end as shown in figure 12.3 can be found in many fracture mechanics books.

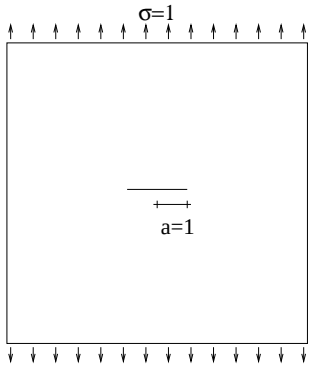

Figure 12.3: Infinite plate with crack.

The displacements of the points on the lip of the crack follow,

$$\begin{aligned} u_x &= 0 \\ u_y &= \frac{a\sigma 2(1-\nu^2)}{E}\sqrt{1-\xi^2} \end{aligned}$$

being ξ the local coordinate on the crack, which varies from -1 to 1.

The sensitivity to the semilenght of the crack a in terms of the material derivative is, evaluated at the boundary of the hole:

$$\begin{aligned} u_{x,a} &= 0 \\ u_{y,a} &= \frac{\sigma 2(1-\nu^2)}{E}\sqrt{1-\xi^2} \end{aligned}$$

The errors on the numerical calculations of these values at the middle point of the crack are shown in figure 12.4, for discretizations of the crack of 2, 4, 8, 16 and 32 elements. The value along the crack is also shown for a discretization of 4 elements.

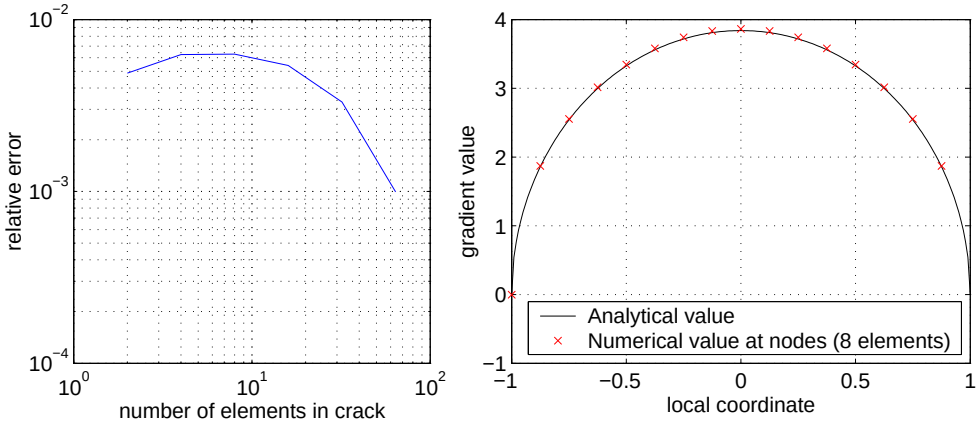

Figure 12.4: Numerical and analytical comparison.

Despite the simplicity of the model, the errors in the numerical figures keep very low and converge properly as the mesh is refined.

12.2 Comparison with numerical solution. Direct derivation

12.2.1 Methodology

The sensitivity tests are performed using a set of simple benchmark problems for the sake of reproductibility and simplility of comparison. The external shape and conditions of the known body are common, and the varying flaw differs depending on the type (crack or cavity) and on the parametrization, which will permit different shapes.

The fixed contour consists of a 2×2 box of a material with constants $E = 1.0$; $\nu = 0.2$, $\rho = 1.0$. In the case of an inclusion, it is made of an identical material changing $E = 0.5$. As boundary conditions the baseline is fixed and the upper side is subjected to an uniform unitary vertical stress. The cavities and inclusions are defined (limited by the geometrical possibilities of the boundary elements) as an ellipse of center $(-0.3, 0.2)$ of semiaxes 0.41 and 0.22, at an angle of 39 degrees with the horizontal. The crack is defined as $x = -0.7 + 0.8\lambda; y = 0.3 + 0.4\lambda + 0.2\sin(2\pi\lambda)$, where the parameter λ goes from 0 to 1. They are built from circle of radius 0.8 at the center, which is perturbed by the six basic 6-parameter vector $[-0.30, 0.20, -0.50, -0.40, 0.20, 0.15]$ (see parametrization chapter for an exact definition) and $[-0.20, 0.20, 0.00, 0.00, 0.00, 0.00, 0.00, 0.00, 0.00, 0.00, 0.00, 0.00]$ for the case of special quadratic, two-point mixed and polar fourier parametrizations. The crack starts from a straight and centered horizontal line of length 0.8, perturbed as well by the tip displacement and fourier parametrization vector $[-0.30, 0.30, -0.30, 0.70, 0.00, 0.20, 0.00, 0.00, 0.00, 0.00, 0.00, 0.00]$.

The model is made of two subboundaries per side of the outer box, and eight subboundaries for the circle or crack. If nothing else is specified, one quadratic element is used at each subboundary. The collocation points are always placed at $0.2a$ from the edge of the element, being a the distance between two geometrical, displacement or stress nodes.

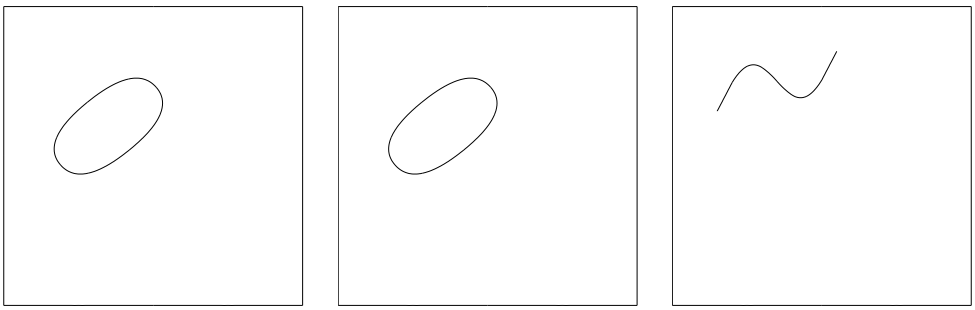

Figure 12.5: Real scale description of cavity benchmark, inclusion benchmark and crack benchmark.

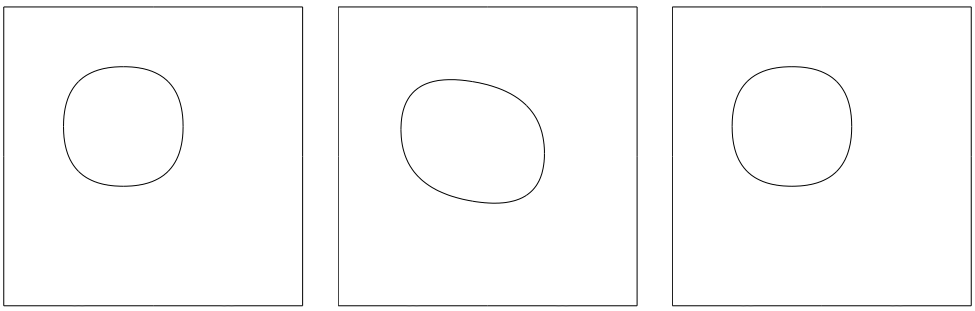

Figure 12.6: Real scale description of cavity benchmarks for special quadratic, two-point mixed and polar fourier parametrizations.

12.2.2 Dependence of gradient value with frequency

To begin this section, the values of the gradients are shown a a couple of simple points, in order to allow for the comparison. Four values are given for each benchmark problem:

1. $\frac{du_x}{d\Theta_n}$ is the variation of the horizontal displacement of the middle point on the upper side when parameter n grows (see chapter 8).

2. $\frac{dp_x}{d\Theta_n}$ is the variation of the horizontal stress vector of the middle point on the lower side when parameter n grows (see chapter 8).

These values were computed using 8 elements per subboundary, excepting the crack benchmark, with 4 elements per subboundary. In the latter case, the distance for the finite differences had to be increased to $\frac{0.002}{\omega}$ instead of 0.001, because a divergence in finite differences was detected for smaller values. The division by ω is justified by the equivalent scaling that the change of frequency implies in the fundamental solutions. The presence of eigenfrequencies, shown below each graphic, gives a jaggy aspect to the graphics. An estimation of the same value using finite differences is made, superimposing it by red dots. A perfect agreement is shown visually, proving that the right value is being calculated. Therefore, the converging solution for refined meshes should give the exact solution.

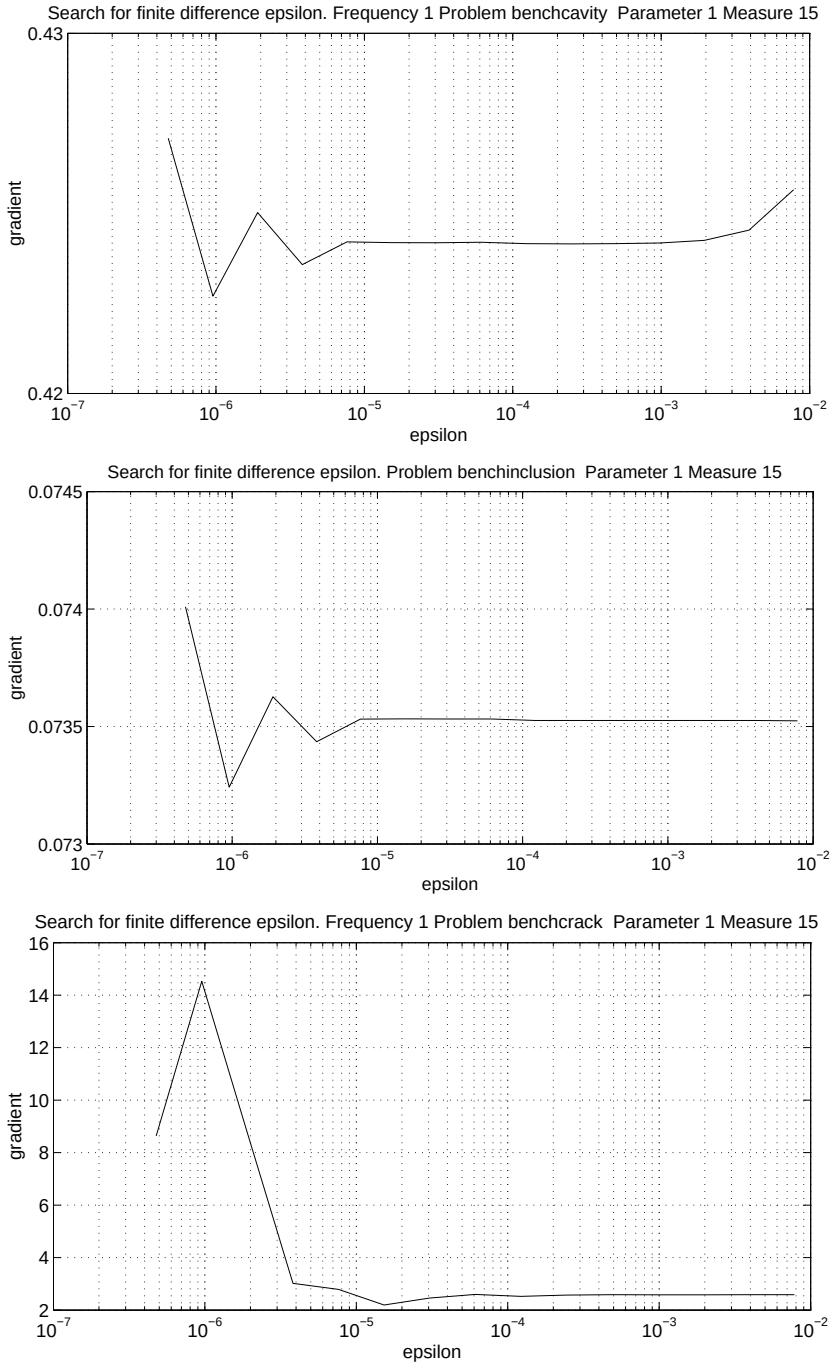

Figure 12.7: Frequency. Test of finite difference distance. Value versus finite epsilon. Cavity, inclusion and crack problems respectively.

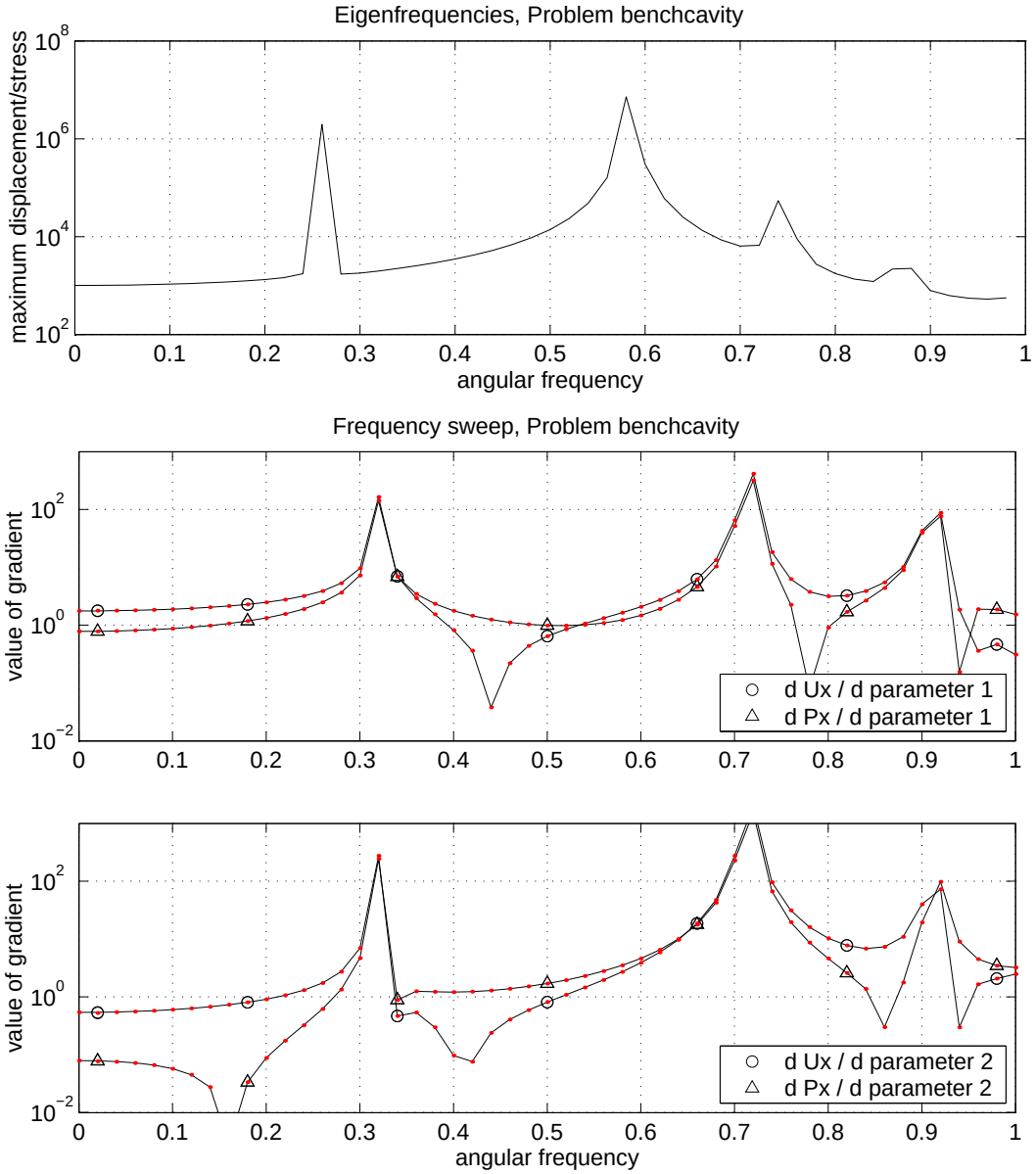

Figure 12.8: Values of gradient. Cavity problem. Continuous line: analytical value by direct derivation. Red dots: finite differences value. Each curve is the derivative with respect to the horizontal (1) and vertical (2) parameters.

12.2.3 Integration precision

In order to have control over the sources of error we now study the accuracy of the integration of the boundary integral equations. To do this we play with the Gauss quadrature.

From figure 12.11 the convergence of an hypersingular integral (first) and two benchmark problems by increasing the number of integration points is confirmed. The reference value is an integral with an extremely high number of points (2500 gauss points for the first and 10 gauss points together with 8 times the actual number of elements).

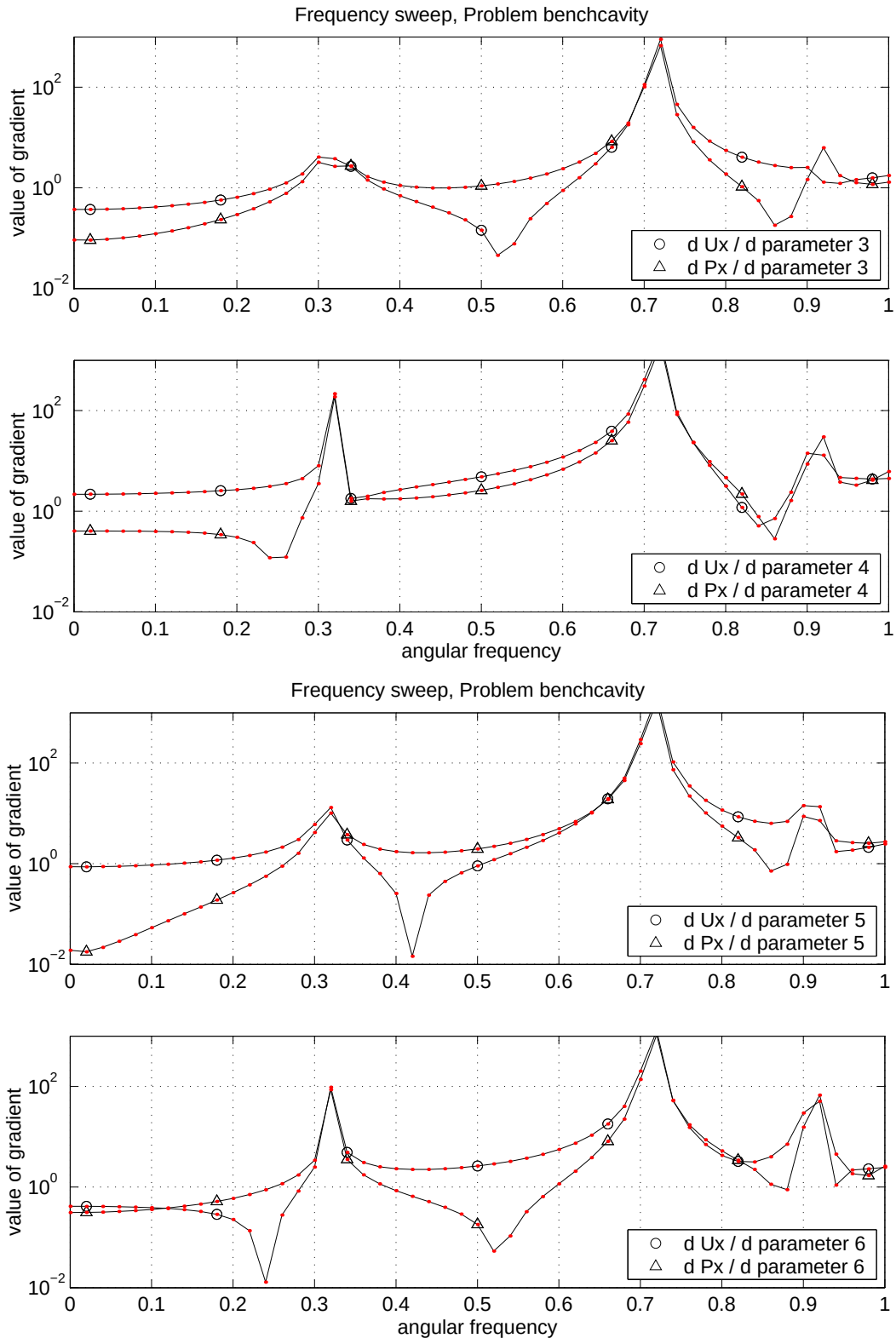

Figure 12.9: Values of gradient. Cavity problem. Continuous line: analytical value by direct derivation. Red dots: finite differences value. Each curve is the derivative with respect to the rotation (3), dilatation (4), elongation (5) and distortion (6) parameters.

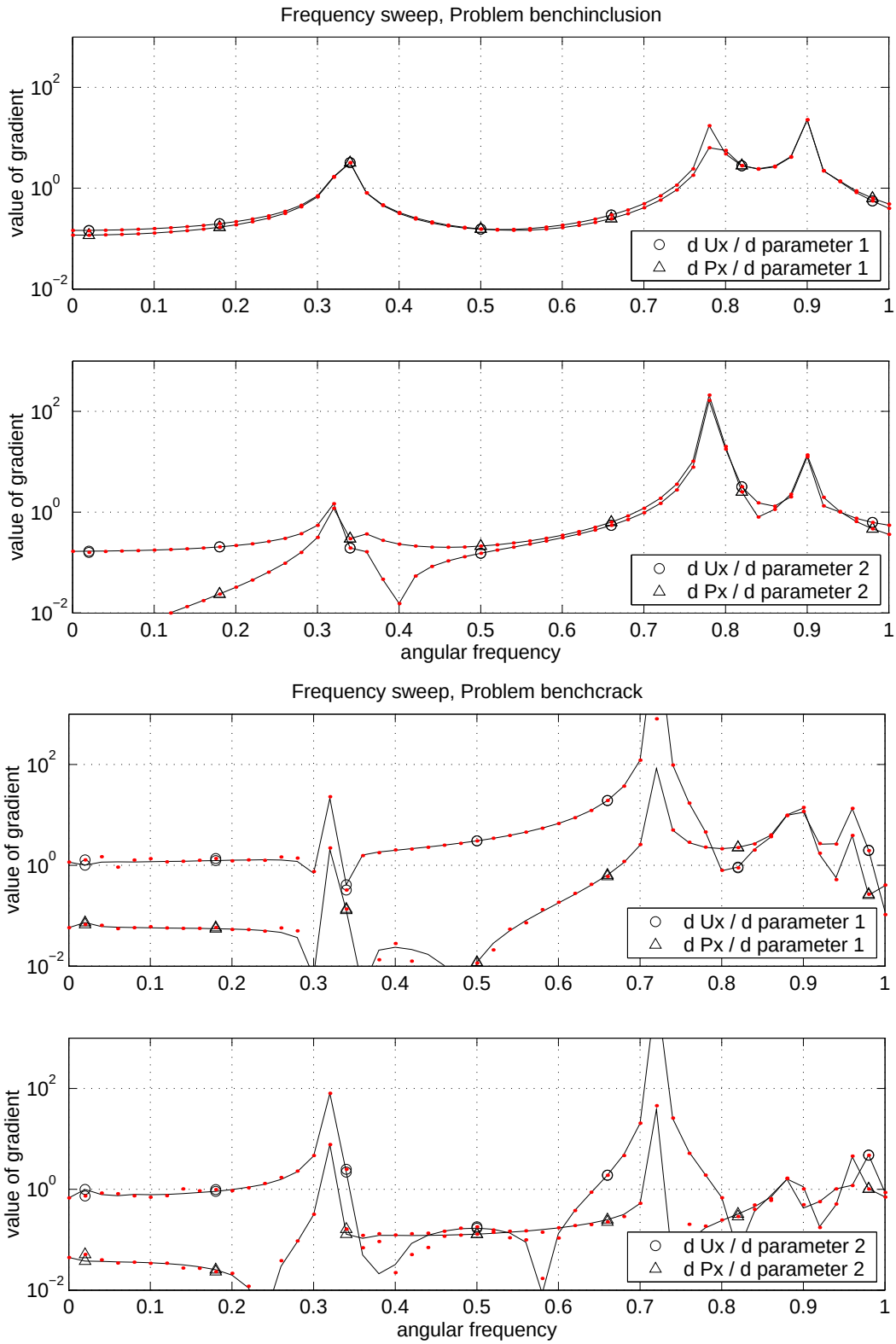

Figure 12.10: Values of gradient. Above: inclusion problem. Below: crack problem. Continuous line: analytical value by direct derivation. Red dots: finite differences value. Each curve is the derivative with respect to the horizontal (1) and vertical (2) parameters.

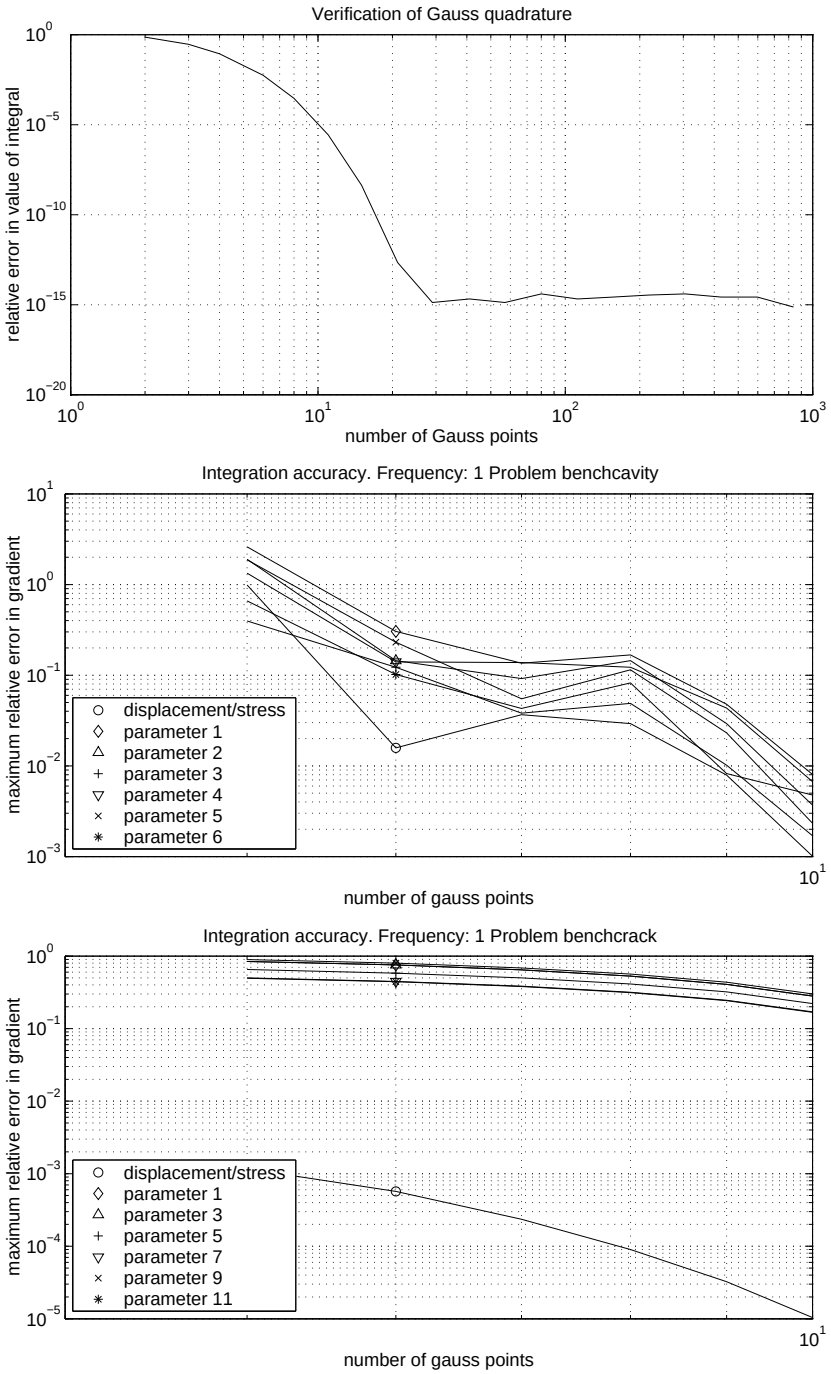

Figure 12.11: Integration precision. Above: relative error in a hypersingular integral. Below: Error in the complete problem gradient calculation in the cavity problem and in the crack problem.

12.2.4 Order of elements

To continue the study of the integration accuracy, the size of the numerical problem is studied, by playing with the number of nodes per element (order of interpolation).

In figure 12.2.4 the initial convergence and later divergence of the calculations depending on the order of the elements is checked for a fixed 12-point gauss quadrature per element. The divergence is caused by the limitation of the gauss quadrature precision in the case of functions of very high order. The reference value is computed refining to $\times 8$ the mesh and keeping 4-order elements (this order was chosen since a higer one would show some divergence).

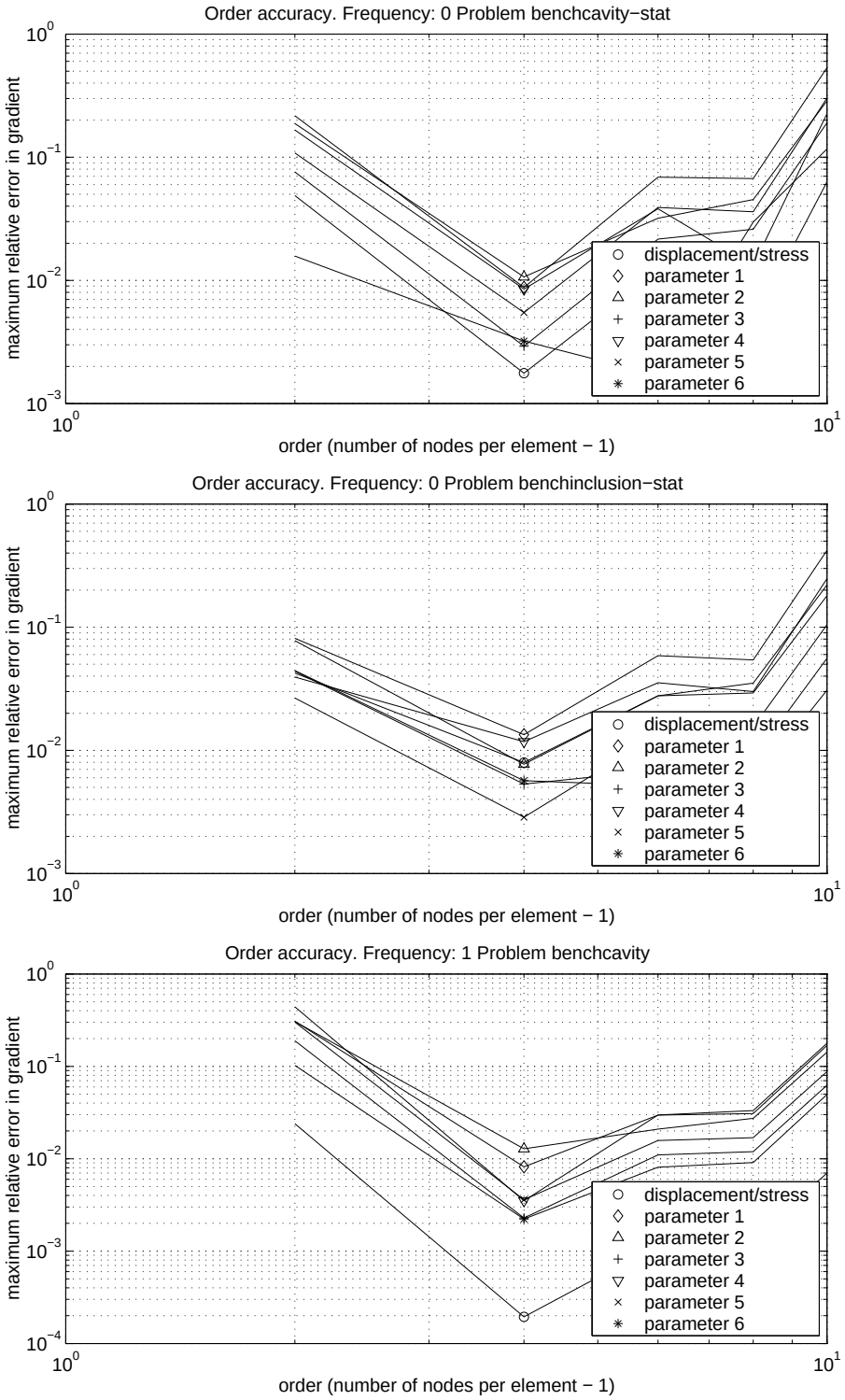

Figure 12.12: Order of elements. Relative error for various number of nodes per element. Static cavity, static inclusion and dynamic cavity problems respectively.

12.2.5 Number of elements

To finish the study of integration accuracy, we here play with the number of elements in which the boundaries are divided into.

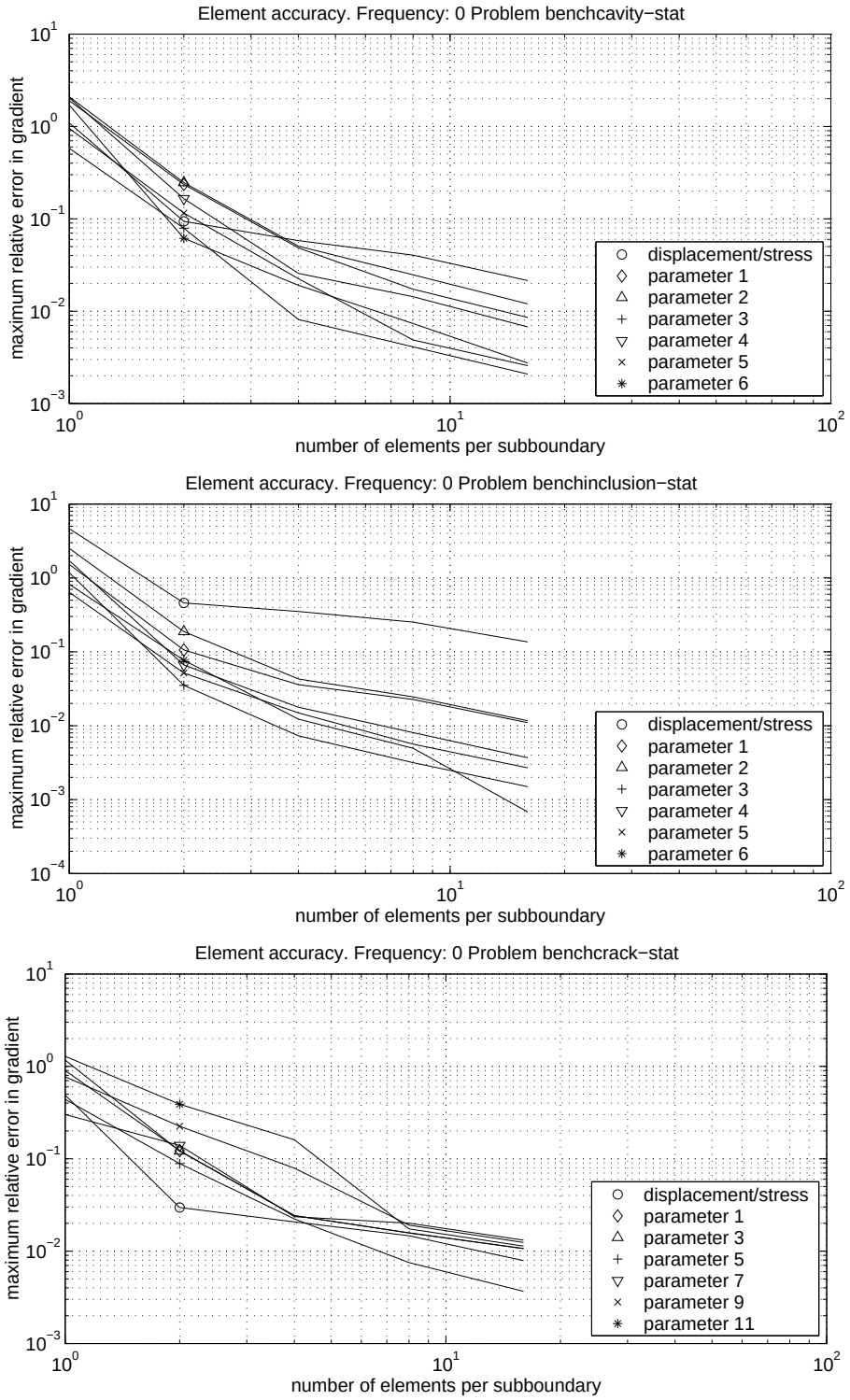

Figure 12.13: Number of elements. Evolution of the relative error as the mesh is refined. Static problem. Cavity, Inclusion and Crack problems respectively.

The figures 12.2.5 prove a clear convergence of the solution by increasing the refinement of the mesh. The reference value is taken from a much more refined mesh.

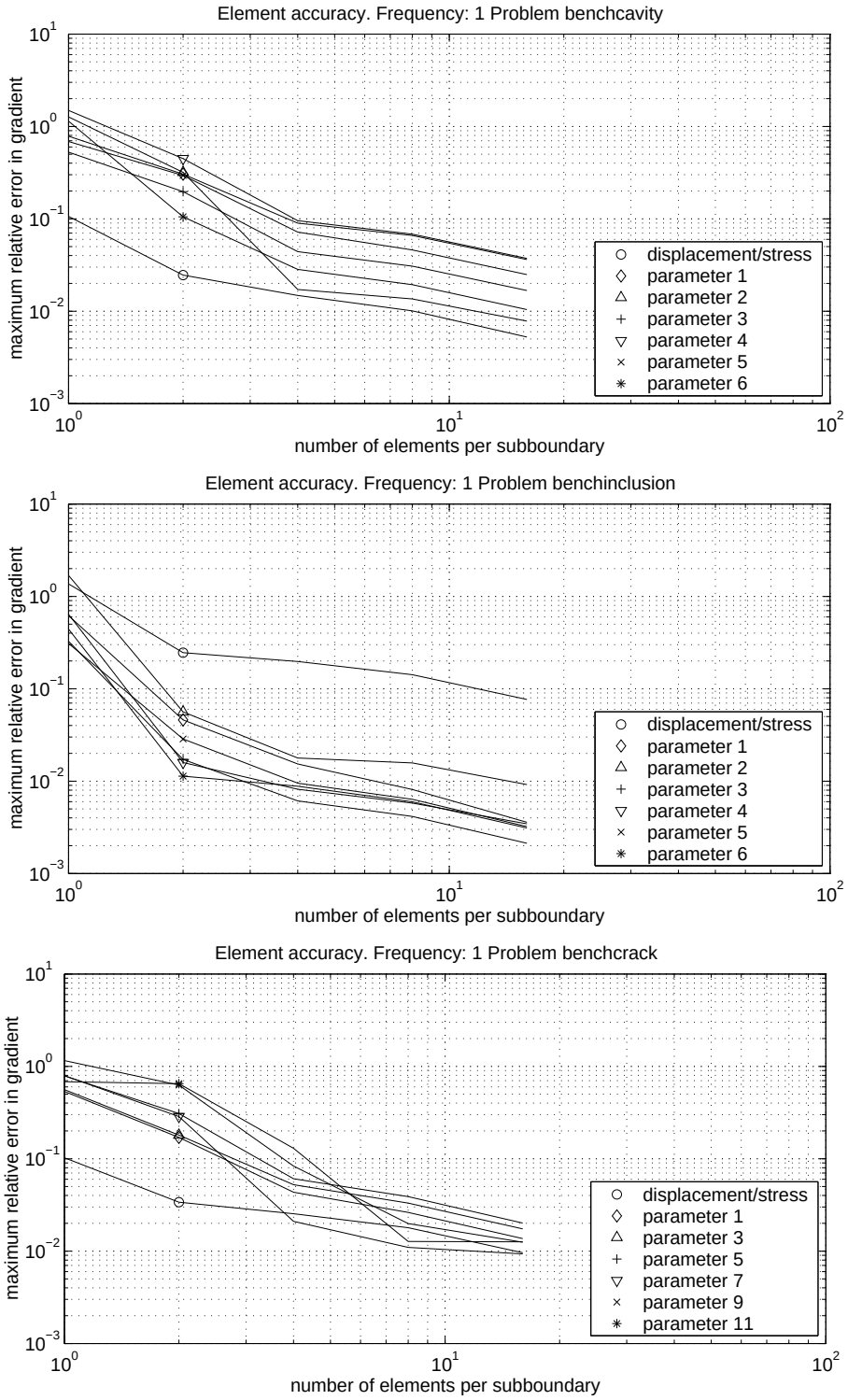

Figure 12.14: Number of elements. Evolution of the relative error as the mesh is refined. Dynamic problem. Cavity, Inclusion and Crack problems respectively.

12.2.6 Influence of frequency

From figure 12.2.2 the epsilon (finite difference distance) chosen for all the frequency comparisons is 10^{-4}.

The errors measured in 12.2.6 are the comparison between the analytic gradient and the one

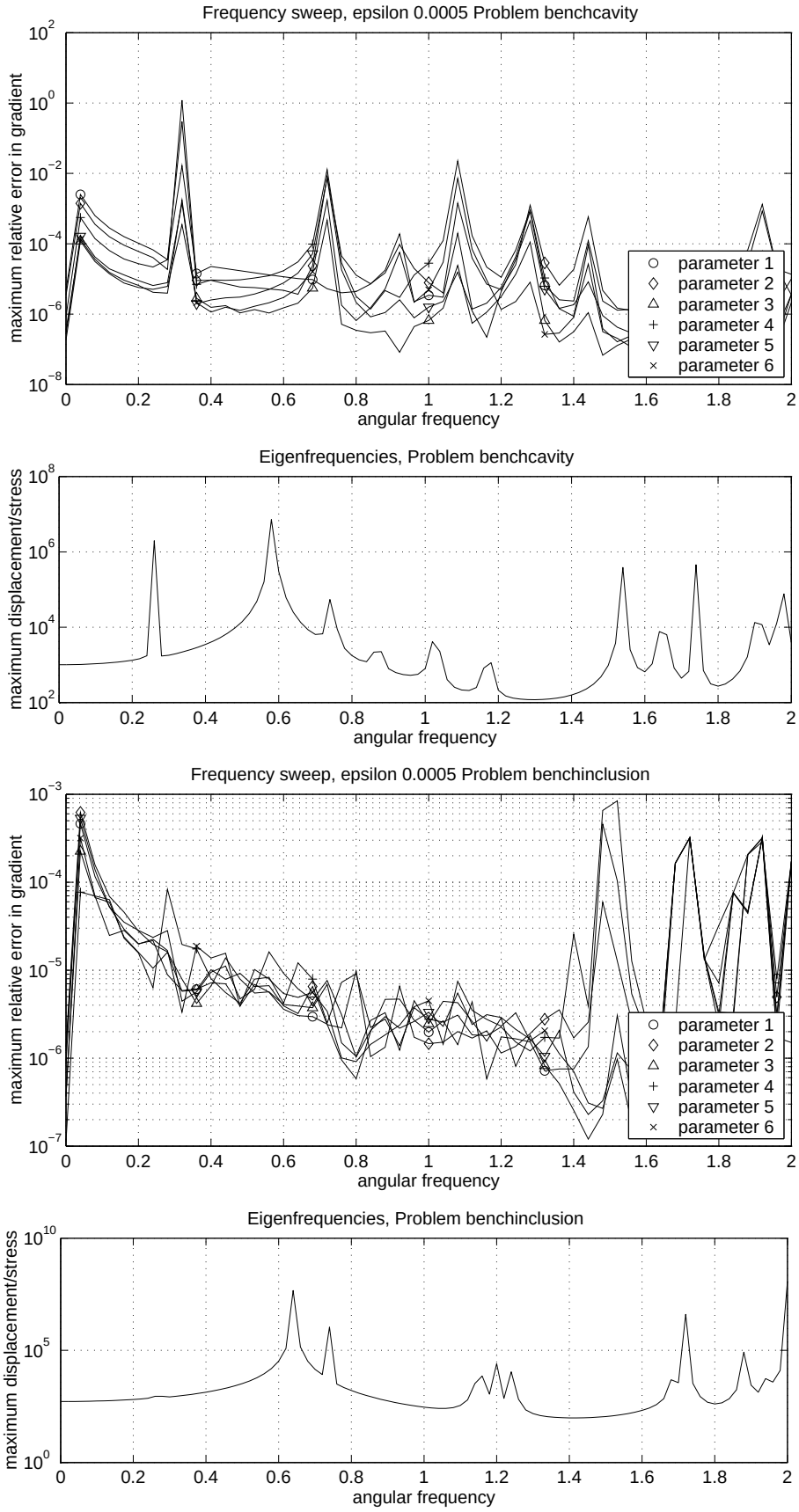

Figure 12.15: Frequency. Relative error and eigenfrequencies. Cavity and inclusion problems.

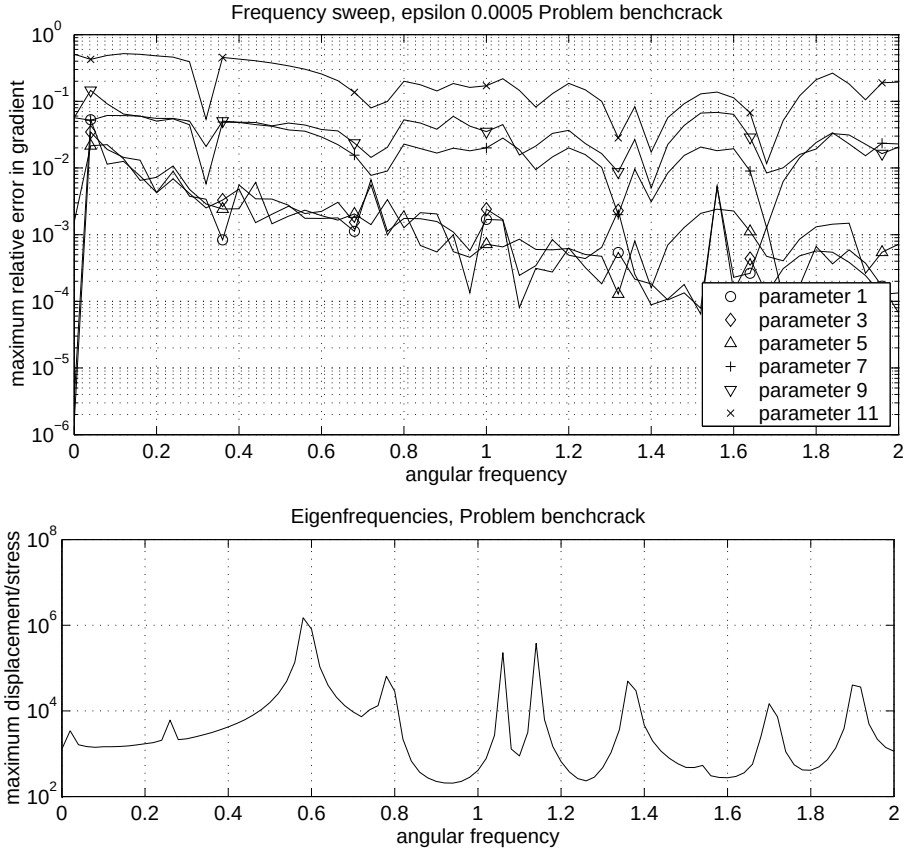

Figure 12.16: Frequency. Relative error and eigenfrequencies. Crack problem.

obtained by centered finite differencies. The eigenfrequencies are also represented to check the relationship between the errors at the edge of the eigenfrequencies, which may cause the finite difference calculations to diverge. It is seen that the errors are low even for frequencies far above the first eigenfrequency.

Unlike in other examples, it is important to note that the reference value is not close to the exact solution of the physical problem, but the finite difference estimation for the same level of meshing. Here, cavity and inclusion problems show a very good agreement, but crack problems show much higher discordancies. If one looks closer to the figure, one sees that this only happens for the last parameters, which involve highly warped geometries. As seen in the next figures, there are indeed high errors at a low number of elements, but all are rapidly reduced by a sufficient mesh refinement. Another interesting effect is that the errors become higher at very low frequencies, which may be due to the numerical difficulties for the numerical convergence of the dynamic fundamental solutions of the BEM to the static ones in the 2D case.

12.2.7 Complex parametrizations

This point is aimed at the verification of the convergence of the results of the gradient when quadratic and other complocated parametrizations are used.

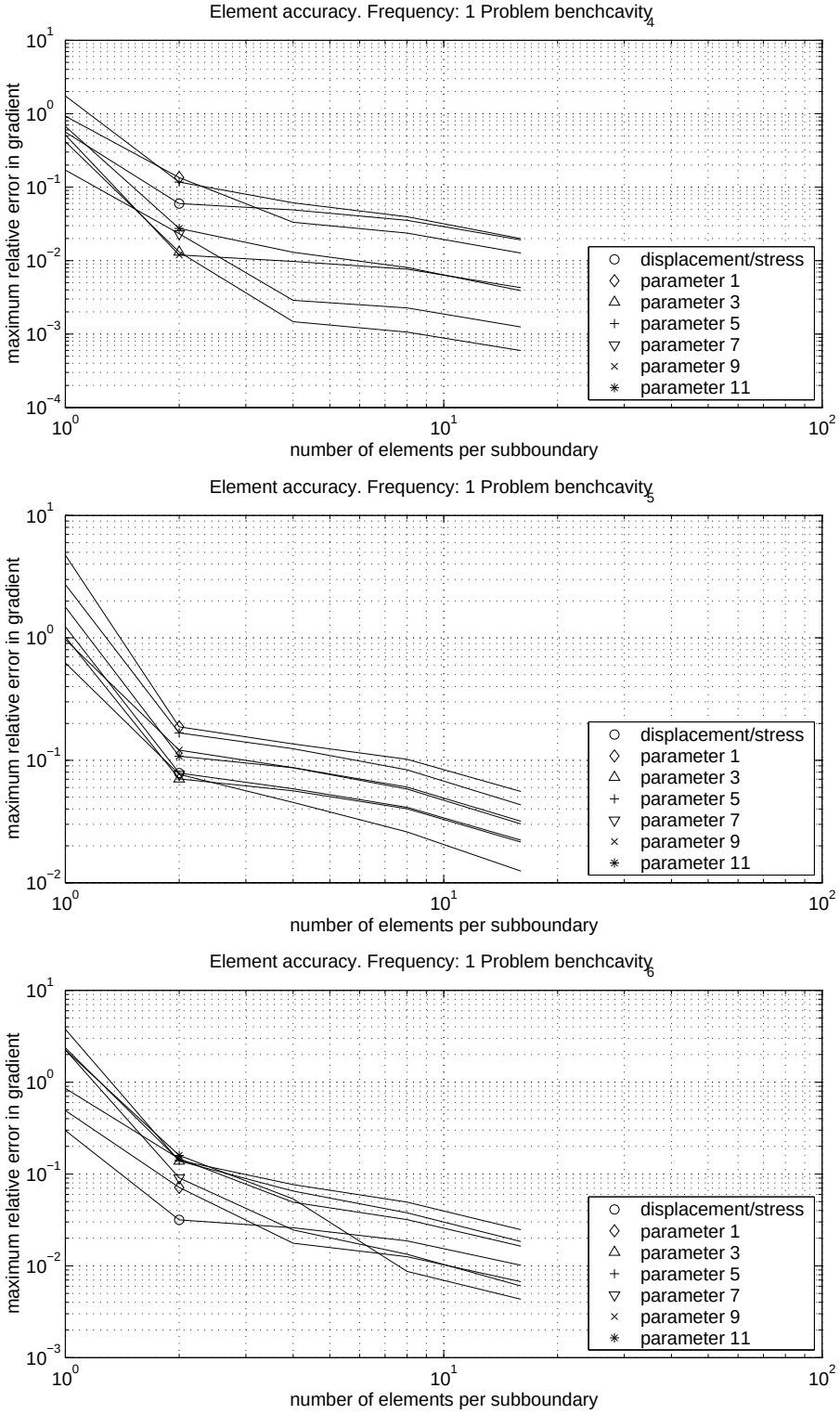

Figure 12.17: Parametrizations. 2-point by 6 parametrization, polar Fourier parametrization and uncoupled quadratic field parametrization respectively. Dynamic cavity problem.

Finally, figure 12.2.7 shows the maximum errors and need for a more strict refinement in the case of more complicated parametrizations. This is simply due to the higher warping of the geometry, which needs elements capable to represent it. The convergence is anyway achieved successfully.

12.3 Adjoint variable method

This section is aimed at the study of the reliability of the gradient of the cost function L with respect to each parameter, taking into account all the variable points in the problem: the discretization, the frequency, the number of given measurements, some variations on the model (boundary conditions), and the chioce of parametrization.

12.3.1 Methodology

Methods to compare

Since we do not have access to the exact value of the sensitivity, we have to compare the results of this formulation with another approximated one, which will be finite central differences.

1. Sensitivity by finite central differences (FD):

$$\overset{*}{L}_g = \lim_{\eta_g \to 0} \frac{L(x_i + \eta_g \Theta_{ig}) - L(x_i)}{\eta_g} \simeq \frac{L(x_i + \eta_g \Theta_{ig}) - L(x_i - \eta_g \Theta_{ig})}{2\eta_g}$$

   where,

$$\begin{aligned} L &= J + A = J = \int_0^T \int_{\Gamma_p} \varphi_u d\Gamma dt + \int_0^T \int_{\Gamma_u} \varphi_p d\Gamma dt + \int_\Gamma \psi d\Gamma \\ &= \frac{\pi}{2\omega} \left[\int_{\Gamma^{m_u}} (u_i^m - u_i)(\overline{u}_i^m - \overline{u}_i) d\Gamma + \int_{\Gamma^{m_p}} (p_i^m - p_i)(\overline{p}_i^m - \overline{p}_i) d\Gamma \right] \end{aligned}$$

2. Sensitivity by the adjoint variable method (AVM):

$$\overset{*}{L}_g \text{ using equation 6.5.}$$

Boundary element calculations

The calculation of the direct problems that arise in both methods is made with bidimensional quadratic boundary elements. The original code, that has been modified conveniently was developed by F. Chirino [29]. The discretization is made with interior collocation points placed at $0.8L/2$ from the center for all the elements, in our examples. The crack is represented by the dual formulation or mixed boundary element method, a combination of equations corresponding to the integral representations of displacements and tractions - one for each lip. The crack tip is modeled by a quarter point straight element, and the stress intensity factors are computed upon the crack opening displacement measured at the quarter node of the tip element. Finally, the singular integrals are evaluated by dividing them into an analytically solved part, which only involves static terms, and a regular part solved with constant standard 10-point Gauss quadrature.

In order to later integrate the expressions along the crack, we should ensure that the data at the crack tips are exactly of the right order of singularity, eliminating numerical alterations of it. This can be done by obliging the $\sqrt{r}$ terms to be identical in the upper and lower lip of the tip. If we represent the behavior of the data as,

$$\begin{aligned} f^+ - f_0 &= \alpha^+ \sqrt{r} + \beta^+ r \\ f^- - f_0 &= \alpha^- \sqrt{r} + \beta^- r \end{aligned}$$

we will force them to behave as $\alpha = \frac{\alpha^+ + \alpha^-}{2}$ by a slight and convenient modification of value at the extreme crack tip node.

Apart from the boundary element software written in fortran 77, which has eventually been used as a black box, we have extensively checked the subroutines, written in both fortran 77 and 90, for the computation of the cost functional and all the formulae for the adjoint variable method. All the calculations are made with double precision.

Parametrization

We use the same parametrization definition for the calculation of the velocity fields in the AVM as for the FD perturbation definition and for the future modification of the geometry throughout an identification procedure. The latter is done by starting always from the initial uniformly meshed crack, in the sense that the final crack will be represented by the initial one perturbed once by the final parameters vector.

All the different parametrizations used with the AVM can be implemented by the use of a generic algorithm that only works with nodal parametrization. The nodal parameter vector is expressed in terms of any other parameter definition as $P_k^{nod} = S_{hj} T_{jk} P_h^{any}$, and reversely, the gradient of this parametrization is expressed in terms of the nodal one as $L_k^{nod} = S_{hj} T_{jk} L_h^{any}$.

Models

The implemented code will be tested in two different models, a circular one and a square-shaped one. The base definitions of both include some variable parameters with which we will play to study their importance.

The first base model on which we work is a circular body of unity radius $R = 1.0$ with a crack inside. The material constants are: Young modulus $E = 1.0$, Poisson coefficient $\nu = 0.2$ and density $\rho = 1.0$. The straight crack of semilenght $a = 0.3$ is placed as shown in figure 12.18, with its center at the coordinates $(0.3, 0.2)$. The boundary conditions consist of a prescribed arc along the boundary of variable length from zero (unconstrained circle) to the whole circle constrained. The non constrained supplementary arch is loaded by an unity stress towards the exterior normal. The measurements are the displacements along an arc of variable lenght on the unconstrained boundary. These displacements correspond to the same problem but with the crack center at the coordinates $(0.1, 0.1)$. The second base model consists of a 2x2 square with a crack in the same

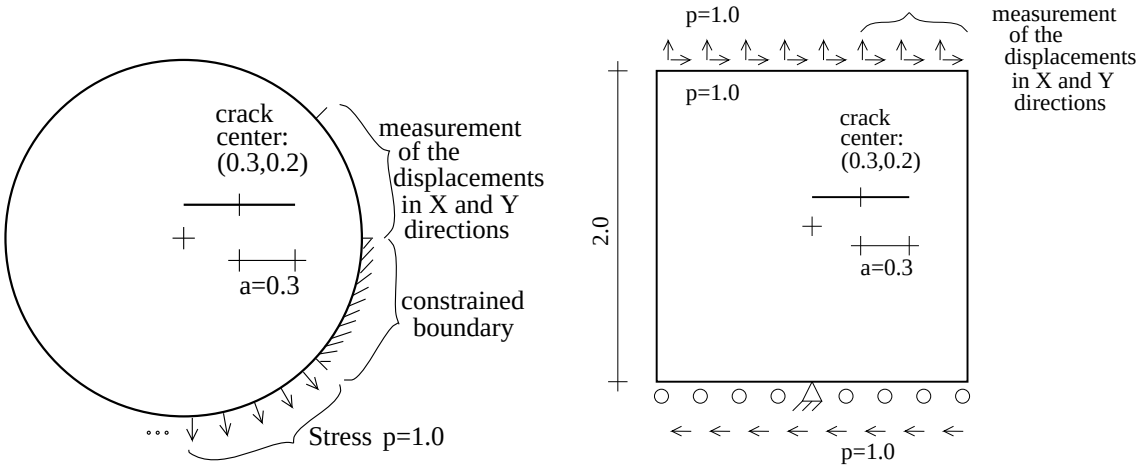

Figure 12.18: Geometry definitions

position. The measurements are made on a fraction of the upper side, and the boundary conditions are fixed as shown in figure 12.18.

These definitions ensure an unsymmetric solution with contribution of all fracture modes.

For the study of all the variable parameters of the geometrical definition, we start from two basic models: a totally unconstrained circular shaped model and the square-shaped model. The parametrization used is the multielemental parametrization for cracks, defined in chapter 8, with two parameters for the crack tip growth, one more for the normal displacement at each variable point along the crack. In both models, the measurements are taken over the whole measureable boundary, the angular frequency of all the magnitudes are $\omega = 1.0$, and the sensitivity is calculated with respect to the horizontal displacement of the crack (first parameter).

12.3.2 Comparison with numerical solution

The distance for the finite differences is chosen so as to minimize the sum of the numerical error at low distances and the nonlinearity of the cost functional at high distances. The choice has been a distance of 10^{-6}, as figure 12.19 suggests (calculated with $36 + 12 + 12$ elements, crack + each lip).

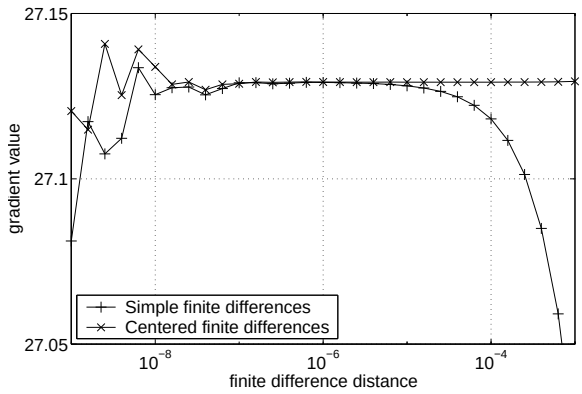

Figure 12.19: Effect of distance finite differences calculation.

The discretization of the crack, in oposition to the uniform mesh on the boundary, is biased so as to concentrate the elements towards the tips according to the rule $\xi = \frac{arctan(s\chi)}{arctan(s)}$, where ξ gives the adimensional coordinates of the nodes when χ is divided uniformly. Both coordinates are understood between -1 and 1. Although any value between $s = 0.0$ (uniform mesh) and $s = 3.0$ give good behaviour, our choice for a good improvement was $s = 2.0$.

Dependence on the discretization

In order to estimate the global errors and to assign the right degree of importance to the mesh. On the pairs of figures 12.20, 12.21 and 12.22, the horizontal axis represents the number of elements on the external boundary (sweeping from 12 to 192), and each curve has a fixed number of elements in each lip of the crack (ranging from 4 to 64). As seen on the value (left figures) and the estimation of the error (left), the values of the gradient or sensitivity appears to converge according to a bilogaritmic law, as expected.

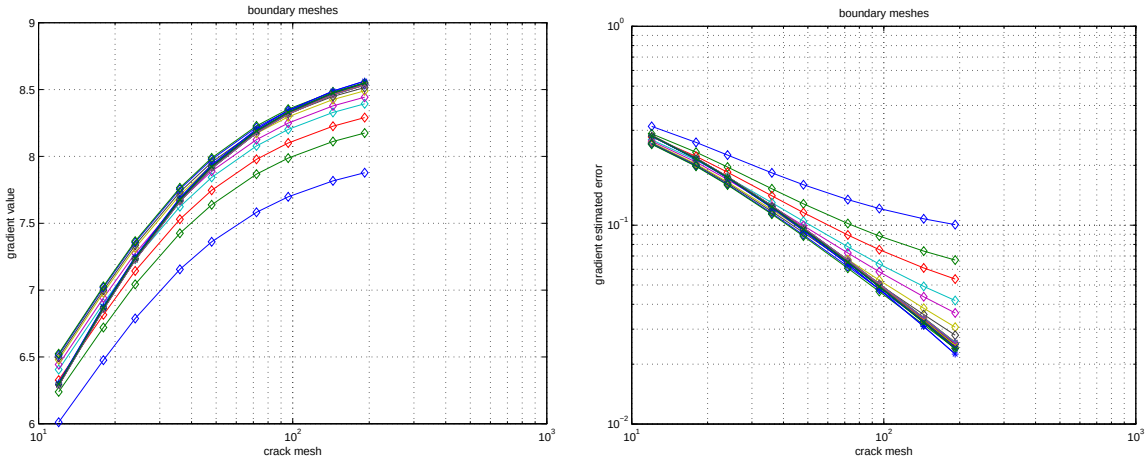

Figure 12.20: Circular model with no displacement prescriptions. Measurements over the *whole* circle. Sensitivity to *horizontal* displacement of the crack. (o) AVM calculation, (x) FD calculation.

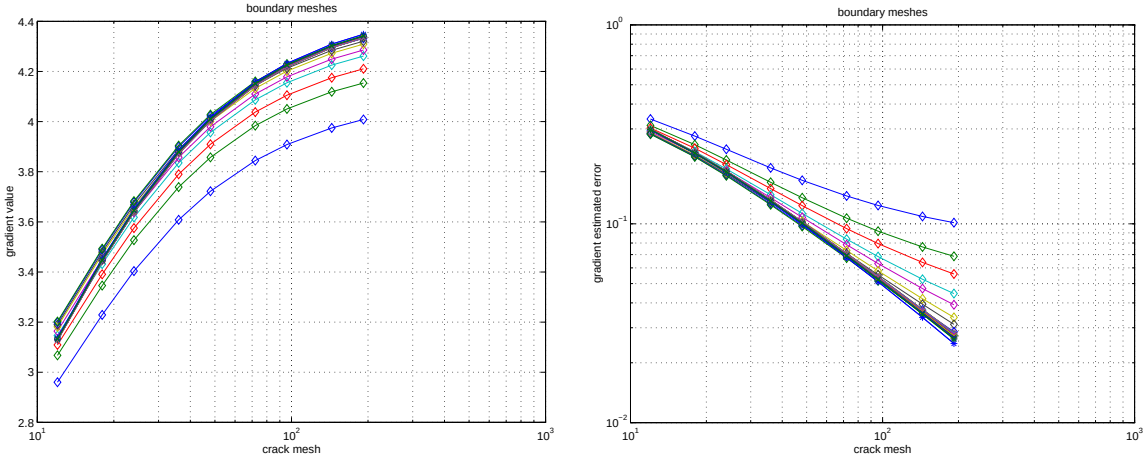

Figure 12.21: Circular model with no boundary prescriptions. Measurements over *a third* of the circle. Sensitivity to *horizontal* displacement of the crack. (o) AVM calculation, (x) FD calculation.

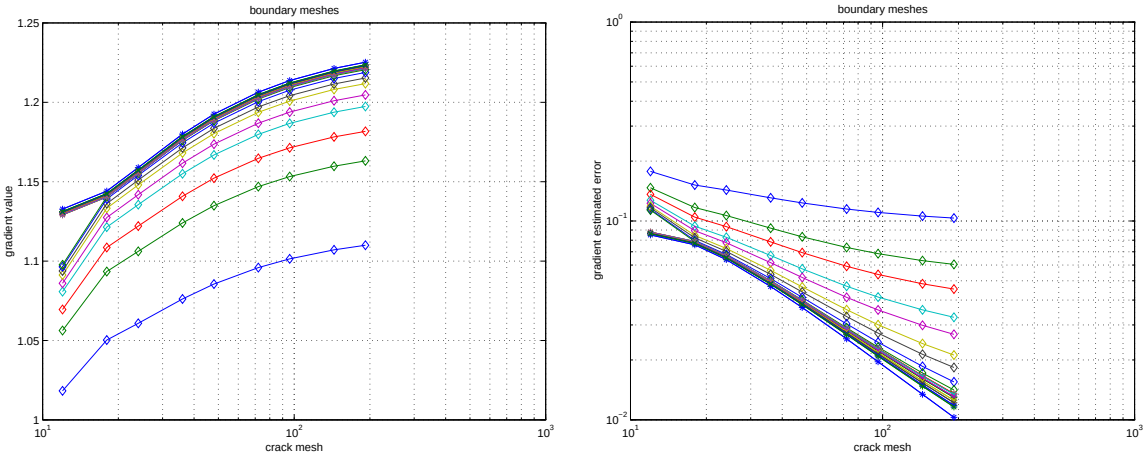

Figure 12.22: Circular model with no boundary prescriptions. Measurements over the *whole* circle. Sensitivity to *vertical* displacement of crack. (o) AVM calculation, (x) FD calculation.

The estimate of the final value has been made from a bilogaritmic extrapolation of the values of the more densely meshed models. The estimated limits for the three examples were 8.76, 4.46 and 1.238 respectively. The extrapolation of the AVM calculation and the finite differences were in reasonable agreement.

Regarding the contour and crack meshes, note that the increase in one mesh independently of the other provokes a blockage of the convergence; i.e. both meshes have to be improved to reach the real value.

The most interesting fact that these graphics show is that both the AVM and the finite difference converge to some value, which moreover appears to be the same. An explanation to why the methods converge with different patterns could be that the AVM is not consistent in the sense that it gives the sensitivity of the continuous problem, not the discretized one, as the finite differences do. The reason is that the AVM equations are valid for a continuous before any discretization. For solving them, we discretize the direct problem, the adjoint problem, and the integration of the AVM formula, introducing errors in all of them. Although the values obtained converge to the gradient of the continuous, they do not coincide with any value. The finite differences do express directly the gradient of the eventually discretized problem.

Dependence on the frequency

We will analyze how the frequency of the excitation affects the computation of the gradient, by plotting the agreement between FD and AVM gradient for each frequency.

Figures 12.23, 12.24 and 12.25 show the relative gradient error versus the frequency, representing each curve a different discretization in terms of a gradually growing number of elements for the circle and each lip of the crack.

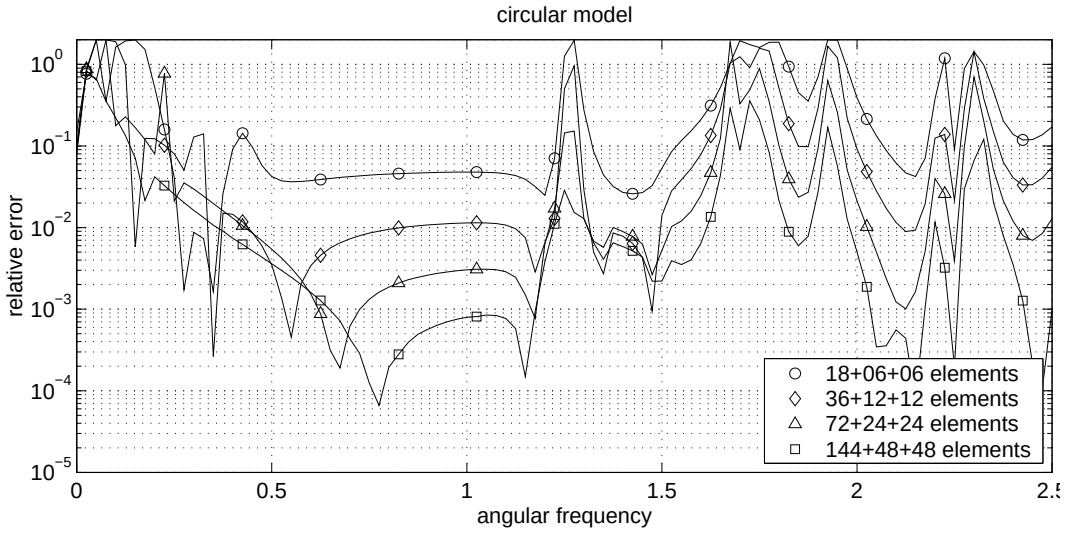

Figure 12.23: Circular model with no displacement prescriptions. Sensitivity to horizontal displacement of the crack.

In the sequel, the errors will be defined as the relative difference between the AVM calculation (avm) and the finite difference (fd) as,

$$error = \frac{|avm - fd|}{\sqrt{\frac{avm^2 + fd^2}{2}}}$$

The main point to notice is that the error, where the results make sense (outside the high error peaks), regularly decays in accordance with the enhacement of the mesh.

The first problem one notes regards the lach of convergence at low frequencies. This is probably due to a bad computation of the FD gradient, since the numerical errors due to the logaritmic dependence of the fundamental solution to the frequency, become too big in comparison with the epsilon chosen for the FD computation. The same logarithmic effect may affect the AVM computation.

At certain frequencies, all graphics show a number of peaks in the errors showing invalid solutions. The explanation could be the presence of eigenfrequencies at these points. To support this hypothesis we have calculated for the problem in figure 12.24 the first eigenfrequencies by finite elements (Abaqus, table on the right) and we have plotted the determinant of the system matrix of the boundary element problem for a $24 + 8 + 8$ discretization (figure 12.24), and the same problem by the finite element method, which gives the data in the following table. These data show an agreement in the values of the frequencies of minimum determinant, eigenfrequencies and peaks in the sensitivity errors. The following table confirms the values of the eigenfrequencies computed by the finite element method.

eigenfrequencies	0.491	0.909	1.149	1.676	1.919	1.962	2.385	2.597	2.644

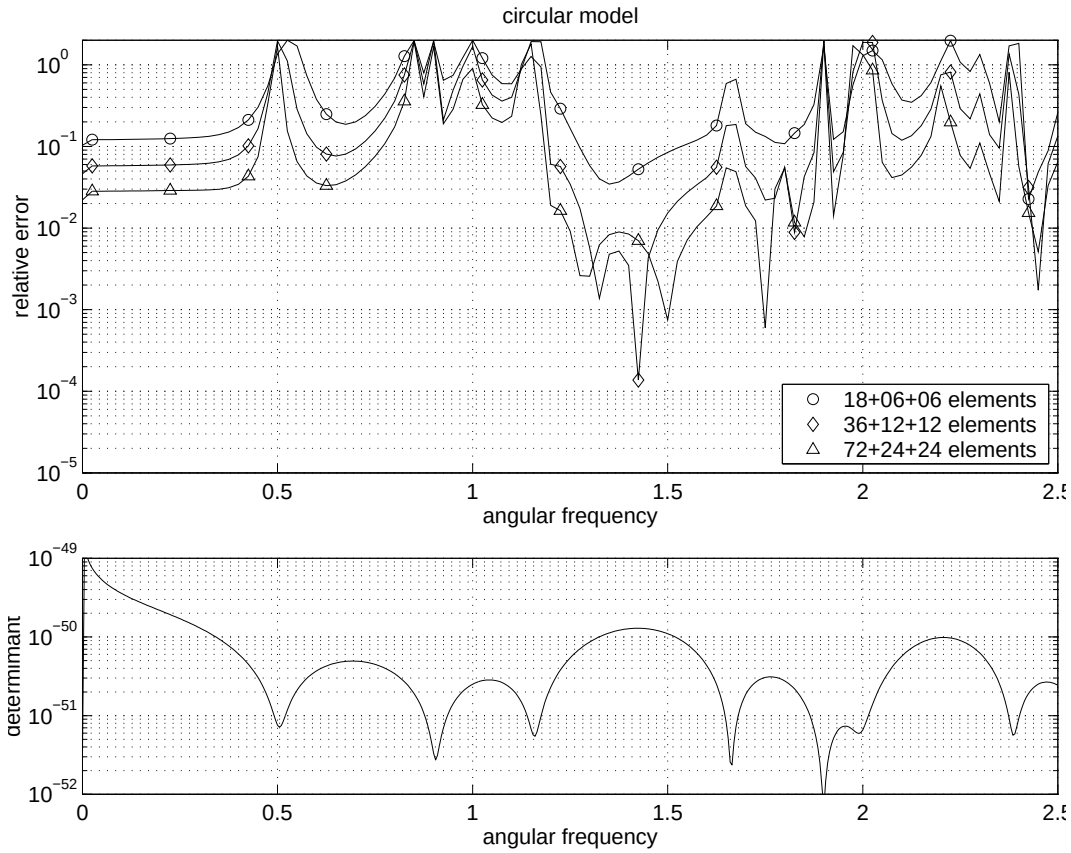

Figure 12.24: Circular model with a third of the circle constrained and measurements on another third. Top: sensitivity to vertical displacement of crack. Bottom: determinant of the BEM system matrix to identify the eigenfrequencies.

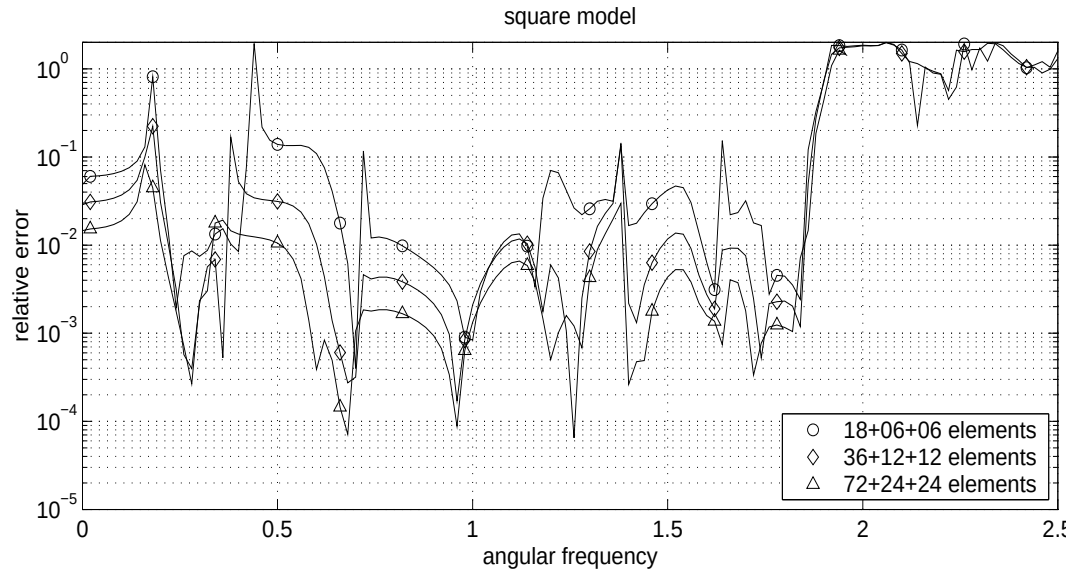

Figure 12.25: Square-shaped model with full measurements. Sensitivity to vertical displacement of crack.

Dependence on the measurements

This section is aimed at studying how the number of data given to the problem (measurements) affects the computation of the gradient.

Figure 12.26 represents the error in the circular model on the left and the square on the right for a range of the non-constrained boundary with measurements on x and y. In the circular model,

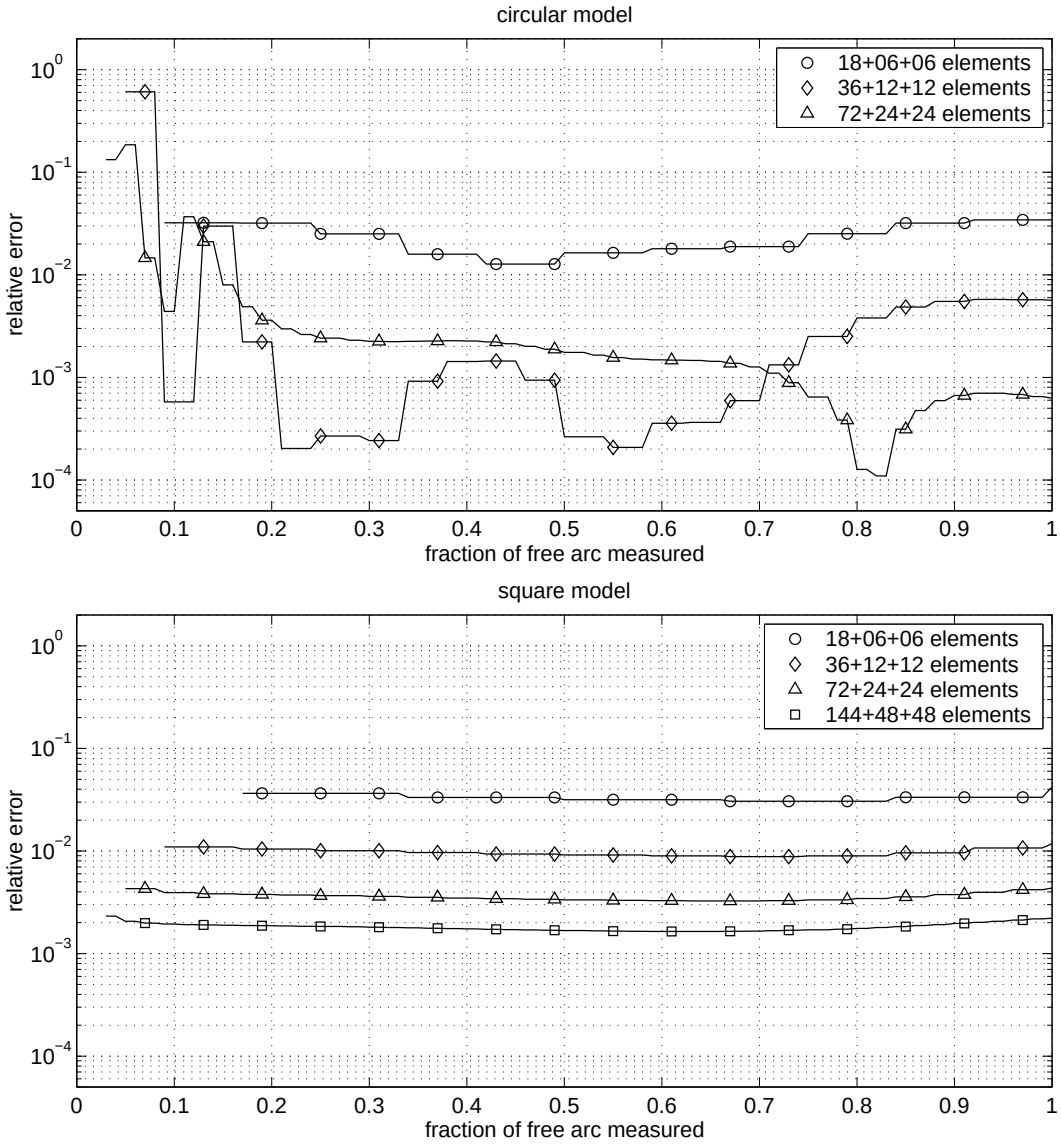

Figure 12.26: Dependence of the relative error on an increasing number of measurements.

one third of the boundary is constrained and the frequency is fixed at $\omega = 1.0$ in both models. The plot is made for a range of growing discretizations.

Dependence on the boundary conditions

In order to catch a wider range of possible problems, we have found that the definition of the boundary prescriptions provides interesting effects to the gradient.

Figure 12.27 represents a similar graphic as above for the circular model, but for a range of constrained arc, fixing the measured area at a third of the boundary. All figures show acceptable errors

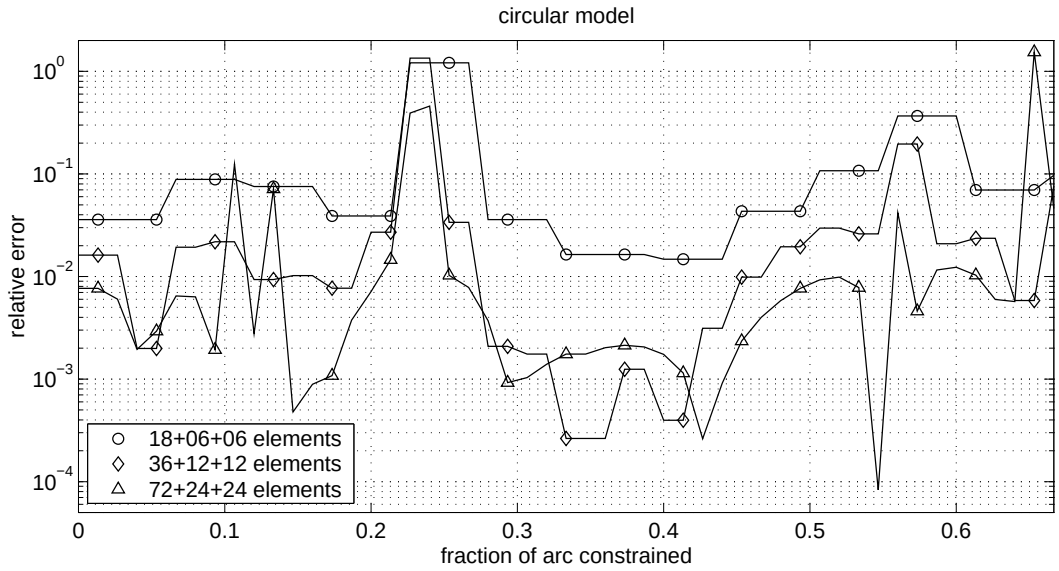

Figure 12.27: Dependence of the relative error on the fraction of constrained boundary.

with the exception of the peaks, probably originated again by the presence of eigenfrequencies.

Comparison of different parametrizations

The sensitivity has been calculated for the four first parameters, which are the only independent ones for a straight crack, and for two more strange parameters, in order to demonstrate that the choice of parametrization is free. The definition of the latter is defined in figure 12.28.

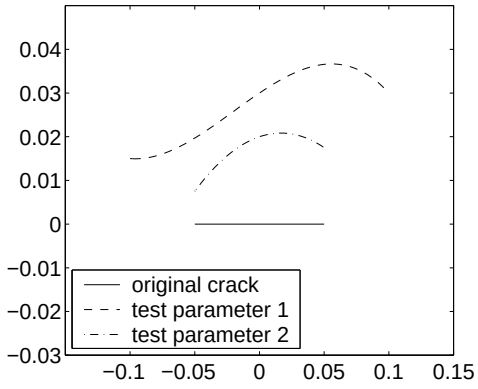

$$\delta\mathbf{x}^1 = [x - x_{cg}, 0.03 + 0.4 * (x - x_{cg}) \\ -3 * (x - x_{cg})^2 - 100 * (x - x_{cg})^3]$$

$$\delta\mathbf{x}^2 = [0, 0.02 + 0.1 * (x - x_{cg}) \\ -3 * (x - x_{cg})^2]$$

Figure 12.28: Free parametrization definition

The relative errors versus the mesh are represented for a fixed frequency of $\omega = 1.5$ and for all parameters mentioned in figure 12.28 for both the circular and square model. The relative errors appear to drop regularly as the mesh is improved.

In figure 12.30 the values of the gradient by the AVM and FD are represented on the right for several discretizations, whereas the left side shows the relative error between them. The model

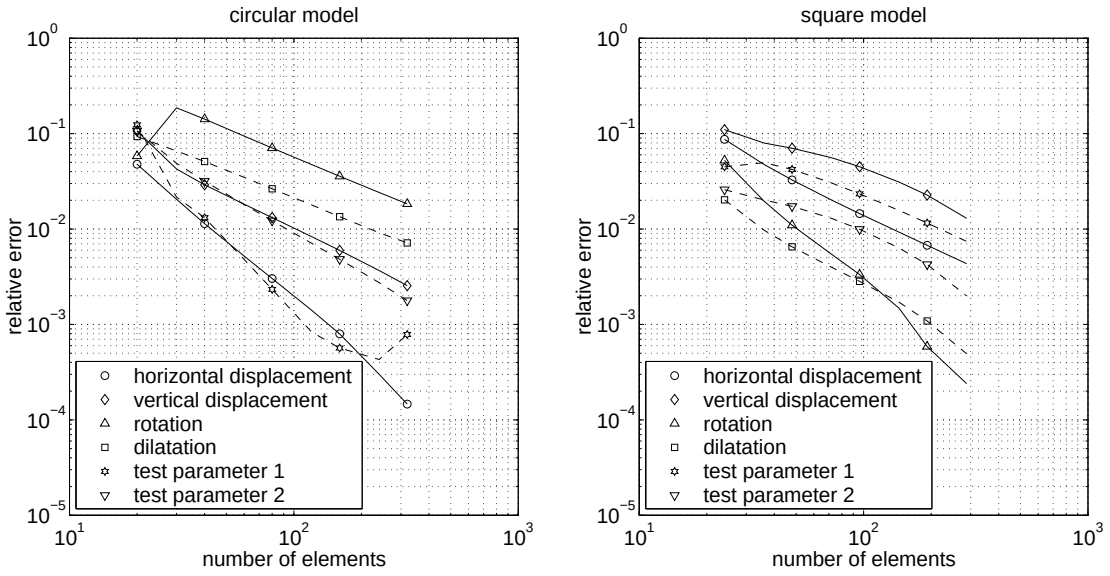

Figure 12.29: Evolution of relative error with the mesh improvement. Circular model (left) and square (right).

chosen in the sequel is the circular one, with a fixed frequency of $\omega = 0.8$ and a third of the boundary constrained. The measures come from the same problem with the crack displaced 0.2 towards the upper normal. As explained earlier, in the element-wise parametrization, the parameters consist of the normal displacements at a set of shape functions centered at the middle of the elements, and two more parameters representing the tip growth in its own direction.

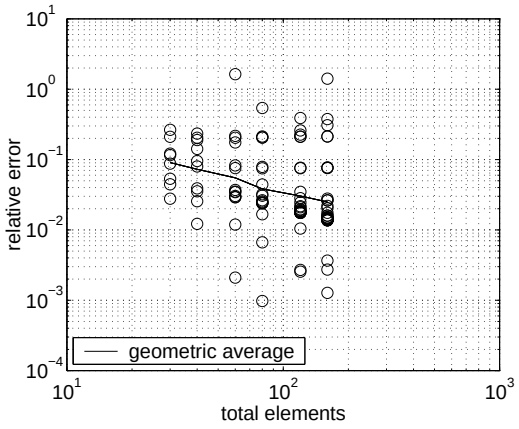

N^o of elements (crack)	N^o of parameters	Geometric average of error	Geometric standard deviation [1]
6	8	0.0905	0.0387
8	10	0.0728	0.0499
12	14	0.0549	0.0506
16	18	0.0383	0.0285
24	26	0.0303	0.0217
32	34	0.0249	0.0172

Figure 12.30: Element-wise parametrization. Evolution of errors with the mesh. At each fixed number of elements, each circle represents the discrepancy between AVM and FD of each parameter. Since the parametrization is mesh-dependent, there is a different set of parameters for each discretization.

We should remark that there is not a correlation in the increasing mesh / gradients, since the parameters are mesh dependent and therefore different for every one. On the other hand, an increase in the density of the mesh should not imply an enhacement in the error since the integrals involved keep sweeping a few elements each. For the case of a straight crack, the errors kept reasonably low, at around 10% except for some peaks around the penultimate nodes from the tips.

Figure 12.31 shows the same figures for the significative parameters 1, 3, 5 and 7 at a fixed discretization of $18 + 6 + 6$ elements at a varying frequency.

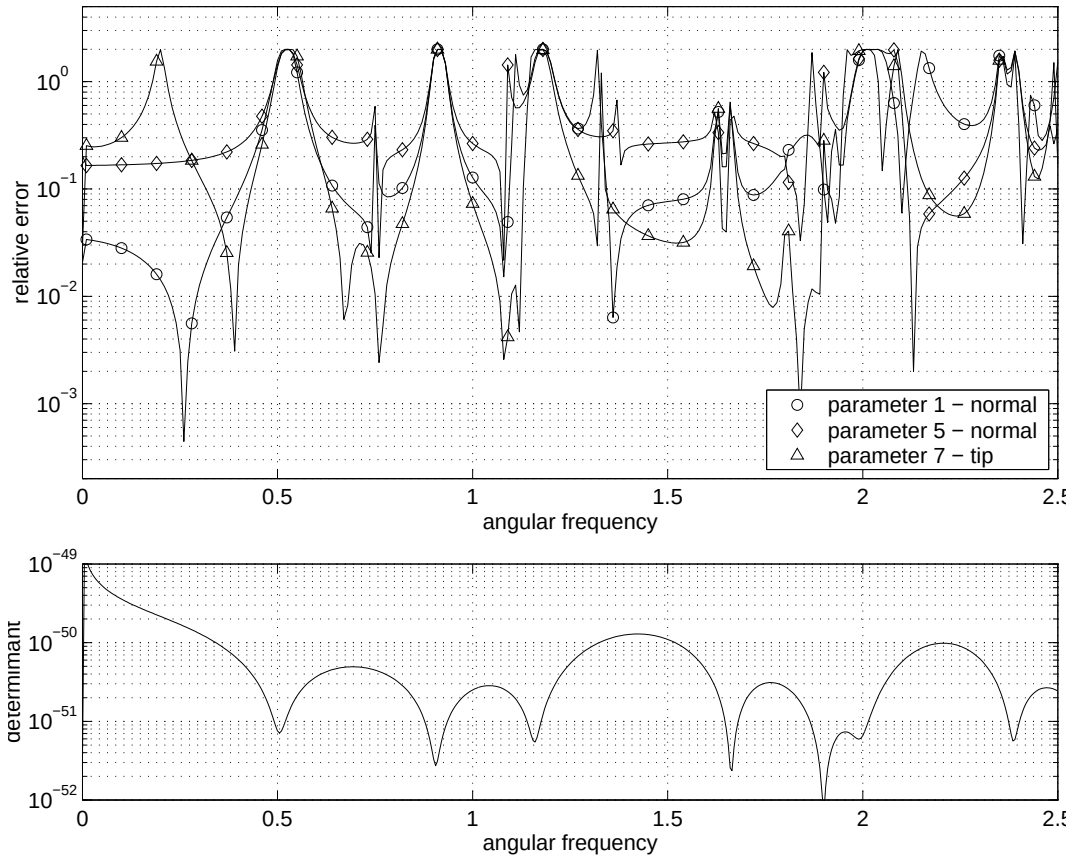

Figure 12.31: Relative errors for some parameters at a range of frequencies.

By the use of any superimposed parametrization mesh that will group these parameters, the errors shown in this graph tend to average each other.

Figure 12.32 shows the convergence of the gradient values for the case of a curved crack. The parametrization mesh is composed by three elements, besides the two remaining parameters for tip growth.

This shows the convenience of using this strategy of separating the discretization and the parametrization in order to have full control over both the desired robustness/detail of the parametrization and the accuracy of the calculations.

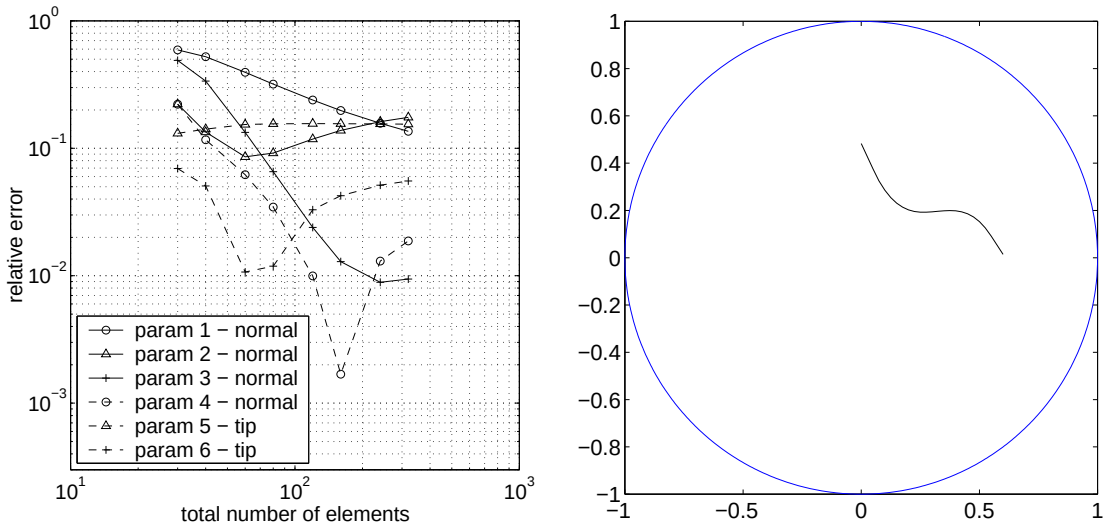

Figure 12.32: Convergence of gradients for curved crack. Frequency $\omega = 0.8$. One third of the circle constrained. Measures over another third of the boundary. Left: Discrepancy between FD and AVM. Right: geometry of the specimen.

Chapter 13

Optimization algorithms test

13.1 Methodology

The following tests are aimed at finding the advantages and disadvantages of the most suitable optimization algorithms for identification IP in static 2D elasticity. The algorithms tested are,

	Method	Gradient (Gr)	Line search (LS)
1	Gauss-Newton (GN)	•	
2		•	•
3			•
4	Levenberg-Marquardt (LM)	•	
5		•	•
6			•
7	BFGS	•	•
8			•
9	GN-Secant Update	•	

The problem is divided in three stages:

1. The first one consists in the calculation of a direct problem with the BEM. For this purpose, a classical code for bidimensional elasticity with quadratic elements and collocation points at the geometrical nodes has been implemented. The details of the formulation can be found in [22], [36]. The code was written in Fortran 90 and run on an HP700 workstation. In all the cases the excitation of the problem was static.

2. The second stage consists in the calculation of the $A = J$ matrix (sensitivity matrix or jacobian) that comes from the sensitivity equations (δbie). This implementation is merged with the former code in order to take advantage of common calculations. The formulation is detailed in [100].

3. Both calculations are repeated in each iteration of the optimization algorithm. This algorithm has been taken from the Matlab Optimization Toolbox, version 5, with the proper modifications so as to match the needs of the problem. It has run on the same workstation.

13.2 Description of problems

We have chosen a set of simple models that enhance different faces of the problem each, as well as some from other authors for a comparison. They range from easy problems to more complicated ones, although practical problems could become much more complicated. For each problem, we

use every one of the algorithms. They are sketched in figure 13.1. The number of elements, free parameters and measurements (data) are shown in the table.

Problems A to D consist of a 3×3 square external boundary with one or two circular flaws. The points of measurements and the position of the assumed and real flaw are plotted on figure 13.1. Problem F was consists of a 100×50 rectangle with different boundary conditions and an elliptical flaw. This problem was solved by Bezerra et al. [9]. Here only two parameters are allowed from a starting circle, allowing horizontal and vertical displacement. The solution converges to a circular configuration close to the real but not identical. Bezerra et al. solved this problem in 35 iterations by the BFGS algorithm.

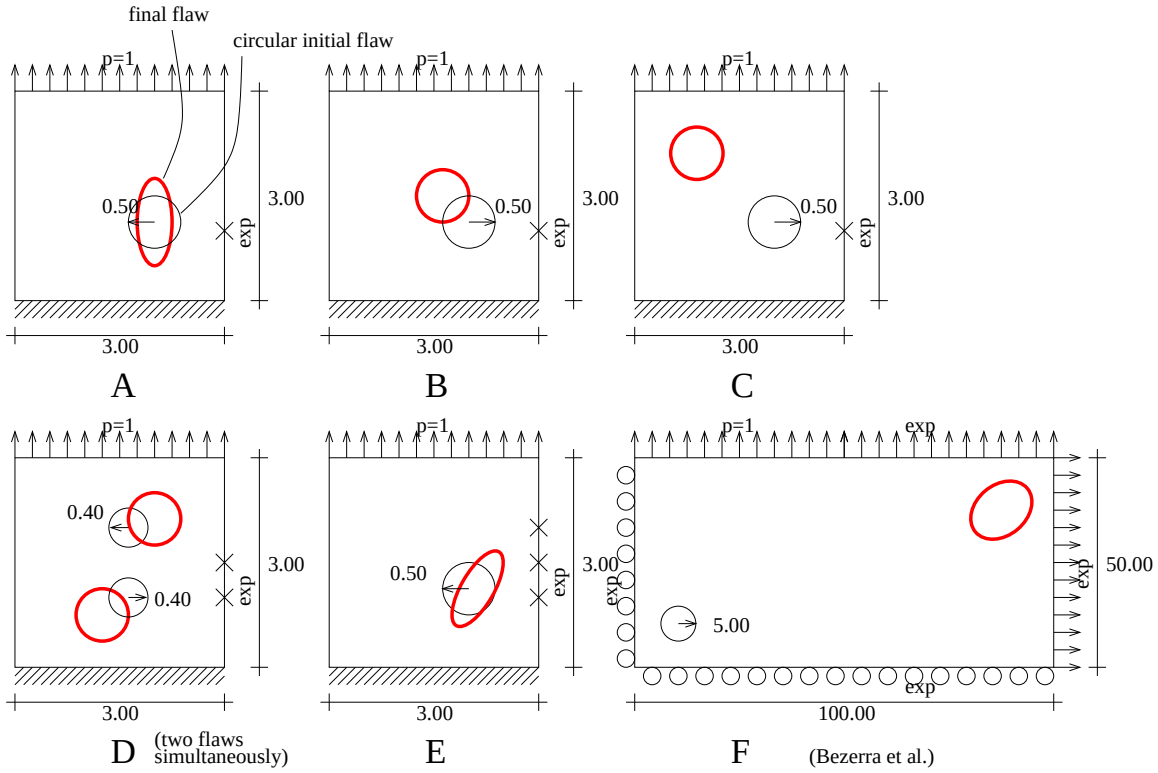

Figure 13.1: Problem definition.

Problem	A	B	C	D	E	F
Exterior Elements	12	12	12	12	12	24
Flaw Elements	4	4	4	2x4	4	8
Total Elements	16	16	16	20	16	32
Parameters	5	2	2	4	5	2
Experimental data	5	2	2	8	5	80

13.3 Results

In the following table we schematize the results in terms of function evaluations (iterations) and gradient evaluations required. The problems have been sorted from easier to more complex, and (-/-) means no convergence.

Method	Gr	LS	A	B	C	D	E	F	Mean	Success
G-N	•		8/8	-/-	-/-	5/5	-/-	31/31	14.67/14.67	50 %
	•	•	13/5	-/-	-/-	17/6	-/-	35/-	21.67/ 5.5	50 %
		•	10/0	-/-	-/-	41/0	-/-	-/-	25.5 / -	33 %
L-M	•		7/7	6/6	6/6	7/7	17/17	15/15	9.67/ 9.67	100%
	•	•	13/5	14/5	23/8	17/6	42/13	-/-	21.8 / 7.4	83 %
		•	10/0	23/0	34/0	41/0	64/0	40/0	42.4 / -	100%
BFGS	•	•	9/3	20/6	23/7	21/5	61/17	35/-	28.17/ 7.6	100%
		•	12/0	32/0	37/0	64/0	61/0	-/-	41.2 / -	83 %
GN-SU	•		5/5	6/6	-/-	4/4	-/-	12/12	5.0 / 5.0	67 %

The graphics of the evolution of the geometry and error defined as the value of the cost functional are shown in the following figures.

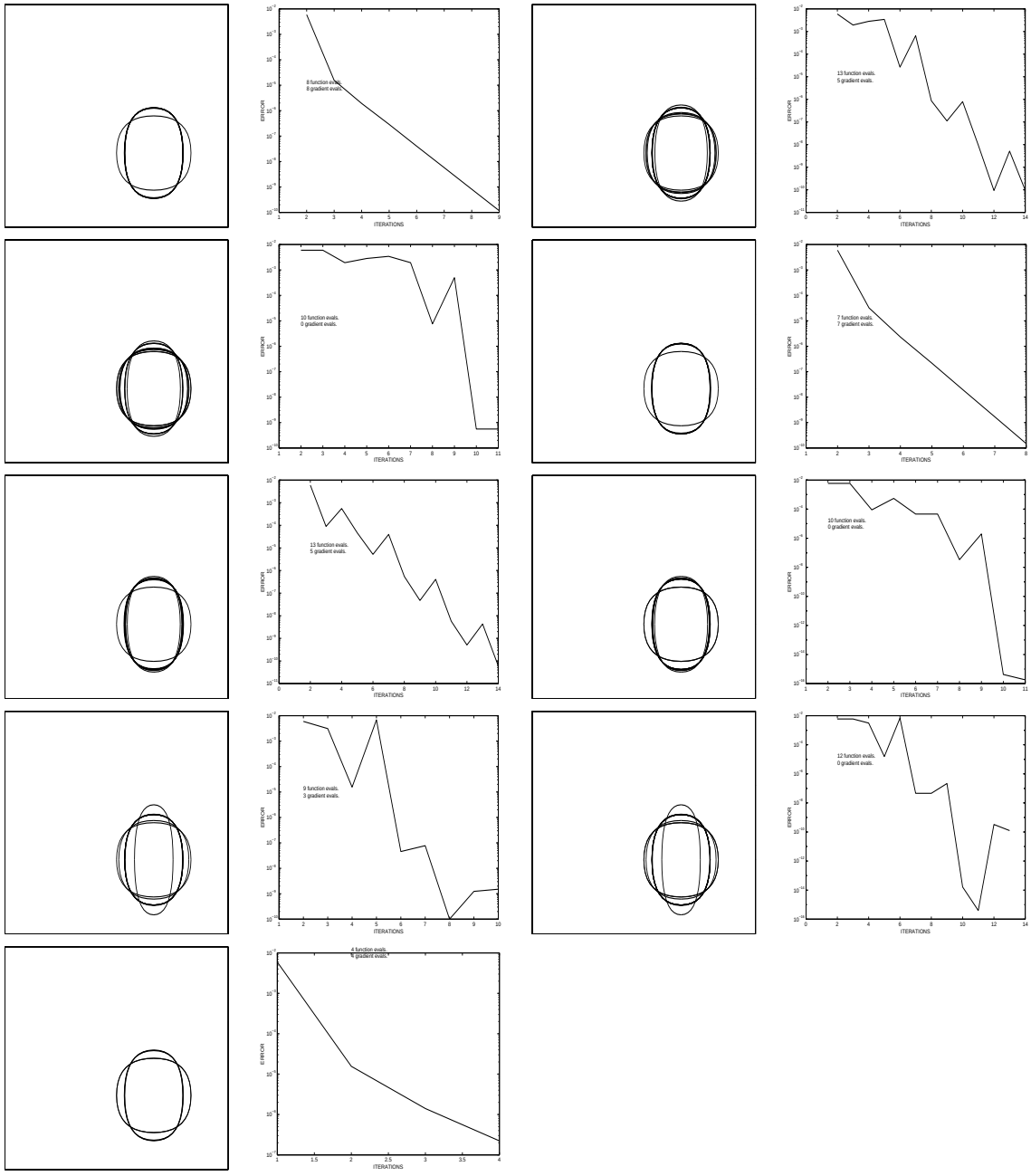

Figure 13.2: Example A. The nine minimization algorithms are used from left to right and then up to down.

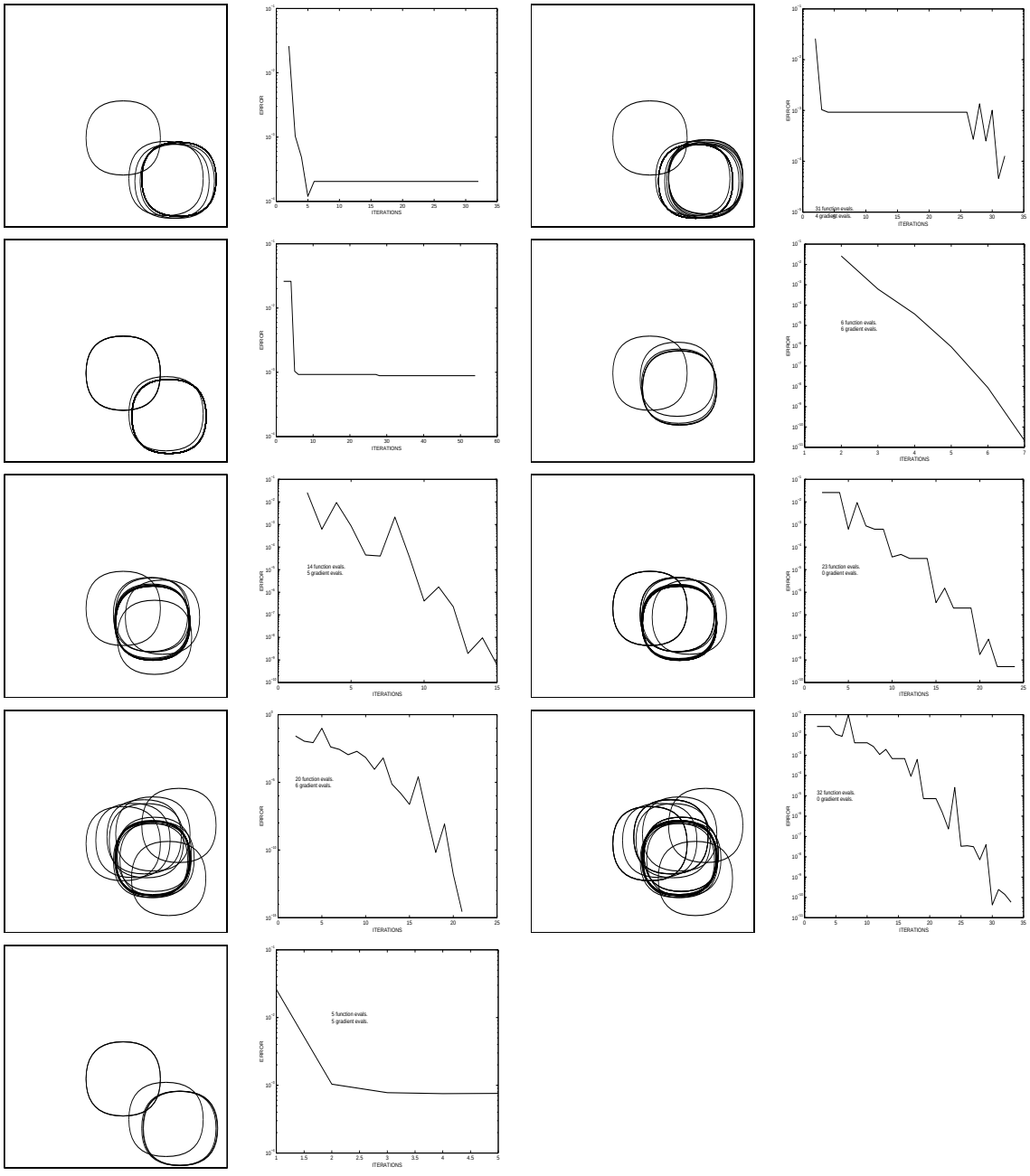

Figure 13.3: Example B. The nine minimization algorithms are used from left to right and then up to down.

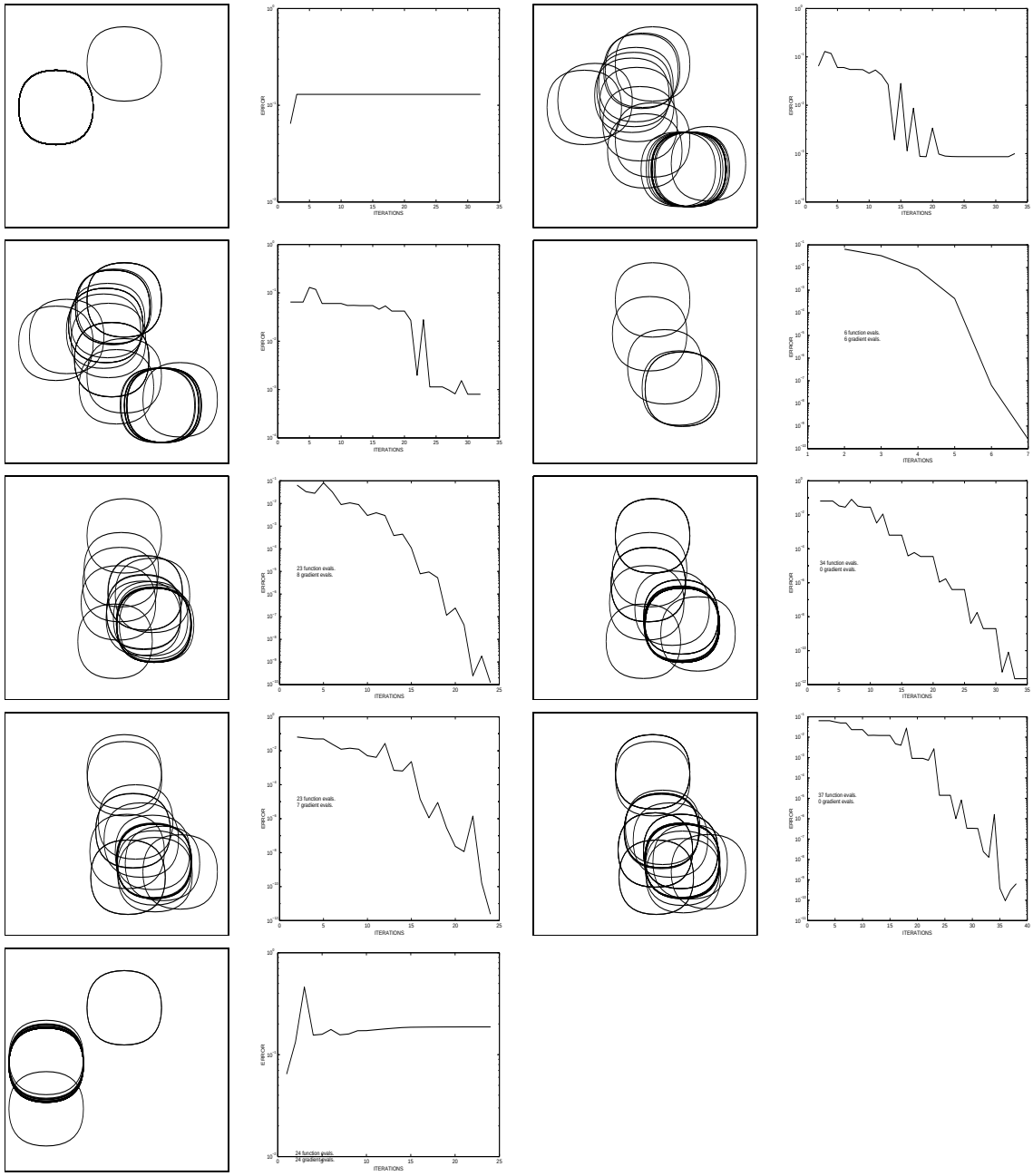

Figure 13.4: Example C. The nine minimization algorithms are used from left to right and then up to down.

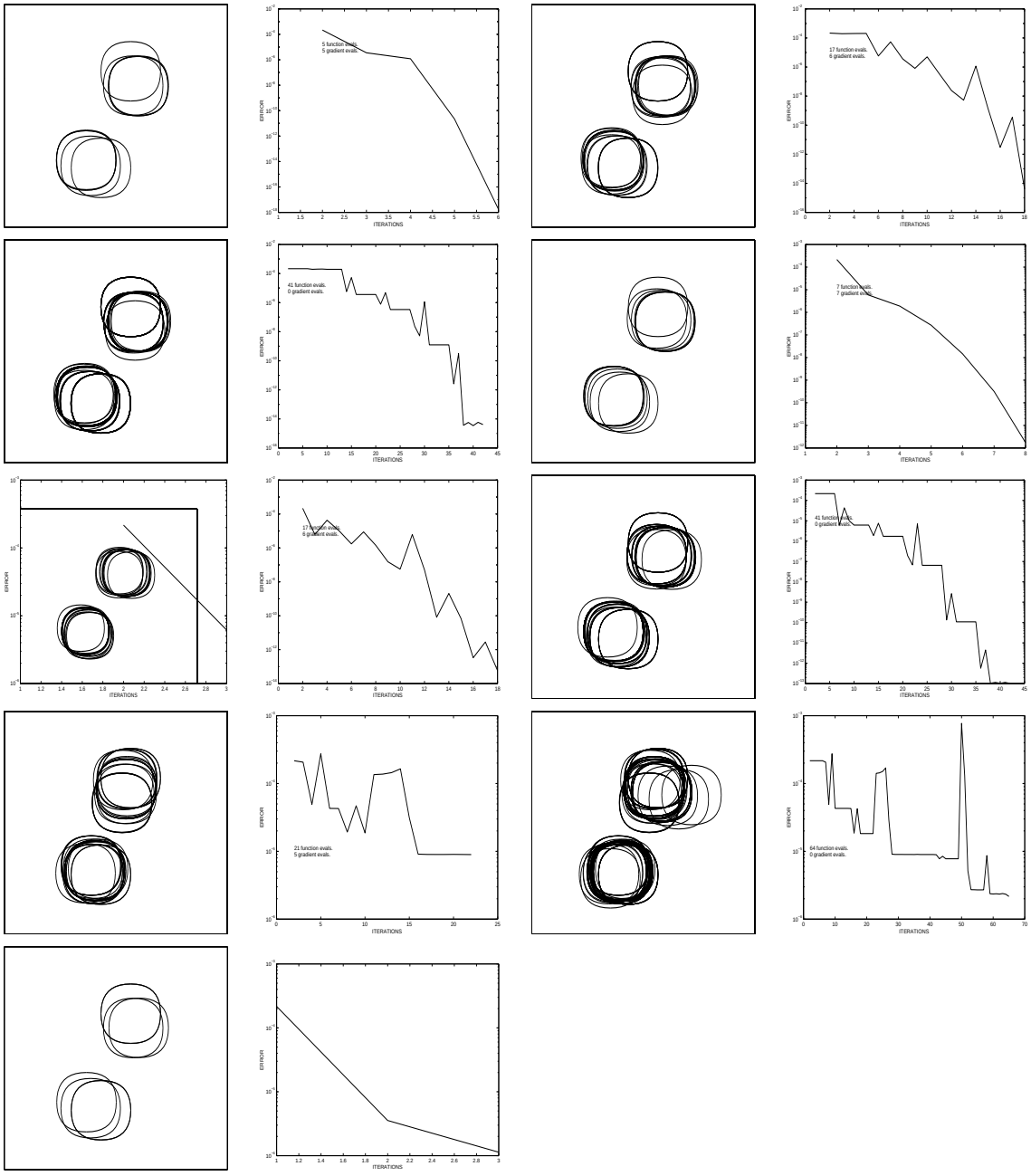

Figure 13.5: Example D. The nine minimization algorithms are used from left to right and then up to down.

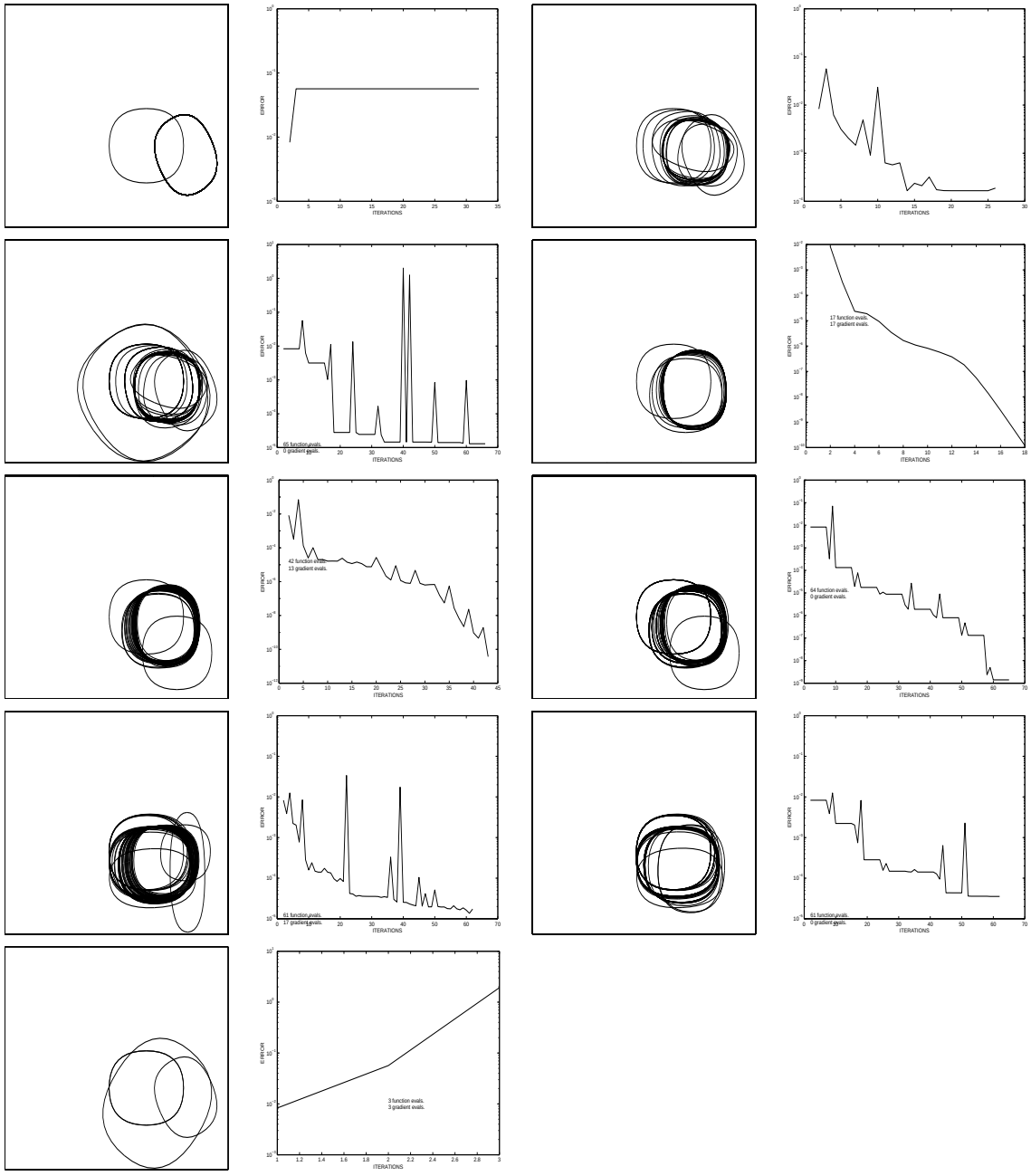

Figure 13.6: Example E. The nine minimization algorithms are used from left to right and then up to down.

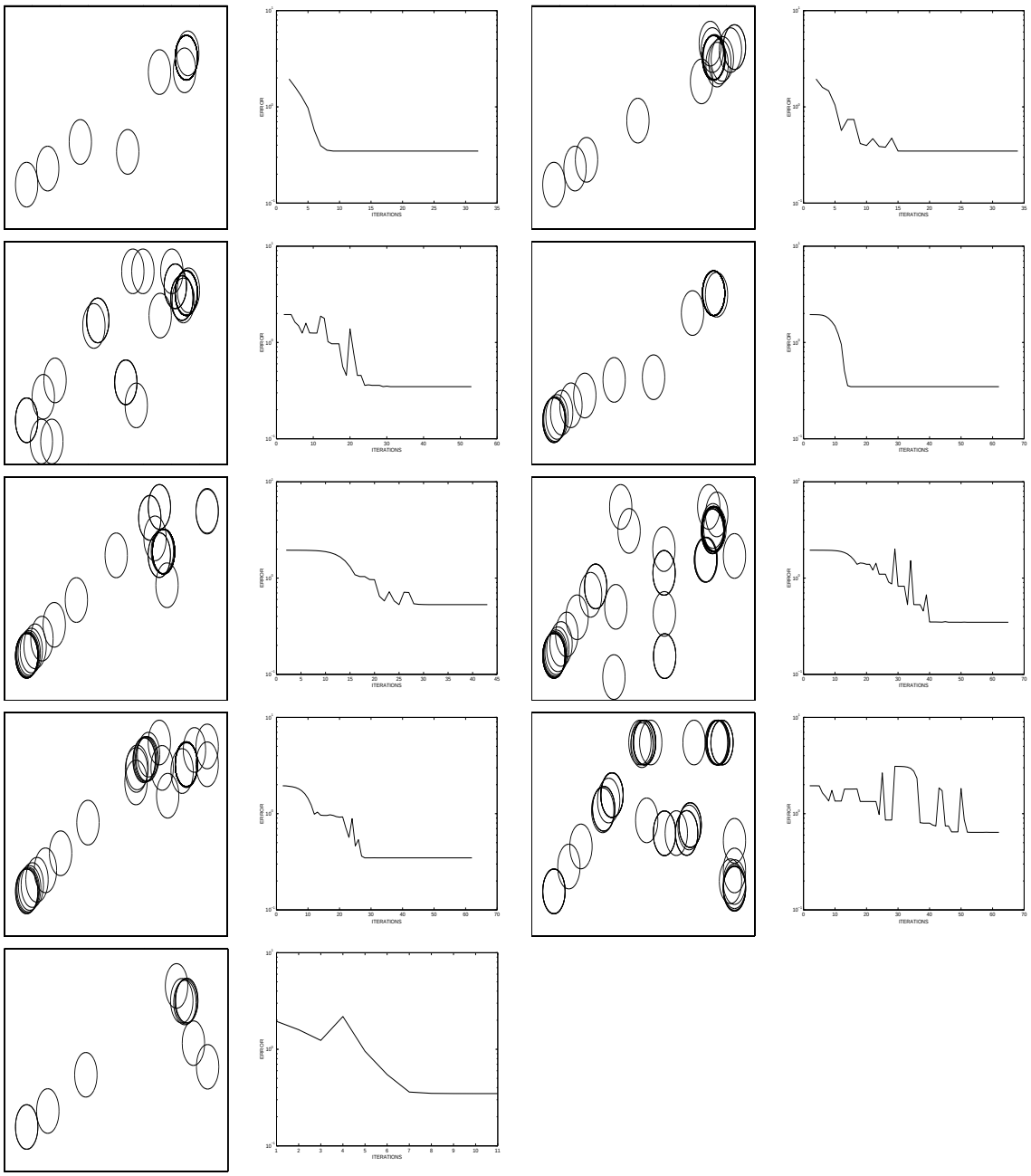

Figure 13.7: Example F. The nine minimization algorithms are used from left to right and then up to down.

Chapter 14

Identification inverse problems

From now on we will solve complete inverse problems by using the nonlinear optimization algorithms just studied and supplying the different gradients developed in this work, to test their accuracy and convergence properties, dependence on errors in the problem and other factors.

14.1 Other authors examples

We have compared the direct derivation together with the basic Gauss-Newton method with the few examples proposed by other authors, achieving better results in all of the examples.

14.1.1 Panel with axial loadings

The first example was studied by L. M. Bezerra and S. Saigal [9]. His method is based on the minimization of a functional defined as the integral of the quadratic difference between calculated and measured displacements over the boundary, by a classical quasi-Newton method. This example consists in a rectangle of 100 by 50 inches constrained horizontally at the left side, and vertically at the lower side. It has uniform loads of 1000 psi outwards at the left and upper sides. The modulus of elasticity is $E = 1.86 \times 10^6$ psi. The measurements are taken as the displacements all over the boundary. The long side is divided into 8 quadratic elements, the short one in 4, and the circle into 8. In order to obtain convergence, we had to try two regularization techniques, both of wich worked properly. The first one, presented here, consisted in using a reduction of the steps defined by $\beta = 10$ (see section 11.2.4). In the other method, like the author in others of his examples, we had allow only the first two parameters (bidimensional rigid solid motion) variation until it stabilized at the 10th iteration, and then release all the variables.

In figures 14.1 and 14.2, we show the original results from L. Bezerra and ours, respectively. We obtained an error below 10^{-5} at the 10th iteration, whereas L. Bezerra obtained good convergence after 35 iterations.

14.1.2 Square plate

The second example is taken from S. C. Mellings and M. H. Aliabadi [85]. Their procedure is almost identical to the one of L. Bezerra, but with the steepest descent method. The example consists in a square plate subject to uniaxial tension with a elliptical hole. The stresses are known at 16 internal sensors. The geometrical dimensions have been taken graphically from the plot. In figures 14.1 and 14.2, we show respectively the original results from S. C. Mellings and M. H. Aliabadi, who need 89 iterations for the exact location, and 10 for an approximate one; and ours, where we need 9 for an error of 10^{-6}.

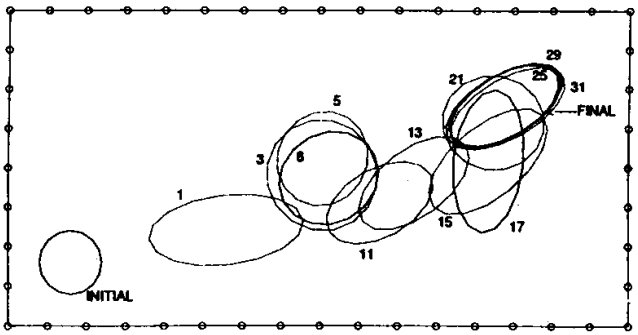

Figure 14.1: Panel with axilal loadings (Source: L. M. Bezerra and S. Saigal)

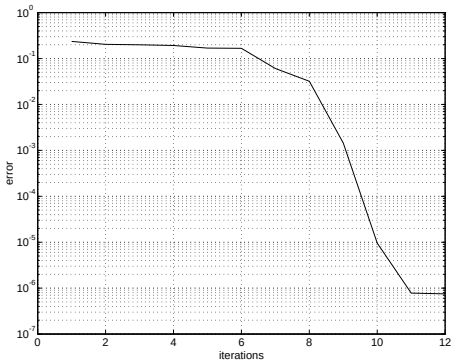

Figure 14.2: Panel with axilal loadings

14.1.3 Two holes

The third example comes from the job of Z. Yao and B. Gong [133]. Using the same method as the other two authors, this example consists in a square plate with a biaxial load: compression vertically and traction horizontally. This time, we have two holes simultaneously, and the data comes from the measured displacements over the whole boundary. The geometrical dimensions have been taken graphically from the plot. In figures 14.5 and 14.6, we show respectively their original results, with a need of 17 iterations for an error of 10^{-4}; and ours, where we need 5 iterations for the same error, and 8 to reduce it to 10^{-15}.

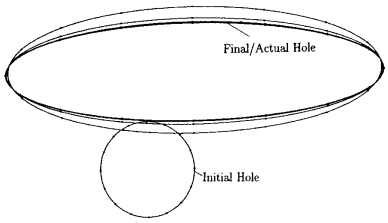

Figure 14.3: Infinite plate (Source: S. C. Mellings and M. H. Aliabadi).

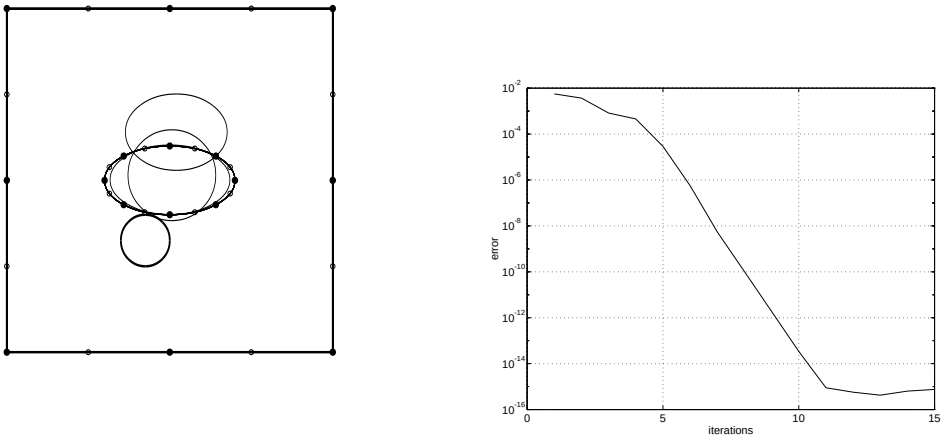

Figure 14.4: Infinite plate.

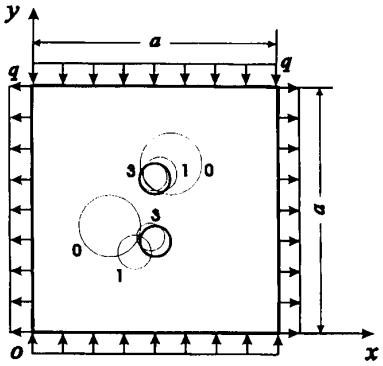

Figure 14.5: Square plate with two holes (Source: Z. Yao and B. Gong).

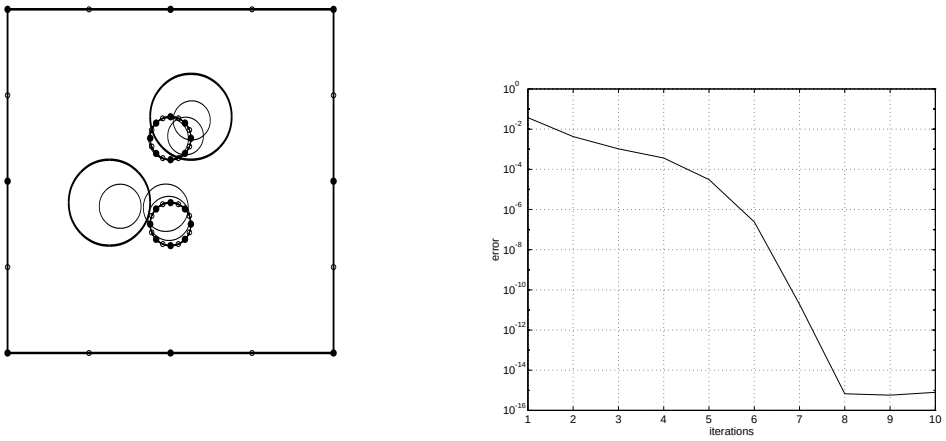

Figure 14.6: Square plate with two holes.

14.2 Convergence tests using Levenberg-Marquardt algorithm and direct derivation

14.2.1 Methodology

The three benchmark problems used at the sensitivity test by direct differenciation are used for the complete solution of an identification inverse problem using a least squares minimization algorithm: the Levenberg-Marquardt method with line search and gradient supply.

The starting configuration or initial guess is the corresponding to figure 14.7. The final configuration to be sought was shown in figure 12.5.

The fixed contour consists of a 2×2 box of a material with constants $E = 1.0$; $\nu = 0.2$, $\rho = 1.0$. In the case of an inclusion, it is made of an identical material changing $E = 0.5$. As boundary conditions the baseline is fixed and the upper side is subjected to an uniform unitary vertical stress. The initial cavities and inclusions are defined as a centered circle of radius 0.8, and the final ones are ellipses of center $(-0.3, 0.2)$ and semiaxes 0.41 and 0.22, at an angle of 39 degrees with the horizontal (like the ones used for the sensitivity tests). The initial crack is a horizontal centered segment of length 0.8, and the final crack is defined by $x = -0.7+0.8\lambda; y = 0.3+0.4\lambda+0.2\sin(2\pi\lambda)$, where the parameter λ goes from 0 to 1.

The model is made of two subboundaries per side of the outer box, and eight subboundaries for the circle or crack. If nothing else is specified, one quadratic element is used at each subboundary. The collocation points are always placed at $0.2a$ from the edge of the element, being a the distance between two geometrical, displacement or stress nodes.

The used parametrization is, unless something else is specified, the basic 6-parametrer one for cavities and inclusions, and the fourier crack parametrization for cracks, all of them defined in chapter 8.

The models are discretized using 2 quadratic elements per subboundary (a total of 8 for the external boundary plus 8 for the flaw). The measurements are the four complex displacements at the four uncontrained nodes of the lower half of the right vertical side.

The identification is made increasing gradually the number of parameters. This is done in four restarts of the optimization algorithm, with the parameters listed in the legend of each problem. The maximum number of iterations per restart is limited to 20, and the maximum increment in the value of each parameter is limited to 0.2 in order to limit possible divergences, using the *arcTan* remapping. The stopping criteria is $\Delta P = 0.001$.

Three plots are made for each benchmark problem: one corresponding to the search with static data; one corresponding to the values at frequency $\omega = 1.0$, and a third graphic with simultaneous data measured at frequencies $\omega = \{0.0, 0.5, 1.0, 1.5, 2.0\}$.

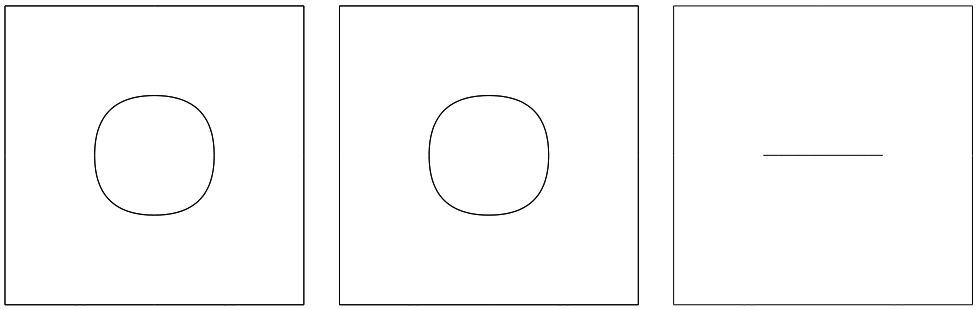

Figure 14.7: Description of cavity benchmark, inclusion benchmark and crack benchmark. Initial guess.

14.2.2 Relationship between convergence and distance

The idea in this section is to chech the scope of convergence for each problem at each frequency. For this purpose we plot the number of iterations (when converged) for a number of distances from the real solution. This distance is simply defined by scaling the parameter vector that defines the initial configuration from the final one.

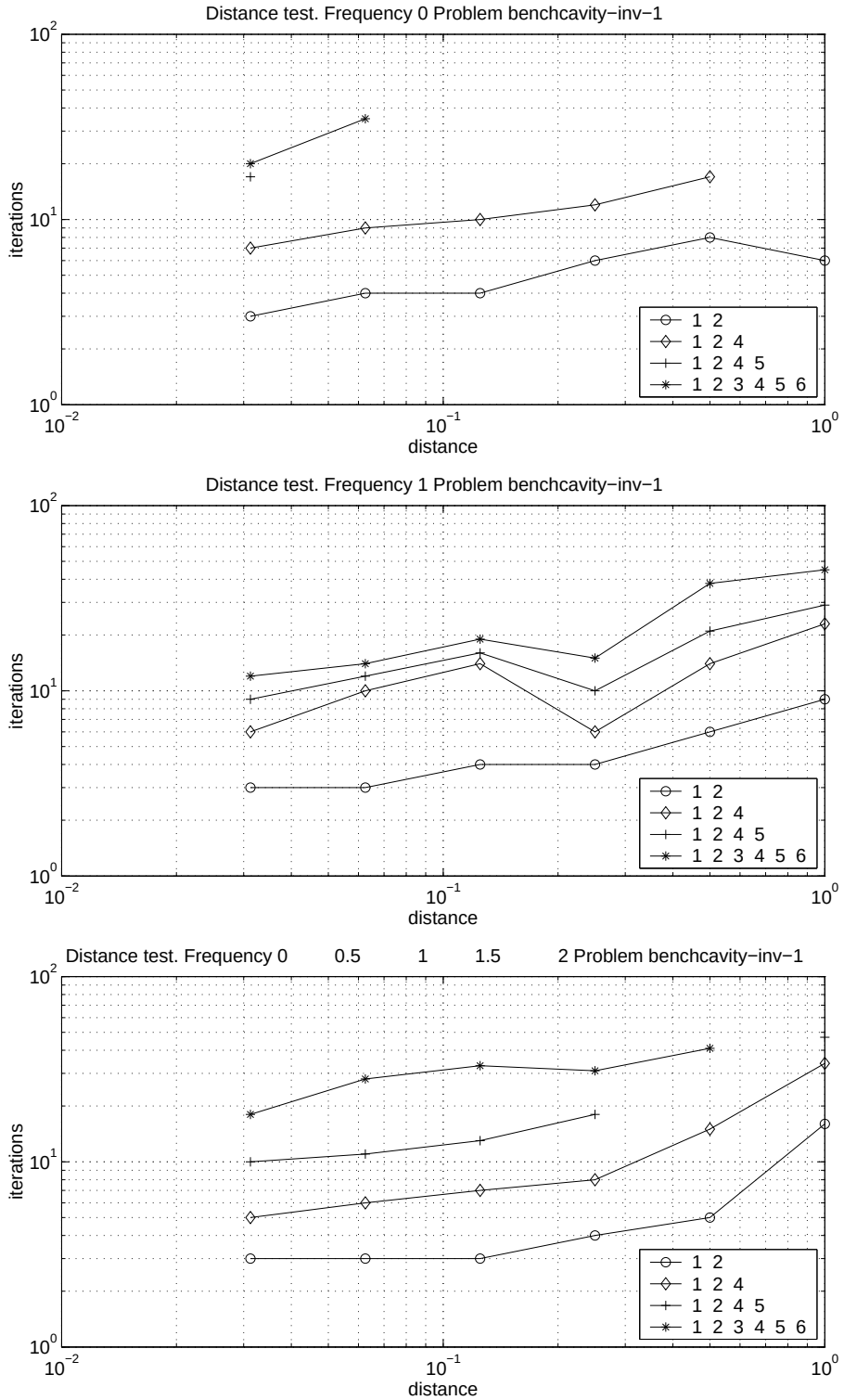

Figure 14.8: Convergence with distance from actual flaw. Cavity problem.

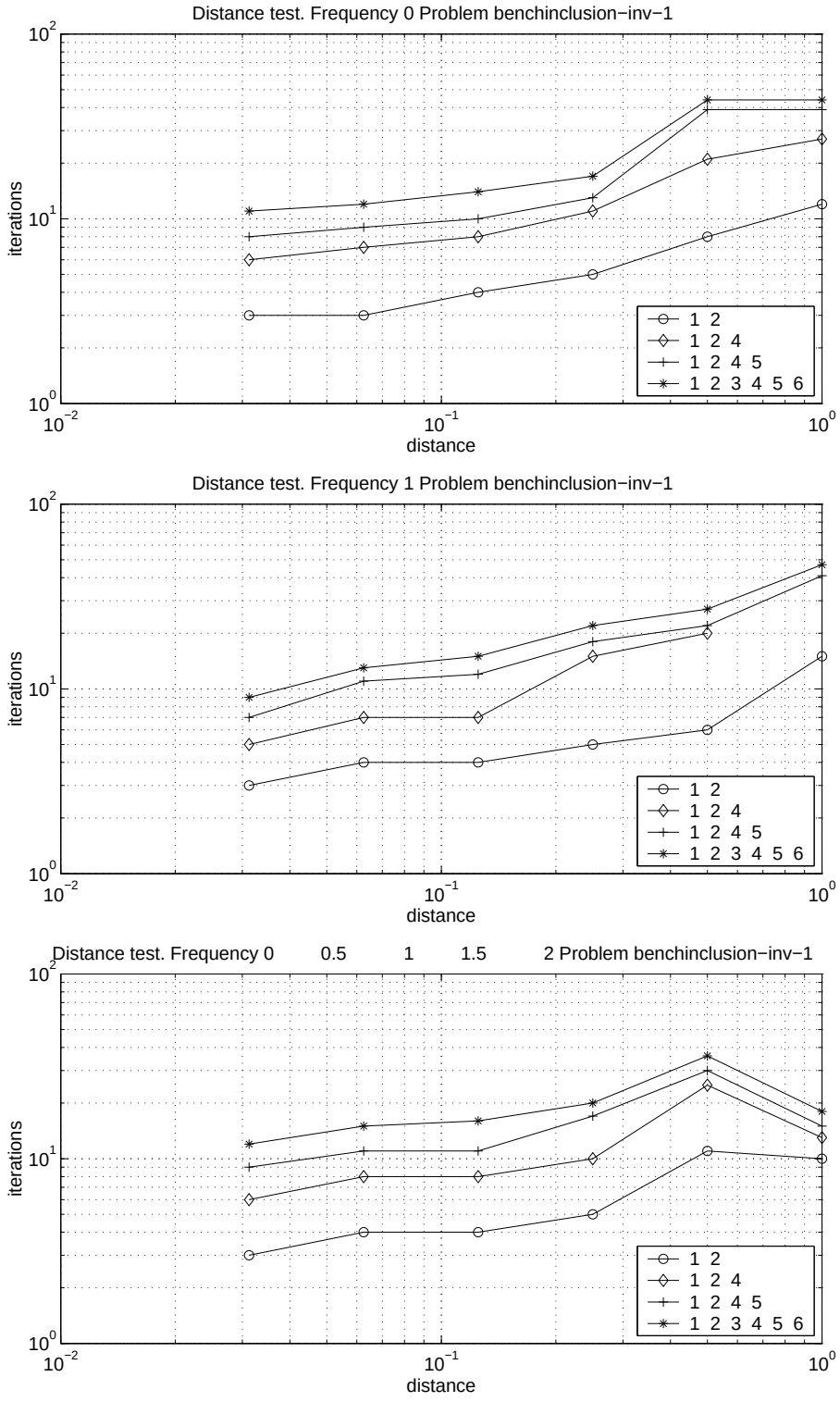

Figure 14.9: Convergence with distance from actual flaw. Inclusion problem.

Figures 14.8, 14.9, 14.10 and 14.11 show the necessary iterations for the convergence placing the initial guess at a proportional value between the zero-vector and the final parameter. In the case of absence of convergence, the corresponding point is not plotted. It should be noted that the convergence is not necessary to the real result. The partial results at each restart are plotted.

One may observe that the necessary iterations increase more or less gradually with the distance and consequent difficulty of the search. A faster and more stable convergence is shown in the

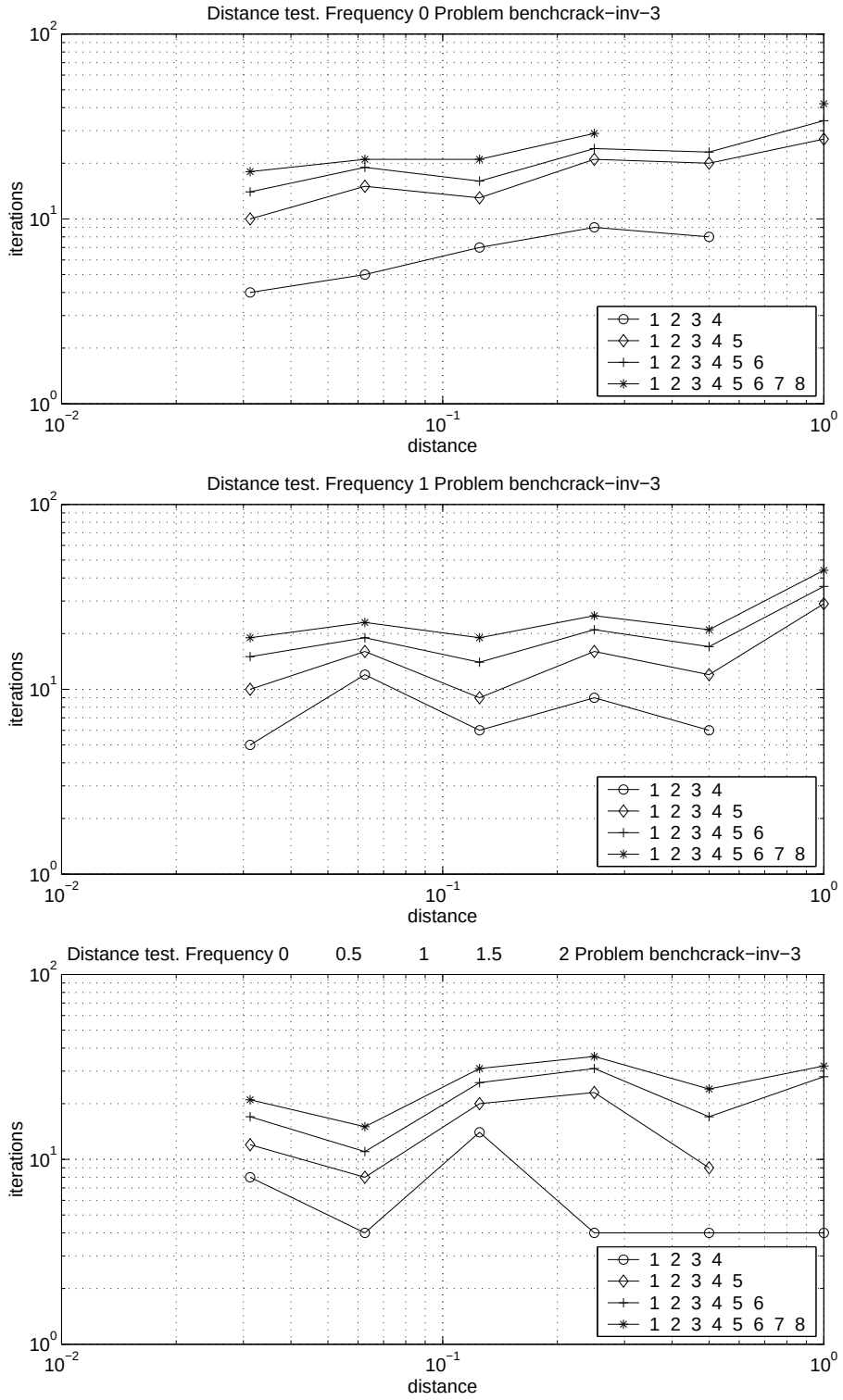

Figure 14.10: Convergence with distance from actual flaw. Crack problem.

case of inclusions, whereas the highest number of iterations is needed for the search of cracks, even at simple parametrizations. Complicated parametrizations show some problems at the last parameters.

Another interesting point is that, as expected, the success in a particular restart is critical for the success of the following one. This justifies the used dosage of parameters.

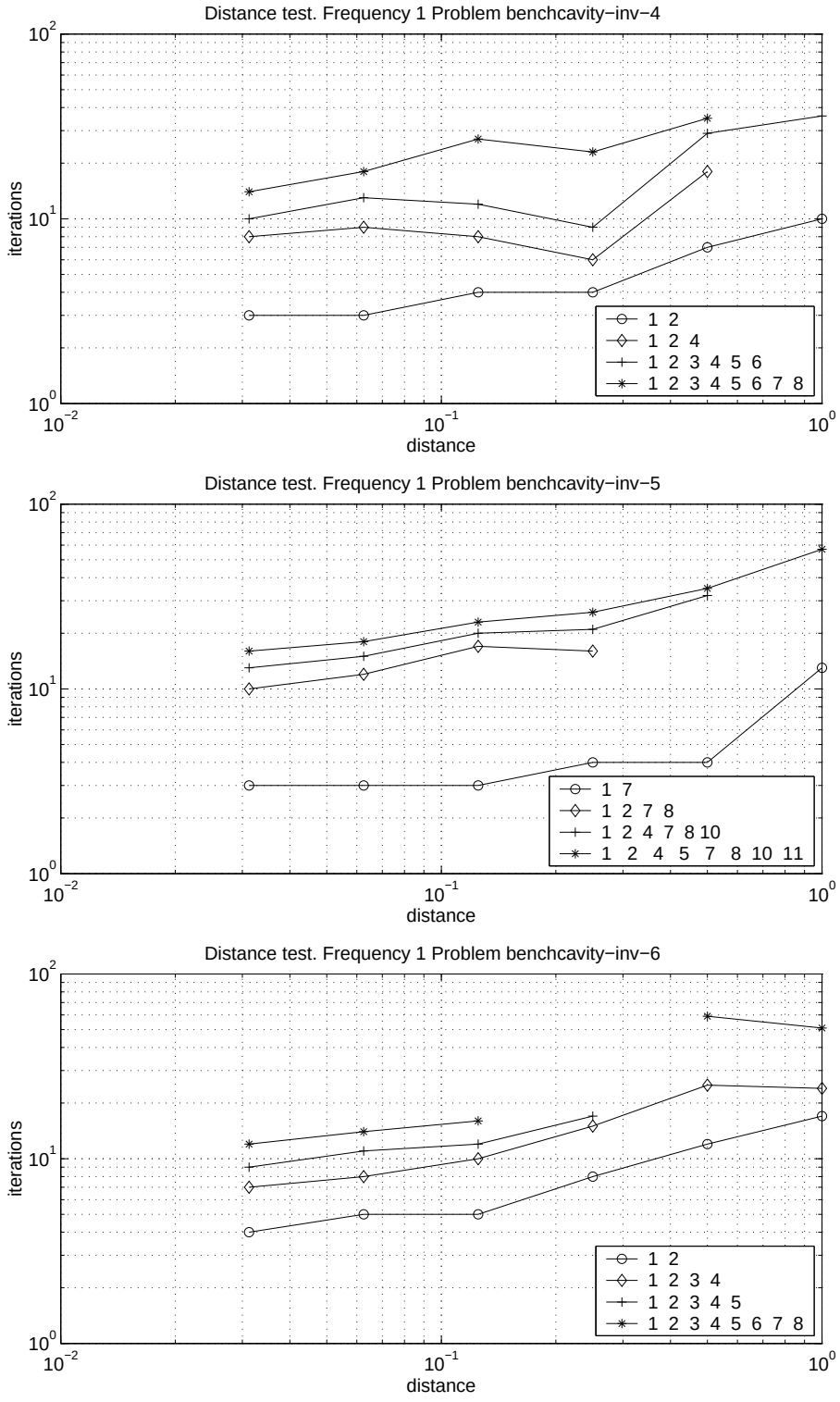

Figure 14.11: Convergence with distance from actual flaw. Complex parametrizations. Cavity problem.

14.2.3 Dependence on the measurements

The number of data supply for an inverse problem is an important factor. Here we solve the problems with a varying number of measurements: from a minimum of 8 (on the half right vertical side), and increasing anti-clock-wise along the external boundary until 64.

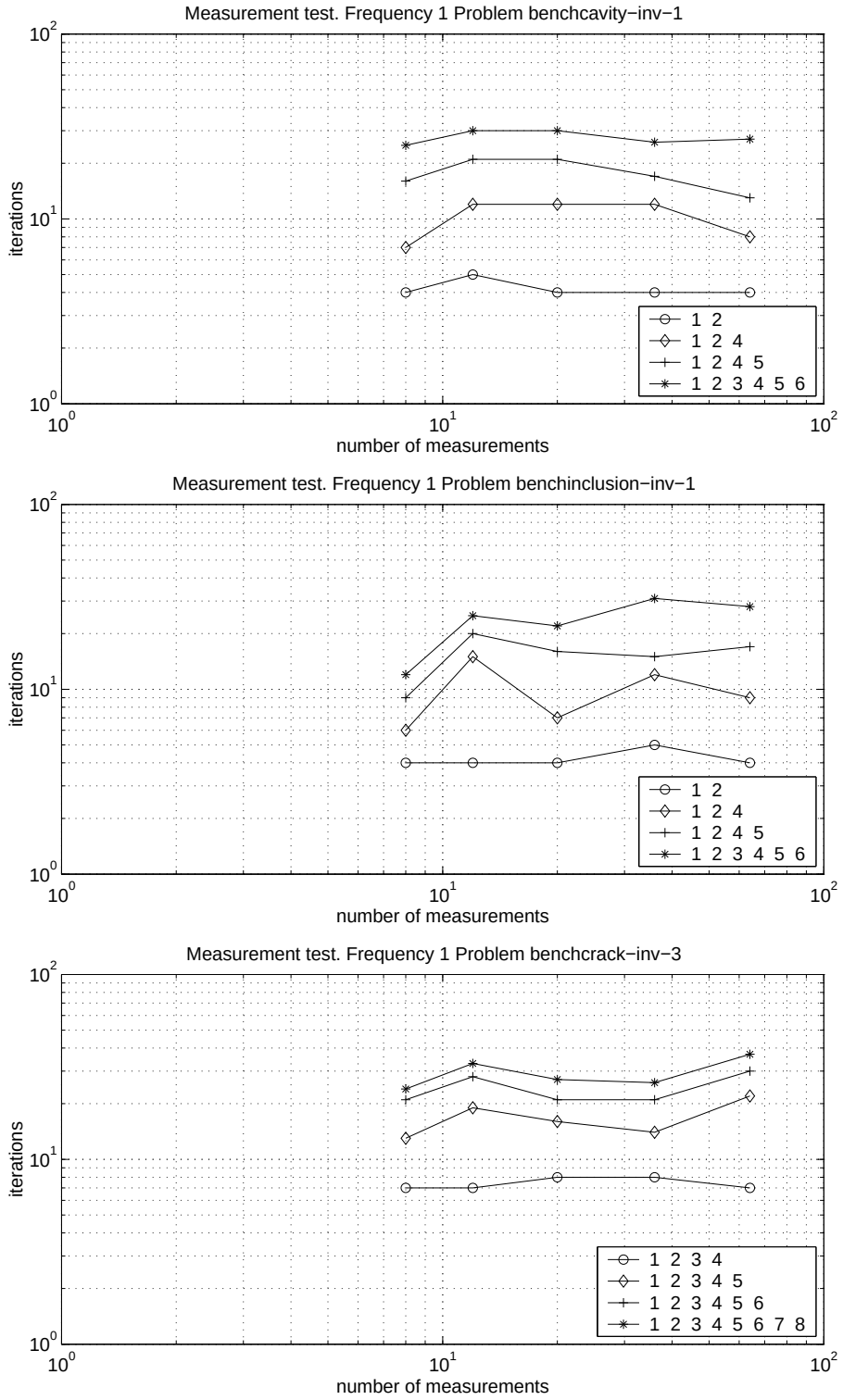

Figure 14.12: Convergence with different number of measurements and parameters. Cavity, inclusion and crack problems respectively.

The graphics are all made for frequency $\omega = 1.0$, and for each benchmark problem. The starting guess is placed at an equivalent distance of 0.2. An increasing number of parameters is also shown at every graphic. The number of measurements does not seem to imply important effects in the process of convergence. It should be noted that, unless special regularization techniques are used,

the number of measurement data should be equal or higher than the number of parameters in order to allow for the convergence to a realistic solution.

14.2.4 Dependence on the errors

In order to simulate real cases, some errors are introduced in all parts of the model: measurements, geometry (alteration of the coordinates of each node), elastic modulus, other elastic constants, and frequency. The errors are defined by a normal distribution of zero mean and variance defined by the percentage of error.

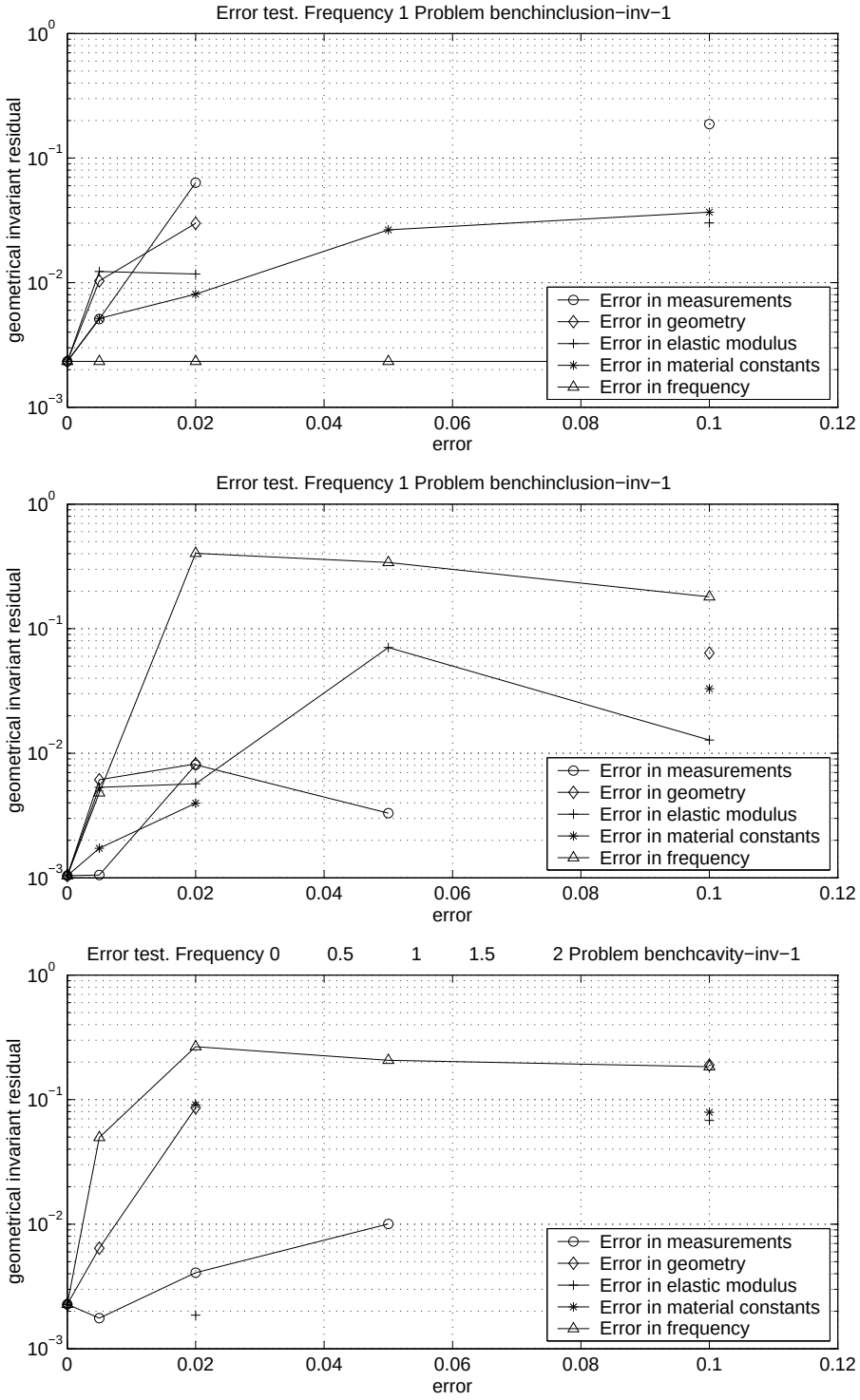

Figure 14.13: Convergence with errors. Cavity problem.

Figures 14.13, 14.14, 14.15 and 14.16 show the final value of the geometrical invariants error

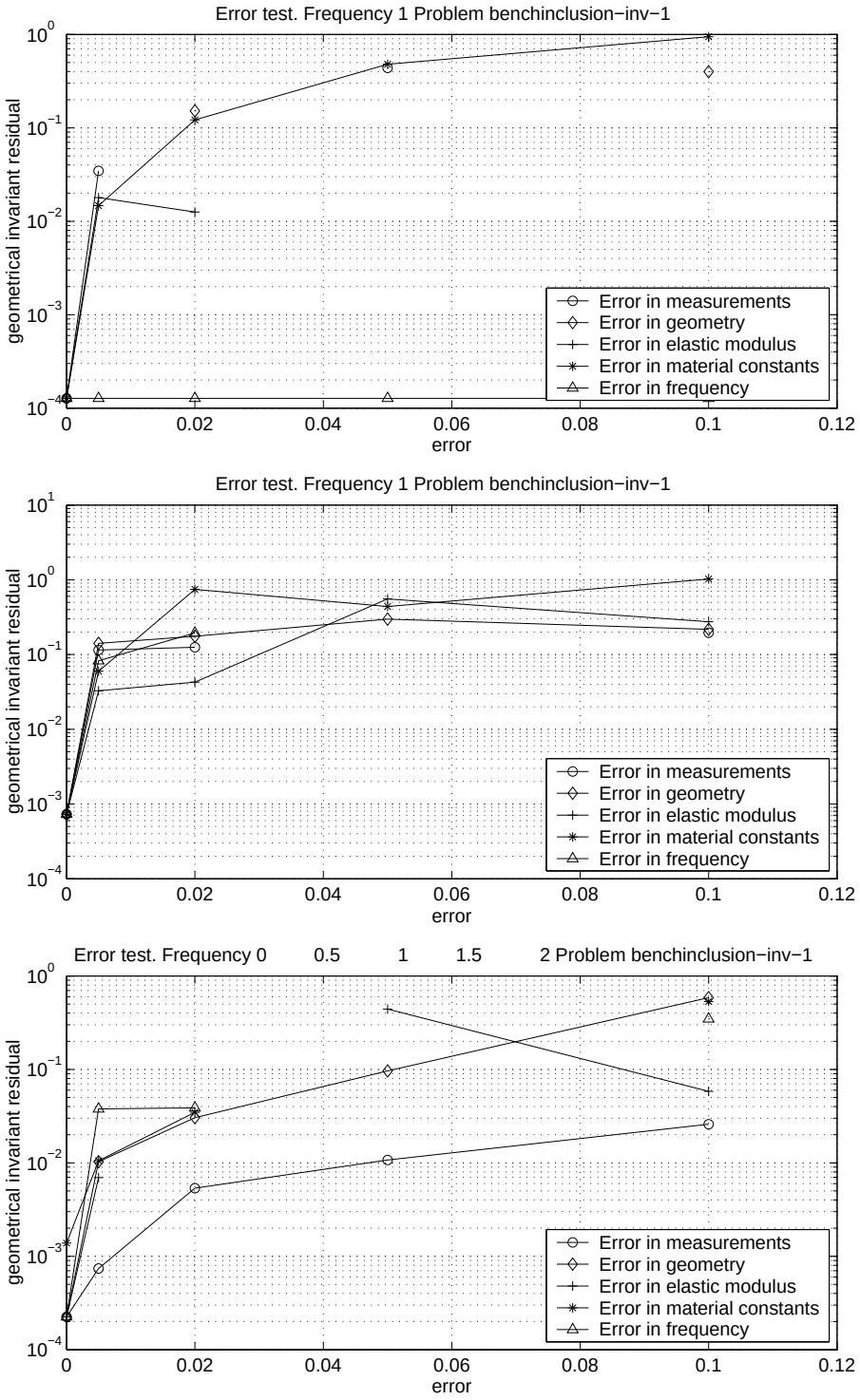

Figure 14.14: Convergence with errors. Inclusion problem.

(area, center of gravity, and the 2D intertias) when the problem has a particular value in the error on the measurements, geometry, elastic modulus, other material constants or frequency. The unitary value of the error is tested at values of 0, 0.005, 0.02, 0.05, 0.10, i.e., up to 10%. Lack of convergence is represented by the absence of plot.

These examples show that the fitness of the final estimation is very fast distorted already at small errors, but looking at the values of the error, the estimation may still be quite reasonable,

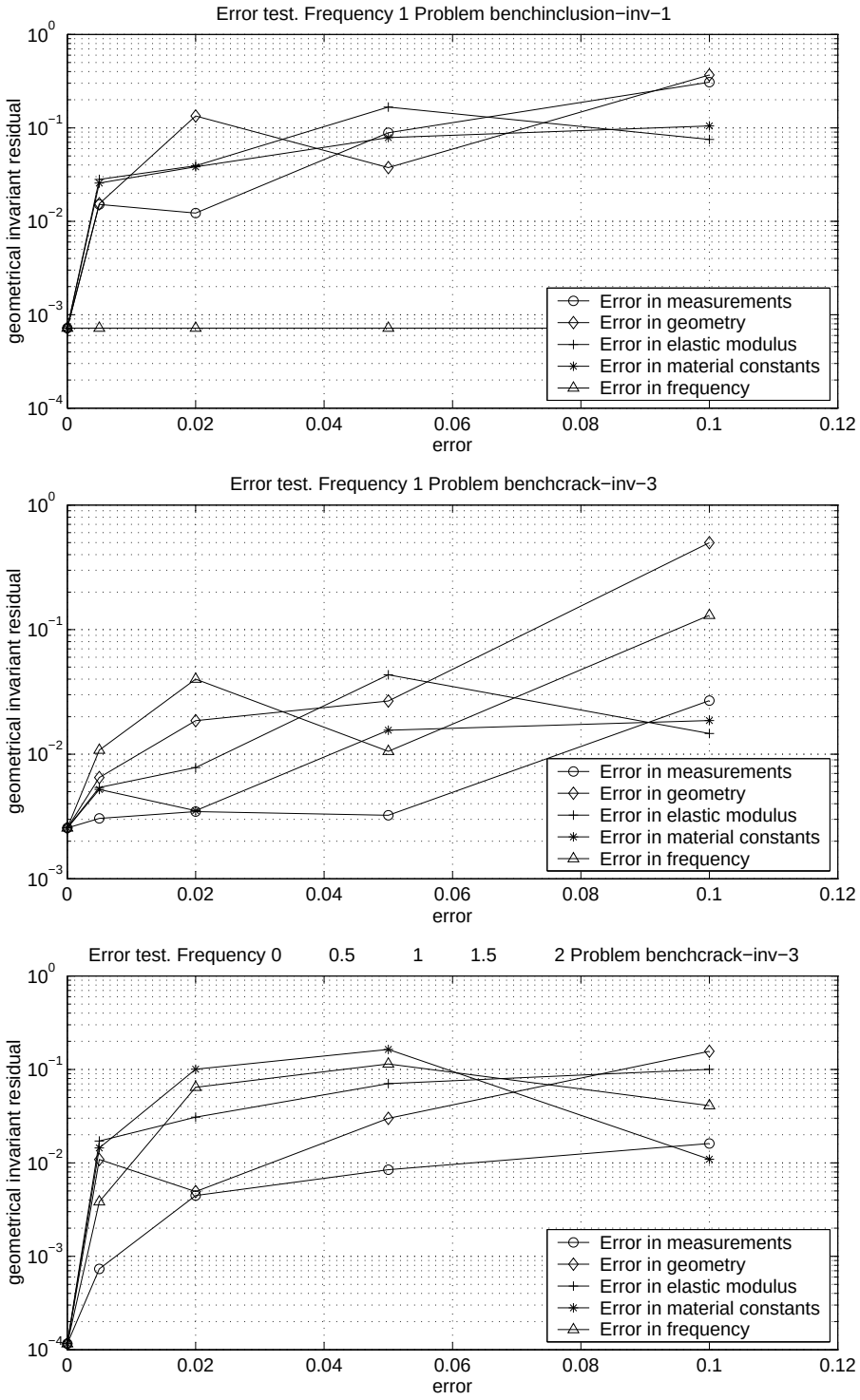

Figure 14.15: Convergence with errors. Crack problem.

taking into account the ill-posedness of the IIP problem.

Inclusion problems show again a much more stable convergence with a higher ratio of success, as well as crack problems do. It is not easy to state the importance of the error in each part of the model, due to a low correlation between different examples.

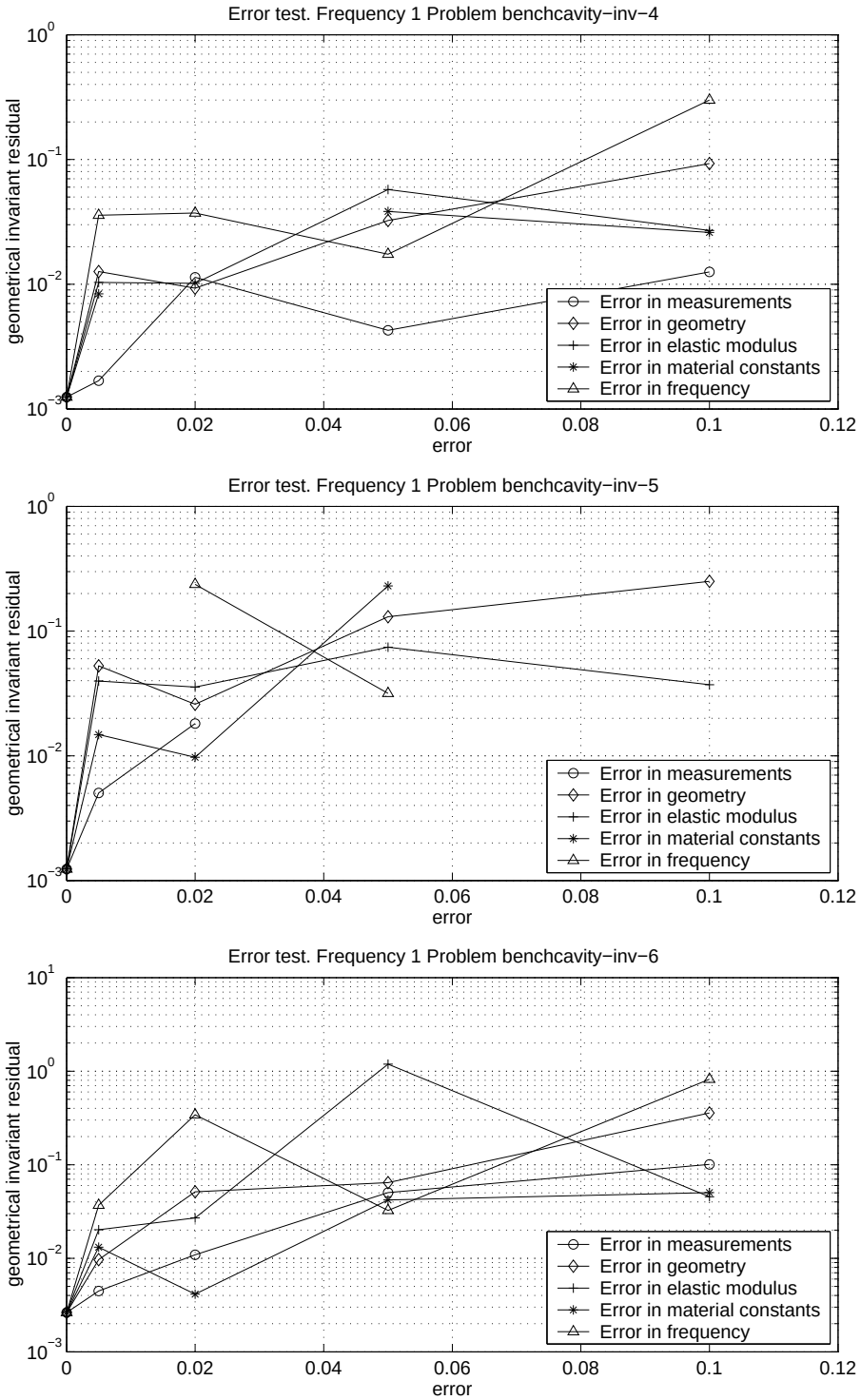

Figure 14.16: Convergence with errors. Complex parametrizations. Cavity problem.

14.3 Convergence with BFGS algorithm using AVM supplied derivative

14.3.1 Methodology

Use of parametrization

We use the same parametrization definition for the calculation of the velocity fields in the AVM as for the modification of the geometry throughout the identification procedure. This is done by starting always from the initial uniformly meshed crack, in the sense that the final crack will be represented by the initial one perturbed once by the final parameters vector.

All the different parametrizations used can be implemented by the use of a generic algorithm that only works with nodal parametrization. The nodal parameter vector is expressed in terms of any other parameter definition as $\eta_k^{nod} = S_{hj} T_{jk} \eta_h^{any}$, and reversely, the gradient of this parametrization is expressed in terms of the nodal one as $L_k^{nod} = S_{hj} T_{jk} L_h^{any}$.

Boundary element calculations

The calculation of the direct problems that arise in both methods is made with bidimensional quadratic boundary elements. The original code, that has been modified conveniently was developed by F. Chirino [29]. The discretization is made with interior collocation points placed at $0.8L/2$ from the center for all the elements, in our examples. The crack is represented by the dual formulation or mixed boundary element method, a combination of equations corresponding to the integral representations of displacements and tractions - one for each lip. The crack tip is modeled by a quarter point straight element, and the stress intensity factors are computed upon the crack opening displacement measured at the quarter node of the tip element. Finally, the singular integrals are evaluated by dividing them into an analytically solved part, which only involves static terms, and a regular part solved with constant standard 10-point Gauss quadrature.

In order to later integrate the expressions along the crack, we should ensure that the data at the crack tips are exactly of the right order of singularity, eliminating numerical alterations of it. This can be done by obliging the $\sqrt{r}$ terms to be identical in the upper and lower lip of the tip. If we represent the behavior of the data as,

$$f^+ - f_0 = \alpha^+ \sqrt{r} + \beta^+ r$$
$$f^- - f_0 = \alpha^- \sqrt{r} + \beta^- r$$

we will force them to behave as $\alpha = \frac{\alpha^+ + \alpha^-}{2}$ by a slight and convenient modification of value at the extreme crack tip node.

Apart from the boundary element software written in fortran 77, which has eventually been used as a black box, we have extensively checked the subroutines, written in both fortran 77 and 90, for the computation of the cost functional and all the formulae for the adjoint variable method. All the calculations are made with double precision.

Banning impossible configurations

Two procedures have been tested for banning impossible configurations that ocur when the sought crack exceeds the expected range of locations, such as the boundary or an area at a safe distance from it. The first one is a remapping of the parameter values. It is based on giving a legal value of each parameter regardless of the trial value of the optimization algorithm. An important point is to give it continuity and derivability so as to have a good conditioning and calculability of gradient and hessian. The suggested mappings of the value and gradient have the following form, being $x \in [-\infty, \infty]$ the trial parameter, $y \in [-r, r]$ the transformed one with physical meaning, L the

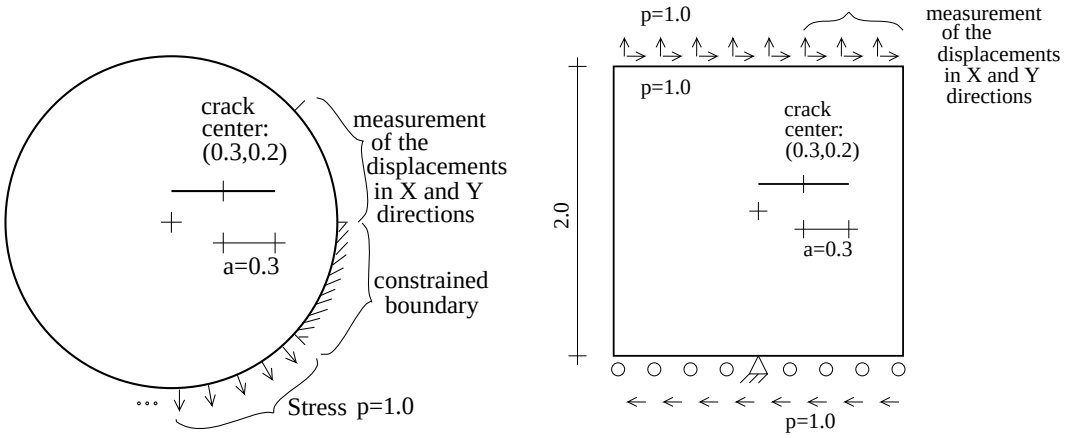

Figure 14.17: Geometry definitions

cost functional, and r the limiting range,

$$y = arctan\left(\frac{\pi x}{2r}\right)\frac{2r}{\pi}$$
$$\frac{\partial L}{\partial x} = \frac{\partial L}{\partial y}\left(1 + \left(\frac{\pi x}{2r}\right)^2\right)$$

The second procedure consists of imposing explicitly a constraint in terms of a nonlinear inequality and solve the problem using sequential quadratic programming, with the use of quadratic programming at each step and the same BFGS method inside.

Models

The implemented code will be tested in two different models, a circular one and a square-shaped one. The base definitions of both include some variable parameters with which we will play to study their importance.

The first base model on which we work is a circular body of unity radius $R = 1.0$ with a crack inside. The material constants are: Young modulus $E = 1.0$, Poisson coefficient $\nu = 0.2$ and density $\rho = 1.0$. The straight crack of semilenght $a = 0.3$ is placed as shown in figure 14.17, with its center at the coordinates $(0.3, 0.2)$. The boundary conditions consist of a prescribed arc along the boundary of variable length from zero (unconstrained circle) to the whole circle constrained. The non constrained supplementary arch is loaded by an unity stress towards the exterior normal. The measurements are the displacements along an arc of variable lenght on the unconstrained boundary. These displacements correspond to the same problem but with the crack center at the coordinates $(0.1, 0.1)$. The second base model consists of a 2×2 square with a crack in the same position. The measurements are made on a fraction of the upper side, and the boundary conditions are fixed as shown in figure 14.17.

This definitions ensure an unsymmetric solution with contribution of all fracture modes.

For the study of all those varying parameters, in a basic models we use the unconstrained circle and, in both models, the measurements are taken over the whole measureable boundary, the angular frequency of all the magnitudes are $\omega = 1.0$, and the sensitivity is calculated with respect to the horizontal displacement of the crack (first parameter).

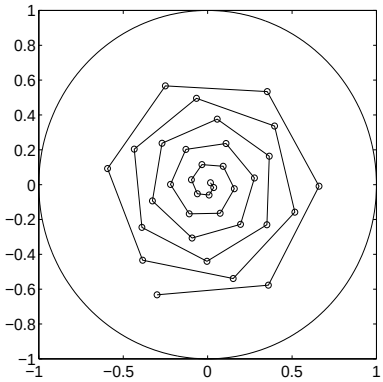

Figure 14.18: Positions of the center of gravity as the distance grows.

14.3.2 Convergence tests

The following graphics show the convergence capabilities with respect to the distance of the initial guess. The idea is to give an estimate of the likelihood of finding the crack as well as the precision of that achievement. This is done by two curves: a curve with the number of iterations, that shows gaps if the maximum number is exceeded without accomplishing the convergence criteria, and below a measurement of the geometrical fitness to the real crack, measured as the square sum of the relative difference of six geometrical parameters: length, center of gravity and inertia tensor (approximating the integrals by sum of nodal values).

The bigger number of start guesses gives rather a probability of success than a single and quite arbitrary result. The distance, on the horizontal axis, is taken into account only for the center of gravity, leaving the other parameters (if any) unchanged from the real position (only at the initial guess, since they will vary during the iterations). The direction is defined as in figure 14.18, giving quite random and well ranged cover.

In the case of curved cracks, the distance is considered by displacing the crack that magnitude along its upper normal.

The convergence criteria have been chosen as a tolerance of 10^{-9} in the function value, and a tolerance of 10^{-4} in the parameter variation. This gives an average of at least three significant digits in the final coordinates.

2 Parameters in dynamics

The following examples start solving the identification of a simple crack in an exactly solvable case with two parameters in various frequencies.

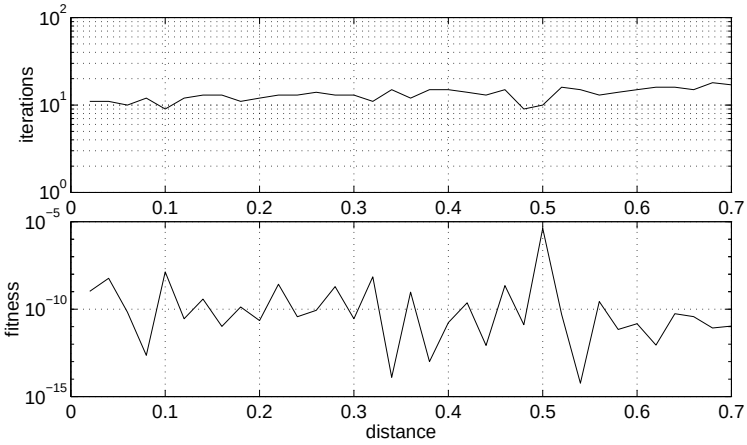

Figure 14.19: Circular model. Static ($\omega = 0.0$). 2 parameters. No errors.

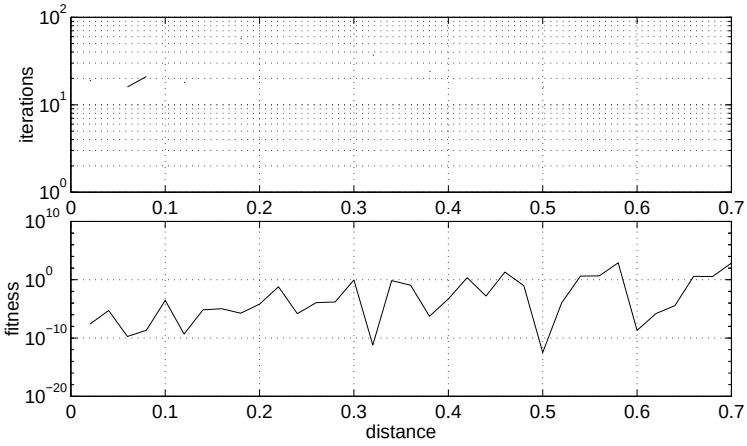

Figure 14.20: Circular model. Dynamic ($\omega = 0.5$, close to an eigenfrequency). 2 parameters. No errors.

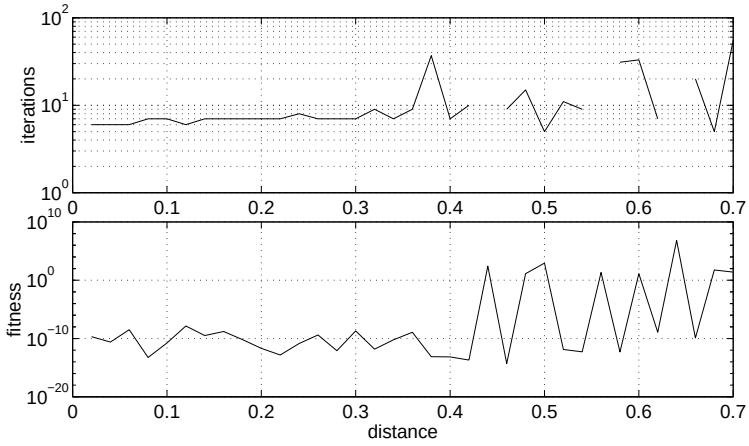

Figure 14.21: Circular model. Dynamic ($\omega = 1.5$). 2 parameters. No errors.

4 Parameters in dynamics

Here we solve a similar problem, but with a doubled number of unknowns.

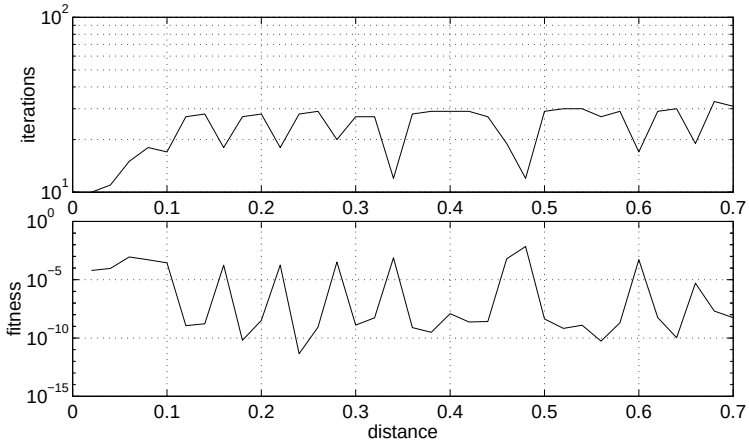

Figure 14.22: Circular model. Static ($\omega = 0.0$). 4 parameters. No errors.

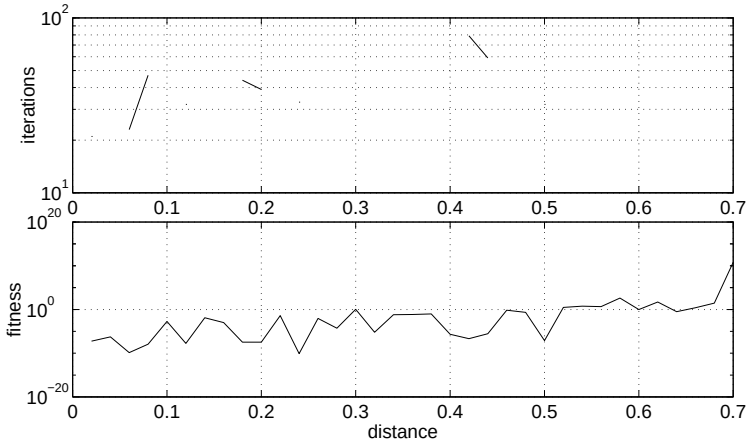

Figure 14.23: Circular model. Dynamic ($\omega = 0.5$, close to an eigenfrequency). 4 parameters. No errors.

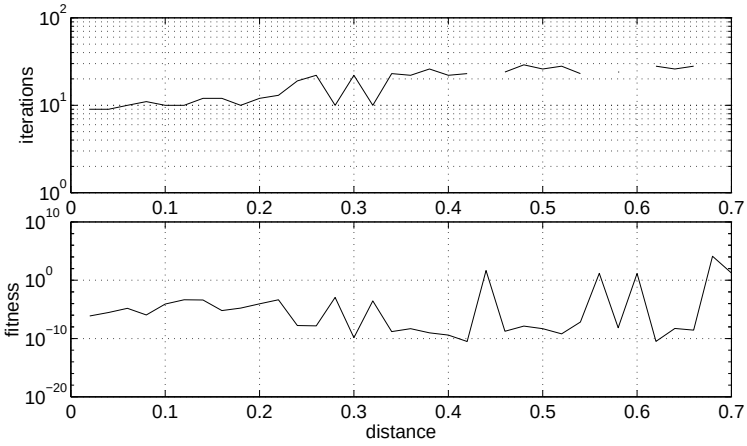

Figure 14.24: Circular model. Dynamic ($\omega = 1.5$). 4 parameters. No errors.

Measurements errors

The following examples introduce errors in the measurements, which is the typical error in inverse problems.

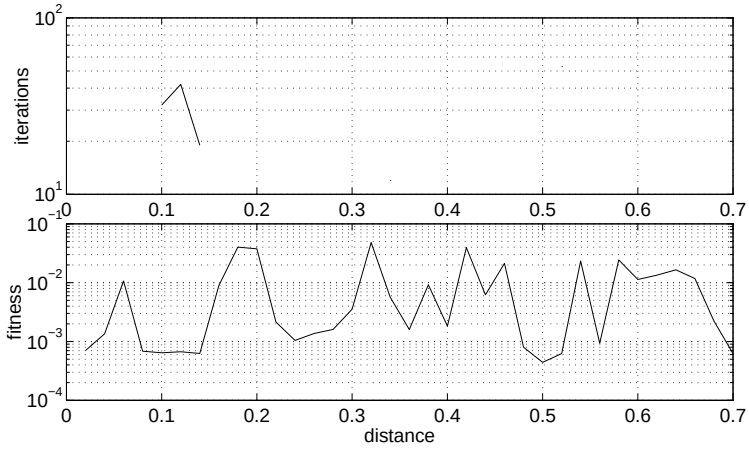

Figure 14.25: Circular model. Static ($\omega = 0.0$). 4 parameters. 2% random error in the measurements.

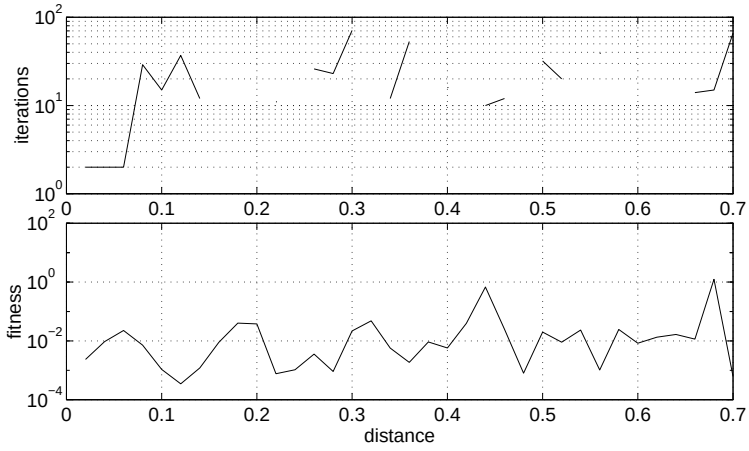

Figure 14.26: Circular model. Static ($\omega = 0.0$). 4 parameters. 2% random error in the measurements. Relaxed convergence criteria (tolerances $\cdot 10$).

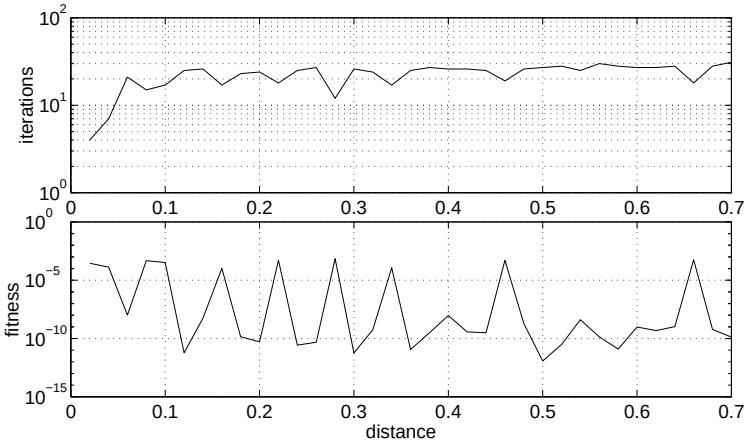

Figure 14.27: Circular model. Static ($\omega = 0.0$). 4 parameters. 2% random error in the measurements. Relaxed convergence criteria (tolerances $\cdot 10$). Refinement of discretization by a factor of 4.

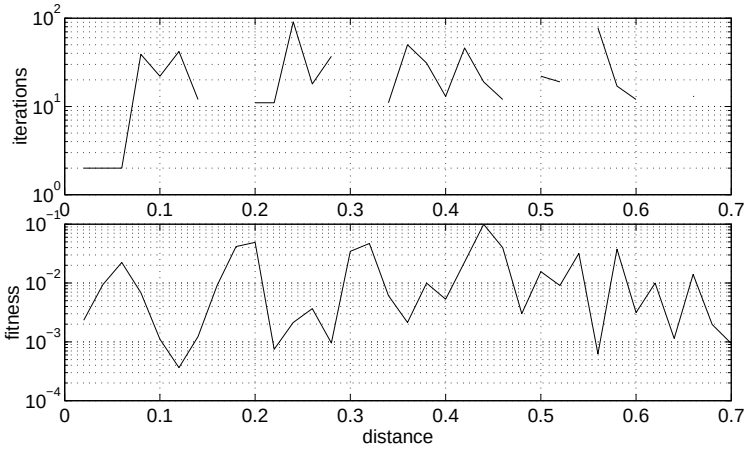

Figure 14.28: Circular model. Static ($\omega = 0.0$). 4 parameters. 2% random error in the measurements. Relaxed convergence criteria (tolerances $\cdot 10$). Remapping of parameters to avoid impossible configurations.

Other errors

The following examples introduce errors in the mechanical parameters and in the geometrical definition of the external body, which are uncertainties that will appear in real problems too.

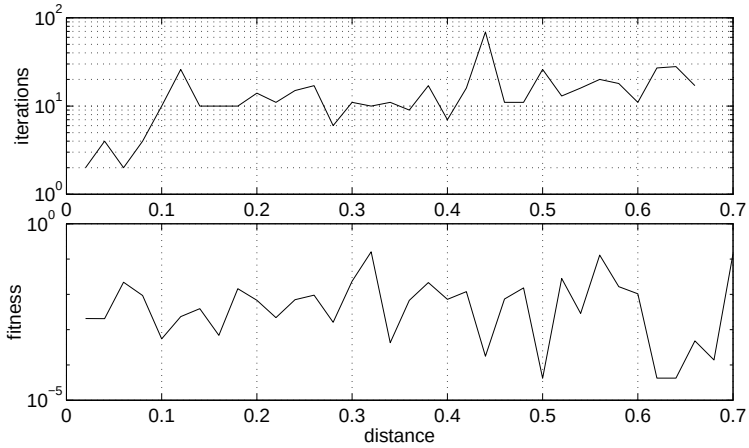

Figure 14.29: Circular model. Static ($\omega = 0.0$). 4 parameters. 2% random error in the measurements. Relaxed convergence criteria (tolerances $\cdot 10$). Remapping of parameters to avoid impossible configurations. Improvement of mesh (by a factor of 4).

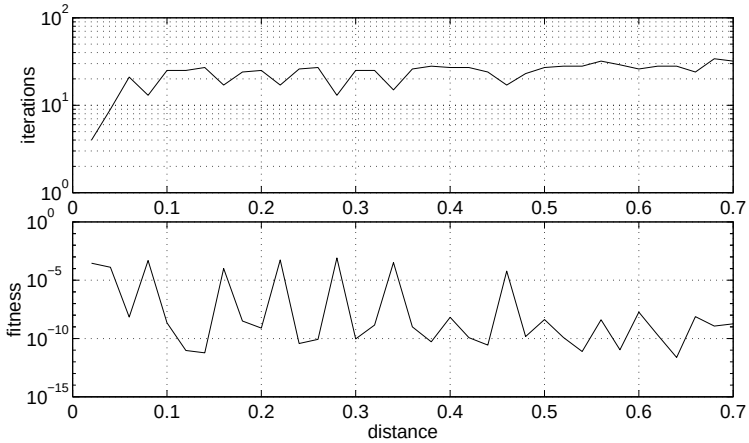

Figure 14.30: Circular model. Static ($\omega = 0.0$). 4 parameters. 2% error in the mechanical properties.

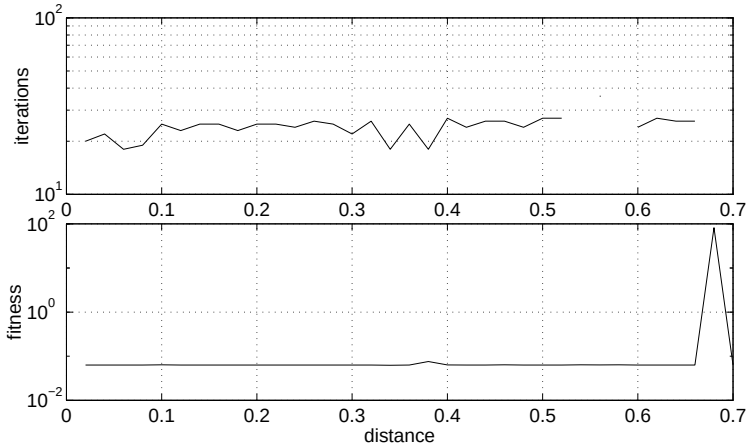

Figure 14.31: Circular model. Static ($\omega = 0.0$). 4 parameters. 2% error in the external geometry (10% in terms of the crack semilength).

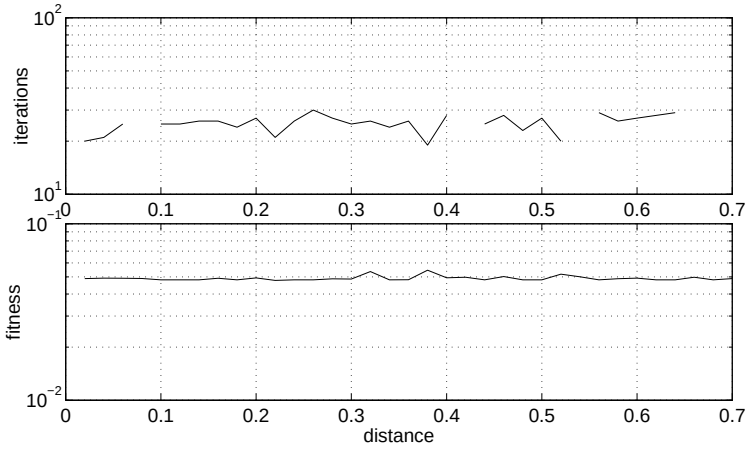

Figure 14.32: Circular model. Static ($\omega = 0.0$). 4 parameters. 2% error in the external geometry (10% in terms of the crack semilength). Remapping of parameters to avoid impossible configurations.

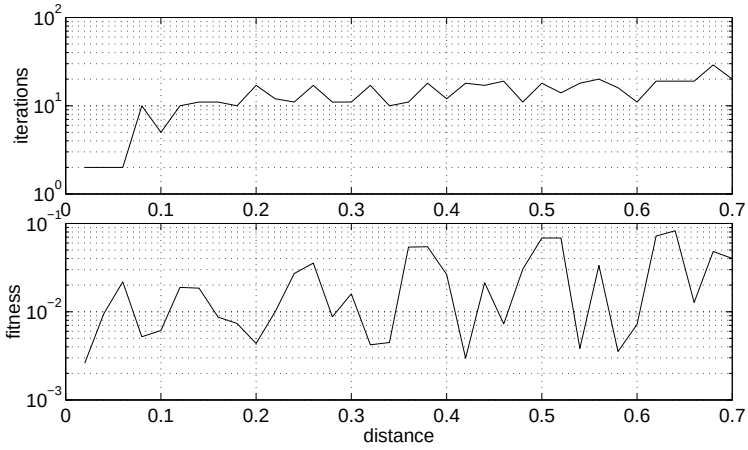

Figure 14.33: Circular model. Static ($\omega = 0.0$). 4 parameters. 2% error in the external geometry (10% in terms of the crack semilength). Remapping of parameters to avoid impossible configurations. Relaxed convergence criteria (tolerances $\cdot 10$).

Sequential Quadrtic Programming

These examples show an alternative to ban impossible configurations, which is the SQP, in which we are allowed to put explicit nonlinear constraints in the parameters.

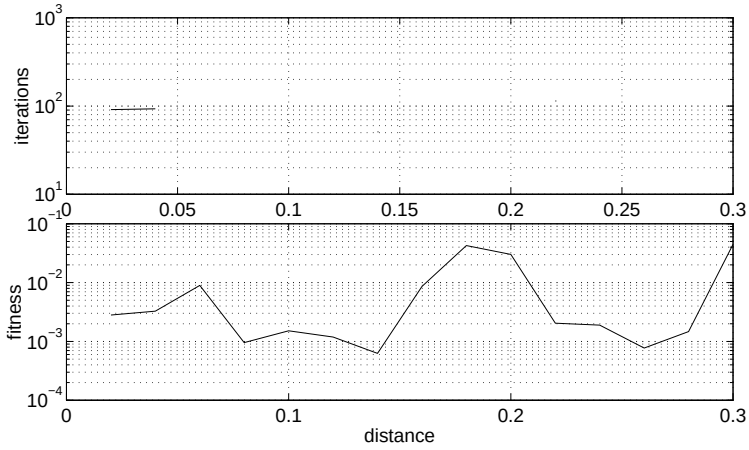

Figure 14.34: Circular model. Static ($\omega = 0.0$). 4 parameters. 2% error in measurements. Constrained solution using sequential quadratic programming.

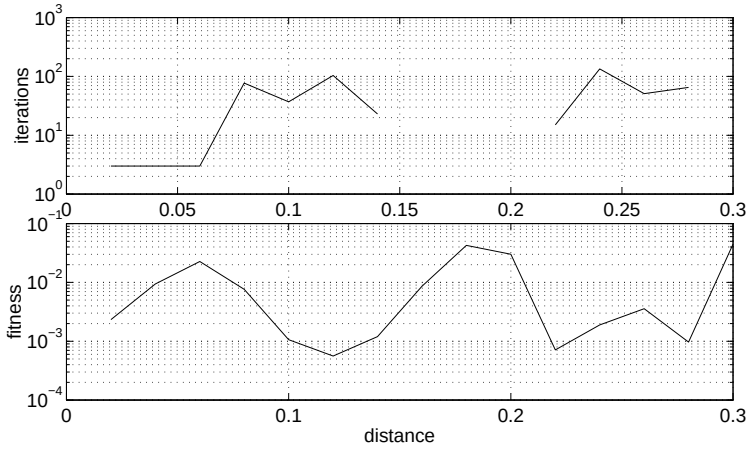

Figure 14.35: Circular model. Static ($\omega = 0.0$). 4 parameters. 2% error in measurements. Constrained solution using sequential quadratic programming. Relaxed convergence criteria (tolerances $\cdot 10$).

Error in crack shape

The following examples show the convergence to a curved crack while we only allow a straight one.

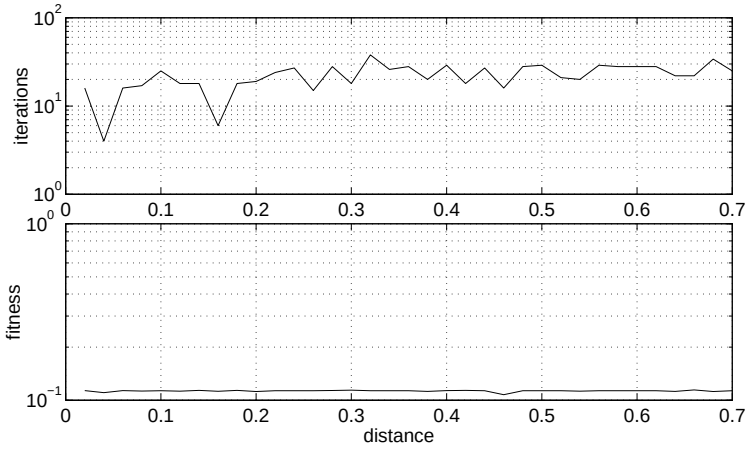

Figure 14.36: Circular model. Curved crack through parameters [0.20 −0.10 0.00 0.00 0.00]. Only straight crack allowed (giving an estimated minimum at [0.0822 0.0437 0.7880 −0.0743]). Static ($\omega = 0.0$). 4 parameters. No error. Remapping of parameters to avoid impossible configurations.

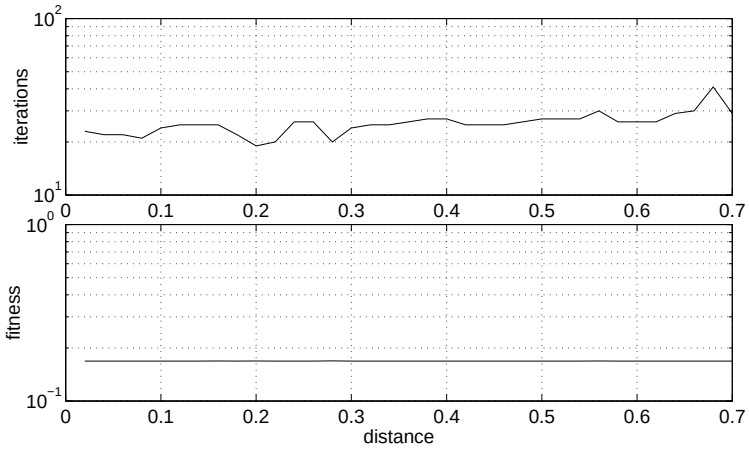

Figure 14.37: Circular model. Curved crack through parameters [0.20 −0.10 0.00 0.00 0.00]. Only straight crack allowed (giving an estimated minimum at [0.0822 0.0437 0.7880 −0.0743]). Static ($\omega = 0.0$). 4 parameters. No error. Remapping of parameters to avoid impossible configurations. Increased number of elements by a factor of 4.

Curve (quadratic)

The following examples show the convergence to a curved crack if the initial guess is close enough. The convergence criteria is stronger now since the distances are smaller, and we have to find more detail.

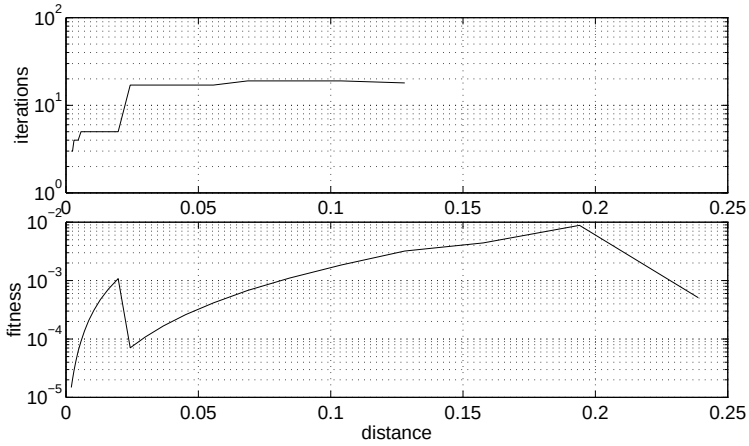

Figure 14.38: Circular model. Curved crack through parameters [0.20 −0.10 0.00 0.00 0.00]. Static ($\omega = 0.0$). 5 parameters. No error. Convergence criteria: tolerances /10.

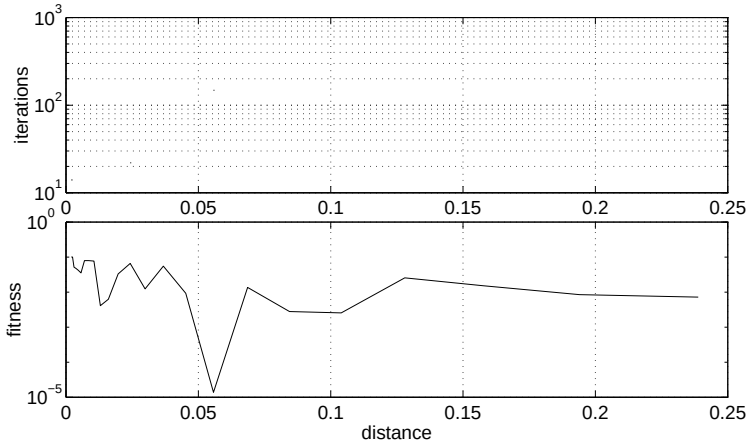

Figure 14.39: Circular model. Curved crack through parameters [0.20 −0.10 0.00 0.00 0.00]. Static ($\omega = 0.0$). 5 parameters. No error. Initial guess from straight crack. Convergence criteria: tolerances /10.

Curve (cubic)

The same procedure is tried for a crack represented by yet another degree of freedom.

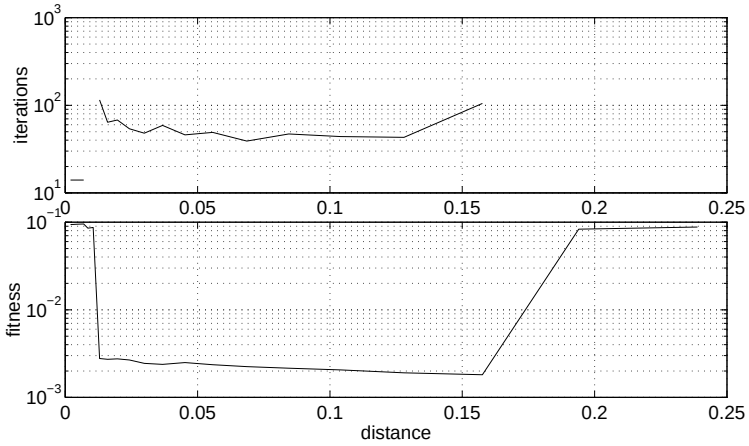

Figure 14.40: Circular model. Curved crack through parameters [0.20 − 0.10 0.00 0.00 0.00 0.00]. Static ($\omega = 0.0$). 6 parameters. No error. Start from straight crack. Convergence criteria: tolerances /10.

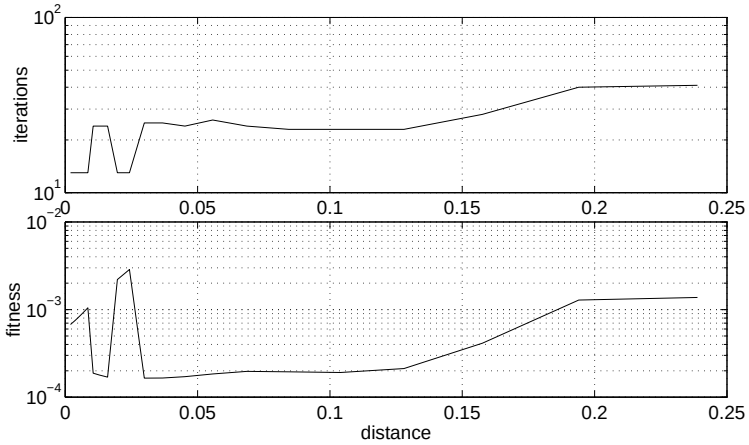

Figure 14.41: Circular model. Curved crack through parameters [0.20 − 0.10 0.00 0.00 0.00 0.00]. Static ($\omega = 0.0$). 6 parameters. No error. Start from quadratic crack ([0.20 0.00 − 0.06667 0.00 0.00 0.00]). Convergence criteria: tolerances /10.

Total strategy

A strategy for achieving a complete search is proposed. It consists of a dosage of the number of parameters, with the aim of having a big range of convergence in the beginning and achieving the desired detail in the end. For the case of a starting distance of 0.2, the evolution of the residual and the geometry of the cracks at the change of stage are shown in the following figures.

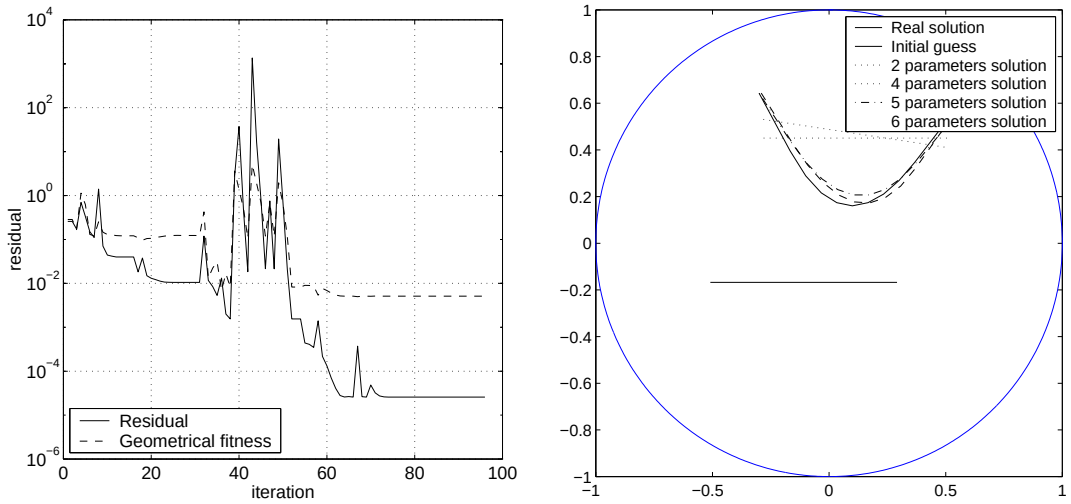

Figure 14.42: Circular model. Curved crack through parameters [0.70 0.20 0.20 0.54 0.10 0.10]. Static ($\omega = 0.0$). 2 - 4 - 5 - 6 parameters sequentially. No error. Start from straight crack at distance 0.2. Convergence criteria: iterations allowed and tolerances: $(10, \cdot 1), (10, \cdot 0.1), (20, \cdot 0.01), (40, \cdot 0.001)$.

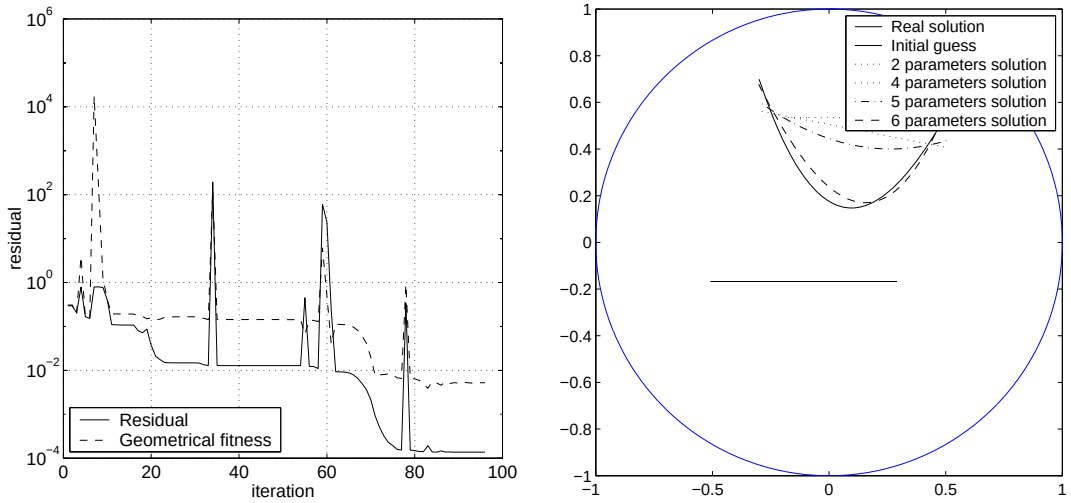

Figure 14.43: Circular model. Curved crack through parameters [0.70 0.20 0.20 0.54 0.10 0.10]. Static ($\omega = 0.0$). 2 - 4 - 5 - 6 parameters sequentially. No error. Start from straight crack at distance 0.2. Convergence criteria: iterations allowed and tolerances: $(10, \cdot 1), (10, \cdot 0.1), (20, \cdot 0.01), (40, \cdot 0.001)$. Crack discretization refined 10 times.

14.3.3 About the inconsistency of the AVM

The cubic line search often gets stuck near the solution, probably due to an inconsistence and therefore divergence between the gradient provided by the AVM calculation and the gradient of the cost functional after the discretization. This implies that the supplied gradient tends to drive the algorithm towards a point that does not coincide with the minimum. The only way to solve this is to allow a higher tolerance for the termination, which will give a lower level of certainty of the final geometry. As an alternative to this, we have allowed a switch to finite differences after the 20th iteration. Figure 14.49 shows this incoherence between the gradient and the cost function, for a close up of the field of two parameters $[x_{cg}, y_{cg}]$ to an area of side 0.080, in the case of an error of 2% in the measurements. Anyway, figure 14.48 shows a good agreement at a large scale.

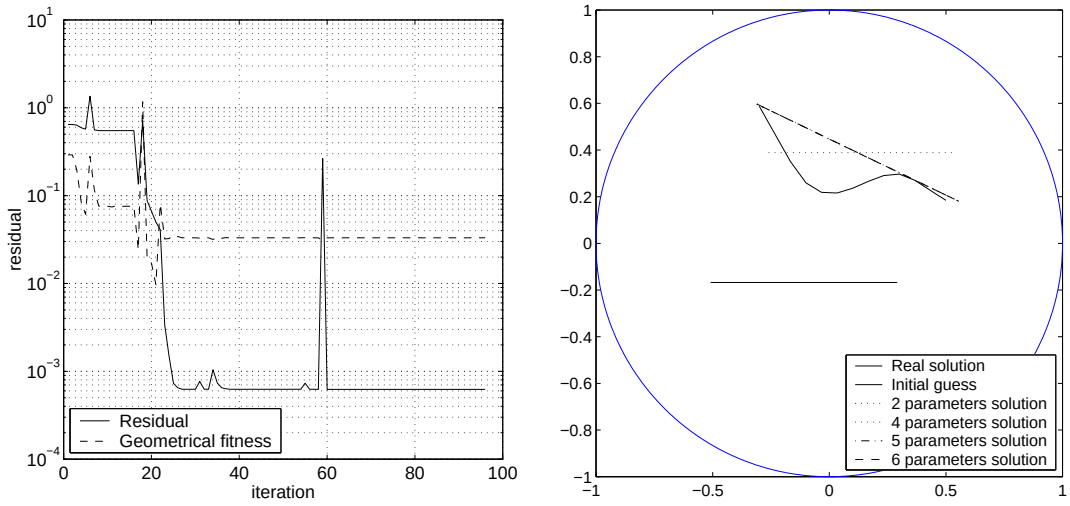

Figure 14.44: Circular model. Curved crack through parameters [0.70 0.20 0.30 0.10 0.10 0.10]. Static ($\omega = 0.0$). 2 - 4 - 5 - 6 parameters sequentially. No error. Start from straight crack at distance 0.2. Convergence criteria: iterations allowed and tolerances: $(10, \cdot 1), (10, \cdot 0.1), (20, \cdot 0.01), (40, \cdot 0.001)$.

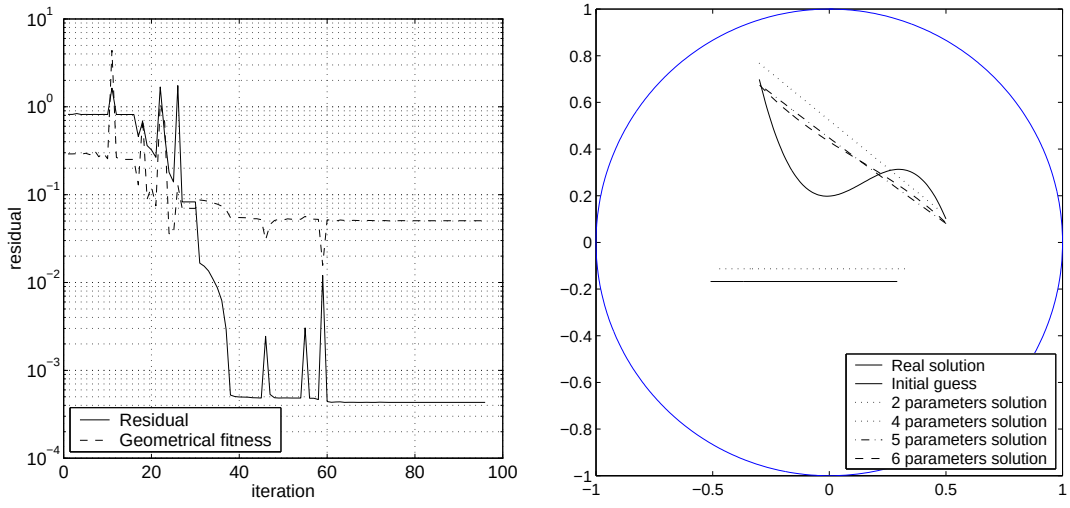

Figure 14.45: Circular model. Curved crack through parameters [0.70 0.20 0.30 0.10 0.10 0.10]. Static ($\omega = 0.0$). 2 - 4 - 5 - 6 parameters sequentially. No error. Start from straight crack at distance 0.2. Convergence criteria: iterations allowed and tolerances: $(10, \cdot 1), (10, \cdot 0.1), (20, \cdot 0.01), (40, \cdot 0.001)$. Crack discretization refined 10 times.

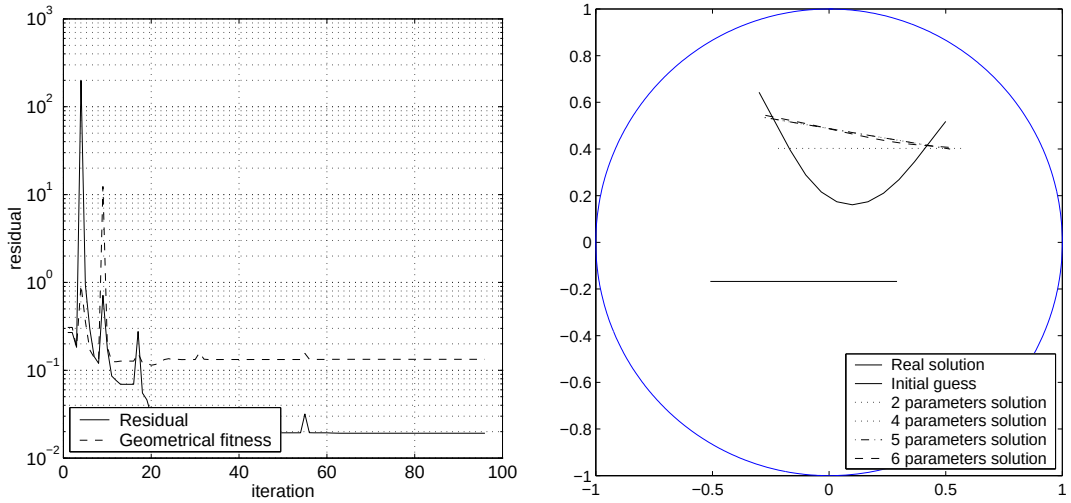

Figure 14.46: Circular model. Curved crack through parameters [0.70 0.20 0.20 0.54 0.10 0.10]. Static ($\omega = 0.0$). 2 - 4 - 5 - 6 parameters sequentially. 10% error in the measurements. Start from straight crack at distance 0.2. Convergence criteria: iterations allowed and tolerances: $(10, \cdot 1), (10, \cdot 0.1), (20, \cdot 0.01), (40, \cdot 0.001)$.

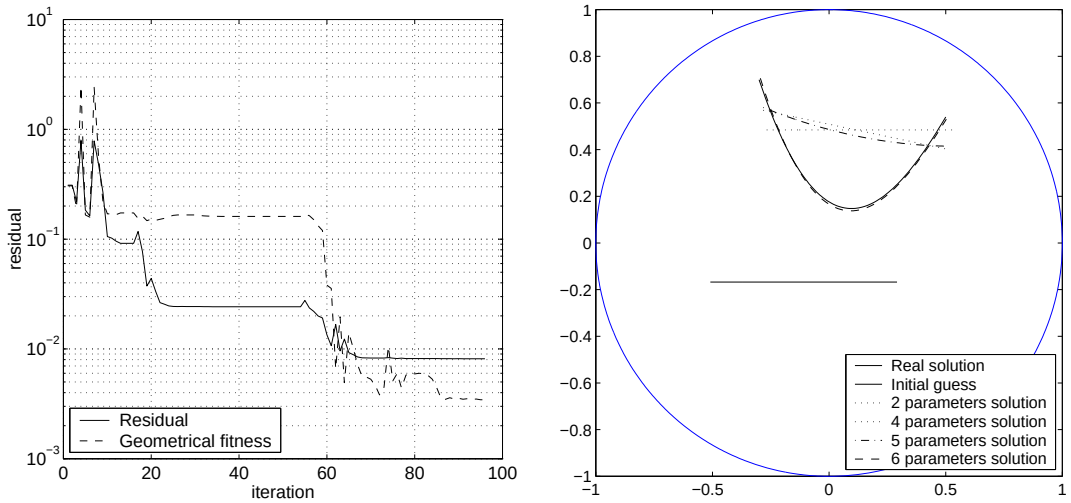

Figure 14.47: Circular model. Curved crack through parameters [0.70 0.20 0.20 0.54 0.10 0.10]. Static ($\omega = 0.0$). 2 - 4 - 5 - 6 parameters sequentially. 10% error in the measurements. Start from straight crack at distance 0.2. Convergence criteria: iterations allowed and tolerances: $(10, \cdot 1), (10, \cdot 0.1), (20, \cdot 0.01), (40, \cdot 0.001)$. Crack discretization refined 10 times.

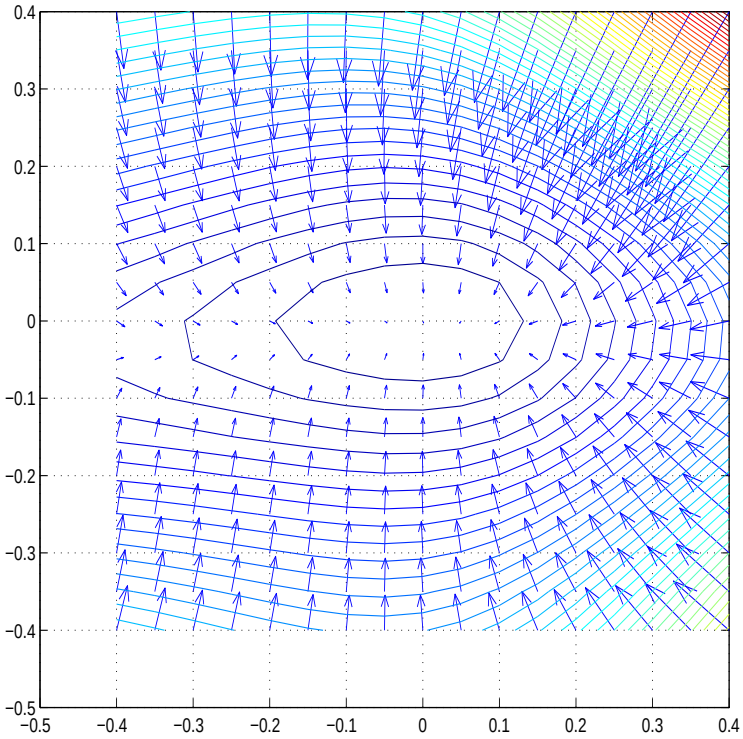

Figure 14.48: Value of the cost functional (contour lines), and gradient (vector plot).

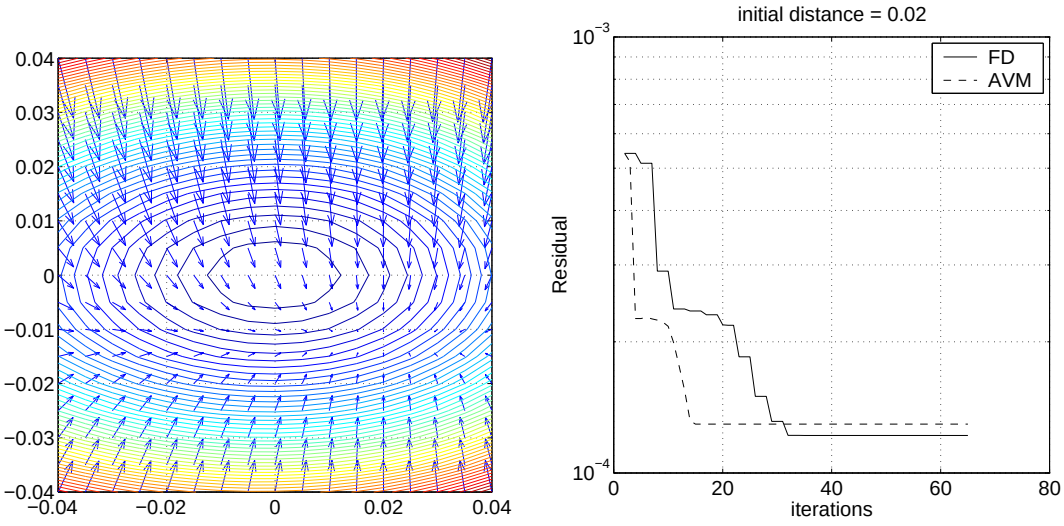

Figure 14.49: Left: close-up of value of the cost functional (contour lines), and gradient (vector plot). Right: evolution of the cost function with AVM and finite differences.

Figure 14.49 shows the differences in the convergence for two supplies of gradient: AVM and finite differences. The calculation starts at a distance of the parameter $[x_{cg}, y_{cg}]$ of 0.02, in the case of an error of 2% in the measurements and a discretization of $18 + 6 + 6$. Figures 14.50 and 14.51 show the same results for enhaced discretizations. Although this effect is reduced as the discretization is improved, the AVM never reaches the minimum that the FD calculation does.

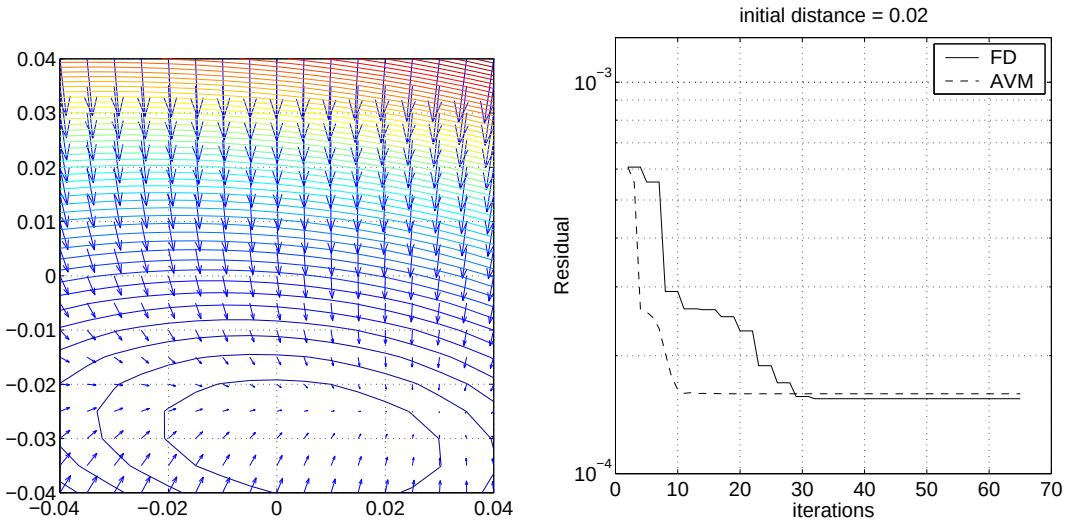

Figure 14.50: Left: close-up of value of the cost functional (contour lines), and gradient (vector plot). Right: evolution of the cost function with AVM and finite differences. Discretization enhaced by a factor of 2.

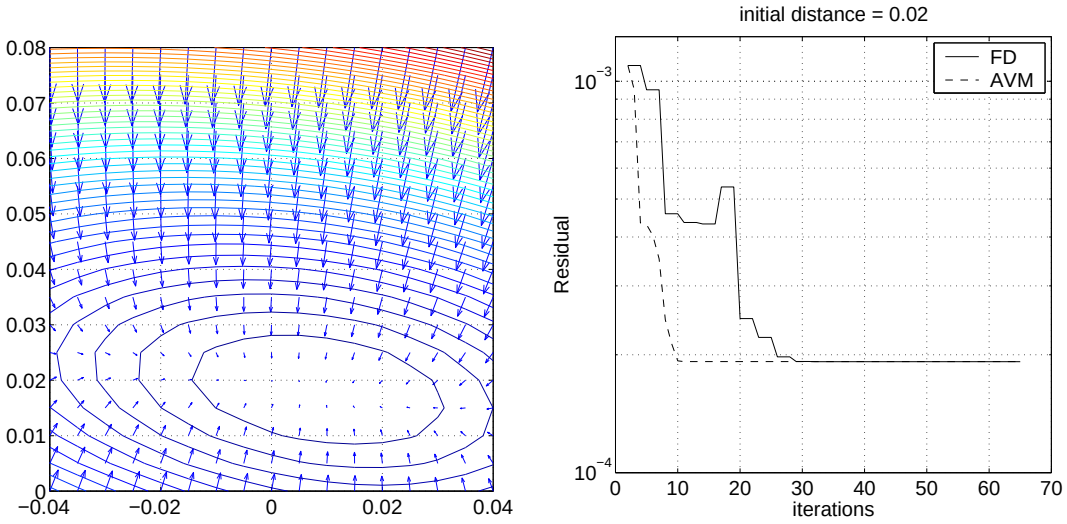

Figure 14.51: Left: close-up of value of the cost functional (contour lines), and gradient (vector plot). Right: evolution of the cost function with AVM and finite differences. Discretization enhaced by a factor of 4.

About highly curved cracks

As seen in the latest examples with different shapes of cracks, and in the convergence versus distance graphics for curved variation, it is possible to notice that the gradient of the local parameters is very warped, leading to local minima even in a very local scope. This is not dependent on the gradient calculation technique since the same behaviour is observed with FD and AVM. The only way to solve this would be to use more global search methods, even in localized areas.

Chapter 15

Topological derivative test

15.1 Verification of radius estimation

The first step in the topological derivative procedure is to determine the size-dependent constant in it's first-order approximation. Two benchmark problems will be used for this purpose, consisting of an unsymmetrically loaded specimen (2×2 square) with either a cavity of radius 0.1 or a crack of semilength 0.1 in the middle (figures 15.1). The boundary conditions are a displacement constraint at the bottom and a parabolic load at the right vertical side of magnitude $[1, 1]$ on its center and $[0, 0]$ on the edges. The measurements are made along the right vertical side in the sequel. The discretization is made by four quadratic elements per bubboundary (16 elements for the external boundary and 16 for the flaw, only during the calculation of the measurements; since the topological derivative does not require the discretization of the flaw).

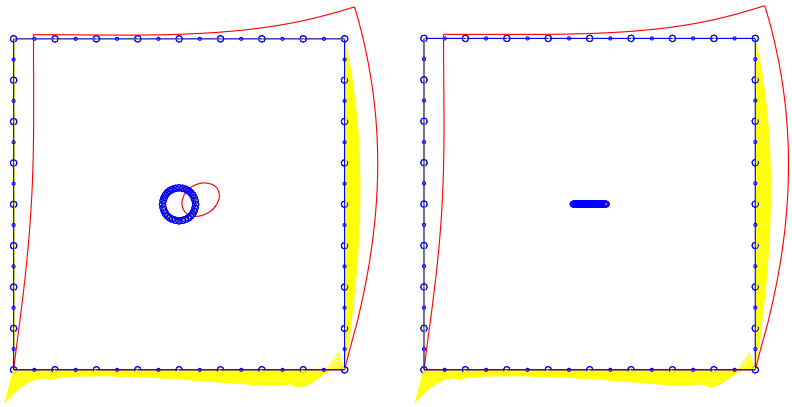

Figure 15.1: Geometry of benchmark problems for cavity and crack.

The correlation between real and estimated size (radius in the case of a cavity and semilength in the case of a crack), is presented in figure 15.2. A perfect agreement is shown but for very small values, due to numerical imprecisions, and for very high values because of the importance of higher order terms. It is interesting to note that higher order terms are $A^{\frac{3}{2}}, A^2, A^{\frac{5}{2}}, ...$, since the topological derivative is expanded in terms of the area.

15.2 Residual

The second step consists in using the above estimated size-dependent constant to build a linearized estimate of the corresponding measurements and give the residual composed from these estimated measurements and the real ones. The exact procedure is explained thoroughly in chapter 10.

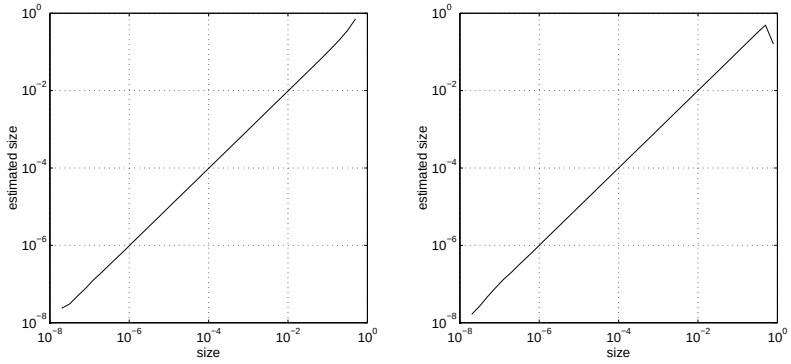

Figure 15.2: Correlation of radius. Cavity and Crack benchmark.

In the sequel, a set of problems involving one or two simultaneous circular cavities and elliptical ones are stidued. The graphics show the mentioned residual for each position of the center of the cavity (fixing the second one if any, at it's right value).

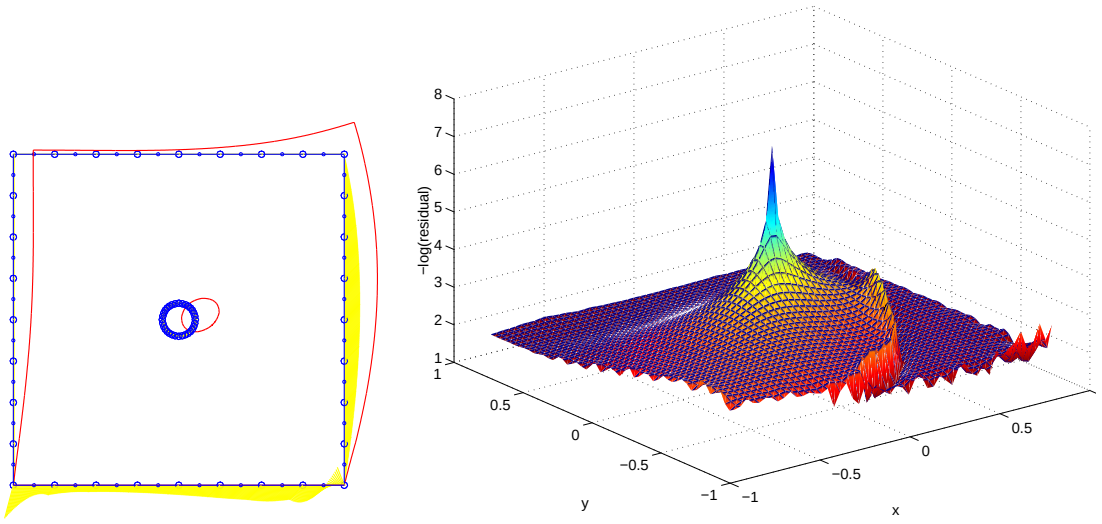

Figure 15.3: Benchmark with one cavity. A precise, isolated and smooth optimum is seen.

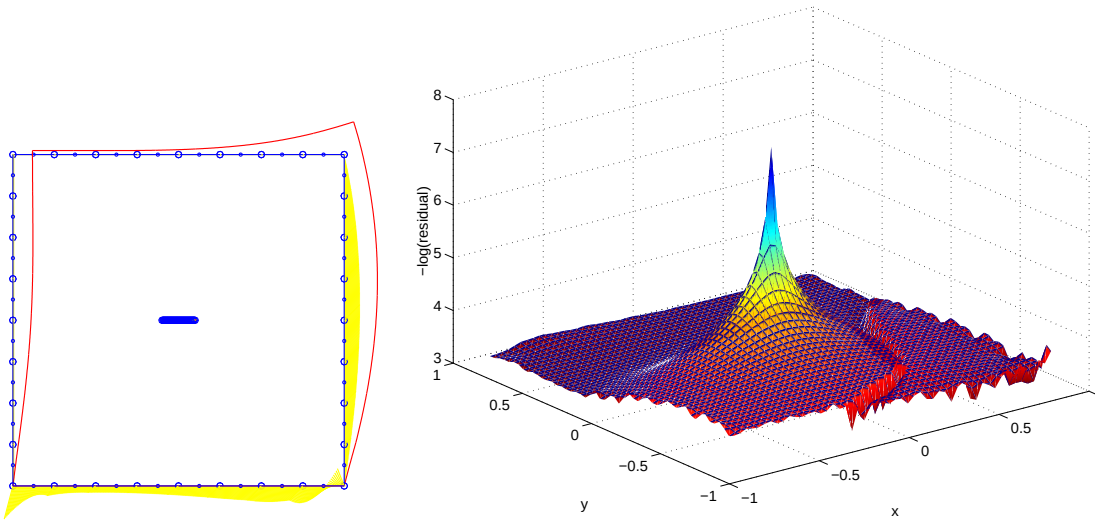

Figure 15.4: Benchmark with one crack. A similarly precise, isolated and smooth optimum is found in this case.

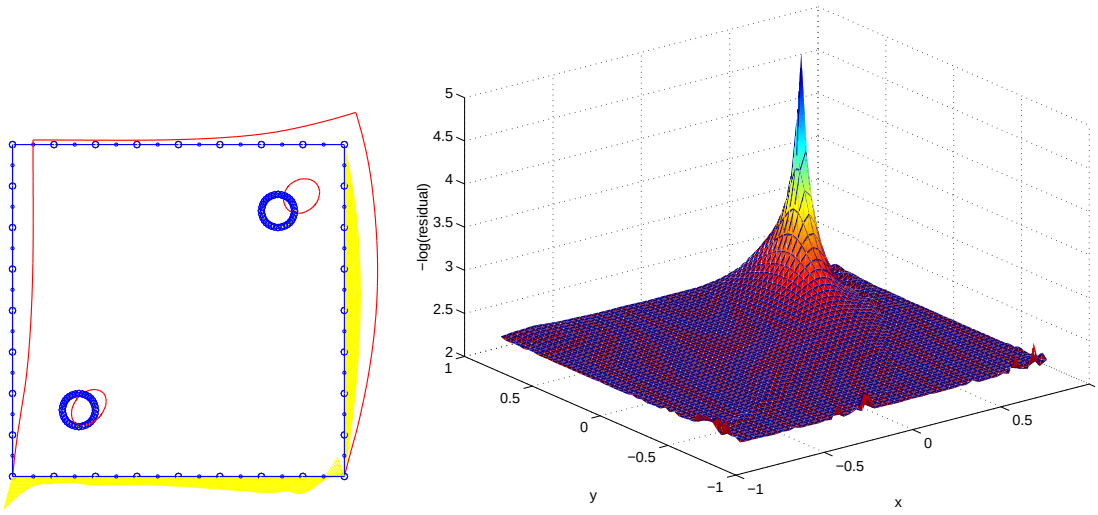

Figure 15.5: Benchmark with two distant cavities. A very sharp maximum is found. The equivalent result with a more coarse mesh would give much worse results in this particular case.

15.3 Genetic algorithms

Once the topological derivative has been tested and shown, and due to the extremely low cost of each computation, a suitable tool to climb to the optimal solution appears to be the genetic algorithms.

A simple genetic algorithm has been programmed and plugged into the topological derivative, giving the following results. The necessary coded was adapted from the one developed by J. Haataja [59]. The objective to be maximized is $-\log$ residual. The parameters used for all the gentic algorithm runs are,

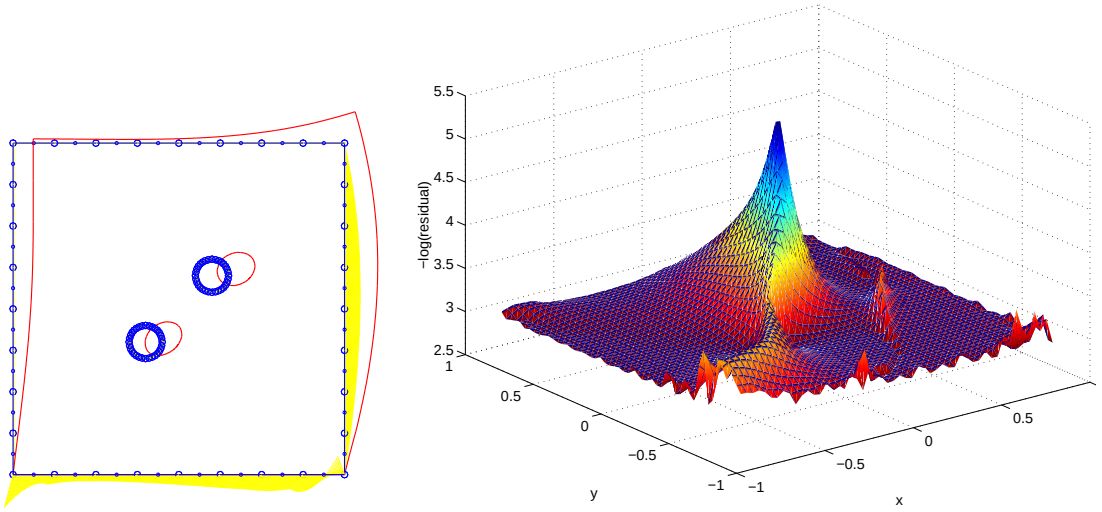

Figure 15.6: Benchmark with two close cavities. More local extrema appear here.

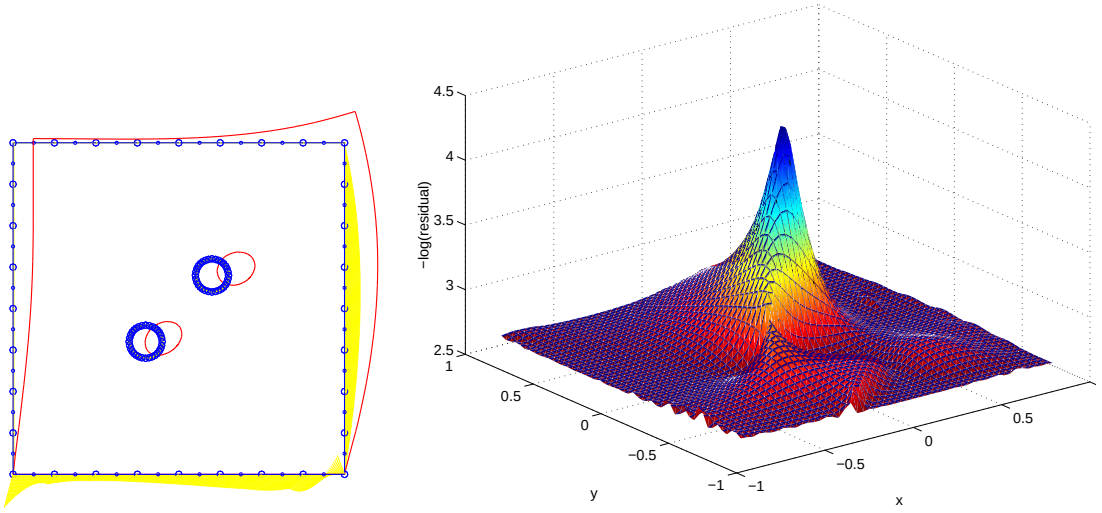

Figure 15.7: Benchmark with two close cavities. Measurements are made along the upper side too. A more precise maximum is found at this point.

Number of members in population	30
Number of generations	100
Probability of mutation	0.02
Probability of crossover	0.8
Tournament probability	0.7
Scale for mutations	0.1
Gens	Real-coded

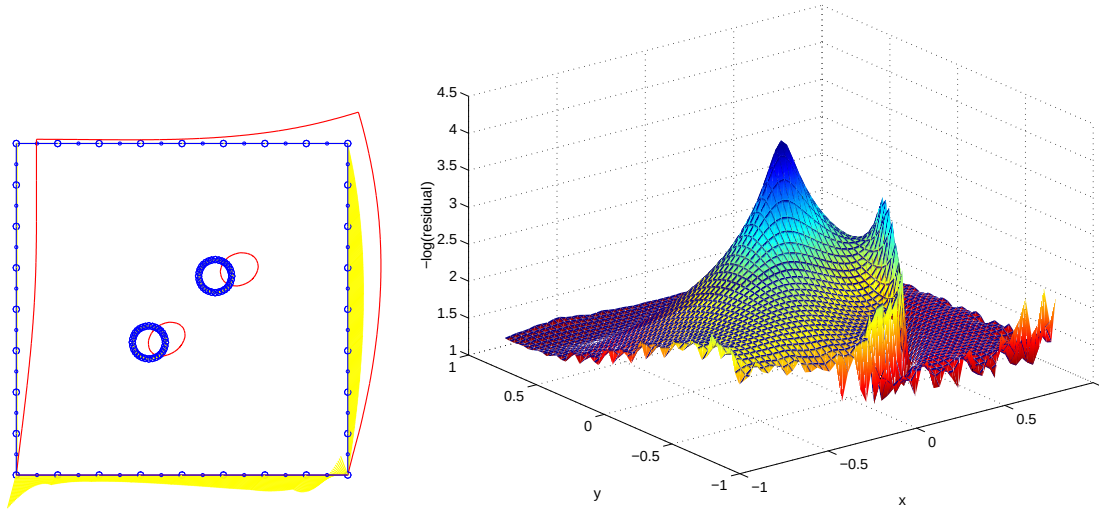

Figure 15.8: Benchmark with two close cavities. Only one is allowed for the topology. A larger area with low residual appears.

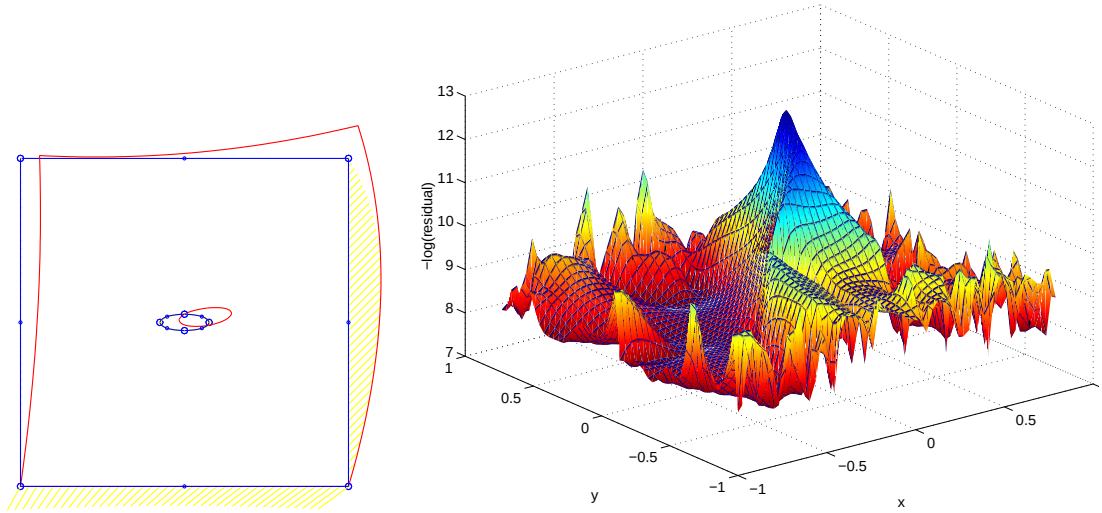

Figure 15.9: Benchmark with one ellyptical cavity. The limitation of the circular shape does not allow for a perfect fitness, and the residual map appears smoother, with large areas of low residual and many local minima.

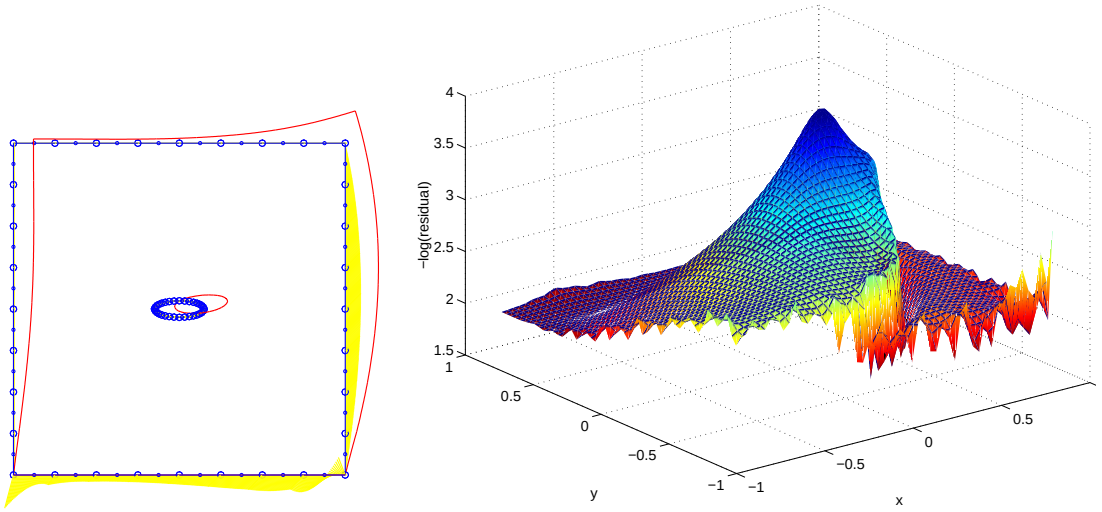

Figure 15.10: Benchmark with one ellyptical cavity. Only one circular cavity is allowed. A very undefined and large area of low residual is found, among several maxima. It is interesting to see that a particular solution far from the real one gives the best fitness.

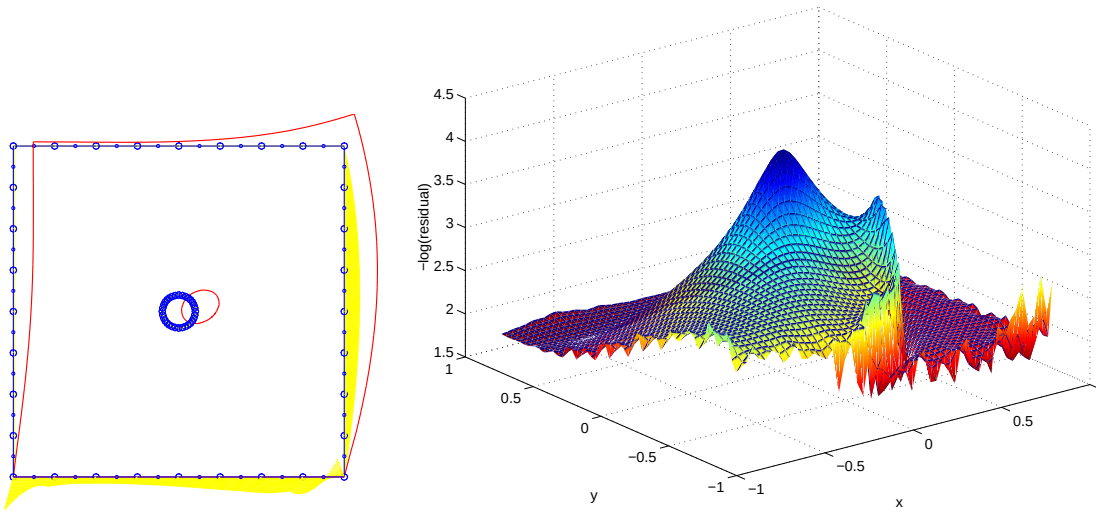

Figure 15.11: Benchmark with one circular cavity. 10% error in the measurement data. The residual is worse and occupies a large area. The optimum does not appear exactly on the real solution.

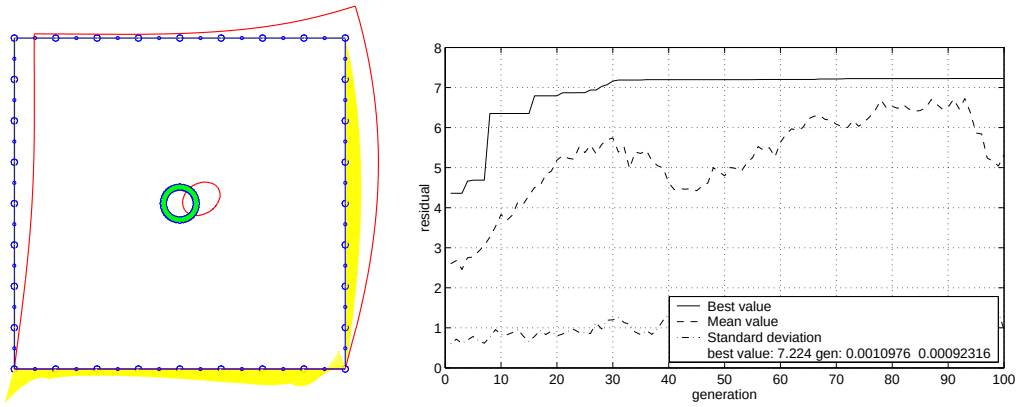

Figure 15.12: Benchmark with one cavity. A very close solution (best gen) is found, with about 0.1% of geometrical distance.

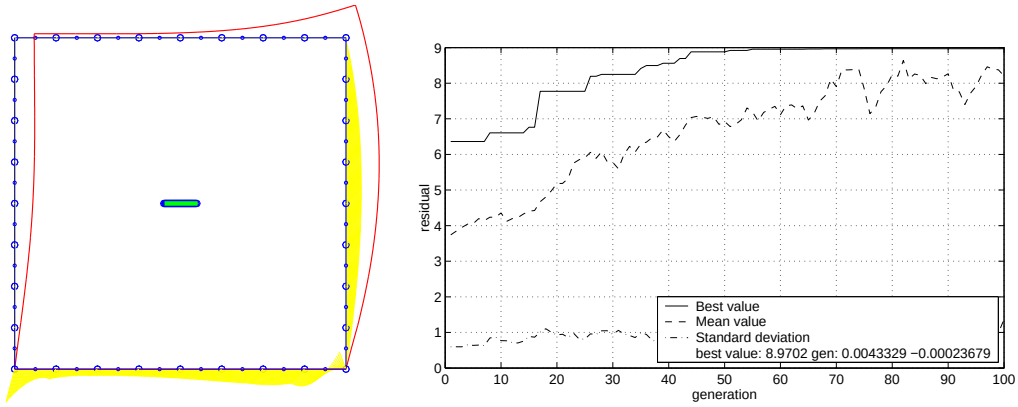

Figure 15.13: Benchmark with one crack. A similar result to the cavity is found.

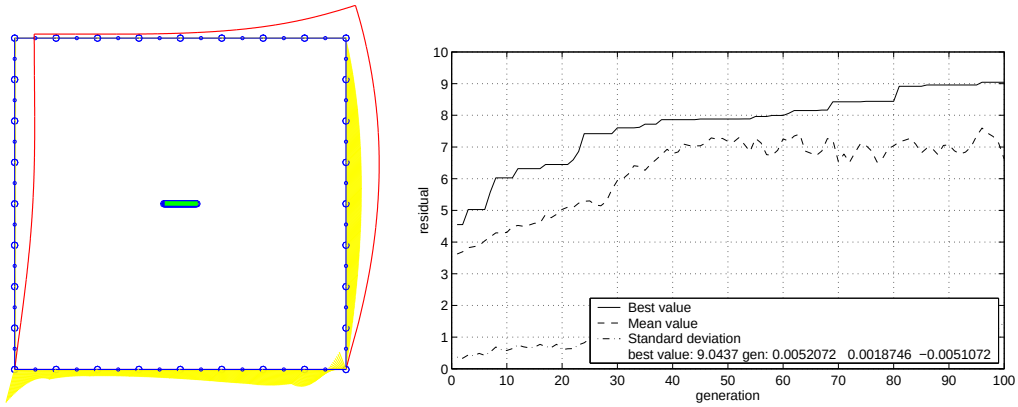

Figure 15.14: Benchmark with one crack. The angle is allowed as the third parameter. The convergence to the right values is attained correctly.

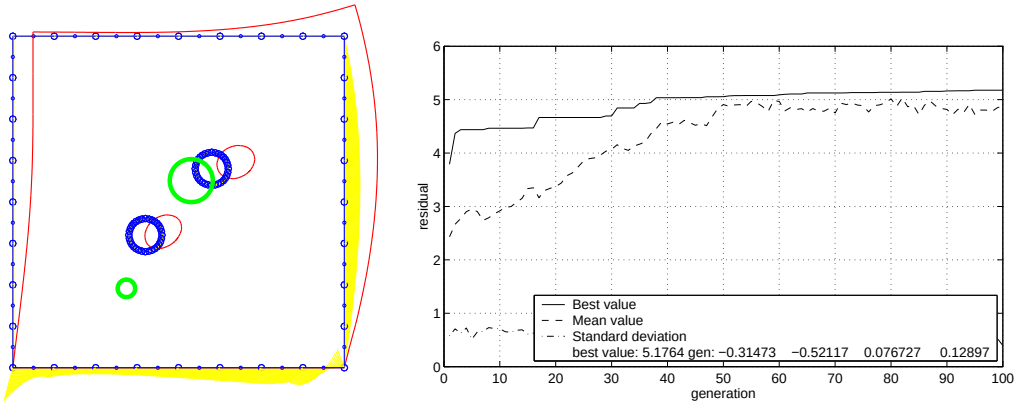

Figure 15.15: Benchmark with two cavities. Four parameters are sought this time. The final values show almost no correlation with the real solution.

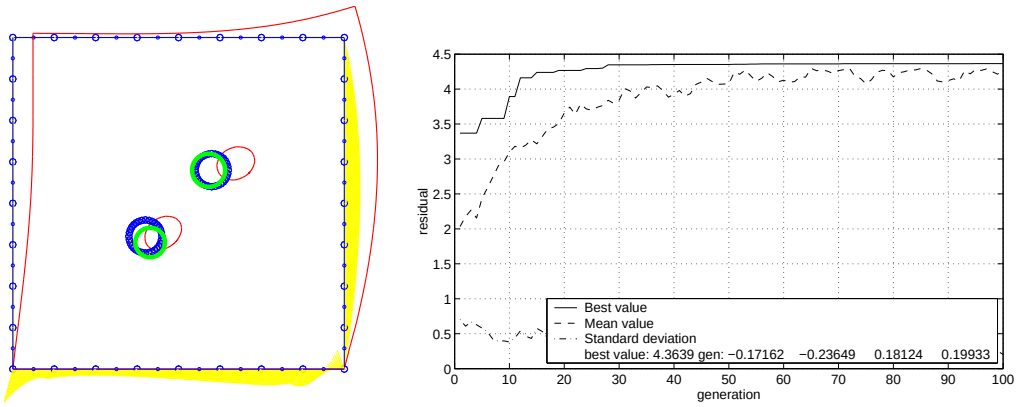

Figure 15.16: Benchmark with two cavities. The use of more measurement data, improves very much. The final values appear to be about 10% of geometrical distance from the real ones.

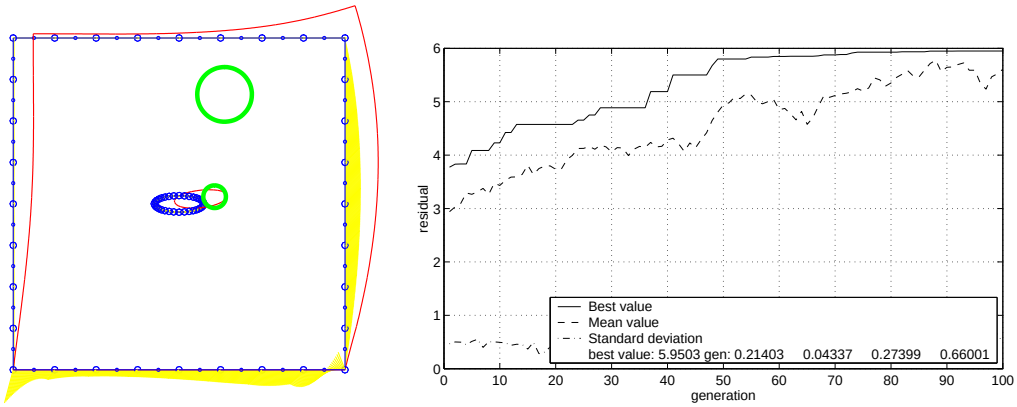

Figure 15.17: Benchmark with one elliptical cavity. Two cavities are allowed to compose the solution. The first one fits reasonably good, with 15% geometrical distance, and the second one appears very far.

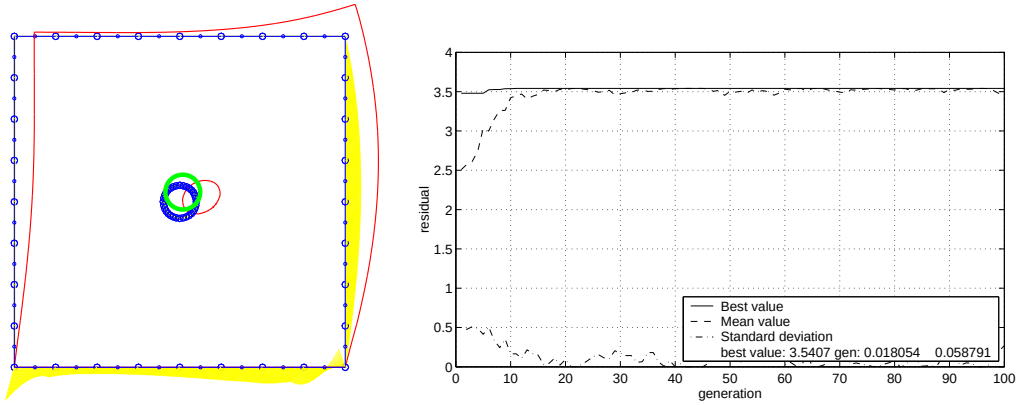

Figure 15.18: Benchmark with one cavity. 10% error on the measurements is introduced. A solution acceptably near the real one appears.

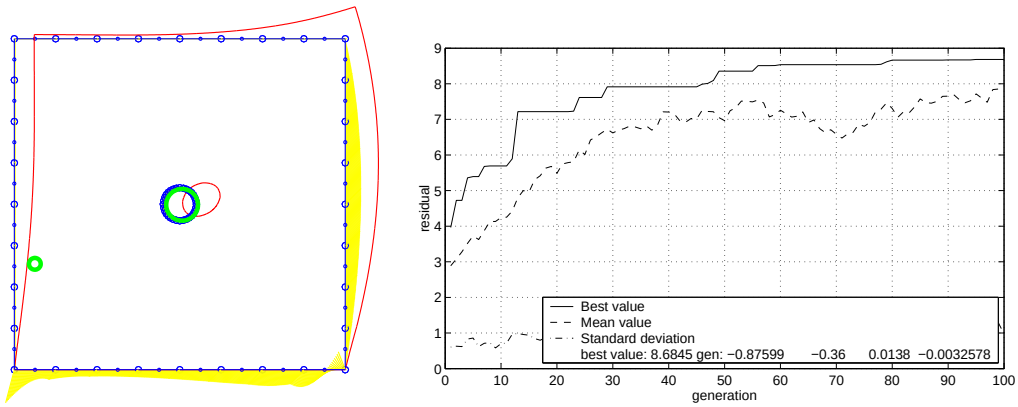

Figure 15.19: Benchmark with one cavity. 2 Cavities allowed. The first cavity converges correctly to the right value (92% of the right area), whereas the second one moves randomly with a vanishing radius (10% of the right area).

Chapter 16

Demonstration examples

16.1 Detection of a subsurface inclusion

A single problem simulating a soil made of two layers is presented. An flatten inclusion in the lower layer is sought by measuring the displacement of a set of 5 nodes, on the area shown in figure 16.1. The excitation of the body is a parabolic load beside the measurement zone. The mechanical properties of the materials in the different layers and the inclusion are given. In addition, the density is 1.0 and the damping ratio 10% throughout, for frequency $\omega = 1.0$. The model is made of 13 quadratic boundary elements altogether (plotted in figure 16.1, in real-scale, from which the geometrical magnitudes can be measured).

This may simulate the search of an oil deposit, a drainpipe or a hollow in piece of cast iron, for instance.

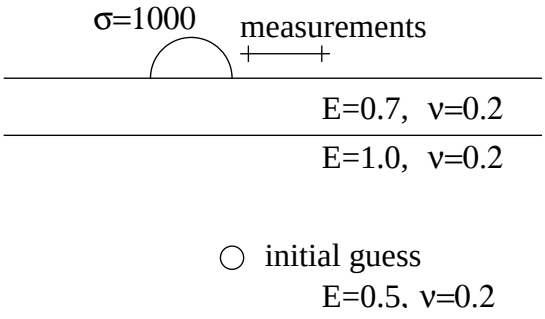

Figure 16.1: Definition of the model.

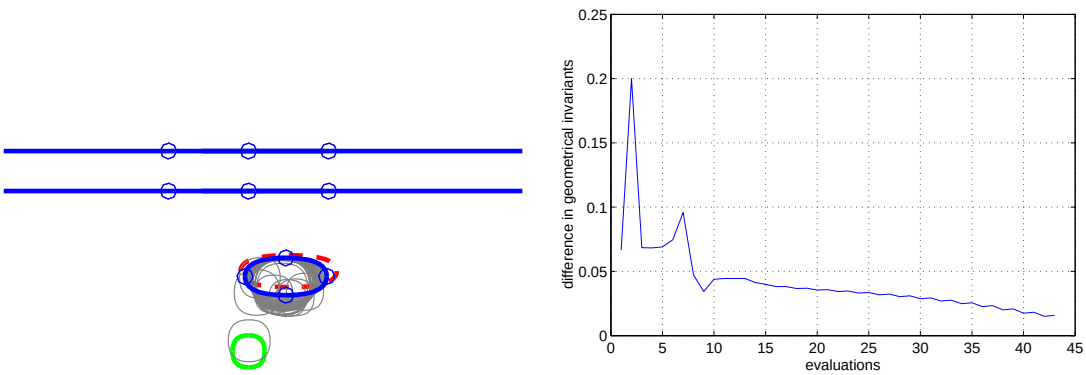

Figure 16.2: Iterations and geometrical error.

Figure 16.2 shows the succesive geometries during the iterative procedure. The real inclusion is plotted in discontinuous red line, and the final guess is plotted in continuous blue line. The problem mesh is refined to 26 elements altogether. The right graphic shows the geometrical error in terms of the square sum of the difference of the geometrical invariants between estimated and real flaws. 43 iterations are needed to reach a good estimation, and a fast convergence is shown at the beginning. The iterative procedure has been divided in two steps: one allowing only the displacement and radial growth of the circular guess (which converges after 13 iterations), and a second step allowing the flattening too.

The same problem is repeated using an unique measurement: the vertical component of the displacement at the point shown in figure 16.3. The data obtained is a sampling of the permanent waveform, which is transformed into its harmonic amplitudes and their phase shift. The first six harmonics are used for the detection, leaving the rest of the definitions as above.

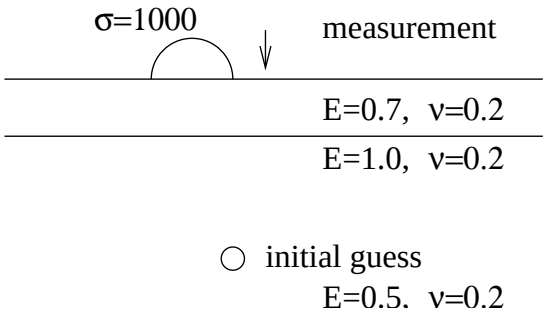

Figure 16.3: Definition of the model.

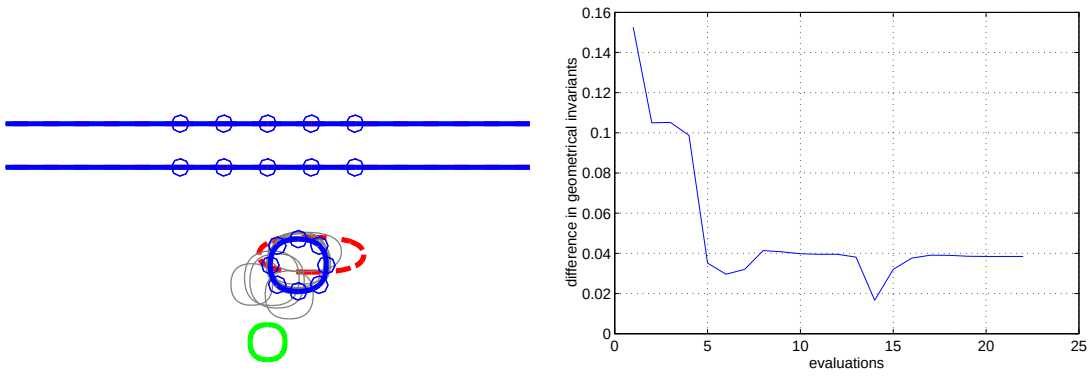

Figure 16.4: Iterations and geometrical error. Use of waveform analysis.

Figure 16.2 shows the iteration procedure and the geometrical error, as before. The convergence is achieved in $13 + 11$ iterations, being a somewhat worse solution the cost of a cheap experimental setup with only one transducer.

16.2 Identification of delamination crack position and length in a beam.

This sample problem simulates the search and control of a crack that appears on a bending beam of 5×1 with the mechanical properties shown in the figure 16.5. A set of 5 nodes is analyzed, on the area shown in the figure, when a parabolic load is applied beside. In addition, the density is 1.0 and the damping ratio 10% throughout, for frequency $\omega = 1.0$.

This may simulate the search of a delamination in an isotropic composite beam of an airplane wing, for instance.

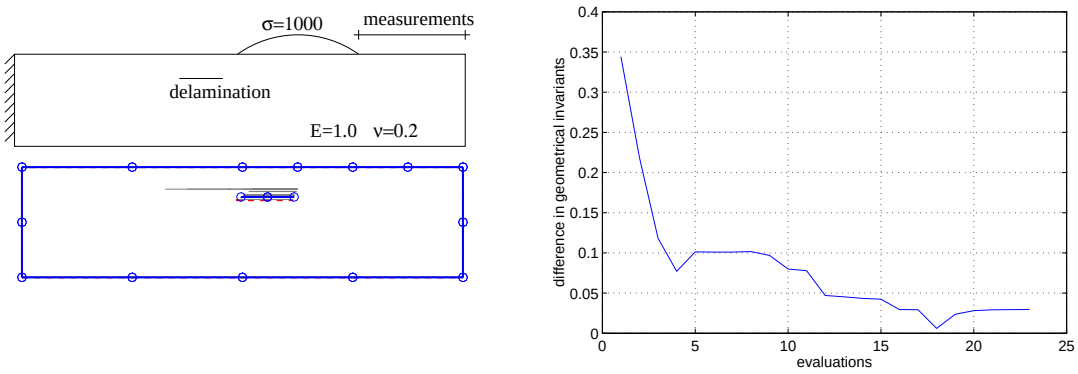

Figure 16.5: Left: definition of the model and iterations. Right: Geometrical error.

In figure 16.5 the correct convergence is shown after $7 + 17$ iterations in a first step that allows horizontal movement, and a second step with all three parameters.

The wave analysis is used as before to this example, giving the results in figure 16.6. A very good convergence is obtained after $11 + 15$ iterations.

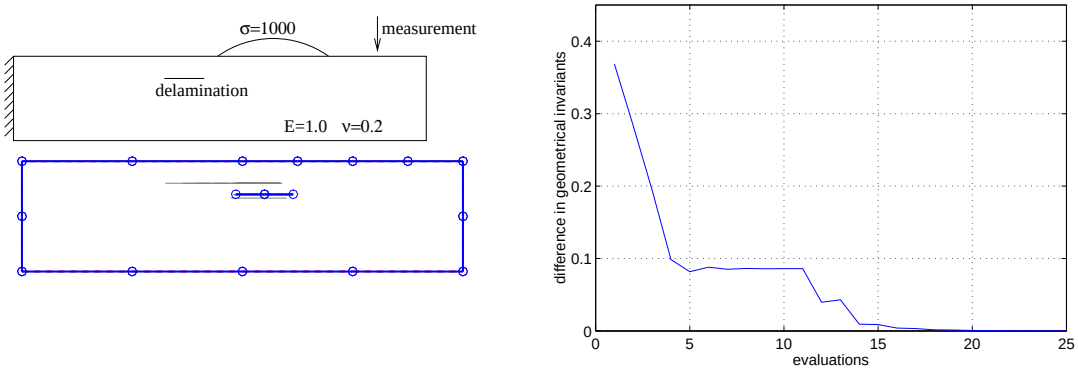

Figure 16.6: Left: definition of the model and iterations. Right: Geometrical error.

Part IV

Conclusions

Chapter 17

Conclusions

This thesis has brought forward and tested the following main ideas:

- Direct derivation of sensitivity to geometry. The derivation is done in an analytic and completely generic way, before any definition of parametrization or discretization (chapter 5).
- Sensitivity by the adjoint variable method. This method extended to the derivation of the sensitivity to a crack geometry in bidimensional elastodynamics by means of a boundary only equation (chapter 6).
- Topological derivative. A method based on the linearized estimation of the presence of a circular cavity or straight crack is presented (see chapter 10).
- Comparison of the most interesting minimization methods in a systematic way in order to reveal their strengths and limitations.

During the development of all the ideas above some new techniques had to be developed:

- A simple regularization formula for hypersingular integrals that does not require the calculation of any derivative (appendix B).
- A programmable algebra for tensorial expressions with a high number of indices is developed (appendix C).
- A generalized formula for the quarter point element for higher order elements (chapter 7).

Besides, some unexpected results arose:

- An equivalence between the optimization methods and the observation equation approach (chapter 11.3).

17.1 About the gradient by direct derivation

A procedure for the obtention of the gradient or sensitivity of singular and hypersingular boundary integral equations (the *ubie* and *qbie* used in the BEM) is developed. The sensitivity is obtained analytically before discretization, and before parametrization (with respect to a generic differential variation field of the geometry).

The conditions required by all the kernels, weights, discretization and parametrization are studied, assuring the applicability. Besides, all the necessary tools for the numerical implementation have been developed and tested.

The numerical values converge perfectly in statics and steady state dynamics, both in simple and complex problems. The convergence of the gradient values while improving the discretization is steady in every example, at similar rates to the solution of the direct problems. This fact together

with a visually identical value in comparison with the gradient estimation by finite differences guarantees that the correct values are being obtained.

In fact, the finite differences (FD) method seems to fail in the low frequency dynamic problems, especially with cracks, since a big finite distance amplifies second order effects, whereas small values are unstabilizing rapidly due to low frequency-related numerical inaccuracies in the direct problem. This inaccuracy together with the much higher computational cost of FD recommends the use of direct differenciation.

The functionality is confirmed by the application to the solution of complete inverse problems by the Levenberg-Marquardt method. The test of convergence has been made including all the possible errors: measurement, model, geometry and frequency, attaining reasonably good results. The scope of convergence has been systematically studied by exploring the range of distances from which the correct solution is reached, in order to show the capabilities and reliability of the method.

Finally, a technique for identification based on the study of the steady state waveform is presented. It simply consists on the harmonic decomposition of the response to a non-sinusoidal harmonic excitation. This permints the measurement of only one point, and allows for much less computing cost that transient analysis as well as more precision in the measurements and less violent methods than the impact used in transient dynamics evaluation.

17.2 About the choice of optimization algorithm

Here we compare different methods taken from unconstrained nonlinear optimization and apply them to identification IP in order to find the most profitable one. Besides, we test and run an analytical derivation of the gradient.

From the point of view of the probability of arriving at a solution, it seems that the Gauss-Newton is the worst, whereas there is not very much difference between Levenberg-Marquardt and BFGS (as seen in the number of achievements in the results table). The use of a line search does not improve very much the solution. A reason for this is the incompatibility of the line search algorithms with the constrained character of the optimization that the ban of impossible configuration brings (when a flaw touches a boundary). The same reason may alter the numerical calculation of the gradient in some cases (e.g. test F).

The convergence speed makes emphasize the difference between BFGS and the two first methods. GN and LM are very similar for easy problems, but when the global strategies go into service (e.g.test F), LM appears to be the fastest. The use of a line search is a critical choice. In easy problems it retards very much the solution, but it becomes necessary for complex problems. A good strategy would be to switch off the line search when the convergence is more or less assured.

The use of analytic gradient instead of finite differences reduces the computations as much as one should expect: by 20-50% for complex cases, and by 50-80% when the line search is not necessary.

To sum up, each method has shown some advantages and disadvantages. The Levenberg-Marquardt method unifies both robustness and speed, but Gauss-Newton is best near the solution. The global strategy is important in complex problems, but retards near the solution. The use of analytic gradient regularly accelerates the calculation.

In addition, a relationship between the two main types of inverse problem layouts, the observation equation methods and the minimization methods has been found. In particular, it is proved that the direct solution of the observation equation by a least square solution of the non-square system of equations is identical to the simple Gauss-Newton method. This may unify the methods allowing for transferring the advantages of one to the other.

17.3 About the Adjoint variable method

A method for the calculation of the sensitivity with boundary only integrals and the adjoint variable method has been adapted, implemented and checked for the case of bidimensional crack in statics and frequency domain. On the other hand, several parametrization strategies have been proposed and tested.

The main benefits of this method are that the computational cost of the calculations is minimal. It only adds a fraction of the computation time of the direct problem, since the solution of the adjoint problem is immediate as it shares the direct one's factorized system matrix, and the further integrals of the formula are unidimensional.

Regarding the numerical results, they are in agreement with the expectations and useful as long as one cares about a few considerations. In particular, the method appeared to be especially sensitive to the computation of the stress intensity factors, since some terms depend directly on them, and on the discretization, especially for the aforementioned nodal parametrization. This last point can be overridden by the proposed modifications, based on a parametrization of a superimposed discretization. As in the case of other methods of sensitivity calculation, special care should be taken in the vicinity of the eigenfrequencies.

It is interesting to notice that the AVM equations give the sensitivity for continuous problems before any discretization. For solving them, we discretize the direct problem, the adjoint problem, and the integration of the AVM formula, introducing errors in all of them. Although the values obtained eventually converge to the gradient of the continuous, they are not consistent in the same sense as the finite differences are, as they give directly the gradient of the discretized problem. It can become necessary to use a high number of elements, especially on the crack, to minimize this effect.

17.4 About the convergence of IP

Two main techniques have been used: the supply of the gradient of the measured displacements by direct derivation together with a least-squares minimization algorithm, and on the other hand a cost functional gradient supply by the AVM with a secant update minimization algorithm.

The supply of the gradient seems important for two reasons: it accelerates substantially the computation, as well as improves the value given by finite differences in many cases, due to the numerical difficulties related to the choice of finite distance.

The scope of convergence has mainly been studied with respect to the supplied data, the errors in the model and the frequency of the excitation. The number of measurements has not shown an important effect, as long as they are more than the number of unknowns. It is just important when the error in them becomes important, in order to compensate the total error.

An important factor is the number of parameters or unknowns. A high number of them rapidly unstabilizes the convergence and reduces the scope. An effective solution is to dose the parameters, allowing a few to act at the beguinning and gradually increasing them as the minimization succeeds. Another factor is that the choice of parametrization should give a good compromise between a good approximation of the sought flaw and a low number of parameters.

The presence of errors in any of the parts of the model affects in a similar way both the convergence and the reliability of the final solution. This can be enhanced by increasing the number of data in form of measurement point and measurement frequencies.

17.5 About topological derivative

The topological derivative gives the variation in the response due to the presence of an infinitesimal flaw (circular cavity or straight crack). This is in turn directly related to the linearized difference

in response when the finite flaw does and does not exist. The main benefits rely on the following points:

- Only an unique direct problem computation is needed for the whole search. The direct problem has moreover no flaw.
- The computation of the topological derivative is based on the already factorized system matrix of the direct problem and on a cheap computation of some values at the center of the sought area, with a similar cost to the stress evaluation at that point.
- The area of the flaws are optimized within the iteration step, reducing significantly the number of parameters. This stabilizes and accelerates the search further.

It shows an excellent response to the presence of errors and to the search of non-circular flaws.

The ability to search several simultaneous flaws easily, gives the possibility of searching a undefined number of faults by allowing for a number of flaws in excess, and letting the non existing flaws vanish by themselves.

17.6 Forthcoming works

- The most immediate work, already being made at present, regards the extension of the topological derivative to steady state dynamics, and later to inclusions.
- Less classical soft computing techniques are an interesting field still to be explored. They seem especially well suited to the coupled use with the topological derivative.
- Since the methods developed so far seem ready for use, the experimental confirmation is the following natural step.
- The geometrical and topological sensitivity formulas are to be extended to anisotropic materials, to fully enter the evaluation of advanced materials.

Functional software and numerical problems for comparison can be obtained from the author at *grus@ugr.es*

Part V

Bibliography

Bibliography

[1] J. B. Abdallah. *Inversion gaussienne appliqué 'la correction paramétrique de modéles structuraux.* PhD thesis, Ecole Polytechnique, 1995.

[2] M. Abramowitz and I. A. Stegun. *Handbook of mathematical functions.* Dover, 1964.

[3] R. Aithal and S. Saigal. Shape sensitivity in thermal problems using bem. *Engineering Analysis with Boundary Elements*, 15:115–120, 1995.

[4] E. Alarcon and P. Reyero. Método de los elementos de contorno. Guía de Introducción.

[5] M. Altmann. About nonuniform rational b-splines - nurbs. Worcester Polytechnic Institute, USA. www.cs.wpi.edu/ matt/cs563/talks/nurbs.html.

[6] S. Andrieux, A. B. Abda, and H. D. Bui. Reciprocity principle and crack identification. *Inverse Problems*, 15:59–65, 1999.

[7] M. R. Barone and R. J. Yang. A boundary element approach for recovery of shape sensitivities in three-dimensional elastic solids. *Computer Methods in Applied Mechanics and Engineering*, 1989.

[8] D. M. Bates and D. G. Watts. *Relative curvature measures of nonlinearity.* D. Jacobs Ed, Academic Press, London, 1980.

[9] L. M. Bezerra and S. Saigal. A boundary element formulation for the inverse elastostatics problem (iesp) of flaw detection. *International Journal for Numerical Methods in Engineering*, 36:2189–2202, 1993.

[10] G. E. Blandford. Two-dimensional stress intensity factor computations using the boundary element method. *International Journal for Numerical Methods in Engineering*, 17:387–404, 1981.

[11] M. Bonnet. On some inverse problems for determining volumic defects by electric current using boundary integral equation approaches: an overview. *JASCOME*, 1989.

[12] M. Bonnet. Shape identification using acoustic measurements: A numerical investigation using bie and shape differentiation. In H. D. Bui M. Tanaka, editor, *Inverse Problems in Engineering Mechanics*, pages 191–200, 1992.

[13] M. Bonnet. Bie and material differenciation applied to the formulation of obstacle inverse problems. *Engineering Analysis with Boundary Elements*, 15:121–136, 1995.

[14] M. Bonnet. Bie formulations for first- and second-order shape sensitivity of elastic fields. *Computer and Structures*, 56:799–811, 1995.

[15] M. Bonnet. *Boundary Integral Equation Methods for Solids and Fluids.* Wiley, 1995.

[16] M. Bonnet. A general boundary-only formula for crack shape sensitivity of integral functionals. *Comptes Rendus de l'Académie des Sciences, Série IIb/ Mécanique des Solides et des Structures*, June 7 1999.

[17] M. Bonnet, R. Gallego, and J. Domínguez. Elementos de contorno de transición para el cálculo de factores de intensidad de tensiones. *Métodos de Contorno*, 1996.

[18] M. Bonnet, G. Rus, and R. Gallego. Convergence of crack identification using avm gradient and bfgs optimization. *to be published*, 2001.

[19] M. Bonnet, G. Rus, and R. Gallego. Crack shape sensitivity by the adjoint variable method using a boundary-only formula. *to be published*, 2001.

[20] A. Boström, G. Johansson, and P. Olsson. On the derivation of a hierarchy of dynamic equations for a homogeneous, isotropic, elastic plate. *International Journal of Solids and Structures*, 38:2487–2501, 2001.

[21] A. Boström and H. Wirdelius. Ultrasonic probe modeling and nondestructive crack detection. *J. Acoust. Soc. Am.*, 97:2836–2848, 1995.

[22] C. A. Brebbia and J. Domínguez. *Boundary Elements, An Introductory Course.* CMP, McGraw Hill, 1992.

[23] D. Broek. *Elementary engineering fracture mechanics.* Kluwer academic publishers, 1997.

[24] K. Bryan, V. Liepa, and M. Vogelius. Reconstruction of multiple cracks from experimental electrostatic boundary measurements. *NASA. ICASE Report*, 93-96:1–28, 1993.

[25] H. D. Bui. *Inverse Problems in the Mechanics of Materials. An Introduction.* CRC, Eyrolles, 1994.

[26] T. Burczynski. Recent advances in boundary element approach to design sensitivity analysis - a survey. In *Design Sensitivity Analysis*, pages 1–25. M. Kleiber, 1993.

[27] T. Burczynski, G. Kuhn, H. Antes, and M. Nowakowski. Boundary element formulation of shape sensitivity analysis for defect identification in free vibration problem. *Engineering Analysis with Boundary Elements*, 1997.

[28] E. Calvo. *Análisis de sensibilidad en elasticidad mediante el método de los elementos de contorno. Aplicación a la optimización de formas.* PhD thesis, Centro Politécnico de la Universidad de Zaragoza, september 1995.

[29] F. Chirino. Hypersingular boundary element program for harmonic crack solution. Fortran 77., 1998.

[30] F. Chirino and R. Abascal. Cálculo de factores de intensidad de tensión estáticos y dinámicos mediante el método de los elementos de contorno con formulación hipersingular. *Métodos numéricos para cálculo y diseño en ingeniería*, 14(3):339–364, 1998.

[31] A. Constantinescu and N. Tardieu. Identification strategies for recovering material parameters from indentation experiments. In M. Tanaka and G. Dulikravich, editors, *Inverse problems in engineering mechanics II*, 2000.

[32] T. A. Cruse. *Boundary Element Analysis in Computational Fracture Mecanics.* Kluwer Academic Publishers, 1988.

[33] D. Delaunay, Y. Jarny, and K. A., editors. *Inverse Problems in Engineering: Theory and Practice.*, Proc. 2nd Conf. on Inverse Problems in Engineering, June 9-14, 1993, Le Croisic, France, 1996.

[34] J. E. Dennis, D. M. Gay, and R. E. Welsch. Algorithm 573 nl2sol - an adaptive nonlinear least-squares algorithm [e4]. *ACM Transactions on Mathematical Software*, 7(3):369–383, 1981.

[35] Manuel Doblaré. *Fundamentos de Elasticidad Lineal.* Sintesis, 1998.

[36] J. Domínguez. *Boundary Elements in Dynamics.* Elsevier, CMP, 1993.

[37] N. A. Dumont. On the efficient numerical evaluation of integrals with complex sigularity poles. *Engng. Analysis With Boundary Elements*, 13:155–168, 1994.

[38] M. Elices. Mecánica de la fractura aplicada a sólidos elásticos bifimensionales. Apuntes del Departamento de Ciencia de Materiales, E.T.S.I. Caminos, C. y P., U.P.M.

[39] D. Elizondo, C. Faure, and B. Cappelare. Automatic- versus manual- differentiation for nonlinear inverse modelling. In *INRIA, Rapport de Recherche*, volume 3981, 2000.

[40] S. Ratnajeevan et al. Inverse problem methodology and finite elements in the identification of cracks, sources, materials, and their geometry in inaccessible locations. *IEEE Transactions on Magnetics*, 27(3), May 1991.

[41] T. Kowalckzyk et al. An extensible evolutionary algorithm approach for inverse problems. In G. S. Dulikravich M. Tanaka, editor, *Inverse problems in Engineering Mechanics*, 1998.

[42] H. L. Ewalds and R. J. H. Wanhill. *Fracture Mechanics.* Arnold DUM, 1984.

[43] C. Faure. Automatic differentiation for adjoint code generation. In *INRIA, Rapport de Recherche*, volume 3555, 1998.

[44] H. E. Fettis. Expressions for divergent integrals in terms of convergent ones. In G. Hammerlin, editor, *Numerical Integration, International Series of Numerical Mathematics 57.* Birkhauser, 1991.

[45] R. Gallego and J. Domínguez. Hypersingular bem for transient elastodynamics. *International Journal for Numerical Methods in Engineering*, 39:1681–1705, 1996.

[46] R. Gallego and J. Domínguez. Solving transient dynamic crack problems by the hypersingular boundary element method. *Fatigue Fract. Engng. Mater. Struct.*, 20(5):799–812, 1997.

[47] R. Gallego and G. Rus. Topological derivatives for elasticity by boundary integral equations. *To be published*, 0:0, 2001.

[48] R. Gallego and J. Suarez. Numerical solution of the variation boundary integral equation for inverse problems, October 1999.

[49] R. Gallego and J. Suarez. Solution of inverse problems by boundary integral equations without residual minimization, September 1999.

[50] R. Gallego and J. Suarez. Solution of inverse problems by boundary integral equations without residual minimization, September 1999.

[51] R. Gallego and J. Suarez. Variation boundary integral equation for flaw shape identification. In *3rd Int. Conf. on Inverse Problems in Engineering: Theory and Practice*, June 1999.

[52] D. Goldberg. *Genetic algorithms in search, optimization and machine learning.* Addison-Wesley Publ, Reading, Massachussets, etc., 1989.

[53] I. S. Gradshteyn and I. M. Ryzhik. *Table of integral, series, and products.* Academic Press, 1963.

[54] M. Guiggiani. Direct evaluation of hypersingular integrals in 2D BEM. In W. Hackbusch / Vieweg, editor, *Proc. 7th GAMM Seminar on Numerical Techniques for Boundary Element Methods / Notes in Numerical Fluid Mechanics*, volume 333, pages 23–34, Kiel, Germany, 1991.

[55] M. Guiggiani. Hypersingular formulation for boundary stress evaluation. *Engineering Analysis with Boundary Elements*, 1993.

[56] M. Guiggiani. Hypersingular boundary integral equations have an additional free term. *Computational Mechanics*, 16:245–248, 1995.

[57] M. Guiggiani, G. Krishnasamy, F. J. Rizzo, and T. J. Rudolphi. Hypersingular boundary integral equations: a new approach to their numerical treatment. In L. Morino and R. Piva / Springer, editors, *Proc. IABEM Symposium / Boundary Integral Methods*, pages 211–220, Rome, Italy / Berlin, Germany, 1990.

[58] M. Guiggiani, G. Krishnasamy, T. J. Rudolphi, and F. J. Rizzo. A general algorithm for the numerical solution of hypersingular boundary integral equations. *J. Appl. Mech.*, 59:604–614, 1992.

[59] J. Haataja. Matlab function for simulating a simple real-coded genetic algorithm. Center for Scientific Computing, Box 405, FIN-02101 Espoo. Internet: Juha.Haataja@csc.fi, 2000.

[60] Per Christian Hansen. *Rank-deficient and discrete ill-posed problems. Numerical aspects of linear inversion.* SIAM, 1997.

[61] John Hertz, Anders Krogh, and Richard G. Palmer. *Introduction to the theory of neural computation.* Addison Wesley, 1991.

[62] Q. Huang and T.A. Cruse. Some notes on singular integral techniques in boundary element analysis. *Int. J. Num. Meth. Engng.*, 36:2643–2659, 1993.

[63] MathWorks Inc. Matlab optimization toolbox user's guide. http://www.mathworks.com, 1996.

[64] J. E. Dennis Jr. and Robert B. Schnabel. *Numerical methods for unconstrained optimization and nonlinear equations.* SIAM, 1983, 1996.

[65] L. Jun, G. Beer, and J. L. Meek. Efficient evaluation of integrals of order $1/r$, $1/r^2$, $1/r^3$ using Gauss method. *Engng. Analys.*, 2:118–123, 1985.

[66] H. Kagawe. The two dimensional inverse acoustic scattering for shape identification. In Tanaka et al. Bui, editor, *Inverse problems in Engineering Mechanics*, 1994.

[67] M. F. Kanninen and C.H. Popelar. *Advanced Fracture Mechanics.* Oxford Science Publications, 1985.

[68] A. Kassab, F. Moshley, and A. Daryapubkar. Nondestructive detection by an inverse elastostatic boundary element method. *Engineering Analysis with Boundary Elements*, 13:45–55, 1994.

[69] A. Kirsch. The domain derivative and two applications in inverse scattering theory. *Inverse Problems*, 9:81–96, 1993.

[70] G. Kirsch. The effect of circular holes on stress distributions in plates. *V.D.I.*, 42, 1898.

[71] H. Koguchi and H. Watabe. Improving defects search in structure by boundary element and genetic algorithm scan method. *Engineering Analysis with Boundary Elements*, 19:105–116, 1997.

[72] G. Krishnasamy, L. W. Schmerr, T. J. Rudolphi, and F. J. Rizzo. Hypersingular boundary integral equations: Some applications in acoustic and elastic wave scattering. *Transactions of the ASME*, pages 404–415, 1990.

[73] A. R. Krommer and C. W. Ueberhuber. *Computational Integration.* SIAM, 1998.

[74] S. Kubo. Classification of inverse problems arising in field problems and their treatments. In H. D. Bui M. Tanaka, editor, *Inverse Problems in Engineering Mechanics*, pages 51–60, 1992.

[75] D. Laplue, G. Guerlement, and D. Lamblin. Implementation of simulated annealing to the optimal plastic design of solid cylindrical shells without axial loading. In B. Suárez E. Oñate, G. Bugeda, editor, *ECCOMAS2000*, 2000.

[76] R. M. Lewis. Numerical computation of sensitivities and the adjoint approach. *Tech. Report No.97-61, ICASE, NASSA Langley Research Center, Hampton, Virginia, USA*, 1997.

[77] J. A. Liggett and J. R. Salmon. Cubic spline boundary elements. *Int. J. for Numerical Methods in Engineering*, 1981.

[78] E. D. Lutz. *Numerical methods for hypersingular and near-singular boundary integrals in fracture mechanics.* PhD thesis, Cornell University, Ithaca, New York, USA, 1991.

[79] V. Mantic and F. Paris. Existence and evaluation of the two free terms in the hypersingular boundary integral equation of potential theory. *Engineering Analysis with Boundary Elements*, 9:1–8, 1995.

[80] J. Martínez and J. Domínguez. On the use of quarter-point boundary elements for stress intensity factor computations. *International Journal for Numerical Methods in Engineering*, 20:1941–1950, 1984.

[81] M. Masmoudi. A synthetic presentation of shape and topological optimization. In *INRIA, Rapport de Recherche*, pages 121–127, 1998.

[82] T. Matsumoto and M. Tanaka. Boundary integral formulation of design sensitivities for potential problems. *Engng Anal Boundary Elements*, 7-1:33–38, 1990.

[83] T. Matsumoto, M. Tanaka, M. Miyigawa, and N. Ishii. Optimum design of cooling lines in injection moulds by using boundary element design sensitivity analysis. *Finite Elements in Analysis and Design*, 14:177–186, 1993.

[84] S. C. Mellings and M. H. Aliabadi. Dual boundary element formulatoin for inverse potential problems in crack identification. *Engineering Analysis with Boundary Elements*, 12:275–283, 1993.

[85] S. C. Mellings and M. H. Aliabadi. Flaw identification using the boundary element method. *International Journal for Numerical Methods in Engineering*, 38:399–419, 1995.

[86] William Menke. *Geophysical data analysis, Discrete Inverse Theory.* Academic Press INC., 1984.

[87] R. A. Meric. Differential and integral sensitivity formulations and shape optimization by bem. *Engineering Analysis with Boundary Elements*, 15:181–188, 1995.

[88] A. K. Mitra and S. Das. Solution of inverse problems by using the boundary element method. *Boundary Element Technology*, 1990.

[89] T. Mura, T. Koya, C. Hsieh, Z. A. Moschovidis, and Z. Gao. Inverse problems associated with nondestructive evaluation of plastic damages in solids.

[90] K. Nakahata and M. Kitahara. Inversion of defects by linearized inverse scattering methods with measured waveforms. In M. Tanaka and G. Dulikravich, editors, *Inverse problems in engineering mechanics II*, 2000.

[91] N. Nishimura. Crack determination problems. *Theoretical and Applied Mechanics*, 46:39–57, 1997.

[92] N. Nishimura and S. Kobayashi. A boundary integral equation method for an inverse problem related to crack detection. *International Journal for Numerical Methods in Engineering*, 32:1371–1387, 1991.

[93] N. Nishimura and S. Kobayashi. Determination of cracks having arbitrary shapes with the boundary integral equation method. *Engineering Analysis with Boundary Elements*, 15:189–195, 1994.

[94] Federico Paris. *Teoría de la Elasticidad.* GERM, 1996.

[95] Polch, Cruse, and Huang. Traction bie solutions for flat cracks. *Computational Mechanics*, 2:253–267, 1987.

[96] M Prud'homme and T. H. Nguyen. Iterative solution to the inverse steady state convection: analysis of the convergence process. In B. Suárez E. Oñate, G. Bugeda, editor, *ECCOMAS2000*, 2000.

[97] L. Råde and B. Westergren. *Mathematics Handbook for Science and Engineering.* Springer, 1999.

[98] T. J. Rudolphi. The use of simple solutions in the regularization of hypesingular boundary integral equations. *Math. Comput. Modelling*, 15:269–278, 1991.

[99] G. Rus and R. Gallego. Acoplamiento del método de los elementos finitos y elementos de contorno en elastodinámica plana armònica. sevilla, june 2000. In R. Abascal, J. Domìnguez, and G. Bugeda, editors, *CIMNE*, 1999.

[100] G. Rus and R. Gallego. Solution of identification inverse problems by a sensitivity boundary integral equation. barcelona, september 2000. In B. Suárez E. Oñate, G. Bugeda, editor, *ECCOMAS2000*, 2000.

[101] G. Rus and R. Gallego. Optimization algorithms for identification inverse problems. In B. Suárez E. Oñate, G. Bugeda, editor, *CMEM2001*, 2001.

[102] J. N. Goodier S. Timoshenko. *Theory of Elasticity.* McGraw-Hill, 1951.

[103] A. Sáez, R. Gallego, and J. Domínguez. Hypersingular quarter-point boundary elements for crack problems. *Int. J. Num. Meth. Engng.*, 38:1681–1701, 1995.

[104] V. Saldek, J. Sladek, and M. Tanaka. Regularization of hypersingular and nearly singular integrals in the potential theory and elasticity. *Int. J. Num. Meth. Engng.*, 36:1609–1628, 1993.

[105] D. Schnur and N. Zabaras. An inverse method for determining elastic material properties and a material interface. *International Journal for Numerical Methods in Engineering*, 33:2039–2057, 1992.

[106] A. A. Schwab. Boundary integral equations for inverse problems in the elasticity theory. *Journal of elasticity*, 1995.

[107] B. Sensale, A. Herrera, and A. Piria. Optimizacion de forma de estructuras continuas por algoritmos naturales y el metodo de los elementos de contorno. In *Métodos Numéricos en la Ingeniería*, 1999.

[108] J. Sokolowski and A. Zochowski. On topological derivative in shape optimization. In *INRIA, Rapport de Recherche*, pages 129–136, 1997.

[109] J. Sokolowski and A. Zochowski. Topological derivatives for elliptic equations. INRIA. Inverse Problems, Control and Shape Optimization, 1998.

[110] G. E. Stavroulakis. *Inverse and crack identification problems in engineering mechanics.* Kluwer Academics, 2000.

[111] G. E. Stavroulakis. *Inverse and crack identification problems in engineering.* Kluwer Academic Publishers, 2001.

[112] G. E. Stavroulakis and H. Antes. Crack detection in elastostatics and elastodynamics. a bem modelling - neural network approach. In M. Tanaka and G. Dulikravich, editors, *Inverse problems in engineering mechanics*, 1998.

[113] G. E. Stavroulakis and H. Antes. Flaw identification in elastomechanics: Bem simulation with local and genetic optimization. *Structural Optimization*, 1998.

[114] F. J. Suárez. *Aplicación del Método de los Elementos de Contorno a la Resulución del Problema Inverso en Elastodinámica.* PhD thesis, Universidad de Granada, E.T.S.I. Caminos, C. y P., Noviembre 1998.

[115] M. Suzuki and A. Murakami. Bayesian estimation for nonlinear inverse problems. In M. Tanaka and G. Dulikravich, editors, *Inverse problems in engineering mechanics II*, 2000.

[116] M. Takadoya, M. Notake, and M. Kitahara. Neural network approach to the inverse problem of crack-depth determination from ultrasonic backscattering data. In M. Tanaka and H. D. Bui, editors, *Inverse problems in engineering mechanics. Proc. IUTAM Symposium Tokyo*, pages 413–422, 1992.

[117] M. Tanaka and H. D. Bui, editors. *Inverse Problems in Engineering Mechanics.*, Proc. IUTAM Symp. on Inverse Problems in Engineering Mechanics 1992, Tokyo, Japan., 1992.

[118] M. Tanaka and H. D. Bui, editors. *Inverse Problems in Engineering Mechanics*, Tokyo, Japan, 1992.

[119] M. Tanaka and H. D. Bui. *Inverse Problems in Engineering Mechanics.* Balkema, 1994.

[120] M. Tanaka and G. S. Dulikravich, editors. *Inverse Problems in Engineering Mechanics*, Proc. Int. Symp. on Inverse Problems in Engineering Mechanics 1998 (ISIP'98), Nagano, Japan, 1998.

[121] M. Tanaka and G. S. Dulikravich, editors. *Inverse Problems in Engineering Mechanics*, Proc. Int. Symp. on Inverse Problems in Engineering Mechanics 2000 (ISIP 2000), Nagano, Japan, 2000.

[122] M. Tanaka and Y. Masuda. Boundary element method applied to some potential inverse problems. *Engineering Analysis*, 3-3:138–143, 1989.

[123] M. Tanaka, T. Matsumoto, and S. Oida. Identification of unknown boundary shape of rotiationally symmetric body in steady heat conduction via bem and filter theories. In M. Tanaka and G. Dulikravich, editors, *Inverse problems in engineering mechanics*, 1998.

[124] M. Tanaka, T. Matsumoto, and T. Yano. A combined use of experimental design and kalman filter-bem for identification of unknown boundary shape for axisymmetric bodies under steady-state hear conduction. In M. Tanaka and G. Dulikravich, editors, *Inverse problems in engineering mechanics II*, 2000.

[125] M. Tanaka and M. Nakamura. Application of genetic algoritm to plural defects identification. In Tanaka et al. Bui, editor, *Inverse problems in Engineering Mechanics*, 1994.

[126] M. Tanaka, V. Sladek, and J. Sladek. Regularization techniques applied to boundary element methods. *Appl. Mech. Rev.*, 47:457–499, 1994.

[127] M. Tanaka and K. Yamagiwa. A boundary element method for some inverse problems in elastodynamics. *Appl. Math. Modelling*, 13, May 1989.

[128] J. C. F. Telles. A self-adaptative coordinate transformation for efficient numerical evaluation of general boundary element integrals. *Int. J. Num. Meth. Engng.*, 24:959–973, 1987.

[129] N. Tosaka and A. Utani. New filter theory - boundary element method and its applicatoin to inverse problem. In Tanaka et al. Bui, editor, *Inverse problems in Engineering Mechanics*, 1994.

[130] G. J. Vass. The bezier curve. a pov-ray tutorial. www.geocities.com/CapeCanaveral/Launchpad/7394/.

[131] H. G. Walters, J. C. Ortiz, G. Steven Gipson, and J. A. Brewer III. Overhauser boundary elements in potential theory and linear elastostatics. *IUTAM Symposium, San Antonio, Texas*, 1987.

[132] S. C. Wooh and I. M. Daniel. Three dimensional ultrasonic imaging of defects and damage in composite materials. *Materials Evaluation*, pages 1199–1206, 1994.

[133] Z. Yao and B. Gong. Defect identification using boundary element methods of elastostatics. In Tanaka et al. Bui, editor, *Inverse problems in Engineering Mechanics*, 1994.

[134] A. Young. A single-domain boundary element method for 3-d elastostatic crack analysis using continuous elements. *Int J Numer Methods Engrg*, 39:1265–1293, 1996.

[135] F. Yuan, X. Cai, and M. Oezisik. Determination of elastic constant by inverse analysis. *Inverse Problem in Engineering*, 3:1–19, 1996.

[136] N. Zabaras, K. A. Woodbury, and M. Raynaud, editors. *Inverse Problems in Engineering: Theory and Practice*, Proc. 1st Conf. on Inverse Problems in Engineering, June 13-18, 1993, Palm Coast, Florida, USA, 1993.

[137] X. Zeng and S. Saigal. An inverse formulation with boundary elements. *Transactions of the ASME*, 59:835–840, December 1992.

Part VI

Appendix

Appendix A

Kernels and limits

A.1 Expressions for the variation boundary integral equation for the 2D potential problem

As stated earlier, this equation can be deduced in a very similar manner for the potential problem. Following the guidelines given above, the substracted process to obtain it is as follows:

The potential problem is defined as:

1. Statics:

$$u_{,jj} = 0 \quad \forall x \in \Omega$$

with some boundary conditions,

$$u = \overline{u} \quad \forall x \in \Gamma_1 \qquad q = \overline{q} \quad \forall x \in \Gamma_2$$

where,

$$\Gamma = \Gamma_1 + \Gamma_2 \qquad q = \frac{\partial u}{\partial n} = u_{,j} n_j$$

2. Steady-state elastodynamics:

$$u_{,jj} + \frac{\omega^2}{c_2^2} u = 0 \quad \forall x \in \Omega$$

with some boundary conditions,

$$u = \overline{u} \quad \forall x \in \Gamma_1 \qquad q = \overline{q} \quad \forall x \in \Gamma_2$$

where,

$$\Gamma = \Gamma_1 + \Gamma_2 \qquad q = \mu \frac{\partial u}{\partial n} = u_{,j} n_j$$
$$u(t) = Real(u e^{i\omega t}) \qquad q(t) = Real(q e^{i\omega t})$$

A.1.1 Variation equation

The problems to compare are:

Known geometry:

$$u = \int_\Gamma \{u^* q - q^* u\}\, d\Gamma \tag{A.1}$$

Perturbed geometry:

$$\tilde{u} = \int_\Gamma \{\tilde{u}^* \tilde{q} - \tilde{q}^* \tilde{u}\}\, d\Gamma \tag{A.2}$$

Series expansion:

$$\begin{aligned}
\tilde{q} &= q + \delta q \\
\tilde{u} &= u + \delta u \\
d\tilde{\Gamma} &= [1 + \delta J] d\Gamma \\
\tilde{u}^* &\simeq u^* + \frac{\partial u^*}{\partial r_m}\delta r_m + hot. \\
\tilde{q}^* &\simeq q^* + u^*_{,j}\delta n_j + n_j \frac{\partial u^*_{,j}}{\partial r_m}\delta r_m + hot.
\end{aligned}$$

The last two expansions are made taking into account the following considerations, and making the product and grouping higher order terms in *hot*.

$$\tilde{q}^* = \tilde{u}^*_{,j}\tilde{n}_j \qquad q^* = u^*_{,j} n_j \qquad \tilde{n}_j = n_j + \delta n_j$$

In order to simplify the expressions, we can define:

$$\begin{aligned}
u^*_{,j} &= \frac{\partial u^*}{\partial y_m} = \frac{\partial u^*}{\partial r_m} \\
u^*_{,jm} &= \frac{\partial u^*_{,j}}{\partial r_m} \\
\delta m_j &= \delta n_j + n_j \delta J
\end{aligned}$$

Subtracting the expanded and simplified versions of A.2 and A.1, we obtain the variation equation A.3.

$$\delta u = \int_\Gamma \left[q u^*_{,m}\delta r_m - u u^*_{,j}\delta m_j + q u^* \delta J - u u^*_{,jm} n_j \delta r_m + u^*\delta q - q^*\delta u\right] d\Gamma \tag{A.3}$$

After taking equation A.3 to the limit (see below), we obtain A.4.

$$\frac{1}{2}\delta u = \int_\Gamma \left[q u^*_{,m}\delta r_m - u u^*_{,j}\delta m_j + q u^* \delta J - u u^*_{,jm} n_j \delta r_m + u^*\delta q - q^*\delta u\right] d\Gamma \tag{A.4}$$

A.1.2 Definition of kernels

1. Fundamental solutions for 2D statics:

   They are the solution to the Laplace equation when the body load is:

$$\begin{aligned}
b^* &= \delta^{pole}_{Dirac} \\
u^* &= \frac{1}{2\pi} ln\left(\frac{1}{r}\right) \\
q^* &= -\frac{1}{2\pi r}\frac{\partial r}{\partial n}
\end{aligned}$$

   Gradient for 2D statics:

$$\begin{aligned}
u^*_{,j} &= \frac{-1}{2\pi r}\left(\frac{r_j}{r}\right) \\
u^*_{,jm} &= \frac{1}{2\pi r^2}\left(\frac{r_j}{r}\frac{r_m}{r} - r\delta_{jm}\right)
\end{aligned}$$

2. Fundamental solutions for 2D harmonic antiplane elastodynamics:

   They are the solution to the Helmholtz equation with body loads,

$$u_{,jj} + \frac{\omega^2}{c_2^2}u + \frac{1}{c_2^2}b = 0$$

   when the load is $\rho b^* = \delta^{pole}_{Dirac} e^{i\omega t}$

$$\begin{aligned} u^* &= \frac{1}{2\pi\mu} K_0\left(\frac{i\omega r}{c_2}\right) \\ q^* &= \frac{-i\omega}{2\pi c_2}\frac{\partial r}{\partial n} K_1\left(\frac{i\omega r}{c_2}\right) \end{aligned}$$

   Gradient for 2D harmonic antiplane elastodynamics:

$$\begin{aligned} u^*_{,j} &= \frac{-i\omega}{2\pi\mu c_2} K_1\left(\frac{i\omega r}{c_2}\right)\frac{r_j}{r} \\ u^*_{,jm} &= \frac{i\omega}{2\pi\mu c_2} K_1\left(\frac{i\omega r}{c_2}\right)\delta_{jm} + \frac{\omega^2}{4\pi\mu c_2^2}\left[K_0\left(\frac{i\omega r}{c_2}\right) + K_2\left(\frac{i\omega r}{c_2}\right)\right]\frac{r_j}{r}\frac{r_m}{r} \end{aligned}$$

A.1.3 Limiting process

Geometrical considerations

Taking into consideration figure A.1,

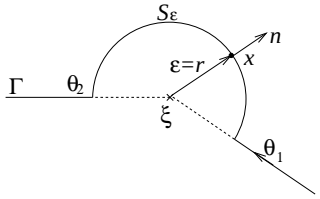

Figure A.1: Protuberance for limiting process

$$\begin{aligned} d\Gamma &= r d\theta \\ \Gamma_\epsilon &\equiv \theta_1 \to \theta_2 \\ r_i &= n_i r \\ r_{,i} &= \frac{r n_i}{r} = n_i \\ n_i &= \begin{bmatrix} -\cos\theta \\ \sin\theta \end{bmatrix} \\ r_{,n} &= r_{,i} n_i = n_i n_i = 1 \\ u(x) &= u(\xi) + \frac{\partial u}{\partial x_j}(x_j - \xi_j) + hot. = u(\xi) + u_{,j} r n_j \\ q(x) &= q(\xi) + \frac{\partial q}{\partial x_j}(x_j - \xi_j) + hot. = q(\xi) + q_{,j} r n_j \\ r &= \epsilon \\ \delta r_l &= \Theta_{l,m} r n_m + \Theta_{l,mn} r^2 n_m n_n + hot. \simeq \Theta_{l,m} r n_m \\ \delta n_j &= t_j t_l \epsilon_{lo} \Theta_{o,m} t_m + \frac{1}{2} r t_j t_l \epsilon_{lo} \Theta_{o,mn} t_m t_n + hot. \simeq t_j t_l \epsilon_{lo} \Theta_{o,m} t_m \\ \delta J &= t_l t_m \Theta_{l,m} + r\frac{1}{2}\Theta_{l,mn} t_l t_m t_n + hot. \simeq t_l t_m \Theta_{l,m} \\ \epsilon_{ij} &= \begin{pmatrix} 0 & 1 \\ -1 & 0 \end{pmatrix} \text{ (permutation tensor)} \end{aligned}$$

Limit of integrals

Statics

1.

$$\lim_{\epsilon\to 0} \quad \left(\int_{\Gamma_\epsilon} q u^*_{,m} \delta r_m d\Gamma\right) = \frac{-q}{2\pi}\Theta_{m,l} \lim_{\epsilon\to 0}\int_{\Gamma_\epsilon} n_l n_m r d\theta = 0$$

2.

$$\begin{aligned}
\lim_{\epsilon\to 0} \quad & \left(\int_{\Gamma_\epsilon} -u u^*_{,jm} n_j \delta r_m d\Gamma\right) \\
&= \frac{-u}{2\pi}\Theta_{m,l}\int_{\Gamma_\epsilon} \lim_{\epsilon\to 0}\left[n_j n_l (n_j n_m - r\delta_{jm})\right] d\theta \\
&= \frac{-u}{2\pi}\Theta_{m,l}\int_{\Gamma_\epsilon} n_l n_m \, d\theta \\
&= \frac{-u}{2\pi}\begin{bmatrix} \left|\frac{\theta}{2} - \frac{\sin 2\theta}{4}\right|_{\theta_2}^{\theta_1} & \left|\frac{\sin^2\theta}{2}\right|_{\theta_2}^{\theta_1} \\ \left|\frac{\sin^2\theta}{2}\right|_{\theta_2}^{\theta_1} & \left|\frac{\theta}{2} + \frac{\sin 2\theta}{4}\right|_{\theta_2}^{\theta_1} \end{bmatrix} : \begin{bmatrix} \Theta_{1,1} & \Theta_{1,2} \\ \Theta_{2,1} & \Theta_{2,2} \end{bmatrix} \\
\Gamma_\epsilon \quad & \textit{smooth} \Rightarrow \frac{u}{4}\left(\Theta_{1,1} + \Theta_{2,2}\right)
\end{aligned}$$

3.

$$\lim_{\epsilon\to 0} \quad \left(\int_{\Gamma_\epsilon} q u^* \delta J d\Gamma\right) = \frac{q}{2\pi}\delta J \int_{\Gamma_\epsilon} \lim_{\epsilon\to 0} r \ln\frac{1}{r} d\theta = 0$$

4.

$$\begin{aligned}
\lim_{\epsilon\to 0} \quad & \left(\int_{\Gamma_\epsilon} -u u^*_{,j} \delta m_j d\Gamma\right) \\
&= \frac{u}{2\pi}\Theta_{o,m}\int_{\Gamma_\epsilon} (n_j t_j t_l \epsilon_{lo} t_m + n_j n_j t_o t_m) d\theta \\
&= \frac{u}{2\pi}\begin{bmatrix} t_1^2 & t_1 t_2 \\ t_1 t_2 & t_2^2 \end{bmatrix} : \begin{bmatrix} \Theta_{1,1} & \Theta_{1,2} \\ \Theta_{2,1} & \Theta_{2,2} \end{bmatrix} \\
&= \frac{u}{2\pi}\begin{bmatrix} \left|\frac{\theta}{2} - \frac{\sin 2\theta}{4}\right|_{\theta_2}^{\theta_1} & \left|\frac{\sin^2\theta}{2}\right|_{\theta_2}^{\theta_1} \\ \left|\frac{\sin^2\theta}{2}\right|_{\theta_2}^{\theta_1} & \left|\frac{\theta}{2} + \frac{\sin 2\theta}{4}\right|_{\theta_2}^{\theta_1} \end{bmatrix} : \begin{bmatrix} \Theta_{1,1} & \Theta_{1,2} \\ \Theta_{2,1} & \Theta_{2,2} \end{bmatrix} \\
\Gamma_\epsilon \quad & \textit{smooth} \Rightarrow \frac{-u}{4}\left(\Theta_{1,1} + \Theta_{2,2}\right)
\end{aligned}$$

5.

$$\lim_{\epsilon\to 0} \quad \left(\int_{\Gamma_\epsilon} u^* \delta q d\Gamma\right) = \frac{1}{2\pi}\delta q \int_{\Gamma_\epsilon} \lim_{\epsilon\to 0} r \ln\frac{1}{r} d\theta = 0$$

6.

$$\lim_{\epsilon\to 0} \quad \left(\int_{\Gamma_\epsilon} -q^*\delta u d\Gamma\right)$$
$$= \frac{-1}{2\pi}\delta u \int_{\Gamma_\epsilon} n_j n_j d\theta = \frac{-1}{2\pi}\delta u(\theta_1 - \theta_2)$$
$$\Gamma_\epsilon \quad smooth \Rightarrow \frac{1}{2}\delta u$$

Dynamics

1.

$$\lim_{\epsilon\to 0} \quad \left(\int_{\Gamma_\epsilon} q u^*_{,m}\delta r_m d\Gamma\right)$$
$$= \frac{-i\omega q}{2\pi\mu c_2}\Theta_{m,l}\lim_{\epsilon\to 0}\int_{\Gamma_\epsilon} n_l n_m r^2 K_1\left(\frac{i\omega r}{c_2}\right)d\theta = 0$$

2.

$$\lim_{\epsilon\to 0} \quad \left(\int_{\Gamma_\epsilon} -u u^*_{,jm} n_j \delta r_m d\Gamma\right)$$
$$= \frac{i\omega u}{2\pi\mu c_2}\Theta_{m,l}\int_{\Gamma_\epsilon}\lim_{\epsilon\to 0}\left[n_j n_l \delta_{jm} K_1\left(\frac{i\omega r}{c_2}\right) r^2\right] d\theta$$
$$-\frac{\omega^2 u}{4\pi\mu c_2^2}\int_{\Gamma_\epsilon}\lim_{\epsilon\to 0} n_j n_l n_j n_m \left[K_0\left(\frac{i\omega r}{c_2}\right) + K_2\left(\frac{i\omega r}{c_2}\right)\right] r^2 s\theta$$
$$= \frac{u}{2\pi}\begin{bmatrix} \left|\frac{\theta}{2} - \frac{\sin 2\theta}{4}\right|_{\theta_2}^{\theta_1} & \left|\frac{\sin^2\theta}{2}\right|_{\theta_2}^{\theta_1} \\ \left|\frac{\sin^2\theta}{2}\right|_{\theta_2}^{\theta_1} & \left|\frac{\theta}{2} + \frac{\sin 2\theta}{4}\right|_{\theta_2}^{\theta_1} \end{bmatrix} : \begin{bmatrix} \Theta_{1,1} & \Theta_{1,2} \\ \Theta_{2,1} & \Theta_{2,2} \end{bmatrix}$$
$$\Gamma_\epsilon \quad smooth \Rightarrow \frac{-u}{4}\left(\Theta_{1,1} + \Theta_{2,2}\right)$$

3.

$$\lim_{\epsilon\to 0} \quad \left(\int_{\Gamma_\epsilon} q u^* \delta J d\Gamma\right)$$
$$= \frac{q}{2\pi\mu}\delta J \int_{\Gamma_\epsilon}\lim_{\epsilon\to 0} r\ln\frac{1}{r}d\theta = 0$$

4.

$$\lim_{\epsilon\to 0} \quad \left(\int_{\Gamma_\epsilon} -u u^*_{,j}\delta m_j d\Gamma\right)$$
$$= \frac{i\omega u}{2\pi\mu c_2}\Theta_{l,m}\int_{\Gamma_\epsilon}\left(n_j t_j t_l \epsilon_{lo} t_m + n_j n_j t_o t_m\right)\lim_{\epsilon\to 0} r K_1\left(\frac{i\omega r}{c_2}\right)d\theta$$
$$= \frac{u}{2\pi}\begin{bmatrix} t_1^2 & t_1 t_2 \\ t_1 t_2 & t_2^2 \end{bmatrix} : \begin{bmatrix} \Theta_{1,1} & \Theta_{1,2} \\ \Theta_{2,1} & \Theta_{2,2} \end{bmatrix}$$
$$= \frac{u}{2\pi}\begin{bmatrix} \left|\frac{\theta}{2} - \frac{\sin 2\theta}{4}\right|_{\theta_2}^{\theta_1} & \left|\frac{\sin^2\theta}{2}\right|_{\theta_2}^{\theta_1} \\ \left|\frac{\sin^2\theta}{2}\right|_{\theta_2}^{\theta_1} & \left|\frac{\theta}{2} + \frac{\sin 2\theta}{4}\right|_{\theta_2}^{\theta_1} \end{bmatrix} : \begin{bmatrix} \Theta_{1,1} & \Theta_{1,2} \\ \Theta_{2,1} & \Theta_{2,2} \end{bmatrix}$$
$$\Gamma_\epsilon \quad smooth \Rightarrow \frac{-u}{4}\left(\Theta_{1,1} + \Theta_{2,2}\right)$$

5.

$$\lim_{\epsilon \to 0} \quad \left(\int_{\Gamma_\epsilon} u^* \delta q d\Gamma \right)$$
$$= \frac{1}{2\pi\mu} \delta q \int_{\Gamma_\epsilon} \lim_{\epsilon \to 0} r K_0 \left(\frac{i\omega r}{c_2} \right) d\theta = 0$$

6.

$$\lim_{\epsilon \to 0} \quad \left(\int_{\Gamma_\epsilon} -q^* \delta u d\Gamma \right)$$
$$= \frac{-i\omega}{2\pi c_2} \delta u \int_{\Gamma_\epsilon} n_j n_j \lim_{\epsilon \to 0} r K_0 \left(\frac{i\omega r}{c_2} \right) d\theta = \frac{-1}{2\pi} \delta u (\theta_1 - \theta_2)$$
$$\Gamma_\epsilon \quad smooth \Rightarrow \frac{1}{2} \delta u$$

A.2 Expressions for the variation boundary integral equation for the 2D elastostatic problem

The expressions defined earlier using the programmable algebra, for the case of the static and steady-state singular and hypersingular boundary integral equations can still be written in a readable and reasonably compact form for the case of the static singular δBIE.

A.2.1 Definition of the gradient of the fundamental Kelvin solution

Kelvin solution

The Kelvin solutions are the displacement and the stress due to a concentrated load applied at the pole towards the direction of the canonical vector e_k,

$$b_k = \delta^{pole}_{Dirac} e_k$$

The solution of this problem in 2D elastostatics is:

$$u^i_k = \frac{1}{8\pi\mu(1-\nu)}\left[(3-4\nu)\log\frac{1}{r}\delta_{ik} + r_{,i}r_{,k}\right]$$

$$\sigma^i_{jk} = \frac{-1}{4\pi(1-\nu)r}\left[(1-2\nu)\left\{\delta_{ik}r_{,j} + \delta_{jk}r_{,i} - \delta_{ij}r_{,k}\right\} + 2r_{,i}r_{,j}r_{,k}\right]$$

$$q^i_k = \sigma^i_{jk}n_j = \frac{-1}{4\pi(1-\nu)r}\left[(1-2\nu)\left\{\delta_{ik}r_{,n} + n_k r_{,i} - n_i r_{,k}\right\} + 2r_{,i}r_{,k}r_{,n}\right]$$

Gradient

The derivative of the latter with respect to y_l or r_l are:

$$\frac{\partial u^i_k}{\partial r_l} = \frac{1}{8\pi\mu(1-\nu)r}\left[-(3-4\nu)\delta_{ik}r_{,l} + \delta_{il}r_{,k} + \delta_{kl}r_{,i} - 2r_{,i}r_{,l}r_{,k}\right]$$

$$\begin{aligned}\frac{\partial \sigma^i_{jk}}{\partial r_l} = \frac{-1}{4\pi(1-\nu)r^2}\big[&(1-2\nu)\left\{\delta_{ik}\delta_{jl} + \delta_{il}\delta_{jk} - \delta_{kl}\delta_{ij}\right.\\ &\left.-2\delta_{ik}r_{,j}r_{,l} - 2\delta_{jk}r_{,i}r_{,l} + 2\delta_{ij}r_{,k}r_{,l}\right\}\\ &+2\delta_{il}r_{,j}r_{,k} + 2\delta_{jl}r_{,i}r_{,k} + 2\delta_{kl}r_{,i}r_{,j} - 8r_{,i}r_{,j}r_{,k}r_{,l}\big]\end{aligned}$$

hence,

$$\begin{aligned}\frac{\partial \sigma^i_{jk}}{\partial r_l}n_j = \frac{-1}{4\pi(1-\nu)r^2}\big[&(1-2\nu)\left\{\delta_{ik}n_l + \delta_{il}n_k - \delta_{kl}n_i\right.\\ &\left.-2\delta_{ik}r_{,l}r_{,n} - 2r_{,i}r_{,l}n_k + 2r_{,k}r_{,l}n_i\right\}\\ &+2\delta_{il}r_{,k}r_{,n} + 2r_{,i}r_{,k}n_l + 2\delta_{kl}r_{,i}r_{,n} - 8r_{,i}r_{,k}r_{,l}r_{,n}\big]\end{aligned}$$

where,

$$\begin{aligned} r_{,n} &= \frac{\partial r}{\partial n}\\ r_{,i} &= \frac{\partial r}{\partial r_i} = \frac{r_i}{r}\\ r_{,ij} &= \frac{\partial r_{,i}}{\partial r_j} = \frac{1}{r}\left(\delta_{ij} - r_{,i}r_{,j}\right)\end{aligned}$$

A.2.2 Limit of the integrals

We are going to evaluate the limits $\lim_{\epsilon\to 0}\left(\int_{\Gamma_\epsilon} f d\Gamma\right)$ of every integral, where Γ_ϵ is a semicircle in the case of the 2D problem.

1.

$$\begin{aligned}\lim_{\epsilon\to 0} \quad & \left(\int_{\Gamma_\epsilon} q_i u^i_{k,l}\delta r_l d\Gamma\right)\\ & = \frac{q_i}{8\pi\mu(1-\nu)}\Theta_{l,m}\lim_{\epsilon\to 0}\int_{\Gamma_\epsilon} n_m r\left[-(3-4\nu)\delta_{ik}r_{,l}\right.\\ & \left.+\delta_{il}r_{,k}+\delta_{kl}r_{,i}-2r_{,i}r_{,l}r_{,k}\right]d\theta = 0\end{aligned}$$

2.

$$\begin{aligned}\lim_{\epsilon\to 0} \quad & \left(\int_{\Gamma_\epsilon} -u_i\sigma^i_{jk,l}n_j\delta r_l d\Gamma\right)\\ & = \frac{u_i}{4\pi(1-\nu)}\Theta_{l,m}\int_{\Gamma_\epsilon}\left[(1-2\nu)\left\{\delta_{ik}n_l+\delta_{il}n_k-\delta_{kl}n_i\right.\right.\\ & \left.-2\delta_{ik}n_l-2n_kn_in_l+2n_in_kn_l\right\}\\ & \left.+2\delta_{il}n_k+2n_ln_in_k+2\delta_{kl}n_i-8n_in_kn_l\right]n_m d\theta\\ & = \frac{u_i}{4\pi(1-\nu)}\Theta_{l,m}\int_{\Gamma_\epsilon}\left[(1-2\nu)\left\{-\delta_{ik}n_l+\delta_{il}n_k-\delta_{kl}n_i\right\}\right.\\ & \left.+2\delta_{il}n_k+2\delta_{kl}n_i-6n_in_kn_l\right]n_m d\theta\\ & = \frac{u_i}{4\pi(1-\nu)}\Theta_{l,m}t^1_{iklm}\\ \Gamma_\epsilon \quad & smooth \Rightarrow \frac{u_i}{16(1-\nu)}\Theta_{l,m}t'^1_{iklm}\end{aligned}$$

3.

$$\begin{aligned}\lim_{\epsilon\to 0} \quad & \left(\int_{\Gamma_\epsilon} q_i u^i_k\delta J d\Gamma\right)\\ & = \frac{q_i}{8\pi\mu(1-\nu)}\delta J\int_{\Gamma_\epsilon}\lim_{\epsilon\to 0}\left[(3-4\nu)r\log\frac{1}{r}\delta_{ik}+rn_in_k\right]d\theta = 0\end{aligned}$$

4.

$$\begin{aligned}\lim_{\epsilon\to 0} \quad & \left(\int_{\Gamma_\epsilon} -u_i\sigma^i_{jk}\delta m_j d\Gamma\right)\\ & = \frac{u_i}{4\pi(1-\nu)}\Theta_{l,m}\int_{\Gamma_\epsilon}\left[(1-2\nu)\left\{\delta_{ik}n_j+\delta_{jk}n_i-\delta_{ij}n_k\right\}\right.\\ & \left.+2n_in_jn_k\right](t_jt_o\epsilon_{ol}t_m+n_jt_lt_m)d\theta\\ & = \frac{u_i}{4\pi(1-\nu)}\Theta_{l,m}t^2_{iklm}\\ \Gamma_\epsilon \quad & smooth \Rightarrow \frac{u_i}{16(1-\nu)}\Theta_{l,m}t'^2_{iklm}\end{aligned}$$

5.

$$\begin{aligned}\lim_{\epsilon\to 0} \quad & \left(\int_{\Gamma_\epsilon} u^i_k\delta q_i d\Gamma\right)\\ & = \frac{1}{8\pi\mu(1-\nu)}\delta\sigma_{ij}\int_{\Gamma_\epsilon}\lim_{\epsilon\to 0}\left[(3-4\nu)r\log\frac{1}{r}\delta_{ik}n_j+rn_in_kn_j\right]d\theta = 0\end{aligned}$$

6.

$$\lim_{\epsilon\to 0} \quad \left(\int_{\Gamma_\epsilon} -p_k^i \delta u_i d\Gamma\right)$$

$$= \frac{-1}{4\pi(1-\nu)}\delta u_i \int_{\Gamma_\epsilon} \lim_{\epsilon\to 0}\left[(1-2\nu)\left\{\delta_{ik}+n_k n_i - n_i n_k\right\} + 2n_i n_k\right] d\theta$$

$$= \frac{-1}{4\pi(1-\nu)} \begin{bmatrix} \delta u_1 \\ \delta u_2 \end{bmatrix} \begin{bmatrix} \int_{\Gamma_\epsilon}(1-2\nu)+2n_1n_1 d\theta & \int_{\Gamma_\epsilon} 2n_1n_2 d\theta \\ \int_{\Gamma_\epsilon} 2n_2n_1 d\theta & \int_{\Gamma_\epsilon}(1-2\nu)+2n_2n_2 d\theta \end{bmatrix}$$

$$= \frac{-1}{4\pi(1-\nu)} \begin{bmatrix} \delta u_1 \\ \delta u_2 \end{bmatrix} \left| \begin{bmatrix} (2-2\nu)\theta + \frac{\sin 2\theta}{2} & \sin^2\theta \\ \sin^2\theta & (2-2\nu)\theta - \frac{\sin 2\theta}{2} \end{bmatrix} \right|_{\theta_2}^{\theta_1}$$

$$\Gamma_\epsilon \qquad smooth \Rightarrow \frac{1}{2}\delta u_k$$

where,

i	k	l	m	t^1_{iklm}	t'^1_{iklm}	t^2_{iklm}	t'^2_{iklm}
1	1	1	1	$(+3+2\nu)cc-6cccc$	$-3+4\nu$	$(+1-2\nu)ss-2ccss$	$+3-4\nu$
2	1	1	1	$(-1-2\nu)sc+6cccs$	0	$(+1-2\nu)sc+2csss$	0
1	2	1	1	$(-3+2\nu)sc+6cccs$	0	$(-1+2\nu)sc+2csss$	0
2	2	1	1	$(-1+2\nu)cc-6ccss$	$-5+4\nu$	$(+1-2\nu)ss-2ssss$	$+5-4\nu$
1	1	2	1	$(+1-2\nu)sc+6cccs$	0	$(+1-2\nu)sc+2cccs$	0
2	1	2	1	$(+3-2\nu)cc-6ccss$	$+3-4\nu$	$(-1+2\nu)ss-2ccss$	$-3+4\nu$
1	2	2	1	$(+1+2\nu)cc-6ccss$	$-1+4\nu$	$(+1-2\nu)ss-2ccss$	$+1-4\nu$
2	2	2	1	$(-3-2\nu)sc+6csss$	0	$(+1-2\nu)sc+2csss$	0
1	1	1	2	$(-3-2\nu)sc+6cccs$	0	$(+1-2\nu)sc+2cccs$	0
2	1	1	2	$(+1+2\nu)cc-6ccss$	$-1+4\nu$	$(+1-2\nu)cc-2ccss$	$+1-4\nu$
1	2	1	2	$(+3-2\nu)cc-6ccss$	$+3-4\nu$	$(-1+2\nu)cc-2ccss$	$-3+4\nu$
2	2	1	2	$(+1-2\nu)sc+6csss$	0	$(+1-2\nu)sc+2csss$	0
1	1	2	2	$(-1+2\nu)cc-6ccss$	$-5+4\nu$	$(+1-2\nu)cc-2cccc$	$+5-4\nu$
2	1	2	2	$(-3+2\nu)sc+6csss$	0	$(-1+2\nu)sc+2cccs$	0
1	2	2	2	$(-1-2\nu)sc+6csss$	0	$(+1-2\nu)sc+2cccs$	0
2	2	2	2	$(+3+2\nu)cc-6ssss$	$-3+4\nu$	$(+1-2\nu)cc-2ccss$	$+3-4\nu$

$$ss = \int_{\theta_2}^{\theta_1} \sin\theta\sin\theta d\theta = \left|\frac{\theta}{2} - \frac{\sin 2\theta}{4}\right|_{\theta_2}^{\theta_1}$$

$$cc = \int_{\theta_2}^{\theta_1} \cos\theta\cos\theta d\theta = \left|\frac{\theta}{2} + \frac{\sin 2\theta}{4}\right|_{\theta_2}^{\theta_1}$$

$$sc = \int_{\theta_2}^{\theta_1} \sin\theta\cos\theta d\theta = \left|\frac{\sin^2\theta}{2}\right|_{\theta_2}^{\theta_1}$$

$$ssss = \int_{\theta_2}^{\theta_1} \sin\theta\sin\theta\sin\theta\sin\theta d\theta = \left|\frac{3\theta}{8} - \frac{3\sin\theta\cos\theta}{8} - \frac{\sin^3\theta\cos\theta}{4}\right|_{\theta_2}^{\theta_1}$$

$$sssc = \int_{\theta_2}^{\theta_1} \sin\theta\sin\theta\sin\theta\cos\theta d\theta = \left|\frac{\sin^4\theta}{4}\right|_{\theta_2}^{\theta_1}$$

$$sscc = \int_{\theta_2}^{\theta_1} \sin\theta\sin\theta\cos\theta\cos\theta d\theta = \left|\frac{\theta}{8} + \frac{\sin\theta\cos\theta}{8} - \frac{\sin\theta\cos^3\theta}{4}\right|_{\theta_2}^{\theta_1}$$

$$sccc = \int_{\theta_2}^{\theta_1} \sin\theta\cos\theta\cos\theta\cos\theta d\theta = \left|-\frac{\cos^4\theta}{4}\right|_{\theta_2}^{\theta_1}$$

$$cccc = \int_{\theta_2}^{\theta_1} \cos\theta\cos\theta\cos\theta\cos\theta d\theta = \left|\frac{3\theta}{8} + \frac{3\sin\theta\cos\theta}{8} + \frac{\sin\theta\cos^3\theta}{4}\right|_{\theta_2}^{\theta_1}$$

δubie for nonsmooth boundary

In th case of a cornered boundary at the collocation point, the *δubie* has two somewhat more complicated terms.

ubie:

$$u_k(\boldsymbol{\xi})U1_k^i + \oint_\Gamma \left[q_k^i u_k(\mathbf{x}) - u_k^i q_k(\mathbf{x})\right] d\Gamma(\mathbf{x}) = 0 \tag{A.5}$$

δubie:

$$\begin{aligned} &\delta u_k(\boldsymbol{\xi})DU1_k^i + u_k(\boldsymbol{\xi})\delta x_{l,j}(\mathbf{x},\boldsymbol{\xi})DU2_{jkl}^i \\ &+ \oint_\Gamma \left[\sigma_{jk}^i(\mathbf{x},\boldsymbol{\xi})n_j(\mathbf{x})\delta u_k(\mathbf{x}) - u_k^i(\mathbf{x},\boldsymbol{\xi})\delta q_k(\mathbf{x})\right] d\Gamma(\mathbf{x}) \\ &+ \oint_\Gamma \big[(\sigma_{jk,m}^i(\mathbf{x},\boldsymbol{\xi})n_j(\mathbf{x})u_k(\mathbf{x}) - u_{k,m}^i(\mathbf{x},\boldsymbol{\xi})q_k)\delta r_m(\mathbf{x},\boldsymbol{\xi}) \\ &\quad + (\sigma_{jk}^i(\mathbf{x},\boldsymbol{\xi})n_j(\mathbf{x})u_k(\mathbf{x}) - u_k^i(\mathbf{x},\boldsymbol{\xi})q_k)\delta J(\mathbf{x}) \\ &\quad + \sigma_{jk}^i(\mathbf{x},\boldsymbol{\xi})u_k(\mathbf{x})\delta n_j(\mathbf{x})\big] d\Gamma(\mathbf{x}) \quad = \quad 0 \end{aligned} \tag{A.6}$$

where,

Free term number 1 in *ubie* and *δuie*: $u_k U1_k^i$ and $\delta u_k DU1_k^i$ $\quad DU1_k^i = U1_k^i =$

$$\begin{pmatrix} 1 - \frac{4(1-\nu)(\pi+\theta_2-\theta_1)+\sin 2\theta_1 - \sin 2\theta_2}{8\pi(1-\nu)} & -\frac{\cos 2\theta_2 - \cos 2\theta_1}{8\pi(1-\nu)} \\ -\frac{\cos 2\theta_2 - \cos 2\theta_1}{8\pi(1-\nu)} & 1 - \frac{4(1-\nu)(\pi+\theta_2-\theta_1)+\sin 2\theta_2 - \sin 2\theta_1}{8\pi(1-\nu)} \end{pmatrix}$$

Free term number 2 in δuie: $u_k\theta_{l,j}DU2^i_{jkl}$ $\quad DU2^i_{jkl} =$

$$\{\frac{1}{32\pi(-1+\nu)}(2(-5+6\nu)\sin[2\theta_1]+(-3+2\nu)\sin[4\theta_1]-$$
$$2(-5+6\nu+(-3+2\nu)\cos[2\theta_2])\sin[2\theta_2]),$$
$$-\frac{(-3+2\nu)(\cos[4\theta_1]-\cos[4\theta_2])}{32\pi(-1+\nu)},$$
$$-\frac{(-3+2\nu)(\cos[4\theta_1]-\cos[4\theta_2])}{32\pi(-1+\nu)},$$
$$\frac{1}{32\pi(-1+\nu)}(2(-5+6\nu)\sin[2\theta_1]+(3-2\nu)\sin[4\theta_1]+$$
$$2(5-6\nu+(-3+2\nu)\cos[2\theta_2])\sin[2\theta_2]),$$
$$-\frac{1}{16\pi(-1+\nu)}((\cos[2\theta_1]-\cos[2\theta_2])$$
$$(8(-1+\nu)+(-3+2\nu)\cos[2\theta_1]+(-3+2\nu)\cos[2\theta_2])),$$
$$-\frac{(-3+2\nu)(2\sin[2\theta_1]+\sin[4\theta_1]-8\cos[\theta_2]^3\sin[\theta_2])}{32\pi(-1+\nu)},$$
$$-\frac{(-3+2\nu)(2\sin[2\theta_1]+\sin[4\theta_1]-8\cos[\theta_2]^3\sin[\theta_2])}{32\pi(-1+\nu)},$$
$$\frac{1}{16\pi(-1+\nu)}((\cos[2\theta_1]-\cos[2\theta_2])$$
$$(2-4\nu+(-3+2\nu)\cos[2\theta_1]+(-3+2\nu)\cos[2\theta_2])),$$
$$-\frac{1}{16\pi(-1+\nu)}((\cos[2\theta_1]-\cos[2\theta_2])$$
$$(-2+4\nu+(-3+2\nu)\cos[2\theta_1]+(-3+2\nu)\cos[2\theta_2])),$$
$$\frac{(-3+2\nu)(2\sin[2\theta_1]-\sin[4\theta_1]-8\cos[\theta_2]\sin[\theta_2]^3)}{32\pi(-1+\nu)},$$
$$\frac{(-3+2\nu)(2\sin[2\theta_1]-\sin[4\theta_1]-8\cos[\theta_2]\sin[\theta_2]^3)}{32\pi(-1+\nu)},$$
$$\frac{1}{16\pi(-1+\nu)}((\cos[2\theta_1]-\cos[2\theta_2])$$
$$(-8(-1+\nu)+(-3+2\nu)\cos[2\theta_1]+(-3+2\nu)\cos[2\theta_2])),$$
$$\frac{1}{32\pi(-1+\nu)}(-2(-5+6\nu)\sin[2\theta_1]+(3-2\nu)\sin[4\theta_1]+$$
$$2(-5+6\nu+(-3+2\nu)\cos[2\theta_2])\sin[2\theta_2]),$$
$$\frac{(-3+2\nu)(\cos[4\theta_1]-\cos[4\theta_2])}{32\pi(-1+\nu)},$$
$$\frac{(-3+2\nu)(\cos[4\theta_1]-\cos[4\theta_2])}{32\pi(-1+\nu)},$$
$$\frac{1}{32\pi(-1+\nu)}(-2(-5+6\nu)\sin[2\theta_1]+(-3+2\nu)\sin[4\theta_1]-$$
$$2(5-6\nu+(-3+2\nu)\cos[2\theta_2])\sin[2\theta_2])\}$$

A.3 Kernels for material properties sensitivity

The definition in terms of the Kelvin functions of all the kernels involved in both variation equations are:

$$\begin{aligned}
d^i_{jk}(x,\xi) &= \lambda\delta_{ij}u^o_{k,o}(x,\xi) + \mu(u^i_{k,j}(x,\xi) + u^j_{k,i}(x,\xi)) \\
t^i_{jkl}(x,\xi) &= \lambda\delta_{ij}\sigma^o_{kl,o}(x,\xi) + \mu(\sigma^i_{kl,j}(x,\xi) + \sigma^j_{kl,i}(x,\xi)) \\
\frac{dd^i_{jk}(x,\xi)}{dm} &= \frac{d\lambda}{dm}\delta_{ij}u^o_{k,o}(x,\xi) + \frac{d\mu}{dm}(u^i_{k,j}(x,\xi) + u^j_{k,i}(x,\xi)) + \\
&\quad \lambda\delta_{ij}\frac{du^o_{k,o}(x,\xi)}{dm} + \mu(\frac{du^i_{k,j}(x,\xi)}{dm} + \frac{du^j_{k,i}(x,\xi)}{dm}) \\
\frac{dt^i_{jkl}(x,\xi)}{dm} &= \frac{d\lambda}{dm}\delta_{ij}\sigma^o_{kl,o}(x,\xi) + \frac{d\mu}{dm}(\sigma^i_{kl,j}(x,\xi) + \sigma^j_{kl,i}(x,\xi)) + \\
&\quad \lambda\delta_{ij}\frac{d\sigma^o_{kl,o}(x,\xi)}{dm} + \mu(\frac{d\sigma^i_{kl,j}(x,\xi)}{dm} + \frac{d\sigma^j_{kl,i}(x,\xi)}{dm})
\end{aligned}$$

where

$$\begin{aligned}
\sigma^i_{jk}(x,\xi) &= \lambda\delta_{jk}u^i_{o,o}(x,\xi) + \mu(u^i_{j,k}(x,\xi) + u^i_{k,j}(x,\xi)) \\
\sigma^i_{jk,l}(x,\xi) &= \lambda\delta_{jk}u^i_{o,ol}(x,\xi) + \mu(u^i_{j,kl}(x,\xi) + u^i_{k,jl}(x,\xi)) \\
\frac{d\sigma^i_{jk}(x,\xi)}{dm} &= \frac{d\lambda}{dm}\delta_{jk}u^i_{o,o}(x,\xi) + \frac{d\mu}{dm}(u^i_{j,k}(x,\xi) + u^i_{k,j}(x,\xi)) + \\
&\quad \lambda\delta_{jk}\frac{du^i_{o,o}(x,\xi)}{dm} + \mu(\frac{du^i_{j,k}(x,\xi)}{dm} + \frac{du^i_{k,j}(x,\xi)}{dm}) \\
\frac{d\sigma^i_{jk,l}(x,\xi)}{dm} &= \frac{d\lambda}{m}\delta_{jk}u^i_{o,ol}(x,\xi) + \frac{d\mu}{dm}(u^i_{j,kl}(x,\xi) + u^i_{k,jl}(x,\xi)) + \\
&\quad \lambda\delta_{jk}\frac{du^i_{o,ol}(x,\xi)}{dm} + \mu(\frac{du^i_{j,kl}(x,\xi)}{dm} + \frac{du^i_{k,jl}(x,\xi)}{dm})
\end{aligned}$$

and,

$$\begin{aligned}
\frac{du^a_b}{dm} &= \frac{\mu}{dm}\frac{-1}{2\pi\mu^2}[\psi\delta_{ab} - \chi r_{,a}r_{,b}] + \frac{1}{2\pi\mu}\left[\frac{d\psi}{dm}\delta_{ab} - \frac{d\chi}{dm}r_{,a}r_{,b}\right] \\
\frac{du^a_{b,c}}{dm} &= \frac{\mu}{dm}\frac{1}{2\pi\mu}[\psi'\delta_{ab}r_{,c} - \chi' r_{,a}r_{,b}r_{,c} - \chi e_{aba'b'}r_{,a'}r_{,b'c}] \\
&\quad + \frac{-1}{2\pi\mu^2}\left[\frac{d\psi'}{dm}\delta_{ab}r_{,c} - \frac{d\chi'}{dm}r_{,a}r_{,b}r_{,c} - \frac{d\chi}{dm}e_{aba'b'}r_{,a'}r_{,b'c}\right] \\
\frac{du^a_{b,cd}}{dm} &= \frac{\mu}{dm}\frac{-1}{2\pi\mu^2}[\psi''\delta_{ab}r_{,c}r_{,d} + \psi'\delta_{ab}r_{,cd} - \chi'' r_{,a}r_{,b}r_{,c}r_{,d} - \chi' r_{,a}r_{,b}r_{,cd} \\
&\quad - e_{aba'b'}(\chi' e_{cdc'd'}r_{,a'}r_{,c'}r_{,b'd'} + \chi r_{,a'cd}r_{,b'} + \chi r_{,a'c}r_{b'd})] \\
&\quad + \frac{1}{2\pi\mu}\left[\frac{d\psi''}{dm}\delta_{ab}r_{,c}r_{,d} + \frac{d\psi'}{dm}\delta_{ab}r_{,cd} - \frac{d\chi''}{dm}r_{,a}r_{,b}r_{,c}r_{,d} - \frac{d\chi'}{dm}r_{,a}r_{,b}r_{,cd}\right. \\
&\quad \left. - e_{aba'b'}(\frac{d\chi'}{dm}e_{cdc'd'}r_{,a'}r_{,c'}r_{,b'd'} + \frac{d\chi}{dm}r_{,a'cd}r_{,b'} + \frac{d\chi}{dm}r_{a'c}r_{b'd})\right]
\end{aligned}$$

where,

$$\frac{d\psi}{dm} = \begin{bmatrix} \frac{d\psi}{dc_s} & \frac{d\psi}{dc_p} \end{bmatrix}\begin{bmatrix} \frac{dc_s}{dm} \\ \frac{dc_p}{dm} \end{bmatrix} \qquad \frac{d\chi}{dm} = \begin{bmatrix} \frac{d\chi}{dc_s} & \frac{d\chi}{dc_p} \end{bmatrix}\begin{bmatrix} \frac{dc_s}{dm} \\ \frac{dc_p}{dm} \end{bmatrix}$$

$$\frac{d\psi'}{dm} = \begin{bmatrix} \frac{d\psi'}{dc_s} & \frac{d\psi'}{dc_p} \end{bmatrix}\begin{bmatrix} \frac{dc_s}{dm} \\ \frac{dc_p}{dm} \end{bmatrix} \qquad \frac{d\chi'}{dm} = \begin{bmatrix} \frac{d\chi'}{dc_s} & \frac{d\chi'}{dc_p} \end{bmatrix}\begin{bmatrix} \frac{dc_s}{dm} \\ \frac{dc_p}{dm} \end{bmatrix}$$

$$\frac{d\psi''}{dm} = \begin{bmatrix} \frac{d\psi''}{dc_s} & \frac{d\psi''}{dc_p} \end{bmatrix}\begin{bmatrix} \frac{dc_s}{dm} \\ \frac{dc_p}{dm} \end{bmatrix} \qquad \frac{d\chi''}{dm} = \begin{bmatrix} \frac{d\chi''}{dc_s} & \frac{d\chi''}{dc_p} \end{bmatrix}\begin{bmatrix} \frac{dc_s}{dm} \\ \frac{dc_p}{dm} \end{bmatrix}$$

If we choose as material properties vector $m = [E, \nu, \rho]$, the last derivatives become:

$$\begin{aligned}
\frac{dc_s}{dm} &= \left[\sqrt{\frac{\nu-1}{4E\rho(1-2\nu)(1+\nu)}} \quad \sqrt{\frac{E\nu^2(\nu-2)^2}{(\nu-1)(1+\nu)^3(1-2\nu)^3\rho}} \quad \sqrt{\frac{E(\nu-1)}{4\rho^3(1+\nu)(1+2\nu)}} \right] \\
\frac{dc_p}{dm} &= \left[\sqrt{\frac{1}{8E\rho(1+\nu)}} \quad \sqrt{\frac{E}{8\rho(1+\nu)^3}} \quad \sqrt{\frac{E}{8\rho^3(1+\nu)}} \right] \\
\frac{d\lambda}{dm} &= \left[\frac{\nu}{(1+\nu)(1-2\nu)} \quad \frac{E(1+2\nu^2)}{(1+\nu)^2(1-2\nu)^2} \quad 0 \right] \\
\frac{d\mu}{dm} &= \left[\frac{1}{2(1+\nu)} \quad \frac{-E}{2(1+\nu)^2} \quad 0 \right]
\end{aligned}$$

Appendix B

Regularization of integrals

When the collocation point is not placed on the integrated element, a regular Gauss quadrature formula can be utilized.

B.1 Singular points

As it uses to happen with integral equation methods, the integrals have singularities of different orders. After the limiting process the integrals are defined outside the "artificial ball" around the pole, and divided into a first one that may have a singularity, and turns to be a Cauchy Principal Value (CPV: $\int_a^b CPV = \lim_{\epsilon \to 0} \left(\int_a^{-\epsilon} + \int_\epsilon^b \right)$), and a second integral that tends to a so called free term, calculated in the appendix:

$$\int_\Gamma f d\Gamma = \lim_{\epsilon \to 0} \left(\int_{\Gamma - \Gamma_\epsilon} f d\Gamma \right) + \lim_{\epsilon \to 0} \left(\int_{\Gamma_\epsilon} f d\Gamma \right)$$

When some values at this point tend to infinite, the first term has singularities: $\log \frac{1}{x}$, $\frac{1}{x}$, $\frac{1}{x^2}$. In order to be able to compute them numerically in an efficient way, we need to use a combination of two techniques:

- Decomposing the kernel in a sum of a regular part (continuous and differentiable, and not tending to infinite), which will be integrated numerically, and a simpler singular part, to be integrated analytically ($\int = \int_{regular} + \int_{analytic}$).
- Placing the collocation points a bit separated from the ends of the elements when necessary. As proved later, this will not be needed for this formulation as long as the varying geometry is smooth.
- Integrating by special gauss quadratures:

$$\int ln\left(\frac{1}{x}\right) f(x) d\Gamma(x) = \sum_{g=gauss} \omega_g^{ln} f(\xi_g^{ln}) J$$

The four different types of integrals that arise here are computed as follows:

B.2 Regular

This arises when the kernel of the integral is bounded and Holder continuous, with finite derivative in the whole range. We use a simple gauss quadrature with a variable change:

$$\int_\Gamma f(s) ds = \int_{-1}^{1} J(\xi) f(s(\xi)) d\xi = \sum_{g=gauss} J(\xi) \omega_g f(s(\xi_g))$$

B.3 Log-Singular

This appears when the integral has the form $\int_\Gamma f(s)+g(s)log\frac{1}{r(s)}ds$, where f and g are also bounded and Holder continuous. We utilize the special gauss quadrature:

$$\int_\Gamma f(s)+g(s)log\frac{1}{r(s)}ds = \sum_{g=gauss} J(\xi)\omega_g f(s(\xi_g))$$
$$+\sum_{g=gauss} J(\xi)\omega_g g(s(\xi_g))log\left(\frac{Abs(\xi_g-nod)J(\xi)}{rJ^{ln}(\xi)}\right)$$
$$+\sum_{g=gauss}^{left} J^{ln}\omega^{ln}\frac{g(s(\xi_g^{ln}))}{log\frac{1}{r}}+\sum_{g=gauss}^{right} J^{ln}\omega^{ln}\frac{g(s(\xi_g^{ln}))}{log\frac{1}{r}}$$

where $J^{ln}(\xi)=J(\xi)(1+Abs(nod))$, and nod is the value of xi where the singularity appears.

B.4 $\frac{1}{r}$ Singular

This means that the integral has the form $\int_G amma\frac{f(s)}{r(s)}ds$, where f is again bounded and Holder continuous. Two methods are mainly used in the literature, one from Gallego [103],

$$\int_a^b \frac{f(s)}{r(s)}ds = \int_a^b \frac{f(s)-f(s_0)\frac{dr}{ds}}{r(s)}ds + f(s_0)\int_a^b \frac{dr}{ds}\frac{1}{r(s)}ds$$
$$= \int_a^b \frac{f(s)-f(s_0)\frac{r_i(s)\frac{\partial y_i(s)}{\partial \xi}}{r(s)J(s)}}{r(s)}ds + f(s_0)\left(Ln(r(b))-Ln(r(a))\right)$$

and one from Giuggiani [54]

$$\int_a^b \frac{f(s)}{r(s)}ds = \int_a^b \left(\frac{f(s)}{r(s)}-\frac{f(s_0)\frac{d\xi}{ds}}{\xi-\xi_0}\right)ds + f(s_0)\int_a^b \frac{d\xi}{ds}\frac{1}{\xi-\xi_0}ds$$
$$= \int_a^b \left(\frac{f(s)}{r(s)}-\frac{f(s_0)}{J(s)(\xi-\xi_0)}\right)ds + f(s_0)\left(Ln|\xi(b)|-Ln|\xi(a)|\right)$$

We propose a simpler variation of this technique inspired in the work by Fettis [44]. It is based in two principles:

- The Cauchy Principal Value consists of evaluating the integral excluding a symmetric and arbitrarily small boundary around the singularity. The singular kernel can be expressed in terms of its series expansion, giving: $f=\frac{a}{r}+b+cx+dx^2+....$ Using the property that the terms of order $2n-1$ are antimetric, $(r)^{2n-1}=-(-r)^{2n-1}$, we can decompose the integral in two parts and do the specular range of one of them in order to get the antimetric terms, which will vanish. Among these terms, the singular one $\frac{a}{r}$ is one of the vanishing terms:

$$\int_{-1}^{1} f(x)dx = \int_{-1}^{-\varepsilon} f(x)dx + \int_{\varepsilon}^{1} f(x)dx =$$
$$\int_{\varepsilon}^{1} f(-x)dx + \int_{\varepsilon}^{1} f(x)dx = \int_{\varepsilon}^{1} (f(x)+f(-x))dx$$

the terms involved are,

$$\int_{\varepsilon}^{1} (f(x)+f(-x))dx =$$
$$\int_{\varepsilon}^{1} ((\frac{a}{x}+b+cx+dx^2+...)+(-\frac{a}{x}+b-cx+dx^2-...))dx =$$
$$\int_{\varepsilon}^{1} (2b+2dx^2+...)dx$$

which is bounded at the singularity and may be written as,

$$\int_{\varepsilon}^{1}(2b+2dx^2+...)dx=\int_{0}^{1}(2b+2dx^2+...)dx=\int_{0}^{1}(f(x)+f(-x))dx$$

- We apply a change of variable in order to center the singularity, transforming any collocation point in natural coordinates into zero. The main property this change needs is to keep the continuity and the derivability over the range, especially at the singularity. The simplest change found is the following,

$$\xi(t)=sign(\xi_c)\left[1-(1-|\xi_c|)(1-sign(\xi_c)\xi)e^{-Ln\frac{1}{1-|\xi_c|}sign(\xi_0)t}\right]$$

The process can be schematized as follows in figure B.1 Therefore the integral is done as

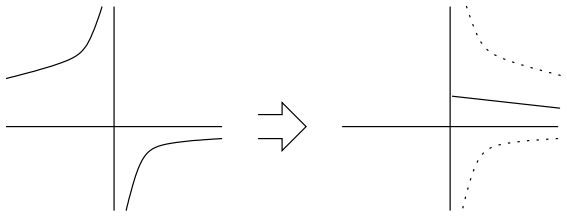

Figure B.1: Steps in the regularization of 1-singular integrals.

$$I = \int_{\Gamma}Ad\Gamma=\int_{-1}^{1}A(\xi)J(\xi)d\xi=\int_{0}^{1}F(t)-F(-t)dt$$

where,

$$A=\frac{\phi}{r}\qquad J=\frac{d\Gamma}{d\xi}\qquad J_1(t)=\frac{d\xi}{dt}$$

$$F(t)=A(\xi(t))J(\xi(t))J_1(t)$$

$$\xi(t)=sign(\xi_c)\left[1-(1-|\xi_c|)(1-sign(\xi_c)\xi)e^{-Ln\frac{1}{1-|\xi_c|}sign(\xi_0)t}\right]$$

$$J_1(t)=(1-|\xi_c|)(1+Ln\frac{1}{1-|\xi_c|}(1-sign(\xi_c)\xi))e^{-Ln\frac{1}{1-|\xi_c|}sign(\xi_0)t}$$

B.5 $\frac{1}{r^2}$-Singular

Following the method for computation of hypersingular Kernels completely defined by Guiggianni ([54] and [55]), one may use the formulas,

$$I = \lim_{\varepsilon\to 0^+}\left\{\int_{\Gamma_s-S_\varepsilon}A(y,x)d\Gamma(x)+\frac{B}{\varepsilon}\right\}$$

$$I = \sum_{m=1}^{2}\left\{\int_{-1}^{1}\left[F^m(\eta,\xi)-\left(\frac{F^m_{-2}(\eta)}{(\xi-\eta)^2}+\frac{F^m_{-1}(\eta)}{\xi-\eta}\right)\right]d\xi\right.$$
$$\left.+F^m_{-1}(\eta)\ln\left|\frac{2}{\beta_m(\eta)}\right|sgn(\xi-\eta)-F^m_{-2}(\eta)\left[sgn(\xi-\eta)\frac{\gamma_m(\eta)}{\beta_m(\eta)^2}+\frac{1}{2}\right]\right\}$$

($\eta=1$ for $m=1$, and $\eta=-1$ for $m=2$) when the singularity is placed between two elements and, in the case of a mid-node collocation point,

$$I = \int_{-1}^{1}\left[F(\eta,\xi)-\left(\frac{F_{-2}(\eta)}{(\xi-\eta)^2}+\frac{F_{-1}(\eta)}{\xi-\eta}\right)\right]d\xi$$
$$+F_{-1}(\eta)\ln\left|\frac{1-\eta}{-1-\eta}\right|-F^{-2}(\eta)\left[\frac{-1}{1-\eta}+\frac{1}{-1-\eta}\right]$$

($\eta \in (-1,1)$) where y and η are the collocation point in real and local coordinates, and x and ξ are the integration point in real and local coordinates ($-1 \leq \xi \leq 1$). The terms β_m and γ_m account for the distortion by the local coordinates transformation of the originally symmetric vicinity of the collocation point:

$$\begin{aligned} F(\eta,\xi) &= A(y(\eta),x(\xi))J^m(\xi) = \frac{F_{-2}(\eta)}{(\xi-\eta)^2} + \frac{F_{-1}(\eta)}{\xi-\eta} + O(1) \\ \beta_m &= \frac{1}{J^m(\eta)} = \frac{1}{\sqrt{\left(\frac{\partial x_1}{\partial \xi}\right)^2 + \left(\frac{\partial x_2}{\partial \xi}\right)^2}} \\ \gamma_m &= -\frac{\frac{\partial x_1}{\partial \xi}\frac{\partial^2 x_1}{\partial \xi^2} + \frac{\partial x_2}{\partial \xi}\frac{\partial^2 x_2}{\partial \xi^2}}{2J^m(\eta)^4} = -\frac{\frac{\partial x_1}{\partial \xi}\frac{\partial^2 x_1}{\partial \xi^2} + \frac{\partial x_2}{\partial \xi}\frac{\partial^2 x_2}{\partial \xi^2}}{2\left\{\left(\frac{\partial x_1}{\partial \xi}\right)^2 + \left(\frac{\partial x_2}{\partial \xi}\right)^2\right\}^2} \end{aligned}$$

An alternative method was later proposed by Saez and Gallego [103], and reads in the case of a collocation point inside the element,

$$\begin{aligned} I &= \int_\Gamma \frac{1}{r^2}\left|\frac{dr(x)}{d\Gamma}\right|\left[\phi(x) - \phi(x_c) - r\frac{d\phi(x_c)}{dr}\right]d\Gamma \\ &\quad -\phi(x_c)\left[\frac{1}{R_1} + \frac{1}{R_2}\right] + \frac{d\phi(x_c)}{\xi}\frac{1}{J(x_c)}\ln\left[\frac{R_2}{R_1}\right] \end{aligned}$$

where,

$$\begin{aligned} A(x,y) &= \frac{1}{r^2}\phi(x) \\ \phi(x) &= \phi(x_c) + r\frac{d\phi(x_c)}{dr} + O(r^2) \\ \frac{d\phi(x_c)}{dr} &= \frac{d\phi(x_c)}{\xi}\frac{1}{J(x_c)}sgn\left(\frac{dr(x_c)}{d\Gamma}\right) \end{aligned}$$

We propose and use a development from the idea of Fettis [44] that yields the following formula, whose main advantage is that it does not require the calculation of a further derivative of the kernel. The main advantages of the change of variable is that it annihilates the free terms by its symmetry, and moreover it simplifies the integrals to only a regular one without need for a second assymetric one, as done in [44].

The integral is eventually implemented as,

$$\begin{aligned} I &= \int_\Gamma A d\Gamma = \int_{-1}^{1} A(\xi)J(\xi)d\xi \\ &= \int_0^1 \frac{F(t)-F(-t)}{t}dt - \phi(x_c)\left[\frac{1}{r(1)} + \frac{1}{r(-1)}\right] \end{aligned}$$

where,

$$A = \frac{\phi}{r^2} \qquad J = \frac{d\Gamma}{d\xi} \qquad J_1(t) = \frac{d\xi}{dt}$$

$$F(t) = \left(\frac{G(\xi(t)) - G_0(\xi(t))\left|\frac{dr(\xi(t))}{d\Gamma}\right|}{t}\right)J(\xi(t))J_1(t)$$

$$G(\xi(t)) = A(\xi(t))t^2 \qquad G_0(\xi(t)) = \phi(\xi_c)\frac{t^2}{r^2(\xi(t))}$$

$$\xi(t) = sign(\xi_c)\left[1 - (1-|\xi_c|)(1-sign(\xi_c)\xi)e^{-Ln\frac{1}{1-|\xi_c|}sign(\xi_0)t}\right]$$

$$J_1(t) = (1-|\xi_c|)(1+Ln\frac{1}{1-|\xi_c|}(1-sign(\xi_c)\xi))e^{-Ln\frac{1}{1-|\xi_c|}sign(\xi_0)t}$$

$$\left|\frac{dr}{d\Gamma}\right| = \left|\frac{r_1t_1 + r_2t_2}{r}\right|$$

The *sign* should always be nonzero for any argument.

This formula can be derived in the following way. The basic steps if the regularization itself are shown in figure B.2. The Hadamard finite part is defined as an integral in which some infinite

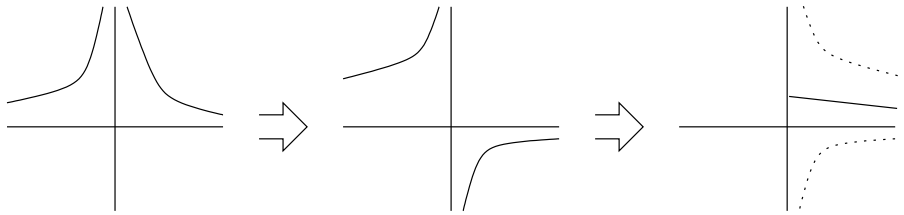

Figure B.2: Steps for regularization of 2-singular integrals.

term is elliminated,

$$\begin{aligned} I &= \int_\Gamma^{FP} A d\Gamma = \int_\Gamma^{FP} \frac{\phi(s)}{r^2(s)} d\Gamma(s) \\ &= \lim_{\varepsilon \to 0} \left[\int_{s_i}^{s_c - \varepsilon} \frac{\phi(s)}{r^2(s)} d\Gamma(s) + \int_{s_c+\varepsilon}^{s_f} \frac{\phi(s)}{r^2(s)} d\Gamma(s) - \phi(s_c) \left(\frac{1}{r(-\varepsilon)} + \frac{1}{r(\varepsilon)} \right) \right] \end{aligned}$$

If we develop the kernel with a simplified notation,

$$\begin{aligned} I &= \int_\Gamma^{FP} A d\Gamma = \int_\Gamma^{FP} \frac{\frac{\phi t^2}{r^2}}{t^2} d\Gamma \\ &= \int_\Gamma^{CPV} \frac{\frac{\phi t^2}{r^2} - \frac{\phi_c t^2}{r^2} \left| \frac{dr}{d\Gamma} \right|}{t^2} d\Gamma + \int_\Gamma^{FP} \frac{\phi_c}{r^2} \left| \frac{dr}{d\Gamma} \right| d\Gamma \end{aligned}$$

Here, $G = \frac{\phi t^2}{r^2}$, doing the symmetric change of variable, doing the same considerations as for the $\frac{1}{r}$ integrals, and defining $F = \frac{\frac{\phi t^2}{r^2} - \frac{\phi_c t^2}{r^2} \left| \frac{dr}{d\Gamma} \right|}{t}$,

$$\begin{aligned} I &= \int_{-1}^{1,CPV} \frac{\frac{\phi t^2}{r^2} - \frac{\phi_c t^2}{r^2} \left| \frac{dr}{d\Gamma} \right|}{t^2} J J_1 dt \\ &\quad + \lim_{\varepsilon \to 0} \phi_c \left[\frac{1}{r(-\varepsilon)^2} - \frac{1}{r(-1)^2} - \frac{1}{r(1)^2} + \frac{1}{r(\varepsilon)^2} \right] \\ &\quad - \lim_{\varepsilon \to 0} \phi_c \left[\frac{1}{r(-\varepsilon)^2} + \frac{1}{r(\varepsilon)^2} \right]^{\text{by FP definition}} \\ &= \int_0^1 \frac{F(t) - F(-t)}{t} dt - \phi_c \left[\frac{1}{r(-1)^2} + \frac{1}{r(1)^2} \right] \end{aligned}$$

Some considerations are useful:

- G is bounded and Holder continuous.
- F is bounded and Holder continuous.
- The kernel of the integral $\frac{F(t)-F(-t)}{t}$ is bounded and Holder continuous, and the range of the integral may be modified from $t(\varepsilon) \to 1$ to $0 \to 1$.

More references about the basics on integration (Krommer [73], Lutz [78]), computation of bessel functions (Abramowitz [53], Gradshteyn [2]) and regularization can be found, in order of appearance, in Jun [65], Telles [128], Fettis [44], Guiggianni et al. [57] [58], Ridolphi [98], Sladek et al. [104], Huang [62], Dumont [37] and Tanaka [126].

Appendix C

Programmable algebra

The main problem of the methods for the gradient computation by analytical procedures and the arguments to avoid them is precisely the high complications of the expression involved in the integrals. Amidst the intention of systematizing this procedure, a way to obtain the values of these expressions in a practical way is here presented.

The expressions obtained so far involve a high number of indices. Since they have to be substituted into each other at several levels the resulting expanded expressions would have too many terms to provide a reasonably long code and a low likelihood of bugs.

To our knowledge, there are not any commercial programs that are capable to combine the manipulation of indices with a capacity of handling many such equations at an affordable speed. Moreover, since the equations should be able to be programmed in many existent languages in which the BEM is actually working, it becomes necessary to come up with some handy transformation of these expressions.

In the code for the sensitivity of dynamics singular and hypersingular BIEs, the value of every term in the kernel is calculated at each quadrature point, by the matricial form defined by means of the transformation of the tensorial form.

C.1 Algebra

We propose a transformation of the indicial elements of the expressions into a systematic matricial algebra by establishing the following rules and operators:

$$
\begin{aligned}
a, b, ... \rightarrow \alpha, \beta, ... & \\
K_{12} &= \delta_{ab}[\delta_{\alpha c}...] \\
K_{12}^T &= \delta_{\alpha\beta}[\delta_{a\gamma}...] \\
d_{12} &= \delta_{a\beta}\delta_{b\alpha}[\delta_{c\gamma}...] \\
I &= [\delta_{a\alpha}...] \\
g_1 &= \overline{\delta}_{a\alpha}[\delta_{b\beta}...] \\
(I + d_{12}) &= e_{ab\alpha\beta}[\delta_{\gamma c}...] \\
(d_{12} + d_{23} + d_{13}) &= e_{abc\alpha\beta\gamma}[\delta_{\delta d}...]
\end{aligned}
$$

The latter elementary operators defined between the indexes $a, b, ...$ and $\alpha, \beta, ...$ can be coupled successively by multiplication (maintaining the order) and defining new sets of the same number of indexes acting as intermediate ones to be contracted by inner summation.

C.2 Proof

If we look at the tensor indices as a series of permutations $x_{ijklm} = x_{12345} = x_A$ with $A = \{12345\}$, then the two basic operations performed are the interchange of permutations,

$$x_{ijklm} \overset{\text{transformation T}}{\longrightarrow} x_{jiklm}$$
$$\{12345\} \xrightarrow{\sigma_1} \{21345\}$$

and contraction or its reverse expansion by inner summation.

$$\delta_{lm} x_{ijklm} \overset{\text{transformation T}}{\longrightarrow} x_{ijk}$$

In either case the transformations can be expressed in terms of a combination of simpler transformations in a multiplicative sense as

$$\sigma_1(A) = \sigma_2(A)\sigma_3(A)$$

This is possible since the transformations are always linear transformations in the sense that

$$\begin{aligned} T(x_A + y_A) &= T(x_A) + T(y_A) \\ T(kx_A) &= kT(x_A) \end{aligned}$$

Since this condition is always accomplished in first order linear elasticity, every linear transformation can be represented in a matricial way.

Reversely, the transformations can be successively chained by doing the matrix multiplication in the right to left sense.

C.3 Subexpressions

Using these definitions, and expanding and inserting the necessary indices, the needed subexpressions can be written as:

$$\begin{aligned}
d^i_{jk}(x,\xi) &= \lambda\delta_{ij}u^o_{k,o}(x,\xi) + \mu(u^i_{k,j}(x,\xi) + u^j_{k,i}(x,\xi)) \\
&= [\lambda K^T_{12}K_{12}d_{23} + \mu(I + d_{12})d_{23}]u^a_{b,c} = dd^{ia}_{jkbc}u^a_{b,c} \\
t^i_{jkl}(x,\xi) &= \lambda\delta_{ij}\sigma^o_{kl,o}(x,\xi) + \mu(\sigma^i_{kl,j}(x,\xi) + \sigma^j_{kl,i}(x,\xi)) \\
&= [\lambda K^T_{12}K_{12}d_{23}d_{34} + \mu(I + d_{12})d_{23}d_{34}]\sigma^a_{bc,d} = tt^{ia}_{jklbcd}\sigma^a_{bc,d} \\
d^i_{jk,m}(x,\xi) &= \lambda\delta_{ij}u^o_{k,om}(x,\xi) + \mu(u^i_{k,jm}(x,\xi) + u^j_{k,im}(x,\xi)) \\
&= [\lambda K^T_{12}K_{12}d_{23} + \mu(I + d_{12})d_{23}]u^a_{b,cd} = dd^{ia}_{jkmbcd}u^a_{b,cd} \\
t^i_{jkl,m}(x,\xi) &= \lambda\delta_{ij}\sigma^o_{kl,om}(x,\xi) + \mu(\sigma^i_{kl,jm}(x,\xi) + \sigma^j_{kl,im}(x,\xi)) \\
&= [\lambda K^T_{12}K_{12}d_{23}d_{34} + \mu(I + d_{12})d_{23}d_{34}]\sigma^a_{bc,de} = tt^{ia}_{jklmbcde}\sigma^a_{bc,de} \\
\sigma^i_{jk}(x,\xi) &= \lambda\delta_{jk}u^i_{o,o}(x,\xi) + \mu(u^i_{j,k}(x,\xi) + u^i_{k,j}(x,\xi)) \\
&= [\lambda d_{13}K^T_{12}K_{12}d_{13} + \mu(I + d_{23})]u^a_{b,c} = dd^{ia}_{jkbc}u^a_{b,c} \\
\sigma^i_{jk,l}(x,\xi) &= \lambda\delta_{jk}u^i_{o,ol}(x,\xi) + \mu(u^i_{j,kl}(x,\xi) + u^i_{k,jl}(x,\xi)) \\
&= [\lambda d_{13}K^T_{12}K_{12}d_{13} + \mu(I + d_{23})]u^a_{b,cd} = dd^{ia}_{jklbcd}u^a_{b,cd} \\
\sigma^i_{jk,lm}(x,\xi) &= \lambda\delta_{jk}u^i_{o,olm}(x,\xi) + \mu(u^i_{j,klm}(x,\xi) + u^i_{k,jlm}(x,\xi)) \\
&= [\lambda d_{13}K^T_{12}K_{12}d_{13} + \mu(I + d_{23})]u^a_{b,cde} = dd^{ia}_{jklmbcde}u^a_{b,cde}
\end{aligned}$$

where

$$
\begin{aligned}
u^a_b &= \tfrac{1}{2\pi\mu} && [\psi\delta_{ab} - \chi r_{,a} r_{,b}] \\
&= \tfrac{1}{2\pi\mu} && \left[\psi K_{12}^T - \chi r_1 r_2\right] \\
u^a_{b,c} &= \tfrac{1}{2\pi\mu} && [\psi'\delta_{ab} r_{,c} - \chi' r_{,a} r_{,b} r_{,c} - \chi e_{aba'b'} r_{,a'} r_{,b'c}] \\
&= \tfrac{1}{2\pi\mu} && \left[\psi' K_{12}^T r_1 - \chi' r_1 r_2 r_3 - \chi(I + d_{12}) r_1 r_{23}\right] \\
u^a_{b,cd} &= \tfrac{1}{2\pi\mu} && [\psi''\delta_{ab} r_{,c} r_{,d} + \psi'\delta_{ab} r_{,cd} - \chi'' r_{,a} r_{,b} r_{,c} r_{,d} - \chi' r_{,a} r_{,b} r_{,cd} \\
& && -e_{aba'b'}(\chi' e_{cdc'd'} r_{,a'} r_{,c'} r_{,b'd'} + \chi r_{,a'cd} r_{,b'} + \chi r_{a'c} r_{b'd})] \\
&= \tfrac{1}{2\pi\mu} && [\psi'' K_{12}^T r_1 r_2 + \psi' K_{12}^T r_{12} - \chi'' r_1 r_2 r_3 r_4 - \chi' r_1 r_2 r_{34} \\
& && -(I + d_{12})(\chi'(I + d_{34}) r_1 r_3 r_2 4 + \chi r_{134} r_2 + \chi r_{13} r_{24})] \\
u^a_{b,cde} &= \tfrac{1}{2\pi\mu} && [\psi'''\delta_{ab} r_{,c} r_{,d} r_{,e} + (-r\psi'' + \psi')\delta_{ab} r_{,cde} - \chi''' r_{,a} r_{,b} r_{,c} r_{,d} r_{,e} \\
& && -\chi''[e_{abca'b'c'} e_{ded'e'} r_{,a'} r_{,b'} r_{,c'd'} r_{,e'} + e_{abea'b'e'} r_{,a'c} r_{,b'} r_{,d} r_{,e'}] \\
& && -\chi'[e_{abca'b'c'}(r_{,a'e} r_{,b} r_{,c'd} + r_{,a'} r_{,b'e} r_{,c'd} + r_{,a'} r_{,b'} r_{,c'de}) \\
& && +e_{aba'b'}(r_{,a'} r_{,b'c} r_{,de} + e_{ded'e'}(r_{,a'e'} r_{,b'c} r_{,d'}))] \\
& && -\chi e_{aba'b'}[r_{,a'de} r_{,b'c} + r_{,a'd} r_{,b'ce} + r_{,a'e} r_{,b'cd} + r_{,b'cde} r_{,a'}]] \\
&= \tfrac{1}{2\pi\mu} && [\psi''' K_{12}^T r_1 r_2 r_3 + (-r\psi'' + \psi') K_{12}^T r_{123} - \chi''' r_1 r_2 r_3 r_4 r_5 \\
& && -\chi''[(d_{12} + d_{13} + d_{23})(I + d_{45}) r_1 r_2 r_{34} r_5 \\
& && +(d_{12} + d_{15} + d_{25}) r_{13} r_2 r_4 r_5] \\
& && -\chi'[(d_{12} + d_{13} + d_{23})(r_{15} r_2 r_{34} + r_1 r_{25} r_{34} + r_1 r_2 r_{345}) \\
& && +(I + d_{12})(r_1 r_{23} r_{45} + (I + d_{45})(r_{15} r_{23} r_4))] \\
& && -\chi(I + d_{12})[r_{145} r_{23} + r_{14} r_{235} + r_{15} r_{234} + r_{2345} r_1]]
\end{aligned}
$$

C.4 Encoding

All the information of one tensor with n indices $A_{123\ldots n}$ is stored in a vector containing 2^n elements. They should be organized in a congruent way. For instance, in the case of $n = 3$ and $\Re^2$,

$$A_{123} = [a_{111} a_{211} a_{121} a_{221} a_{112} a_{212} a_{122} a_{222}]$$

A transformation tensor $T^{123\ldots m}_{123\ldots n}$ with n input and m output indices that transforms $A_{123\ldots n}$ into $B_{123\ldots m}$ is therefore encoded as a $2^n \times 2^m$ matrix.

Obviously, a congruent number of indices is needed, making it necessary to append or prepend mute indices in order to reach the necessary order (for instance a preposition of one index to A_i is made so that $A_{1i} = A_{2i}$).

The radius terms are defined as vectors - and multiplied element by element giving another vector - in the following way:

$$
\begin{aligned}
r_1 &= \frac{r_1}{|r|} \\
r_{12} &= \frac{1}{|r|}(K_{12}^T - r_1 r_2) \\
r_{123} &= \frac{-1}{|r|}(d_{12} + d_{23} + d_{13}) r_{12} r_3 \\
r_{1234} &= \frac{-1}{|r|}(r_{123} r_4 + (d_{12} + d_{23} + d_{13})(r_{124} r_3 + r_{12} r_{34}))
\end{aligned}
$$

where

$$r_1 = \begin{pmatrix} r_x \\ r_y \end{pmatrix} \qquad \text{in the case of 2D.}$$